

# Electroweak corrections to gauge boson production at large transverse momenta

Zur Erlangung des akademischen Grades eines  
DOKTORS DER NATURWISSENSCHAFTEN  
von der Fakultät für Physik der Universität (TH)

Karlsruhe

genehmigte

DISSERTATION

von

Dipl.-Phys. Markus Schulze  
aus Karlsruhe

Tag der mündlichen Prüfung: 18. April 2008

Referent: Prof. Dr. Johann H. Kühn

Korreferent: Prof. Dr. Dieter Zeppenfeld







# Zusammenfassung

Die Erzeugung von elektroschwachen Eichbosonen stellt eine wichtige Prozessklasse an Beschleunigerexperimenten dar. Der Vergleich zwischen dem experimentell gemessenen Wirkungsquerschnitt und der Theorievorhersage ermöglicht eine genaue Überprüfung des zugrunde liegenden Modells. Um die erforderliche Genauigkeit einer Vorhersage zu erreichen, müssen im Rahmen des quantenfeldtheoretischen Modells der Teilchenphysik Strahlungskorrekturen berechnet werden.

In dieser Arbeit werden die elektroschwachen Korrekturen zur hadronischen Produktion von Eichbosonen bei hohen transversalen Impulsen untersucht. Die Berechnung der Ein-Schleifen-Korrekturen für Endzustände mit Photonen und  $Z$ -Bosonen umfasst die schwachen Korrekturen, während für die Produktion von  $W$ -Bosonen die vollständigen elektroschwachen Korrekturen berücksichtigt werden. Letztere beinhalten insbesondere die Beiträge reeller Photonabstrahlung. Die Methoden der Rechnung werden eingehend dokumentiert und die Ergebnisse für das unpolarisierte quadrierte Matrixelement in analytischer Form präsentiert. Weiterhin werden kompakte Formeln angegeben, die für Reaktionen hoher Energie die exakte Ein-Schleifen-Korrektur annähern. In diesem Fall liefern Logarithmen des Verhältnisses  $\hat{s}/M_W^2$  die dominanten Beiträge zum Wirkungsquerschnitt. Ferner sind dominante Zwei-Schleifen-Beiträge bis zur nächst-führenden logarithmischen Ordnung in den Korrekturen berücksichtigt.

Numerische Resultate werden für den *Large Hadron Collider* (LHC) und den Tevatron präsentiert. Es zeigt sich, dass die elektroschwachen Korrekturen negativ sind und mit der Energie anwachsen. Am LHC, an dem transversale Impulse mit bis zu 2 TeV erreicht werden können, belaufen sich die Ein-Schleifen-Beiträge auf Korrekturen bis zu -30%. Die Zwei-Schleifen-Korrekturen sind zudem signifikant und müssen für präzise Analysen berücksichtigt werden. Am Tevatron sind die elektroschwachen Korrekturen weniger bedeutend. Jedoch im Bereich transversaler Impulse bis zu 200 GeV erreichen sie Werte, die größer oder vergleichbar mit dem erwarteten statistischen Fehler sind.



# Abstract

To match the precision of present and future measurements of gauge boson production at hadron colliders, electroweak radiative corrections must be included in the theory predictions. In this work their effect on the transverse momentum ( $p_T$ ) distribution of a photon, a  $Z$  or a  $W$  boson in association with a jet is considered. For neutral gauge boson production the virtual weak corrections are presented, while for  $W$  production the full electroweak corrections are considered, including virtual and real photonic contributions. The steps of the calculations are discussed in detail. Explicit analytical results for the unpolarized squared matrix element are presented. In addition, compact approximate expressions are given, which are valid in the high-energy region where the electroweak corrections are strongly enhanced by logarithms of  $\hat{s}/M_W^2$ . Furthermore, the leading and next-to-leading logarithms at two-loop level are also calculated.

Numerical results are presented for the Large Hadron Collider (LHC) and the Tevatron. The electroweak corrections are negative and their size increases with  $p_T$ . At the LHC, where transverse momenta of 2 TeV or more can be reached, the one-loop corrections amount up to several tens of percent. For a precise analysis also the two-loop contributions will be important. The electroweak corrections for reactions at the Tevatron are less significant. However, for transverse momenta up to 200 GeV the size of the corrections is well above the expected statistical error.

# Contents

<b>1</b>	<b>Introduction</b>	<b>1</b>
<b>2</b>	<b>Definitions and conventions</b>	<b>7</b>
2.1	Partonic processes . . . . .	7
2.2	Kinematics . . . . .	8
2.3	Crossing symmetries . . . . .	11
2.4	Couplings . . . . .	13
2.5	Leading order contribution . . . . .	14
<b>3</b>	<b>Electroweak one-loop corrections</b>	<b>19</b>
3.1	Preliminaries . . . . .	19
3.2	Algebraic reduction . . . . .	20
3.2.1	Couplings for neutral gauge boson production . . . . .	22
3.2.2	Couplings for charged gauge boson production . . . . .	23
3.2.3	Standard matrix elements and scalar integrals . . . . .	25
3.3	Renormalization . . . . .	28
3.3.1	Renormalization of the photon vertex . . . . .	29
3.3.2	Renormalization of the $Z$ vertex . . . . .	31
3.3.3	Renormalization of the $W$ vertex . . . . .	32
3.4	Soft and collinear singularities for $W$ boson production . . . . .	34
3.5	Results . . . . .	38
<b>4</b>	<b>High energy limit</b>	<b>41</b>
4.1	NNLL approximation at one-loop . . . . .	42
4.2	NLL approximation at one-loop . . . . .	46
4.3	NLL approximation at two-loop . . . . .	51
<b>5</b>	<b>Real photonic corrections for <math>W</math>+jet production</b>	<b>55</b>
5.1	Mass regularization . . . . .	57
5.2	Dimensional regularization . . . . .	62
<b>6</b>	<b>Phase space integrations</b>	<b>67</b>
6.1	Three-particle phase space generation . . . . .	67
6.2	Multi-particle phase space generation . . . . .	69



6.2.1	Generation of soft and collinear limits . . . . .	71
<b>7</b>	<b>Checks and implementations</b>	<b>75</b>
<b>8</b>	<b>Numerical results</b>	<b>77</b>
8.1	Results for $Z$ production at partonic level . . . . .	77
8.2	Results for the LHC . . . . .	79
8.3	Results for the Tevatron . . . . .	90
<b>9</b>	<b>Conclusions</b>	<b>97</b>
<b>A</b>	<b>Input parameters for the numerical results</b>	<b>98</b>
<b>B</b>	<b>Recombination and exclusive <math>W</math>+jet cross section</b>	<b>101</b>
<b>C</b>	<b>On-shell coupling renormalization for <math>Z</math>+jet production</b>	<b>104</b>
<b>D</b>	<b>Explicit results</b>	<b>107</b>
D.1	Virtual corrections . . . . .	107
D.2	Real corrections for $W$ +jet . . . . .	111
	<b>References</b>	<b>113</b>
	<b>Acknowledgment</b>	<b>121</b>



# Chapter 1

## Introduction

The era of particle physics may be said to have begun with the discovery of the electron by J. Thomson in 1897. Followed by the advent of fundamental new concepts through the theory of relativity and the quantum picture of nature, this opened up a century of great discoveries and deep insights into the laws of nature. Most of the theoretical developments were always formulated in close interplay with experiments. Most of the new concepts included the previously established models in some limit.

With the formulation of Quantum Electrodynamics (QED) by Feynman, Schwinger and Tomonaga in the late 1940's the first relativistic quantum field theory was set up. It describes electromagnetism by interactions between quantized fields of photons and charged fermions. The great success in predicting the anomalous moment of the muon, via quantum corrections, makes QED to one of the most accurate physical theories ever. On the other hand, since 1934 the Fermi theory allowed to describe the nuclear beta-decay. This theory was formulated in a less stringent way but anticipated the concept of weak interactions and put the neutrino on a firm basis.

With the beginning of the second half of the 20th century more and more particles were found. The invention of the bubble chamber and the synchrotron principle led, together with discoveries of new particles from cosmic rays, to the development of large accelerators. Resonances of the proton were found and experiments with Kaons suggested the strangeness quantum number. Besides the discoveries of new particles, parity violation of weak interactions has been experimentally confirmed in beta-decays of  $^{60}\text{Co}$ , and was followed by the V-A theory of weak interactions. Furthermore, CP violation showed up completely unexpected in decays of short and long-lived Kaons. On the theoretical side, in 1954 Yang and Mills developed classes of new theories, which turned out to constitute the modern non-Abelian gauge theories, many years later. The Higgs mechanism of spontaneous symmetry breaking was presented in 1964. It was inspired by the BCS theory of superconductivity. In the same year, receiving strong support from the observation of the  $\Omega^-$  baryon with strangeness -3, Gell-Mann and Zweig introduced the quark picture of hadrons. This

viewpoint suggests a regular arrangement of baryons and mesons into representations of a  $SU(3)$  symmetry, such as octets and decuplets. The problem of the totally symmetric wave functions of the  $\Delta^{++}$  and  $\Omega^-$  baryons could be reconciled with the Pauli-principle by the proposal of color degrees of freedom for quarks in 1965. Only four years later, the discovery of Bjorken scaling in deep inelastic scattering led to the parton model, which was completely unrelated to that of quarks in the first moment. In the same year, with the advent of the Glashow-Salam-Weinberg (GSW) model the first step towards a unification of interactions was done. This theory proposed the heavy vector bosons  $Z^0$  and  $W^\pm$  in order to explain neutral and charged currents, respectively. Their masses are generated by spontaneous symmetry breaking of a  $SU(2)\times U(1)$  gauge group via the Higgs mechanism. The photon field is incorporated in a unique way, which reproduces the theory of QED at low energies. Similarly, the Fermi theory can be derived from charged current interactions at low energies. With the proof of renormalizability by 't Hooft in 1971 the theory was on par with QED and radiative corrections were possible without loss of predictability. On the experimental side, the study of charged and neutral weak currents and associated coupling parameters provided more and more evidence for the GSW model. Finally, in the year 1983 the experiments UA1 and UA2 at the CERN Sp $\bar{p}$ S collider reported the observation of the heavy  $Z^0$  and  $W^\pm$  bosons. Their masses were found to match the expected values from parameters of neutral currents derived ten years before.

The development in understanding strong interactions went on with the discovery of asymptotic freedom. Gross, Wilzcek and Politzer investigated this specific possibility of Yang-Mills theories in the year 1973. Together with the formulation of the theory of Quantum Chromo Dynamics (QCD) by Fritzsche and Gell-Mann, a non-Abelian gauge theory was found that was able to encompass the quark model with color degrees of freedom as well as the parton model including confinement. Subsequent experiments of deep inelastic lepton-nucleon scattering confirmed the quark picture and anticipated the gluon content of hadrons. In 1979, the observation of three-jet events at the PETRA storage ring brought the discovery of the gluon as mediator of strong interactions.

With the beginning of the 1990's, the Large-Electron-Positron collider LEP at CERN and the SLAC Linear Collider SLC began operating at energies of the  $Z^0$  mass. Over the years, these colliders produced millions of  $Z^0$  particles, confirming the predictions of the GSW model with high precision. Various parameters as for example the  $Z^0$ -boson mass and its width, as well as the electroweak and strong coupling constants were measured in perfect agreement with the underlying theory. Even the mass of the top quark could be derived indirectly from virtual loop effects. The proton-antiproton collider Tevatron at Fermilab finally detected the decay of a top quark in the year 1995. Its mass was found to be in agreement with the earlier derived value. It was also the Tevatron that showed the direct detection of the  $\tau$ -neutrino in the year 2000, which has been expected from the  $Z$  resonance curve at LEP. These discoveries completed the picture of three generations of quarks and lep-

tons in the GSW model, which today constitutes the Electroweak Standard Model (SM) of particle physics. The only not yet discovered particle of the Electroweak SM is the Higgs boson, whose existence is crucial for the spontaneous symmetry breaking of the gauge groups. Even with the upgrade of LEP to energies of the  $Z^0$  pair threshold no discovery signal was found. From these experiments, the lower limit on the Higgs boson mass is set at around 114 GeV, while the upper limit is expected by electroweak precision measurements at around 190 GeV. With the upcoming Large Hadron Collider (LHC) at CERN the full mass range of the Standard Model Higgs particle is within reach and can be explored with adequate statistics. Also many extensions of the Electroweak Standard Model can be tested with experiments at the LHC.

With this historical perspective in mind, it is evident that the study of gauge boson production has been among an important process at hadron colliders. The investigation of the production dynamics, strictly predicted by the electroweak theory, constitutes one of the important tests of the Standard Model. Furthermore, being embedded in the environment of hadronic collisions, the reaction necessarily involves hadronic physics, like parton distributions, and depends on the strong coupling constant.

Direct photon production at hadron colliders consists of the QCD Compton process  $gq \rightarrow \gamma q$  and the annihilation process  $\bar{q}q \rightarrow \gamma g$ . Diverse studies have been performed for these processes, theoretically [1, 2] as well as experimentally [3]. Since the photons do not fragment and can be clearly identified experimentally, direct photon production provides a much clearer probe of the hard-scattering dynamics than jet production processes. Therefore the study of large transverse momentum direct (prompt) photon production constitutes an important test of perturbative QCD and the point-like nature of quarks and gluons. In turn, the cross section for direct production of photons, their transverse momentum ( $p_T$ ) and rapidity distributions can be used to gauge the parton distribution functions. Since the gluon distribution enters already at the leading order, the measurement of the direct photon production is an important means to constrain information on the gluon content of the proton [4]. In particular, large transverse momentum production provides a unique opportunity for determination of gluon densities at large  $x$ .

Apart from the direct process, prompt photons can also be produced through a fragmentation process. However, most of the fragmentation contribution can be removed by applying an isolation criterion. The importance of the remaining contribution from fragmentation, after applying the isolation cut, is expected to decrease with higher  $p_T$ . Moreover, background processes to isolated direct photon production, i.e. photon production through decays of neutral mesons ( $\pi^0, \eta$ ) coming from jet fragmentation, are shown to be less important at large  $p_T$  [5].

The production processes for massive gauge bosons are of equal importance at hadron colliders. In the region of small  $p_T$ , multiple gluon emission plays an impor-

tant role and contributions of arbitrary many gluons must be resummed to arrive at a reliable prediction [6, 7]. At larger transverse momenta the final state consists of a  $W$  or  $Z$  boson plus one (or more) recoiling jet(s). The large cross sections for these processes provide sizable event rates, which allow to extract experimental and theoretical parameters with high precision. In particular, massive gauge boson production can be used to monitor the collider luminosity as well as to calibrate jet energy scales [8]. Furthermore, their study can constrain the error on the parton distribution functions [9]. In view of new physics searches, these processes contribute as background.

In order to match the precision of present and future measurements at hadron colliders, radiative corrections must be included in the theory predictions. In particular, for the correct description of gauge boson production in association with a recoiling jet, QCD as well as electroweak corrections are mandatory. At next-to-leading order in QCD the corrections can amount to several tens of per cent depending on the observable under consideration, including jet definition, as well as the renormalization and factorization scales [2, 5, 10, 11]. The evaluation of next-to-next-to-leading order corrections in QCD involves two-loop virtual plus a variety of combined virtual plus real corrections and is a topic presently pursued by various groups (see e.g. Ref. [12]).

For experiments at the Large Hadron Collider a new aspect comes into play. The high center-of-mass energy in combination with the enormous luminosity will allow to explore parton-parton scattering up to energies of several TeV and correspondingly production of gauge bosons with transverse momenta up to 2 TeV or even beyond. In this kinematic region electroweak corrections from virtual weak boson exchange are strongly enhanced by large logarithms. The dominant terms in  $L$ -loop approximation are leading logarithms of the form  $\alpha^L \log^{2L}(\hat{s}/M_W^2)$  and next-to-leading logarithms of the form  $\alpha^L \log^{2L-1}(\hat{s}/M_W^2)$ , and so on. These corrections, also known as electroweak Sudakov logarithms, may well amount to several tens of percent [13, 14, 15, 16, 17, 18, 19, 20, 21, 22, 23, 24]. A recent survey of the literature on logarithmic electroweak corrections can be found in Ref. [25].

The evaluation of the electroweak corrections to hadronic production of gauge bosons at large transverse momenta are the subject of this work. The corresponding results have been published in Refs. [18, 19] and [20] for  $Z$  boson and photon production respectively, and for  $W$  boson production in [22, 24]. In addition, numerical results for the weak one-loop corrections to the hadronic production of photons or  $Z$  bosons in association with a jet have also been presented in Ref. [17]. Results on charged gauge boson production at large transverse momentum have also been reported in [23].

In this work, we consider the partonic processes  $q\bar{q} \rightarrow Vg$ ,  $qg \rightarrow Vq$  and  $\bar{q}g \rightarrow V\bar{q}$ . For the neutral gauge boson production ( $V = \gamma, Z$ ) we present the results of the weak one-loop calculation. These corrections contribute with large Sudakov logarithms and can be split off from the pure photonic corrections in a gauge invariant manner. In contrast, as a consequence of the non-vanishing  $W$  charge, the photonic

corrections to the above partonic processes for  $W$  production cannot be separated from the purely weak ones and will thus be included in our analysis. In addition to the exact one-loop corrections, we also derived compact approximate expressions in the high energy limit. We include quadratic and linear logarithms as well as those terms that are not logarithmically enhanced at high energies but neglect all contributions of  $\mathcal{O}(M_W^2/\hat{s})$ . The accuracy of this approximation is discussed in detail. Furthermore, in view of their numerical importance we also derive the dominant two-loop terms, up to the next-to-leading logarithmic accuracy for photon,  $Z$  and  $W$  boson production at large transverse momenta. As the virtual photonic corrections for  $W$ +jet production involve soft and collinear singularities, real photon emission must be included in order to obtain a finite and well defined cross section. In these events, the  $p_T$  of the  $W$  boson is balanced both by the  $p_T$  of the recoiling parton (quark or gluon) and the photon. Configurations involving a small- $p_T$  parton and a hard photon are better described as  $W\gamma$  final states. We thus define the  $W$ +jet cross section imposing a lower limit on the jet transverse momentum, which is chosen independent of the  $W$ -boson  $p_T$ . The corresponding cancellation of singularities between virtual and real corrections is performed within the dipole subtraction formalism. Remaining collinear singularities from photon radiation off initial state quarks are absorbed in renormalized parton distribution functions. Final state singularities are avoided by recombination of collinear quark-photon configurations.

The virtual electroweak one-loop corrections to the process  $V$ +jet with  $V = \gamma, Z, W^\pm$  are formally connected with the real emission of  $W$  and  $Z$  bosons. This leads to  $VV'$ +jet final states, where  $V' = W, Z$ . Both contributions are of  $\mathcal{O}(\alpha^2\alpha_S)$ . If integrated over the full phase space, the real emission of massive gauge bosons produces large Sudakov logarithms that partially cancel those resulting from virtual gauge bosons. However, in exclusive measurements of  $V$ +jet processes, the available phase space for additional gauge boson emission is strongly suppressed by the experimental cuts. We thus expect that such real emission provides relatively small contributions while the bulk of electroweak effects originates from virtual corrections. In fact, for  $pp \rightarrow Z$ +jet it was shown in Ref. [21] that, in presence of realistic (and relatively less exclusive) experimental cuts, the contribution of real emission is about five times smaller than the virtual corrections. Moreover, real emission can be further reduced with a veto on additional jets, which suppresses multiple-jet events resulting from the hadronic decay of the radiated gauge bosons. Therefore we will restrict ourselves to the investigation of virtual electroweak corrections (and photon bremsstrahlung in the case of  $W$  production). The real emission of additional  $W$  and  $Z$  bosons can be non-negligible and certainly deserves further detailed studies, however we do not expect a dramatic impact on our results.

This work is organized as follows: In Ch. 2 we give the relevant partonic processes and define the observable as well as the kinematic variables for the two- and three particle phase space. The crossing and CP symmetries are discussed and our conventions for couplings are collected. Furthermore, first numerical results for the lowest order cross sections are presented. The calculation of the virtual corrections

is described in Ch. 3. We discuss the algebraic reductions in Sect. 3.2 and present analytic expressions for the structure of the one-loop amplitude. The different renormalization schemes for the production of photons,  $Z$  and  $W$  bosons are described in Sect. 3.3. Soft and collinear singularities arising from the virtual photonic corrections to the process  $W$ +jet are extracted in Sect. 3.4. We regularize these singularities in two different schemes: using small quark and photon masses which are set to zero at the end of the calculation and, alternatively, dimensional regularization. Ch. 4 is concerned with the compact analytic results in the high energy limit. The next-to-next-leading logarithmic (NNLL) approximation at one-loop level is derived from the exact one-loop calculation in Sect. 4.1. In order to check the dominant logarithmic contributions we re-derive the next-to-leading logarithmic (NLL) terms in Sect. 4.2 by means of an independent method. Furthermore, this introduces the specific notation that will be used to derive the two-loop contributions in Sect. 4.3. The calculation of the real corrections to the  $W$ +jet process is presented in Ch. 5. For this process, we give a detailed description of the dipole subtraction method regularized with small masses as well as with dimensional regularization. The corresponding phase space integration that is necessary to evaluate the three-particle phase space is described in Ch. 6. In addition, a modification of these integration methods is discussed, which allows to check the cancellations between matrix elements and dipoles for soft and collinear momentum configurations with high precision. The checks, which we carried out in order to ensure the correctness of the results are summarized in Ch. 7. Finally, we present our numerical results in Ch. 8. After convolution with parton distribution functions, we obtain radiatively corrected results for  $p_T$ -distributions of the electroweak gauge bosons in association with a jet at the LHC and Tevatron. The size of the electroweak corrections is discussed in detail. The quality of the one-loop NLL and NNLL approximations is investigated and the size of the dominant two-loop terms is compared with the expected statistical precision of the experiments. Concerning perturbative QCD, our results are based on the lowest order. To obtain realistic predictions for the cross sections, higher-order QCD corrections [2, 5, 10, 11] must be included. However, the relative rates for photon,  $Z$ ,  $W^+$  and  $W^-$  production are expected to be more stable against QCD effects. Therefore, the impact of the electroweak corrections on these ratios is also presented in Ch. 8. The conclusions and a brief summary can be found in Ch. 9. Explicit analytic results for the unpolarized squared matrix elements of the exact one-loop calculation and real corrections to the  $W$ +jet process are collected in the Appendices.



# Chapter 2

## Definitions and conventions

In this chapter we introduce the partonic processes relevant for the hadronic production of a gauge boson at large transverse momentum. Furthermore, we define all kinematic variables and discuss the definition of the transverse momentum distribution for the two- and three-particle phase space. Crossing and CP symmetries are presented, which relate various partonic channels, and the conventions for all couplings are given. We also show first numerical results for the lowest order cross sections at the LHC and the Tevatron.

### 2.1 Partonic processes

The  $p_T$ -distribution for electroweak gauge bosons in the reaction  $h_1 h_2 \rightarrow V j(+\gamma)$  is given by

$$\frac{d\sigma^{h_1 h_2}}{dp_T} = \sum_{a,b,k} \int_0^1 dx_1 \int_0^1 dx_2 \theta(x_1 x_2 - \hat{\tau}_{\min}) f_{h_1,a}(x_1, \mu^2) f_{h_2,b}(x_2, \mu^2) \frac{d\hat{\sigma}^{ab \rightarrow V k(+\gamma)}}{dp_T}. \quad (2.1)$$

The hadronic initial state is denoted by  $h_1$  and  $h_2$ . The electroweak gauge boson  $V$  can be a photon, a  $Z$  or a  $W$  boson recoiling against a jet, which is denoted by  $j$ . In the case of the real corrections to  $W$  production an additional photon is present in the final state. The indices  $a, b$  in (2.1) denote initial-state partons and  $f_{h_1,a}(x, \mu^2)$ ,  $f_{h_2,b}(x, \mu^2)$  are the corresponding parton distribution functions (PDFs).  $\hat{\sigma}^{ab \rightarrow V k(+\gamma)}$  is the partonic cross section for the subprocess  $ab \rightarrow V k(+\gamma)$ . The quantity  $\hat{\tau}_{\min}$  is related to the minimum partonic energy that is needed to produce the final state,

$$s\hat{\tau}_{\min} = \left( p_{T,j}^{\min} + \sqrt{(p_{T,V}^{\min})^2 + p_V^2} \right)^2, \quad (2.2)$$

where  $\sqrt{s}$  is the collider energy,  $p_{T,j}^{\min}$  and  $p_{T,V}^{\min}$  are the lower limits on the transverse momentum of the jet and the gauge boson, respectively. The squared mass of the gauge boson is given by  $p_V^2$ . The sum in (2.1) runs over all combinations corresponding to the contributing subprocesses. For the leading contribution of  $\mathcal{O}(\alpha\alpha_s)$  and

the virtual corrections of  $\mathcal{O}(\alpha^2\alpha_s)$  the partonic processes are

$$\begin{aligned}\bar{q}q' &\rightarrow Vg, & q'\bar{q} &\rightarrow Vg, \\ gq' &\rightarrow Vq, & q'g &\rightarrow Vq, \\ \bar{q}g &\rightarrow V\bar{q}', & g\bar{q} &\rightarrow V\bar{q}'.\end{aligned}\tag{2.3}$$

The processes for the production of neutral gauge bosons involve only external quarks of equal flavor, while for  $W$  production the two quark flavors are different. In particular, this is given by the assignment

$$\{q, q'\} = \begin{cases} \{u_n, u_n\} \text{ or } \{d_n, d_n\} & \text{for } V = \gamma, Z, \\ \{d_n, u_m\} & \text{for } V = W^+, \\ \{u_n, d_m\} & \text{for } V = W^-.\end{cases}\tag{2.4}$$

The indices  $m, n$  denote the family dependence of the quarks. We do not consider (anti-)top quarks in the initial or final states and treat all other quarks as massless.

Similarly to (2.3), the real photonic corrections of  $\mathcal{O}(\alpha^2\alpha_s)$  to  $W$ +jet production contribute with the processes

$$\begin{aligned}\bar{q}q' &\rightarrow W^\pm g\gamma, & q'\bar{q} &\rightarrow W^\pm g\gamma, \\ gq' &\rightarrow W^\pm q\gamma, & q'g &\rightarrow W^\pm q\gamma, \\ \bar{q}g &\rightarrow W^\pm \bar{q}'\gamma, & g\bar{q} &\rightarrow W^\pm \bar{q}'\gamma.\end{aligned}\tag{2.5}$$

Furthermore, in the case of  $W$  production the dependence on the family indices  $m, n$  in (2.4) amounts to an overall CKM factor  $|V_{u_m d_n}|^2$ . This factor can be easily absorbed by redefining the parton distribution functions as

$$\begin{aligned}\tilde{f}_{h,d_m} &= \sum_{n=1}^3 |V_{u_m d_n}|^2 f_{h,d_n}, & \tilde{f}_{h,\bar{d}_m} &= \sum_{n=1}^3 |V_{u_m d_n}|^2 f_{h,\bar{d}_n}, \\ \tilde{f}_{h,u_m} &= f_{h,u_m}, & \tilde{f}_{h,\bar{u}_m} &= f_{h,\bar{u}_m}, & \tilde{f}_{h,g} &= f_{h,g}.\end{aligned}\tag{2.6}$$

Thus, the hadronic cross section (2.1) for  $W$ +jet production can be computed using the trivial CKM matrix  $\tilde{V}_{u_i d_j} = \delta_{ij}$  and the redefined PDFs (2.6). Since we do not consider initial or final states involving (anti-)top quarks, only the contributions of the first two quark families ( $m = 1, 2$ ) have to be included. The corresponding redefined PDFs ( $\tilde{f}_{h,q}$  with  $q = u, d, c, s$ ) automatically include the (small) contributions associated with initial- and final-state bottom quarks.

## 2.2 Kinematics

For the  $2 \rightarrow 2$  subprocesses  $ab \rightarrow Vk$  the Mandelstam variables are defined in the standard way,

$$\hat{s} = (p_a + p_b)^2, \quad \hat{t} = (p_a - p_V)^2, \quad \hat{u} = (p_b - p_V)^2.\tag{2.7}$$

The momenta  $p_a, p_b, p_k$  of the partons are assumed to be massless, whereas  $p_V$  is the momentum vector of the gauge boson with mass 0,  $M_Z, M_W$  for photons,  $Z$  and  $W$  bosons, respectively. In terms of  $x_1, x_2, p_T$  and the collider energy  $\sqrt{s}$  we have

$$\hat{s} = x_1 x_2 s, \quad \hat{t} = \frac{p_V^2 - \hat{s}}{2}(1 - \cos\theta), \quad \hat{u} = \frac{p_V^2 - \hat{s}}{2}(1 + \cos\theta), \quad (2.8)$$

with  $\cos\theta = \sqrt{1 - 4p_T^2 \hat{s} / (\hat{s} - p_V^2)^2}$  corresponding to the cosine of the angle between the momenta  $p_a$  and  $p_V$  in the partonic center-of-mass frame.

The  $p_T$ -distribution for the unpolarized partonic subprocess  $ab \rightarrow Vk$  reads

$$\frac{d\hat{\sigma}^{ab \rightarrow Vk}}{dp_T} = \mathcal{N}_{ab} \int d\Phi_2 \overline{\sum} |\mathcal{M}^{ab \rightarrow Vk}|^2 F_{O,2}(\Phi_2), \quad (2.9)$$

where  $\overline{\sum} = \frac{1}{4} \sum_{\text{pol}} \sum_{\text{col}}$  involves the sum over polarization and color as well as the average factor  $1/4$  for initial-state polarization. The normalization factor is given by

$$\mathcal{N}_{ab} = \frac{(2\pi)^4}{2\hat{s}N_{ab}}, \quad (2.10)$$

where  $N_{\bar{q}q'} = N_{q\bar{q}'} = N_c^2$  and  $N_{gq} = N_{qg} = N_{\bar{q}g} = N_{g\bar{q}} = N_c(N_c^2 - 1)$ , with  $N_c = 3$ , account for the initial-state color average. The two-particle phase-space measure is

$$d\Phi_2 = \frac{d^3 p_V}{(2\pi)^3 2p_V^0} \frac{d^3 p_k}{(2\pi)^3 2p_k^0} \delta^4(p_a + p_b - p_V - p_k). \quad (2.11)$$

The function  $F_{O,2}$  in (2.9) defines the observable of interest, i.e. the gauge boson  $p_T$ -distribution in presence of a cut on the transverse momentum of the jet,

$$F_{O,2}(\Phi_2) = \delta(p_T - p_{T,V}) \theta(p_{T,j} - p_{T,j}^{\min}). \quad (2.12)$$

In the two-particle phase space the jet is identified with the parton  $k$  and momentum conservation implies  $p_{T,j} = p_{T,k} = p_{T,V}$ . In practice, since we always consider the  $p_T$ -distribution in the region  $p_T > p_{T,V}^{\min} \geq p_{T,j}^{\min}$ , the cut on  $p_{T,j}$  in (2.12) is irrelevant. The phase-space integral in (2.9) yields two contributions originating from kinematic configurations in the forward and backward hemispheres with opposite values of  $\cos\theta$  in the center-of-mass frame,

$$\frac{d\hat{\sigma}^{ab \rightarrow Vk}}{dp_T} = \frac{d\hat{\sigma}_{\text{fwd}}^{ab \rightarrow Vk}}{dp_T} + \frac{d\hat{\sigma}_{\text{bkwd}}^{ab \rightarrow Vk}}{dp_T}, \quad (2.13)$$

with

$$\frac{d\hat{\sigma}_{\text{fwd}}^{ab \rightarrow Vk}}{dp_T} = \frac{p_T}{8\pi N_{ab} \hat{s} |\hat{t} - \hat{u}|} \overline{\sum} |\mathcal{M}^{ab \rightarrow Vk}|^2, \quad \frac{d\hat{\sigma}_{\text{bkwd}}^{ab \rightarrow Vk}}{dp_T} = \left. \frac{d\hat{\sigma}_{\text{fwd}}^{ab \rightarrow Vk}}{dp_T} \right|_{\hat{t} \leftrightarrow \hat{u}}. \quad (2.14)$$

For the  $2 \rightarrow 3$  subprocess  $ab \rightarrow Wk\gamma$  we define the following five independent invariants

$$\begin{aligned}\hat{s} &= (p_a + p_b)^2, & \hat{t} &= (p_a - p_W)^2, & \hat{u} &= (p_b - p_W)^2, \\ \hat{t}' &= (p_a - p_\gamma)^2, & \hat{u}' &= (p_b - p_\gamma)^2,\end{aligned}\quad (2.15)$$

and the five dependent invariants

$$\begin{aligned}\hat{s}' &= (p_k + p_\gamma)^2 = \hat{s} + \hat{t} + \hat{u} - M_W^2, & \hat{s}'' &= (p_W + p_k)^2 = \hat{s} + \hat{t}' + \hat{u}', \\ \hat{t}'' &= (p_a - p_k)^2 = M_W^2 - \hat{s} - \hat{t} - \hat{t}', & \hat{u}'' &= (p_b - p_k)^2 = M_W^2 - \hat{s} - \hat{u} - \hat{u}', \\ \hat{s}_5 &= (p_W + p_\gamma)^2 = 2M_W^2 - \hat{s} - \hat{t} - \hat{t}' - \hat{u} - \hat{u}'.\end{aligned}\quad (2.16)$$

The  $p_T$ -distribution for this subprocess reads

$$\frac{d\hat{\sigma}^{ab \rightarrow W^\sigma k \gamma}}{dp_T} = \mathcal{N}_{ab} \int d\Phi_3 \overline{\sum} |\mathcal{M}^{ab \rightarrow W^\sigma k \gamma}|^2 F_{O,3}(\Phi_3), \quad (2.17)$$

where  $\sigma$  indicates the charge of the  $W$  boson and

$$d\Phi_3 = \frac{d^3 p_W}{(2\pi)^3 2p_W^0} \frac{d^3 p_k}{(2\pi)^3 2p_k^0} \frac{d^3 p_\gamma}{(2\pi)^3 2p_\gamma^0} \delta^4(p_a + p_b - p_W - p_k - p_\gamma). \quad (2.18)$$

In the three-particle phase space, the gauge boson  $p_T$ -distribution is defined by the observable function

$$F_{O,3}(\Phi_3) = \delta(p_T - p_{T,W}) \theta(p_{T,j} - p_{T,j}^{\min}). \quad (2.19)$$

The cut on the jet transverse momentum rejects events where the  $W$ -boson  $p_T$  is balanced by an isolated photon plus a parton with small transverse momentum. This observable is thus free from singularities associated with soft and collinear quarks or gluons. When applying the cut on the jet momentum in the three-particle phase space, care must be taken that the definition of the jet  $p_T$  is collinear-safe. For the real photonic corrections the jet cannot be identified with the parton  $k$ , since in presence of collinear photon radiation the transverse momentum of a charged parton is not a collinear-safe quantity. Thus we identify the jet with the parton  $k$  only if  $k$  is a gluon or a quark well separated from the photon. Otherwise, i.e. for collinear quark-photon configurations, the recombined momentum of the quark and photon is taken as momentum of the jet. In practice, we define the separation variable

$$R(q, \gamma) = \sqrt{(\eta_q - \eta_\gamma)^2 + (\phi_q - \phi_\gamma)^2}, \quad (2.20)$$

where  $\eta_i$  is the pseudo-rapidity and  $\phi_i$  is the azimuthal angle of a particle  $i$ . If  $R(q, \gamma) < R_{\text{sep}}$ , then the photon and quark momenta are recombined by simple four-vector addition into an effective momentum  $p_j$  and then  $p_{T,j} = \sqrt{(\vec{p}_{T,q} + \vec{p}_{T,\gamma})^2}$ ,

otherwise  $p_{T,j} = p_{T,q}$ . We note that, in the collinear region, lowest-order kinematics implies  $p_{T,j} = p_{T,q} + p_{T,\gamma} = p_{T,W} > p_{T,j}^{\min}$ . This means that the recombination procedure effectively removes the cut on  $p_{T,q}$  inside the collinear cone  $R(q, \gamma) < R_{\text{sep}}$ . For instance the recombined  $gq' \rightarrow W^\sigma q\gamma$  cross section is given by

$$\hat{\sigma}_{\text{rec.}}^{gq' \rightarrow W^\sigma q\gamma} = \int_{R(q,\gamma) < R_{\text{sep}}} d\hat{\sigma}^{gq' \rightarrow W^\sigma q\gamma} + \int_{R(q,\gamma) > R_{\text{sep}}} \theta(p_{T,q} - p_{T,j}^{\min}) d\hat{\sigma}^{gq' \rightarrow W^\sigma q\gamma}. \quad (2.21)$$

In contrast, for the case of final-state gluons, we do not perform photon-gluon recombination and the cut on  $p_{T,g}$  is imposed in the entire phase space.

This procedure has the advantage to avoid both collinear-photon and soft-gluon singularities. However it implies a different treatment of quark and gluon final states and can thus be regarded as an arbitrary cut-off prescription for the final-state collinear singularity. Moreover, the recombined cross section (2.21) has a logarithmic dependence on the cut-off parameter  $R_{\text{sep}}$ . These aspects are discussed in detail in Appendix B. There we compare the recombination procedure with a realistic experimental definition of exclusive  $pp \rightarrow Wj$  production, where final-state quarks are subject to the same cut as final state gluons ( $p_{T,q} > p_{T,j}^{\min}$ ) within the entire phase space. Describing the exclusive  $gq' \rightarrow W^\sigma q\gamma$  cross section,

$$\hat{\sigma}_{\text{excl.}}^{gq' \rightarrow W^\sigma q\gamma} = \int \theta(p_{T,q} - p_{T,j}^{\min}) d\hat{\sigma}^{gq' \rightarrow W^\sigma q\gamma}, \quad (2.22)$$

by means of quark fragmentation functions, we find that the quantitative difference between the two definitions (2.21) and (2.22) amounts to less than two permille. Moreover, we show that the recombined cross section is extremely stable with respect to variations of the parameter  $R_{\text{sep}}$ . This means that the recombination procedure used in our calculation provides a very good description of exclusive  $pp \rightarrow Wj$  production.

Another treatment of the singularities, which does not require recombination and treats quark- and gluon-induced jets uniformly, has been proposed in Ref. [23]. There, contributions from  $W$ +jet production and  $W + \gamma$  production to a more inclusive observable, i.e. high- $p_T$   $W$  production, are both calculated. All soft and collinear singularities in the final state cancel in the approach of Ref. [23] as a result of the more inclusive observable definition than associated production of the  $W$  boson together with a jet, considered in this work. The comparison of our results with those of Ref. [23] seems to indicate that these differences in the jet definitions have a quite small impact on the size of the electroweak corrections.

## 2.3 Crossing symmetries

In order to minimize the number of matrix elements to be calculated we exploit crossing-symmetry and CP (charge-conjugation and parity transformation) invari-

ance. All  $2 \rightarrow 2$  processes in (2.3) can be related to the unpolarized squared matrix elements

$$\overline{\sum} |\mathcal{M}^{\bar{q}q' \rightarrow Vg}|^2 \quad (2.23)$$

for the process  $\bar{q}q' \rightarrow Vg$ . Crossing-symmetry yields the other contributions with

$$\begin{aligned} \overline{\sum} |\mathcal{M}^{gq' \rightarrow Vq}|^2 &= - \overline{\sum} |\mathcal{M}^{\bar{q}q' \rightarrow Vg}|^2 \Big|_{\hat{s} \leftrightarrow \hat{t}}, \\ \overline{\sum} |\mathcal{M}^{\bar{q}g \rightarrow V\bar{q}'}|^2 &= - \overline{\sum} |\mathcal{M}^{\bar{q}q' \rightarrow Vg}|^2 \Big|_{\hat{s} \leftrightarrow \hat{u}}, \\ \overline{\sum} |\mathcal{M}^{ba \rightarrow Vk}|^2 &= \overline{\sum} |\mathcal{M}^{ab \rightarrow Vk}|^2 \Big|_{\hat{t} \leftrightarrow \hat{u}}. \end{aligned} \quad (2.24)$$

Furthermore, as a result of CP symmetry we have

$$\overline{\sum} |\mathcal{M}^{\bar{q}q' \rightarrow Vg}|^2 = \overline{\sum} |\mathcal{M}^{q\bar{q}' \rightarrow \bar{V}g}|^2, \quad (2.25)$$

where  $\bar{V}$  denotes the charge conjugated gauge boson  $V$ . In particular, Eq. (2.25) relates the unpolarized partonic cross section for the production of positively and negatively charged  $W$  bosons and implies invariance under  $p_a \leftrightarrow p_b$  for the quark induced channels of neutral gauge boson production.

As a result of these symmetries the explicit computation of the unpolarized squared matrix element for the leading order and the virtual corrections needs to be performed only once.

Similarly, for the  $2 \rightarrow 3$  processes (2.5) of the real photonic corrections for  $W$  production we can relate all unpolarized squared matrix elements to the single process  $\bar{q}q' \rightarrow W^\sigma g\gamma$  with

$$\overline{\sum} |\mathcal{M}^{\bar{q}q' \rightarrow W^\sigma g\gamma}|^2. \quad (2.26)$$

Using the crossing-symmetry we have

$$\begin{aligned} \overline{\sum} |\mathcal{M}^{gq' \rightarrow W^\sigma q\gamma}|^2 &= - \overline{\sum} |\mathcal{M}^{\bar{q}q' \rightarrow W^\sigma g\gamma}|^2 \Big|_{\{\hat{s} \leftrightarrow \hat{u}'', \hat{t} \leftrightarrow \hat{s}'', \hat{t}' \leftrightarrow \hat{s}'\}}, \\ \overline{\sum} |\mathcal{M}^{\bar{q}g \rightarrow W^\sigma \bar{q}'\gamma}|^2 &= - \overline{\sum} |\mathcal{M}^{\bar{q}q' \rightarrow W^\sigma g\gamma}|^2 \Big|_{\{\hat{s} \leftrightarrow \hat{t}'', \hat{u} \leftrightarrow \hat{s}'', \hat{u}' \leftrightarrow \hat{s}'\}}, \\ \overline{\sum} |\mathcal{M}^{ba \rightarrow W^\sigma k\gamma}|^2 &= \overline{\sum} |\mathcal{M}^{ab \rightarrow W^\sigma k\gamma}|^2 \Big|_{\{\hat{t} \leftrightarrow \hat{u}, \hat{t}' \leftrightarrow \hat{u}'\}} \end{aligned} \quad (2.27)$$

and CP symmetry implies

$$\overline{\sum} |\mathcal{M}^{\bar{d}u \rightarrow W^+ g\gamma}|^2 = \overline{\sum} |\mathcal{M}^{d\bar{u} \rightarrow W^- g\gamma}|^2. \quad (2.28)$$

It is thus enough to perform calculation of the matrix element only for the  $\bar{q}q' \rightarrow W^\sigma g\gamma$  subprocess.

## 2.4 Couplings

For gauge couplings we adopt the conventions of Ref. [26]. With this notation the  $gq\bar{q}$  vertex and the  $Vq'\bar{q}$  vertices with  $V = \gamma, Z, W^\pm$  read

$$\begin{array}{c} \bar{q} \\ \swarrow \\ \bullet \\ \nwarrow \\ q \end{array} \begin{array}{c} G_a^\mu \\ \text{ooooo} \end{array} = -ig_S t^a \gamma^\mu, \quad \begin{array}{c} \bar{q} \\ \swarrow \\ \bullet \\ \nwarrow \\ q' \end{array} \begin{array}{c} V^\mu \\ \text{~~~~~} \end{array} = ie\gamma^\mu \sum_{\lambda=R,L} \omega_\lambda I_{q_\lambda q'_\lambda}^V, \quad (2.29)$$

where all particles are considered as incoming.  $\omega_\lambda$  are the chiral projectors

$$\omega_R = \frac{1}{2}(1 + \gamma_5), \quad \omega_L = \frac{1}{2}(1 - \gamma_5), \quad (2.30)$$

$t^a$  are the Gell-Mann matrices and  $I^V$  are electroweak coupling matrices in the weak isospin space. For diagonal matrices such as  $I^\gamma$  and  $I^Z$  we write  $I_{q_\lambda q'_\lambda}^V = \delta_{qq'} I_{q_\lambda}^V$ . In terms of the weak isospin  $T_{q_\lambda}^3$  and the weak hypercharge  $Y_{q_\lambda}$  we have

$$I_{q_\lambda}^Z = \frac{c_W}{s_W} T_{q_\lambda}^3 - \frac{s_W}{c_W} \frac{Y_{q_\lambda}}{2}, \quad I_{q_\lambda}^\gamma = -Q_{q_\lambda} = -T_{q_\lambda}^3 - \frac{Y_{q_\lambda}}{2}, \quad (2.31)$$

with the shorthands  $c_W = \cos \theta_W$  and  $s_W = \sin \theta_W$  for the weak mixing angle  $\theta_W$ . The eigenvalues of isospin and hypercharge for quarks are

$$\begin{aligned} T_{u_L}^3 = -T_{d_L}^3 = \frac{1}{2}, \quad T_{u_R}^3 = T_{d_R}^3 = 0, \\ Y_{u_L} = Y_{d_L} = \frac{1}{3}, \quad Y_{u_R} = \frac{4}{3}, \quad Y_{d_R} = -\frac{2}{3}. \end{aligned} \quad (2.32)$$

Concerning  $I^{W^\sigma}$ , the only non-vanishing components of the generators associated with  $W$  bosons are

$$I_{u_L d_L}^{W^+} = I_{d_L u_L}^{W^-} = \frac{1}{\sqrt{2}s_W}. \quad (2.33)$$

Combining the gauge boson couplings to quarks into the electroweak Casimir operator in the fundamental representation, we obtain

$$C_{q'_\lambda q_\lambda}^{\text{ew}} = C_{q_\lambda}^{\text{ew}} = \sum_{\Gamma=\gamma,Z,W^\pm} (I^\Gamma I^{\bar{\Gamma}})_{q'_\lambda q_\lambda} = \frac{1}{c_W^2} \left( \frac{Y_{q_\lambda}}{2} \right)^2 + \frac{1}{s_W^2} C_{F,q_\lambda} \quad (2.34)$$

and similar for the pure  $SU(2)$  Casimir operators

$$C_{F,q_L} = \frac{3}{4}, \quad C_{F,q_R} = 0, \quad C_A = 2 \quad (2.35)$$

in the fundamental (F) and adjoint (A) representation. The electroweak triple gauge-boson vertices read

$$\begin{array}{c} V_a^{\mu_1} \\ \swarrow \\ \bullet \\ \nwarrow \\ V_c^{\mu_3} \end{array} \begin{array}{c} \text{~~~~~} \\ \text{~~~~~} \\ \text{~~~~~} \end{array} \begin{array}{c} V_b^{\mu_2} \\ \swarrow \\ \bullet \\ \nwarrow \\ \end{array} = \frac{e}{s_W} \varepsilon^{V_a V_b V_c} [g^{\mu_1 \mu_2} (k_1 - k_2)^{\mu_3} + g^{\mu_2 \mu_3} (k_2 - k_3)^{\mu_1} \\ + g^{\mu_3 \mu_1} (k_3 - k_1)^{\mu_2}], \quad (2.36)$$

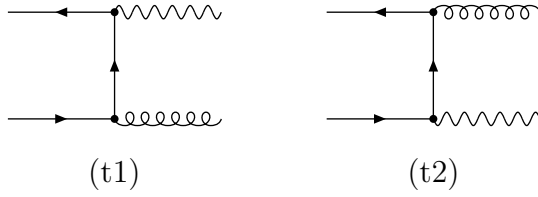


Figure 2.1: Tree-level Feynman diagrams for the process  $\bar{q}q' \rightarrow Vg$ .

where the totally anti-symmetric tensor  $\varepsilon^{V_1 V_2 V_3}$  is defined through the commutation relations

$$[I^{V_1}, I^{V_2}] = \frac{i}{s_w} \sum_{V_3=A,Z,W^\pm} \varepsilon^{V_1 V_2 V_3} I^{V_3}, \quad (2.37)$$

and has components  $\varepsilon^{ZW^+W^-} = -ic_w$  and  $\varepsilon^{AW^+W^-} = is_w$ .

## 2.5 Leading order contribution

To lowest order in  $\alpha$  and  $\alpha_S$ , the matrix element for the process  $\bar{q}q' \rightarrow Vg$  is given by two Feynman diagrams as shown in Fig. 2.1. The resulting unpolarized squared matrix element reads

$$\overline{|\mathcal{M}_0^{\bar{q}q' \rightarrow Vg}|^2} = 8\pi^2 \alpha \alpha_S (N_c^2 - 1) \sum_{\lambda=L,R} \left( I_{q_\lambda q'_\lambda}^{\bar{V}} \right)^2 \frac{\hat{t}^2 + \hat{u}^2 + 2p_V^2 \hat{s}}{\hat{t}\hat{u}}, \quad (2.38)$$

where  $\alpha = e^2/(4\pi)$  and  $\alpha_S = g_S^2/(4\pi)$  are the electromagnetic and the strong coupling constants.

In the following, numerical results for the leading order (LO) cross section shall be presented first. For a detailed discussion of the input parameter we refer to Appendix A. The unpolarized transverse-momentum distributions for  $pp \rightarrow \gamma j$  and  $pp \rightarrow Zj$  at the LHC are shown in Fig. 2.2a (thick curves). The corresponding results for the processes  $pp \rightarrow W^+ j$  and  $pp \rightarrow W^- j$  are shown in Fig. 2.2b. At the LHC the production rates for positively and negatively charged  $W$  bosons are different as the quark and antiquark densities in the  $pp$  initial state differ. In the range  $100 \text{ GeV} \leq p_T \leq 2 \text{ TeV}$  the cross section for all four gauge bosons falls off by about seven orders of magnitude. Considering the total cross section

$$\sigma_{\text{tot}}(p_T^{\text{cut}}) = \int_{p_T^{\text{cut}}}^{\infty} dp_T \frac{d\sigma_{\text{LO}}^{pp \rightarrow Vj}}{dp_T} \quad (2.39)$$

for contributions with  $p_T \geq p_T^{\text{cut}}$  we still find  $\sigma_{\text{tot}}(1 \text{ TeV}) \approx \mathcal{O}(10 \text{ fb})$  for all gauge bosons. For example, this corresponds to about 700  $Z$  bosons per year with  $p_T \geq$



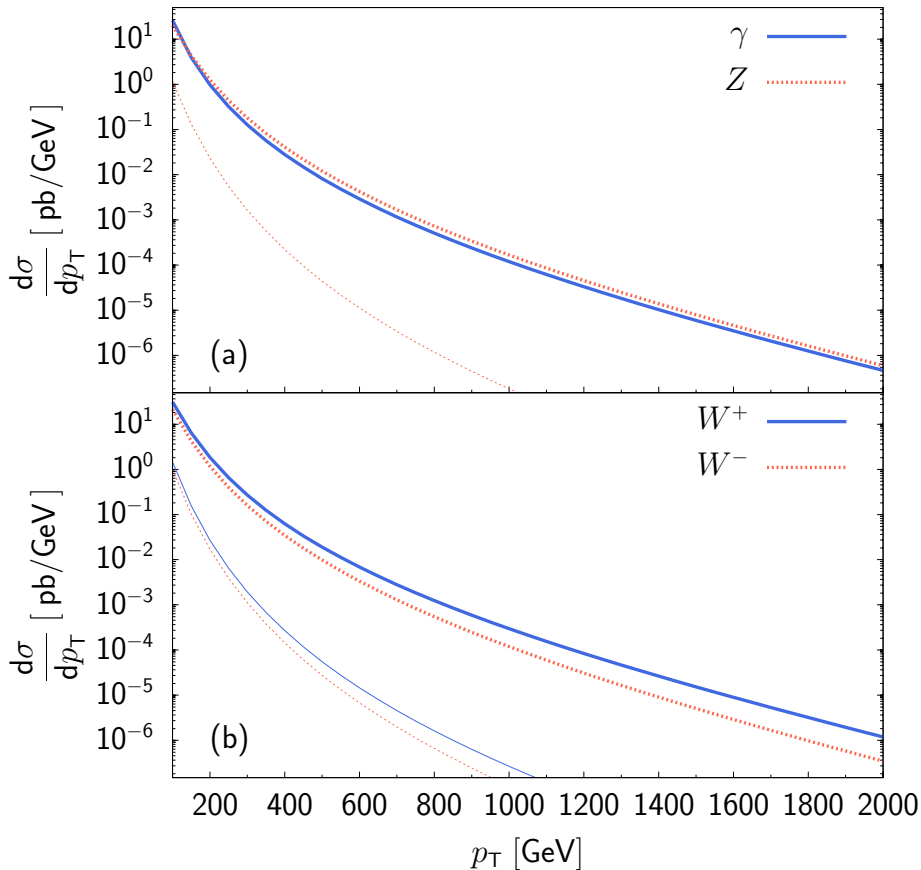


Figure 2.2: Transverse-momentum distribution for gauge boson production at the LHC. Thick lines describe the unpolarized cross section. Thin lines correspond to the contribution of a longitudinal polarized gauge boson. (a) LO distribution for  $pp \rightarrow \gamma j$  (solid) and  $pp \rightarrow Z j$  (dotted), (b) LO distribution for  $pp \rightarrow W^+ j$  (solid) and  $pp \rightarrow W^- j$  (dotted).

1 TeV, assuming a luminosity of  $10^{34} \text{ cm}^{-2} \text{ s}^{-1}$  [27] and leptonic  $Z$  decays with  $\text{BR}(Z \rightarrow l^+ l^-) = 9.9\%$ . Thin lines in Fig. 2.2a and Fig. 2.2b. correspond to the LO transverse-momentum distribution for  $Z$  and  $W$  bosons with longitudinal polarization only. These contributions are suppressed by several orders of magnitude wrt. the unpolarized  $p_T$ -distribution. Furthermore, in Fig. 2.3a-d we show the different partonic contributions to the production of photons,  $Z$  and  $W^\pm$  bosons, respectively. Plotted is the relative size of the contributions from the quark-gluon, antiquark-gluon and antiquark-quark initial states wrt. the total contribution at the LHC. For all four processes the quark-gluon channel constantly dominates with at least 60% of the total rate. The initial states involving an antiquark account for the remaining contribution. At high energies the antiquark-quark induced process dominates these contributions with at least 20% for all four gauge bosons, while the antiquark-gluon channel becomes less relevant.

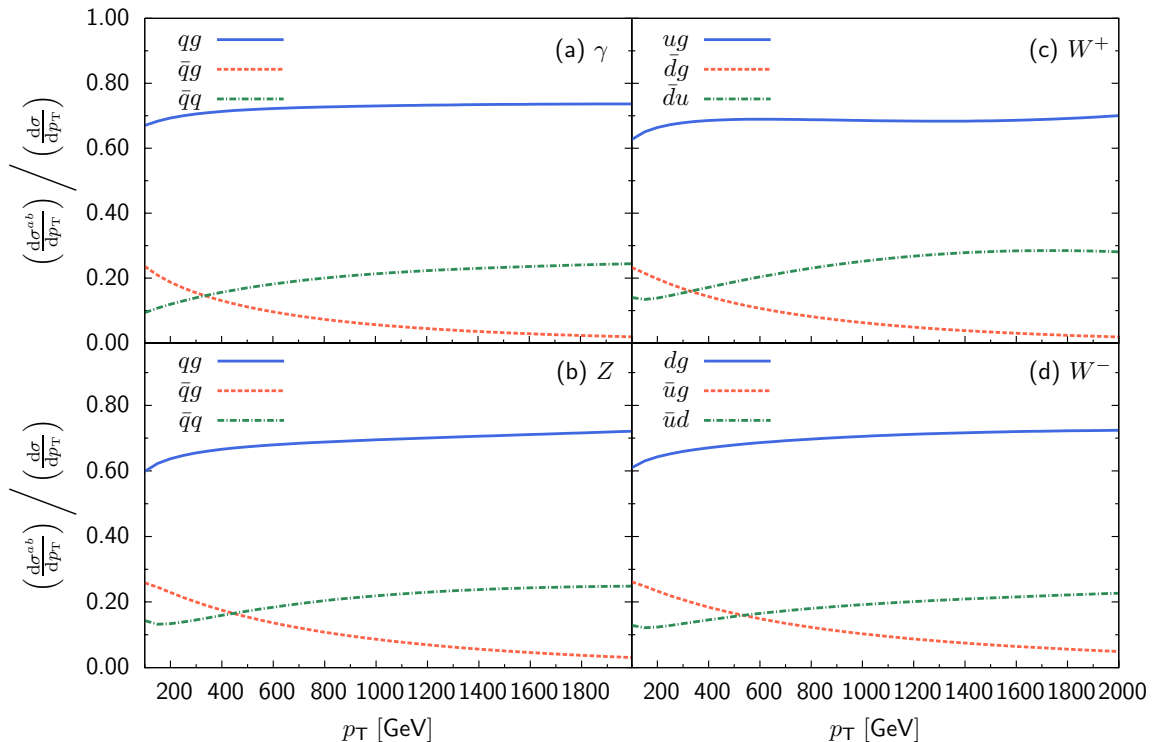


Figure 2.3: Relative size of contributions from different partonic channels wrt. the transverse-momentum distribution for gauge bosons at the LHC. The classification is according to quark-gluon (solid), antiquark-gluon (dotted) and quark-antiquark (dash-dotted) initial states. (a)-(d) shows the dependence for the production of  $\gamma$ ,  $Z$ ,  $W^+$ ,  $W^-$  bosons, respectively.

At the Tevatron the unpolarized LO transverse-momentum distributions for all gauge bosons fall off by about five order of magnitude in the range of  $50 \text{ GeV} \leq p_T \leq 400 \text{ GeV}$ , as shown in Fig. 2.4 (thick curves). Again, we find similar rates for photon and  $Z$  boson production in Fig. 2.4a and for  $W$  boson production in Fig. 2.4b. Due to the CP-symmetric hadronic initial state at the Tevatron the cross sections for  $W^+$  and  $W^-$  bosons are equal. The  $p_T$ -distribution of the purely longitudinal polarized  $Z$  and  $W$  bosons is depicted by thin lines. These contributions are suppressed by about one order of magnitude at low  $p_T$  and decrease further to almost two order of magnitude at  $p_T = 400 \text{ GeV}$  wrt. to the unpolarized cross section.

The partonic contributions to the cross section at the Tevatron are shown in Fig. 2.5a-c for photons,  $Z$  and  $W$  bosons, respectively. At higher energies the purely quark induced channels  $\bar{q}q$  dominate the cross section. More precisely, in the range  $200 \text{ GeV} \leq p_T \leq 400 \text{ GeV}$  these processes contribute with 70-90% for photon and  $Z$  production and 60-85% for  $W$  production wrt. the total rate. Partonic channels involving a gluon in association with a quark or antiquark in the initial state become

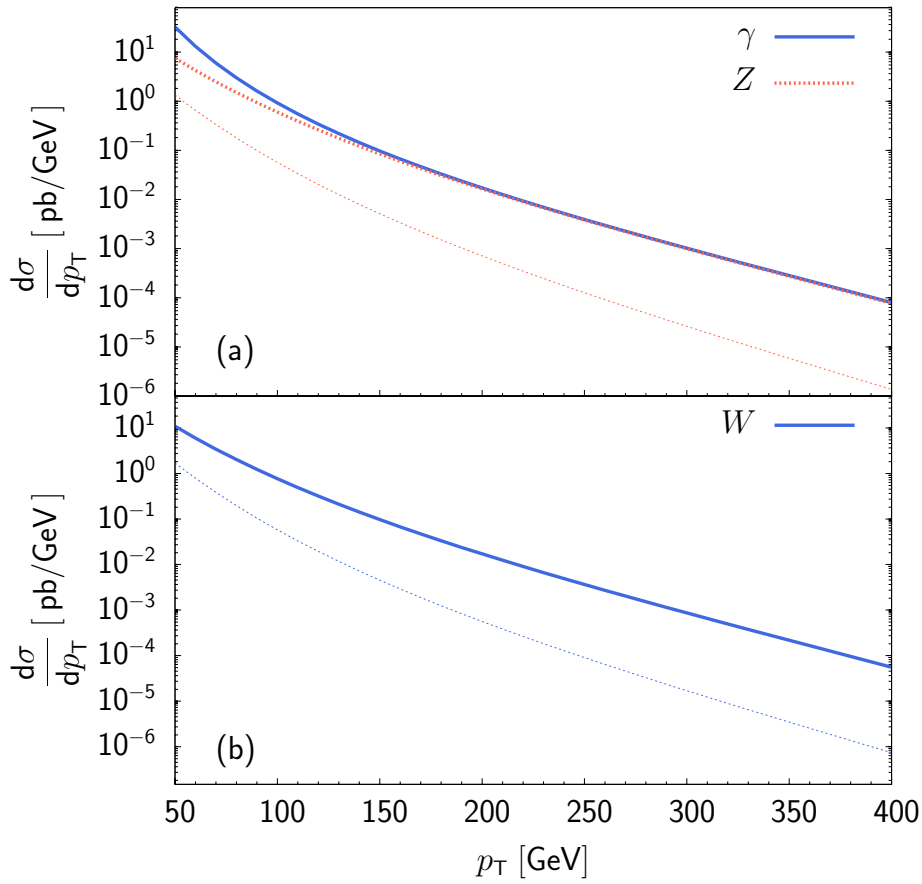


Figure 2.4: Transverse-momentum distribution for gauge boson production at the Tevatron. Thick lines describe the unpolarized cross section. Thin lines correspond to the contribution of a longitudinal polarized gauge boson. (a) LO distribution for  $p\bar{p} \rightarrow \gamma j$  (solid) and  $p\bar{p} \rightarrow Z j$  (dotted), (b) LO distribution for  $p\bar{p} \rightarrow W^\pm j$  (solid).

more important at  $p_T \leq 150 \text{ GeV}$ . For photon production these channels even exceed the contribution from  $\bar{q}q$  channels, while for  $Z$  and  $W$  production they are of comparable size.

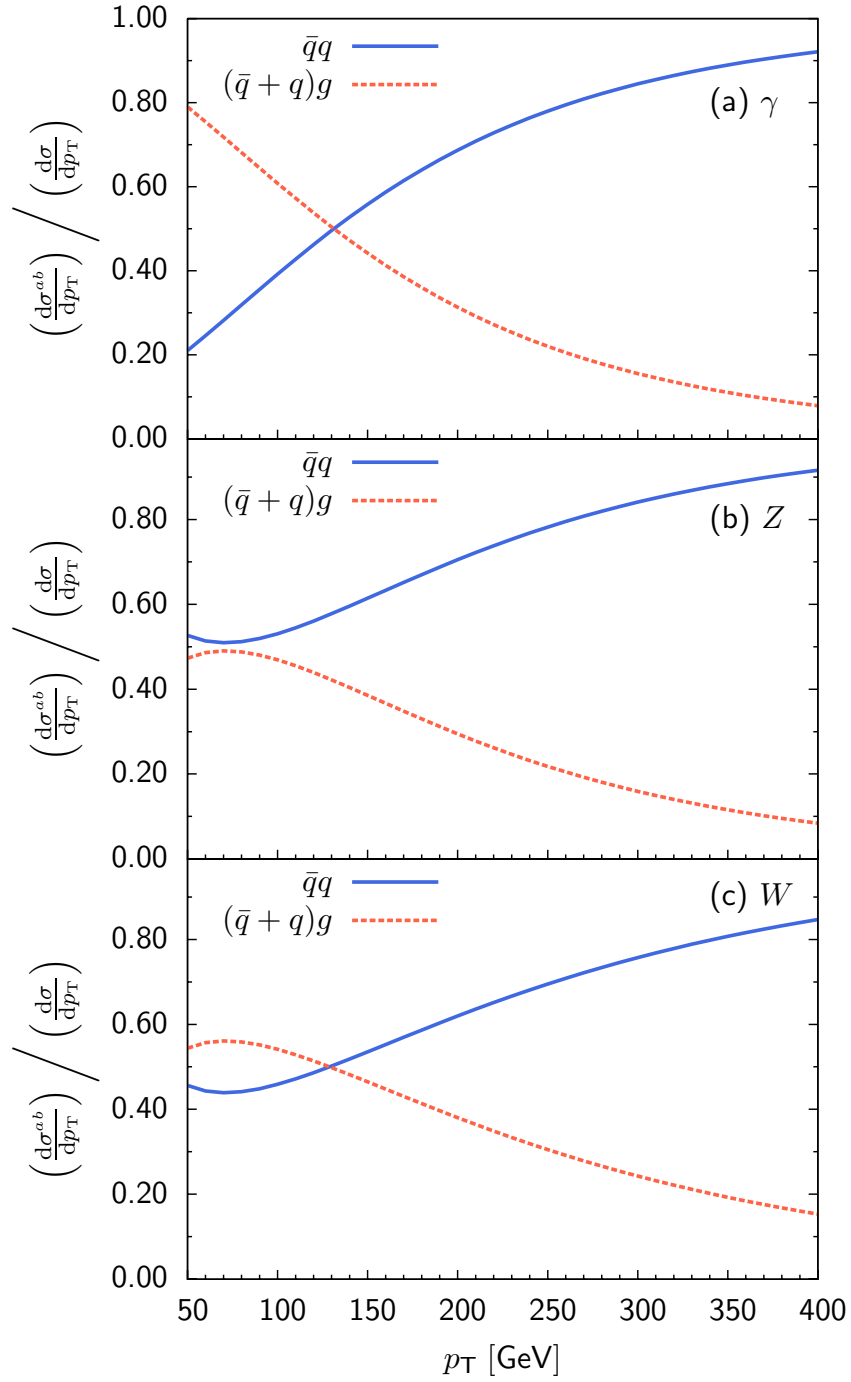


Figure 2.5: Relative size of contributions from different partonic channels wrt. the transverse-momentum distribution for gauge bosons at the Tevatron. The classification is according to quark-antiquark (solid) initial states and gluon induced initial states with quarks and antiquarks. (a)-(c) shows the dependence for the production of  $\gamma$ ,  $Z$ ,  $W^\pm$  bosons, respectively.

# Chapter 3

## Electroweak one-loop corrections

In this chapter we present the electroweak one-loop corrections to the process  $\bar{q}q' \rightarrow Vg$ , where  $V$  represents an electroweak gauge boson. In the case of photon and  $Z$  boson production we consider the purely weak one-loop corrections. These contributions constitute the dominating part of the electroweak one-loop corrections and can be split off from photonic loop corrections in a gauge invariant manner. For  $W$  boson production this is not possible. Thus, for the process  $\bar{q}q' \rightarrow Wg$  we also include photonic corrections at one-loop level. Where possible, we present the results in generic form denoting the external gauge boson by  $V$ . Otherwise, we specify the gauge boson under consideration explicitly. In Sect. 3.1 we introduce our notation and specify the relevant Feynman diagrams for the one-loop calculations. The algebraic reduction to gauge-coupling structures, standard matrix elements and one-loop scalar integrals is described in Sect. 3.2. The renormalization of ultraviolet divergencies is discussed in Sect. 3.3. The subtraction of infrared singularities originating from soft and collinear virtual photons in the case of  $W$ +jet production is presented in Sect. 3.4. These singularities cancel with the corresponding ones from the real corrections (cf. Ch. 5). In Sect. 3.5 we summarize the one-loop results for the unpolarized squared matrix element.

### 3.1 Preliminaries

As discussed in Sect. 2.3, the different partonic processes relevant for gauge boson production at large transverse momenta are related by CP and crossing symmetries. It is thus sufficient to consider only one of these processes. In the following we derive the one-loop corrections for the quark-antiquark induced process  $\bar{q}q' \rightarrow Vg$ . The corresponding one-loop matrix element

$$\mathcal{M}_1^{\bar{q}q' \rightarrow Vg} = \mathcal{M}_0^{\bar{q}q' \rightarrow Vg} + \delta\mathcal{M}_1^{\bar{q}q' \rightarrow Vg} \quad (3.1)$$

is expressed as a function of the Mandelstam invariants

$$\hat{s} = (p_{\bar{q}} + p_{q'})^2, \quad \hat{t} = (p_{\bar{q}} - p_V)^2, \quad \hat{u} = (p_{q'} - p_V)^2 \quad (3.2)$$

and the squared masses  $p_V^2$  and  $M_\Gamma^2$  of the external gauge boson  $V$  and gauge bosons  $\Gamma = \gamma, Z, W^\pm$  from loops, respectively. The Born contribution  $\mathcal{M}_0^{\bar{q}q' \rightarrow Vg}$  results from the  $t$ - and  $u$ -channel diagrams of Fig. 2.1. The loop and counterterm diagrams contributing to the correction

$$\delta\mathcal{M}_1^{\bar{q}q' \rightarrow Vg} = \delta\mathcal{M}_{1,\text{loop}}^{\bar{q}q' \rightarrow Vg} + \delta\mathcal{M}_{1,\text{CT}}^{\bar{q}q' \rightarrow Vg}, \quad (3.3)$$

are depicted in Fig. 3.1 and Fig. 3.2, respectively<sup>1</sup>.

The quarks that are present in the loop diagrams of Fig. 3.1 are treated as massless, and the regularization of the collinear singularities that arise in this limit is discussed in Sect. 3.4 for the process  $\bar{q}q' \rightarrow W^\sigma g$ . The only quark-mass effects that we take into account are contributions from bottom and top quarks that enter the counterterms through gauge-boson self-energies.

Our calculation has been performed at the amplitude level and provides full control over polarization effects. However, in this work we concentrate on the unpolarized squared matrix element and present results for this quantity.

## 3.2 Algebraic reduction

The matrix element (3.1) has the general form

$$\mathcal{M}_1^{\bar{q}q' \rightarrow Vg} = ie g_S t^a \sum_{\lambda=R,L} \bar{v}(p_{\bar{q}}) \mathcal{M}_{1,V}^{\lambda,\mu\nu} \omega_\lambda u(p_{q'}) \varepsilon_\mu^*(p_V) \varepsilon_\nu^*(p_g). \quad (3.4)$$

Since we neglect quark masses in the one-loop diagrams,  $\mathcal{M}_{1,V}^{\lambda,\mu\nu}$  consists of terms involving an odd number of matrices  $\gamma^\rho$  with  $\rho = 0, \dots, 3$ . The  $\gamma^5$ -terms are isolated in the chiral projectors  $\omega_\lambda$  defined in (2.30). The polarization dependence of the quark spinors and gauge-boson polarization vectors is implicitly understood. In analogy to (3.1) and (3.3) we write

$$\mathcal{M}_{1,V}^{\lambda,\mu\nu} = \mathcal{M}_{0,V}^{\lambda,\mu\nu} + \delta\mathcal{M}_{1,V}^{\lambda,\mu\nu}, \quad \delta\mathcal{M}_{1,V}^{\lambda,\mu\nu} = \delta\mathcal{M}_{1,\text{loop}}^{\lambda,\mu\nu} + \delta\mathcal{M}_{1,\text{CT}}^{\lambda,\mu\nu}. \quad (3.5)$$

We isolate the  $\text{SU}(2) \times \text{U}(1)$  couplings that appear in the Feynman diagrams and reduce the one-loop amplitude to a sum of contributions associated with independent coupling structures. The coupling structure of the Born amplitude is trivial and consists simply of the  $q_L q_L'$  component of the gauge group generator  $I^{\bar{V}}$ ,

$$\mathcal{M}_{0,V}^{\lambda,\mu\nu} = I_{q_\lambda q'_\lambda}^{\bar{V}} \mathcal{S}_0^{\mu\nu}, \quad \mathcal{S}_0^{\mu\nu} = \frac{\gamma^\mu (\not{p}_q - \not{p}_g) \gamma^\nu}{\hat{t}} + \frac{\gamma^\nu (\not{p}_g - \not{p}_q) \gamma^\mu}{\hat{u}}. \quad (3.6)$$

The contribution of the loop diagrams in Fig. 3.1 can be written in the generic form

---

<sup>1</sup>We note that, in addition to the contributions depicted in Fig. 3.1, there is a fermion triangle diagram, which is coupled to two electroweak gauge bosons and the gluon. Owing to the fact that the Gell-Mann matrices are traceless, i.e.  $\text{Tr}[t^a] = 0$ , these contributions vanish at the amplitude level.

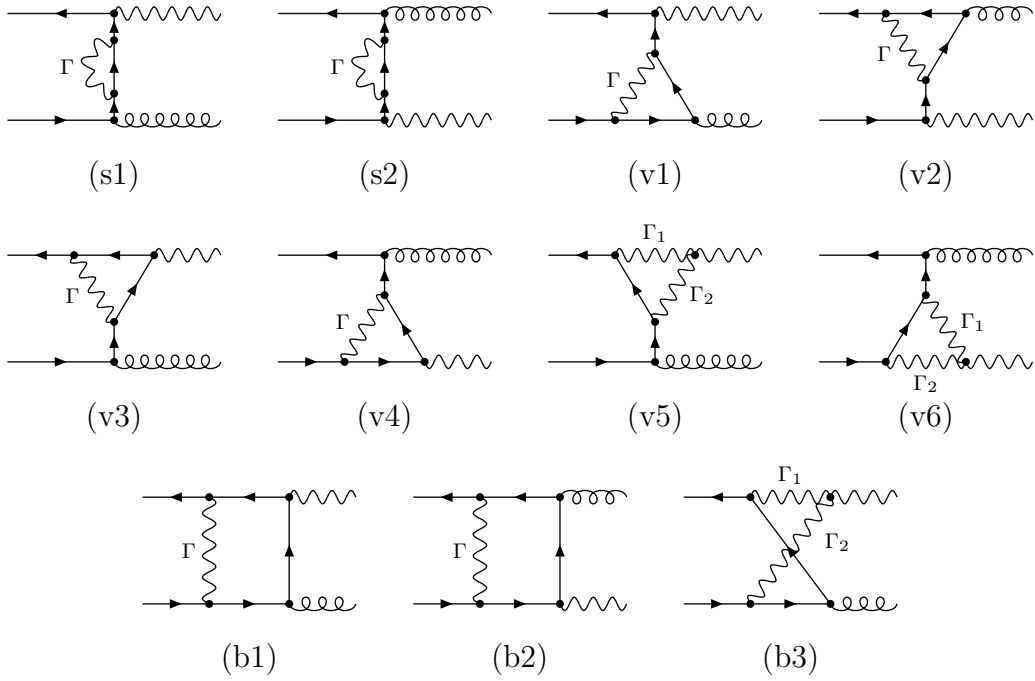


Figure 3.1: One-loop Feynman diagrams for the process  $\bar{q}q' \rightarrow Vg$ .

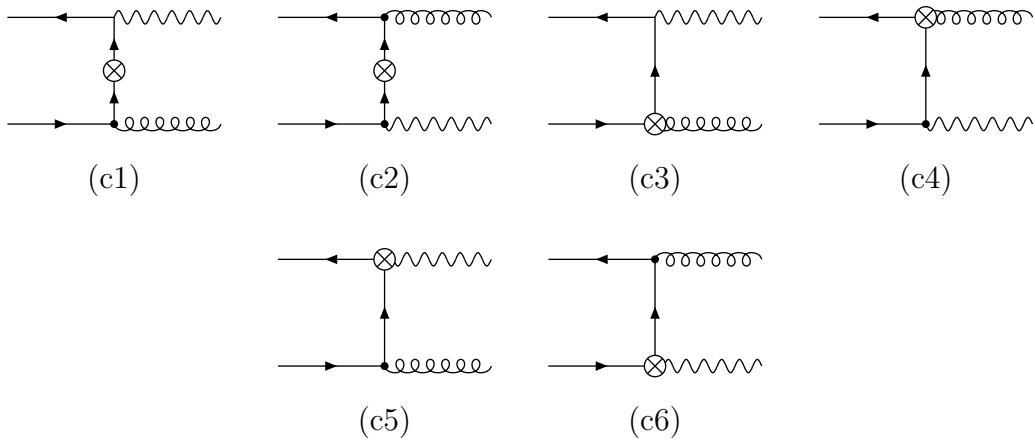


Figure 3.2: Counterterm diagrams for the process  $\bar{q}q' \rightarrow Vg$ .

$$\begin{aligned}
\delta\mathcal{M}_{1,\text{loop}}^{\lambda,\mu\nu} = \frac{\alpha}{4\pi} \left\{ \sum_{\Gamma \in K_{12}(V)} \left[ (I^{\bar{V}} I^{\Gamma} I^{\bar{\Gamma}})_{q_{\lambda} q'_{\lambda}} D_1^{\mu\nu}(M_{\Gamma}^2) + (I^{\Gamma} I^{\bar{\Gamma}} I^{\bar{V}})_{q_{\lambda} q'_{\lambda}} D_2^{\mu\nu}(M_{\Gamma}^2) \right] \right. \\
+ \sum_{\Gamma \in K_3(V)} \left[ (I^{\Gamma} I^{\bar{V}} I^{\bar{\Gamma}})_{q_{\lambda} q'_{\lambda}} D_3^{\mu\nu}(M_{\Gamma}^2) \right] \\
\left. + \sum_{\Gamma, \Gamma' \in K_4(V)} \left[ \frac{i}{s_w} \varepsilon^{\Gamma' V \Gamma} (I^{\Gamma} I^{\Gamma'})_{q_{\lambda} q'_{\lambda}} D_4^{\mu\nu}(M_{\Gamma}^2, M_{\Gamma'}^2) \right] \right\}. \quad (3.7)
\end{aligned}$$

The tensors  $D_1^{\mu\nu}(M_{\Gamma}^2)$  and  $D_2^{\mu\nu}(M_{\Gamma}^2)$  describe the contributions of the diagrams s1, v1 and s2, v2, respectively.  $D_3^{\mu\nu}(M_{\Gamma}^2)$  corresponds to the diagrams v3, v4, b1, b2 and  $D_4^{\mu\nu}(M_{\Gamma}^2, M_{\Gamma'}^2)$  represents the diagrams v5, v6 and b3. The classes of insertions of virtual gauge bosons  $\Gamma$  in the loops depend on the process under consideration. They will be specified by the sets  $K_{12}(V)$ ,  $K_3(V)$  and  $K_4(V)$  in the following subsections for neutral and charged gauge boson production separately. Each of these sets is a subset of the electroweak gauge bosons  $\gamma$ ,  $Z$ ,  $W^{\pm}$ . Furthermore, we will give explicit expressions for the coupling matrices.

### 3.2.1 Couplings for neutral gauge boson production

For the production of neutral gauge bosons ( $V = \gamma, Z$ ) we restrict ourselves to the calculation of weak corrections, i.e. no virtual photons are considered. This is possible as the QED corrections form a gauge independent subset and can consistently be omitted. The diagrams v5, v6 and b3, which contribute to the tensor  $D_4^{\mu\nu}$ , involve only virtual  $W$  bosons whereas the other diagrams receive contributions from virtual  $Z$  and  $W$  bosons. Thus, the sums in (3.7) are defined by the sets

$$\begin{aligned}
K_{12}(\gamma) = K_{12}(Z) &= \{Z, W^+, W^-\}, \\
K_3(\gamma) = K_3(Z) &= \{Z, W^+, W^-\}, \\
K_4(\gamma) = K_4(Z) &= \{W^+, W^-\}. \quad (3.8)
\end{aligned}$$

The electroweak gauge couplings in (3.7) have to be treated as matrices in the weak isospin space. As  $[I^Z, I^{\gamma}] = 0$ , the diagrams involving virtual  $Z$  bosons ( $\Gamma = Z$ ) are simply proportional to  $(I^Z)^2 I^V$ . Instead, the diagrams with virtual  $W$  bosons ( $\Gamma = W^{\pm}$ ) yield combinations of non-commuting gauge-group generators and triple gauge-boson couplings  $\varepsilon^{W^{\pm} W^{\mp} V}$ . These structures in (3.7) can be simplified by using the commutator relation (2.37) according to

$$\begin{aligned}
\sum_{\sigma=\pm} I^V I^{W^{\sigma}} I^{W^{-\sigma}} &= \sum_{\sigma=\pm} I^{W^{\sigma}} I^{W^{-\sigma}} I^V && \text{(corresp. to } D_1^{\mu\nu}, D_2^{\mu\nu}), \\
\sum_{\sigma=\pm} I^{W^{\sigma}} I^V I^{W^{-\sigma}} &= \sum_{\sigma=\pm} I^V I^{W^{\sigma}} I^{W^{-\sigma}} - \frac{U_{VW^3}}{s_w^3} T^3 && \text{(corresp. to } D_3^{\mu\nu}), \\
\sum_{\sigma=\pm} \frac{i}{s_w} \varepsilon^{W^{\sigma} W^{-\sigma} V} I^{W^{\sigma}} I^{W^{-\sigma}} &= \frac{U_{VW^3}}{s_w^3} T^3 && \text{(corresp. to } D_4^{\mu\nu}), \quad (3.9)
\end{aligned}$$



where

$$U_{\gamma W^3} = -s_w, \quad U_{ZW^3} = c_w \quad (3.10)$$

are components of the Weinberg mixing matrix  $U$ . Now, it is possible to define new tensors by

$$\delta\mathcal{A}_{1,A}^{\mu\nu}(M_\Gamma^2) = D_1^{\mu\nu}(M_\Gamma^2) + D_2^{\mu\nu}(M_\Gamma^2) + D_3^{\mu\nu}(M_\Gamma^2), \quad (3.11)$$

$$\delta\mathcal{A}_{1,N}^{\mu\nu}(M_W^2) = D_4^{\mu\nu}(M_W^2, M_W^2) - D_3^{\mu\nu}(M_W^2), \quad (3.12)$$

so that the one-loop amplitude (3.7) for neutral gauge boson production can be expressed in terms of two independent coupling structures according to

$$\delta\mathcal{M}_{1,\text{loop}}^{\lambda,\mu\nu} = \frac{\alpha}{4\pi} \left\{ I_{q_\lambda}^V \sum_{\Gamma=Z,W^\pm} (I^\Gamma I^{\bar{\Gamma}})_{q_\lambda} \delta\mathcal{A}_{1,A}^{\mu\nu}(M_\Gamma^2) + \frac{U_{VW^3}}{s_w^3} T_{q_\lambda}^3 \delta\mathcal{A}_{1,N}^{\mu\nu}(M_W^2) \right\}. \quad (3.13)$$

The labels (A) and (N) denote the Abelian and non-Abelian contributions, respectively, since the latter originates from the non-commutativity of weak interactions, whereas the former is present also in Abelian theories. The sum in (3.13) involving the product of gauge couplings can explicitly be evaluated with

$$(I^Z I^Z)_{q_\lambda} = (I_{q_\lambda}^Z)^2, \quad \sum_{\Gamma=W^\pm} (I^\Gamma I^{\bar{\Gamma}})_{q_\lambda} = \frac{\delta_{\lambda L}}{2s_w^2}. \quad (3.14)$$

### 3.2.2 Couplings for charged gauge boson production

In the case of charged gauge boson production ( $V = W^\sigma$  and  $\sigma = \pm$ ) the purely weak corrections cannot be separated in a gauge-invariant manner. We thus consider the full electroweak corrections for this process. The diagrams s1, s2, v1 and v2 receive contributions from neutral and charged gauge bosons whereas the diagrams v3, v4, b1 and b2 involve only neutral gauge bosons. The remaining diagrams, v5, v6 and b3 involve two contributions with one charged and one neutral gauge boson. Hence, the sums in (3.7) for this process are defined by the sets

$$\begin{aligned} K_{12}(W^\sigma) &= \{\gamma, Z, W^+, W^-\}, \\ K_3(W^\sigma) &= \{\gamma, Z\}, \\ K_4(W^\sigma) &= \{\gamma, Z, W^{-\sigma}\}. \end{aligned} \quad (3.15)$$

The tensors  $D_1^{\mu\nu}(M_\Gamma^2)$  and  $D_2^{\mu\nu}(M_\Gamma^2)$  in (3.7) correspond to the contributions of the diagrams s1, v1 and s2, v2, respectively. In the case of charged gauge bosons ( $\Gamma = W^\pm$ ) in these loop diagrams, the corresponding couplings read

$$\sum_{\rho=\pm} I^{W^{-\sigma}} I^{W^\rho} I^{W^{-\rho}} = \sum_{\rho=\pm} I^{W^\rho} I^{W^{-\rho}} I^{W^{-\sigma}} = \frac{C_F - (T^3)^2}{s_w^2} I^{W^{-\sigma}}. \quad (3.16)$$

For  $\Gamma = \gamma, Z$  the coupling factors read

$$\begin{aligned} I^{W^{-\sigma}} I^\Gamma I^\Gamma &= \left[ \delta_{\Gamma\Gamma}^{\text{SU}(2)} \frac{(T^3)^2}{s_W^2} + X_\Gamma T^3 Y + \delta_{\Gamma\Gamma}^{\text{U}(1)} \frac{Y^2}{4c_W^2} \right] I^{W^{-\sigma}}, \\ I^\Gamma I^\Gamma I^{W^{-\sigma}} &= \left[ \delta_{\Gamma\Gamma}^{\text{SU}(2)} \frac{(T^3)^2}{s_W^2} - X_\Gamma T^3 Y + \delta_{\Gamma\Gamma}^{\text{U}(1)} \frac{Y^2}{4c_W^2} \right] I^{W^{-\sigma}}. \end{aligned} \quad (3.17)$$

Here, we used the abbreviations

$$\delta_{\Gamma\Gamma}^{\text{SU}(2)} = (U_{\Gamma W^3})^2, \quad X_\Gamma = \frac{U_{\Gamma W^3} U_{\Gamma B}}{s_W c_W}, \quad \delta_{\Gamma\Gamma}^{\text{U}(1)} = (U_{\Gamma B})^2, \quad (3.18)$$

where the relevant components of the electroweak mixing matrix  $U$  are given in (3.10). For  $\Gamma = \gamma, Z$  we have  $\delta_{\gamma\gamma}^{\text{SU}(2)} = s_W^2$ ,  $X_A = -1$ ,  $\delta_{\gamma\gamma}^{\text{U}(1)} = c_W^2$ , and  $\delta_{ZZ}^{\text{SU}(2)} = c_W^2$ ,  $X_Z = 1$ ,  $\delta_{ZZ}^{\text{U}(1)} = s_W^2$ . Furthermore, we note that

$$\sum_{\Gamma=\gamma,Z} \delta_{\Gamma\Gamma}^{\text{SU}(2)} = \sum_{\Gamma=\gamma,Z} \delta_{\Gamma\Gamma}^{\text{U}(1)} = 1, \quad \sum_{\Gamma=\gamma,Z} X_\Gamma = 0. \quad (3.19)$$

The tensor  $D_3^{\mu\nu}(M_\Gamma^2)$  in (3.7) corresponds to the diagrams v3, v4, b1 and b2. These diagrams receive contributions from neutral gauge bosons ( $\Gamma = \gamma, Z$ ) only. For the corresponding couplings we have

$$I^\Gamma I^{W^{-\sigma}} I^\Gamma = \left[ \delta_{\Gamma\Gamma}^{\text{SU}(2)} \frac{C_F - C_A/2}{s_W^2} + \delta_{\Gamma\Gamma}^{\text{U}(1)} \frac{Y^2}{4c_W^2} \right] I^{W^{-\sigma}}. \quad (3.20)$$

Finally,  $D_4^{\mu\nu}(M_\Gamma^2, M_W^2)$  represents the diagrams v5, v6 and b3. These diagrams involve a neutral gauge boson and a  $W$  boson. The coupling factors yield

$$\begin{aligned} \frac{i}{s_W} \varepsilon^{W^{-\sigma} W^\sigma \Gamma} I^\Gamma I^{W^{-\sigma}} &= \left[ \delta_{\Gamma\Gamma}^{\text{SU}(2)} \frac{C_A}{4s_W^2} - X_\Gamma T^3 Y \right] I^{W^{-\sigma}}, \\ \frac{i}{s_W} \varepsilon^{\Gamma W^\sigma W^{-\sigma}} I^{W^{-\sigma}} I^\Gamma &= \left[ \delta_{\Gamma\Gamma}^{\text{SU}(2)} \frac{C_A}{4s_W^2} + X_\Gamma T^3 Y \right] I^{W^{-\sigma}}, \end{aligned} \quad (3.21)$$

where  $\Gamma$  can be either  $\gamma$  or  $Z$ . Using the above identities it is possible to express the one-loop amplitude (3.7) for  $W$ -boson production in a form that is analogous to (3.13) for the production of neutral gauge bosons. To this end we define

$$\begin{aligned} \delta\mathcal{A}_{1,A}^{\mu\nu}(M_\Gamma^2) &= D_1^{\mu\nu}(M_\Gamma^2) + D_2^{\mu\nu}(M_\Gamma^2) + D_3^{\mu\nu}(M_\Gamma^2), \\ \delta\mathcal{A}_{1,N}^{\mu\nu}(M_\Gamma^2) &= \frac{1}{2} \left[ D_4^{\mu\nu}(M_\Gamma^2, M_W^2) + D_4^{\mu\nu}(M_W^2, M_\Gamma^2) \right] - D_3^{\mu\nu}(M_\Gamma^2), \\ \delta\mathcal{A}_{1,X}^{\mu\nu}(M_\Gamma^2) &= D_1^{\mu\nu}(M_\Gamma^2) + D_2^{\mu\nu}(M_\Gamma^2), \\ \delta\mathcal{A}_{1,Y}^{\mu\nu}(M_\Gamma^2) &= D_4^{\mu\nu}(M_\Gamma^2, M_W^2) - D_4^{\mu\nu}(M_W^2, M_\Gamma^2) + D_2^{\mu\nu}(M_\Gamma^2) - D_1^{\mu\nu}(M_\Gamma^2). \end{aligned} \quad (3.22)$$

The tensor  $\delta\mathcal{A}_{1,A}^{\mu\nu}(M_\Gamma^2)$  is identical to the Abelian tensor defined in (3.11), and  $\delta\mathcal{A}_{1,N}^{\mu\nu}(M_\Gamma^2)$  is equal to the non-Abelian tensor in (3.12) for  $M_\Gamma^2 = M_W^2$ . The remaining two tensors,  $\delta\mathcal{A}_{1,X}^{\mu\nu}(M_\Gamma^2)$  and  $\delta\mathcal{A}_{1,Y}^{\mu\nu}(M_\Gamma^2)$ , are new contributions. Using

(3.16)–(3.22) we can write the one-loop amplitude (3.7) for  $W$ -boson production as

$$\begin{aligned} \delta\mathcal{M}_{1,\text{loop}}^{L,\mu\nu} = & \frac{\alpha}{4\pi\sqrt{2}s_w} \left\{ \sum_{\Gamma=\gamma,Z} \left[ \left( \delta_{\Gamma}^{\text{SU}(2)} \frac{C_F}{s_w^2} + \delta_{\Gamma}^{\text{U}(1)} \frac{Y_{q_L}^2}{4c_w^2} \right) \delta\mathcal{A}_{1,A}^{\mu\nu}(M_\Gamma^2) \right. \right. \\ & + \delta_{\Gamma}^{\text{SU}(2)} \frac{C_A}{2s_w^2} \delta\mathcal{A}_{1,N}^{\mu\nu}(M_\Gamma^2) - \delta_{\Gamma}^{\text{SU}(2)} \frac{C_F - (T_{q_L}^3)^2}{s_w^2} \delta\mathcal{A}_{1,X}^{\mu\nu}(M_\Gamma^2) \\ & \left. \left. - X_\Gamma T_{q_L}^3 Y_{q_L} \delta\mathcal{A}_{1,Y}^{\mu\nu}(M_\Gamma^2) \right] + \frac{C_F - (T_{q_L}^3)^2}{s_w^2} \delta\mathcal{A}_{1,X}^{\mu\nu}(M_W^2) \right\}. \end{aligned} \quad (3.23)$$

### 3.2.3 Standard matrix elements and scalar integrals

The tensors  $\delta\mathcal{A}_{1,I}^{\mu\nu}(M_\Gamma^2)$  with  $I = A, N$  for neutral gauge boson production and  $I = A, N, X, Y$  for  $W$  boson production contain the kinematical information of the loop corrections. The spinor structure of these tensors has been simplified and isolated into a set of standard matrix elements. The tensor loop integrals have been reduced to scalar ones by means of the Passarino-Veltman technique [28]. Thus, we can express the result in the form<sup>2</sup>

$$\delta\mathcal{A}_{1,I}^{\mu\nu}(M_\Gamma^2) = \sum_{i=1}^{10} \sum_j \mathcal{F}_I^{ij}(M_\Gamma^2) \mathcal{S}_i^{\mu\nu} J_j(M_\Gamma^2), \quad (3.24)$$

for  $I=A,N,X,Y$ . The quantities  $\mathcal{F}_I^{ij}(M_\Gamma^2)$  are rational functions of Mandelstam invariants and masses. The symbols  $J_j$  denote the scalar loop integrals resulting from the reduction. The 10 tensors  $\mathcal{S}_i^{\mu\nu}$  correspond to the massless subset of the standard matrix elements of Ref. [29], which are given by

$$\begin{aligned} \mathcal{S}_1^{\mu\nu} &= \gamma^\mu (\not{p}_V - \not{p}_{\bar{q}}) \gamma^\nu, \\ \mathcal{S}_2^{\mu\nu} &= (\not{p}_V - \not{p}_g) g^{\mu\nu}, \\ \mathcal{S}_3^{\mu\nu} &= \gamma^\mu p_V^\nu, \\ \mathcal{S}_4^{\mu\nu} &= -\gamma^\nu p_g^\mu, \\ \mathcal{S}_5^{\mu\nu} &= \gamma^\mu p_{q'}^\nu, \\ \mathcal{S}_6^{\mu\nu} &= -\gamma^\nu p_{\bar{q}}^\mu, \\ \mathcal{S}_7^{\mu\nu} &= (\not{p}_V - \not{p}_g) p_g^\mu p_V^\nu, \\ \mathcal{S}_8^{\mu\nu} &= (\not{p}_V - \not{p}_g) p_{\bar{q}}^\mu p_{q'}^\nu, \\ \mathcal{S}_9^{\mu\nu} &= (\not{p}_V - \not{p}_g) p_g^\mu p_{q'}^\nu, \\ \mathcal{S}_{10}^{\mu\nu} &= (\not{p}_V - \not{p}_g) p_{\bar{q}}^\mu p_V^\nu. \end{aligned} \quad (3.25)$$

---

<sup>2</sup>We note that the dependence on the squared mass  $p_V^2$  of the external gauge boson is suppressed.

This decomposition for the one-loop matrix element (3.4) has been derived by:

- using the Clifford algebra of the  $\gamma$ -matrices and  $\not{p}_i \not{p}_i = p_i^2$ ,
- elimination of the slashed quark momenta  $\not{p}_{\bar{q}}$  and  $\not{p}_{q'}$  by applying the Dirac equation,
- using the identity  $p^\mu \epsilon_\mu(p) = 0$  for gauge-boson polarization vectors
- and replacing the products  $\epsilon_\mu^*(p_V) p_{q'}^\mu$  and  $\epsilon_\nu^*(p_g) p_{\bar{q}}^\nu$  through exploiting energy-momentum conservation  $p_{\bar{q}} + p_{q'} = p_V + p_g$ .

Let us now list the scalar integrals  $J_i(M_\Gamma^2)$  from the tensor reduction. For convenience we define the constant terms

$$J_0(M_\Gamma^2) = 1 \tag{3.26}$$

and adopt the notation of [30] for the definition<sup>3</sup> of the scalar integrals  $A_0, B_0, C_0$  and  $D_0$ . The appearing integrals can generically be listed for neutral and charged gauge boson production. The UV-divergent one- and two-point functions are given by

$$\begin{aligned} J_{1a}(M_\Gamma^2) &= B_0(m^2; M_\Gamma^2, m^2), \\ J_{1b}(M_\Gamma^2) &= B_0(m^2; M_W^2, m^2) = J_{1a}(M_W^2), \\ J_2(M_\Gamma^2) &= B_0(p_V^2; m^2, m^2), \\ J_3(M_\Gamma^2) &= B_0(p_V^2; M_W^2, M_\Gamma^2), \\ J_4(M_\Gamma^2) &= B_0(\hat{s}; m^2, m^2), \\ J_{5a}(M_\Gamma^2) &= B_0(\hat{u}; M_\Gamma^2, m^2), \\ J_{5b}(M_\Gamma^2) &= B_0(\hat{u}; M_W^2, m^2) = J_{5a}(M_W^2), \\ J_{6a}(M_\Gamma^2) &= B_0(\hat{t}; M_\Gamma^2, m^2), \\ J_{6b}(M_\Gamma^2) &= B_0(\hat{t}; M_W^2, m^2) = J_{6a}(M_W^2), \end{aligned} \tag{3.27}$$

where  $m$  is an infinitesimal quark mass regulator. The remaining loop integrals are free from UV singularities. The following three-point functions are finite if  $M_\Gamma$  and the transverse momentum of the gauge boson are non-vanishing:

$$\begin{aligned} J_7(M_\Gamma^2) &= C_0(\hat{s}, m^2, m^2; m^2, m^2, M_\Gamma^2), \\ J_8(M_\Gamma^2) &= C_0(\hat{u}, p_V^2, m^2; M_\Gamma^2, m^2, m^2), \\ J_{9a}(M_\Gamma^2) &= C_0(\hat{u}, p_V^2, m^2; m^2, M_W^2, M_\Gamma^2), \\ J_{9b}(M_\Gamma^2) &= C_0(\hat{u}, p_V^2, m^2; m^2, M_\Gamma^2, M_W^2) = J_{9a}(M_\Gamma^2) \Big|_{M_\Gamma^2 \leftrightarrow M_W^2}, \end{aligned}$$

---

<sup>3</sup>However, we choose their normalization according to Ref. [29], i.e. we include the factor  $(2\pi\mu)^{4-D}$  which is omitted in the conventions of [30].

$$\begin{aligned}
J_{10}(M_\Gamma^2) &= C_0(\hat{t}, p_V^2, m^2; M_\Gamma^2, m^2, m^2) = J_8(M_\Gamma^2)\Big|_{\hat{t} \leftrightarrow \hat{u}}, \\
J_{11a}(M_\Gamma^2) &= C_0(\hat{t}, p_V^2, m^2; m^2, M_W^2, M_\Gamma^2) = J_{9a}(M_\Gamma^2)\Big|_{\hat{t} \leftrightarrow \hat{u}}, \\
J_{11b}(M_\Gamma^2) &= C_0(\hat{t}, p_V^2, m^2; m^2, M_\Gamma^2, M_W^2) = J_{9b}(M_\Gamma^2)\Big|_{\hat{t} \leftrightarrow \hat{u}}, \tag{3.28}
\end{aligned}$$

In addition, the box diagrams b1–b3 in Fig. 3.1, provide the following combinations of three- and four-point functions

$$\begin{aligned}
J_{12}(M_\Gamma^2) &= D_0(m^2, 0, p_V^2, m^2, \hat{u}, \hat{s}; M_\Gamma^2, m^2, m^2, m^2) - \frac{1}{\hat{s}\hat{u} + (\hat{t} + \hat{u})M_\Gamma^2} \\
&\quad \times \left[ (\hat{u} - p_V^2)C_0(\hat{u}, p_V^2, m^2; M_\Gamma^2, m^2, m^2) + \hat{u}C_0(\hat{u}, 0, m^2; M_\Gamma^2, m^2, m^2) \right. \\
&\quad \left. + (\hat{s} - p_V^2)C_0(\hat{s}, p_V^2, 0; m^2, m^2, m^2) \right], \\
J_{13}(M_\Gamma^2) &= J_{12}(M_\Gamma^2)\Big|_{\hat{t} \leftrightarrow \hat{u}}, \\
J_{14a}(M_\Gamma^2) &= D_0(p_V^2, m^2, 0, m^2, \hat{t}, \hat{u}; M_\Gamma^2, M_W^2, m^2, m^2) \\
&\quad - \frac{\hat{t}\hat{u}C_0(\hat{t}, 0, m^2; M_\Gamma^2, m^2, m^2) + \hat{u}C_0(\hat{u}, 0, m^2; M_W^2, m^2, m^2)}{\hat{t}\hat{u} - \hat{t}M_W^2 - \hat{u}M_\Gamma^2}, \\
J_{14b}(M_\Gamma^2) &= J_{14a}(M_\Gamma^2)\Big|_{M_W^2 \leftrightarrow M_\Gamma^2} = J_{14a}(M_\Gamma^2)\Big|_{\hat{t} \leftrightarrow \hat{u}}. \tag{3.29}
\end{aligned}$$

For non-vanishing values of  $M_\Gamma$  and transverse momentum of the gauge boson, the functions  $J_{12}$ – $J_{14b}$  are finite. The fact that the scalar four-point functions in (3.29) appear always in combination with three-point functions is due to a cancellation of collinear singularities that are associated with the  $gq\bar{q}$  vertex. Such singularities originate from the tensor integral reduction of the box diagrams b1–b3 in Fig. 3.1 where the propagators of virtual massless quarks couple to the real gluon according to



$$\tag{3.30}$$

More specifically, these singularities arise from the integration region where the momenta of the quarks become collinear to the gluon momentum, i.e.  $k^\mu \rightarrow xp_g^\mu$ . However, the box diagrams are finite since the quark-gluon vertex (3.30) yields

$$(\not{k} - \not{p}_g)\not{\epsilon}_g\not{k} \rightarrow x(x-1)\not{p}_g\not{\epsilon}_g\not{p}_g = x(x-1) \left[ 2\not{p}_g(p_g \cdot \epsilon_g) - \not{\epsilon}_g p_g^2 \right] = 0, \tag{3.31}$$

in the collinear limit. Thus, these singularities emerging in  $C_0$  and  $D_0$  functions from the reduction of the tensor four-point function are supposed to cancel.

In order to check these cancellations at the analytical level we used quark masses  $m$  as regulators and expressed the singular parts of  $D_0$  functions through singular  $C_0$  functions, using Ref. [31]. To illustrate this general algorithm let us give an example for the four-point function that appears in  $J_{12}(p_V^2, M_\Gamma^2)$  of Eq. (3.29) with

the parameters  $p_V^2 = M_Z^2$  and  $M_\Gamma^2 = M_W^2$ . Diagrammatically, this decomposition is

$$\begin{array}{c}
 p_q^2=0 \quad m^2 \quad p_V^2=M_Z^2 \\
 \hline
 M_W^2 \quad m^2 \\
 \hline
 p_q^2=0 \quad m^2 \quad p_g^2=0
 \end{array}
 \Big|_{\text{IR-sing}}
 = f_1 \times
 \begin{array}{c}
 p_q^2=0 \quad p_V^2=M_Z^2 \\
 \hline
 M_W^2 \quad m^2 \\
 \hline
 p_q^2=0 \quad m^2 \quad p_g^2=0
 \end{array}
 + f_2 \times
 \begin{array}{c}
 p_q^2=0 \quad p_V^2=M_Z^2 \\
 \hline
 m^2 \quad m^2 \\
 \hline
 p_q^2=0 \quad m^2 \quad p_g^2=0
 \end{array}$$

with  $f_1 = \hat{u}/(\hat{s}\hat{u} + (\hat{t} + \hat{u})M_W^2)$  and  $f_2 = (\hat{s} - M_Z^2)/(\hat{s}\hat{u} + (\hat{t} + \hat{u})M_W^2)$ . It shows that the collinear singularity at the gluon vertex is still present in the  $C_0$  functions, while the other non-singular propagators of the  $D_0$  functions have been shrunk to a point. The explicit formula for this particular result is

$$\begin{aligned}
 D_0(0, 0, M_Z^2, 0, \hat{u}, \hat{s}; M_W^2, m^2, m^2, m^2) \Big|_{\text{IR-sing}} &= f_1 C_0(\hat{u}, 0, 0; M_W^2, m^2, m^2) \\
 &+ f_2 C_0(\hat{s}, M_Z^2, 0; m^2, m^2, m^2).
 \end{aligned} \quad (3.32)$$

Thus, the fictitious singularities can be removed by proper combinations of four- and three-point functions. The functions  $J_{12}-J_{14b}$  in (3.29) are constructed in such a way that they are free from fictitious singularities. We checked that all (fictitious) singular  $C_0$  functions resulting from the reduction cancel. Furthermore, we checked numerically that the functions in (3.29) are finite and numerically stable for  $m/M_Z \ll 1$ . The numerical results presented in Ch. 8 have been obtained using  $m/M_Z = 10^{-6}$ .

In the case of the photonic corrections for  $W$  boson production the scalar integrals  $J_i(M_\Gamma^2)$  in (3.27)-(3.29) contain also soft and collinear singularities that appear when  $M_\Gamma = M_\gamma \rightarrow 0$  and  $m \rightarrow 0$ . These singularities will be discussed in Sect. 3.4.

### 3.3 Renormalization

The ultraviolet (UV) divergencies of the one-loop corrections (3.13) and (3.23) to neutral and charged gauge boson production, respectively, have the same structure: The tensors  $\delta\mathcal{A}_{1,X}^{\mu\nu}$  and  $\delta\mathcal{A}_{1,Y}^{\mu\nu}$  which only contribute to the loop corrections for  $W$  boson production are UV finite, while the Abelian and non-Abelian tensors  $\delta\mathcal{A}_{1,A/N}^{\mu\nu}$  give rise to ultraviolet divergencies, which are the same for neutral and charged gauge boson production. The UV singular part for the corresponding tensors is

$$\delta\mathcal{A}_{1,A}^{\mu\nu}(M_\Gamma^2) \Big|_{\text{UV}} = \bar{\Delta}_{\text{UV}} \mathcal{S}_0^{\mu\nu}, \quad \delta\mathcal{A}_{1,N}^{\mu\nu}(M_\Gamma^2) \Big|_{\text{UV}} = 2\bar{\Delta}_{\text{UV}} \mathcal{S}_0^{\mu\nu}, \quad (3.33)$$

where  $\mathcal{S}_0^{\mu\nu}$  is the tensor structure of the Born amplitude (3.6), and

$$\bar{\Delta}_{\text{UV}} = \left( \frac{4\pi\mu^2}{M_Z^2} \right)^\varepsilon \frac{\Gamma(1+\varepsilon)}{\varepsilon} = \frac{1}{\varepsilon} - \gamma_E + \ln(4\pi) + \ln\left( \frac{\mu^2}{M_Z^2} \right) + \mathcal{O}(\varepsilon) \quad (3.34)$$

in  $D = 4 - 2\varepsilon$  space-time dimensions. In (3.34) we have included a logarithmic term that renders the renormalized amplitude independent of the scale  $\mu$  of dimensional regularization. This is equivalent to the choice  $\mu = M_Z$  within the usual  $\overline{\text{MS}}$  scheme. The above UV singularities are cancelled by the counterterm diagrams depicted in Fig. 3.2. The counterterms that are responsible for the contributions of diagrams c1, c2, c3 and c4 read

$$\begin{aligned} \text{---} \otimes \text{---} &= i\not{p} \sum_{\lambda=R,L} \omega_\lambda \delta Z_{q_\lambda}, & \text{---} \otimes \text{---} &= -ig_S t^a \gamma^\mu \sum_{\lambda=R,L} \omega_\lambda \delta Z_{q_\lambda}. \end{aligned} \quad (3.35)$$

Since there is no  $\mathcal{O}(\alpha)$  contribution to the renormalization of the strong coupling constant  $g_S$ , these counterterms depend only on the wave-function renormalization constants for quarks,  $\delta Z_{q_\lambda}$ . Their combined contribution to the process  $\bar{q}q' \rightarrow Vg$ , i.e. the sum of the diagrams c1, c2, c3 and c4, vanishes. This is a consequence from the QED-like Ward identity, which holds for the gluon in this calculation. The renormalization of the processes  $\bar{q}q' \rightarrow Vg$  is thus provided by the diagrams c5, c6, which originate from counterterms

$$\text{---} \otimes \text{---}^{V=\gamma,Z} = ie\gamma^\mu \sum_{\lambda=R,L} \omega_\lambda \left[ I_{q_\lambda}^V \delta C_{q_\lambda,V}^A + \frac{U_{VW^3}}{s_W} T_{q_\lambda}^3 \delta C_{q_\lambda,V}^N \right] \quad (3.36)$$

for photon and  $Z$ -boson couplings and

$$\text{---} \otimes \text{---}^{W^\sigma} = ie\gamma^\mu \omega_L I_{q_L q_L'}^{W^{-\sigma}} \left[ \delta C_{q_L,W}^A + \delta C_{q_L,W}^N \right] \quad (3.37)$$

for  $W$ -boson couplings to quarks. The symbols  $\delta C^A$  and  $\delta C^N$  denote the Abelian and non-Abelian counterterms, respectively, and will be specified for photon,  $Z$  and  $W$  boson production separately.

### 3.3.1 Renormalization of the photon vertex

In the case of photon production the Abelian counterterm in (3.36) is given by

$$\delta C_{q_\lambda,\gamma}^A = \delta Z_{q_\lambda}^{\text{weak}} + \frac{1}{2} \left( \delta Z_{AA} + \frac{s_W}{c_W} \delta Z_{ZA} + \frac{\delta e^2}{e^2} \right), \quad (3.38)$$

where  $\delta Z_{q_\lambda}^{\text{weak}}$  is the wave-function renormalization constants for massless chiral quarks,  $\delta Z_{AA}$  and  $\delta Z_{ZA}$  describe the renormalization constants for the photon wave-function and  $\delta e$  is the renormalization constant for the electric charge. The wave-function renormalization constants for massless chiral quarks are given by

$$\delta Z_{q_\lambda}^{\text{weak}} = -\text{Re} \left[ \Sigma_{q,\lambda}^{\text{weak}}(0) \right] = \frac{\alpha}{4\pi} \sum_{\Gamma=Z,W^\pm} (I^\Gamma I^{\bar{\Gamma}})_{q_\lambda} \left[ \frac{3}{2} - \frac{A_0(M_\Gamma^2)}{M_\Gamma^2} \right], \quad (3.39)$$

where  $\Sigma_{q,\lambda}^{\text{weak}}(p^2)$  are the chiral components of the weak contributions to the one-particle irreducible two-point function of massless fermions,

$$\Gamma^{q\bar{q}}(p) = i\not{p} \left[ 1 + \sum_{\lambda=R,L} \omega_\lambda \Sigma_{q,\lambda}(p^2) \right]. \quad (3.40)$$

In the following we adopt the on-shell renormalization scheme [29], with  $c_w^2 = 1 - s_w^2 = M_W^2/M_Z^2$  and the electromagnetic coupling constant defined in the Thompson limit, i.e. at the scale zero. In this scheme, Ward identities [29] yield the charge renormalization constant in terms of photonic wave-function renormalization constants according to

$$\frac{\delta e^2}{e^2} = -\delta Z_{AA} - \frac{s_w}{c_w} \delta Z_{ZA}, \quad (3.41)$$

where the explicit expressions for the counterterms  $\delta Z_{AA}$ ,  $\delta Z_{ZA}$  and  $\delta e^2/e^2$  can be found in Ref. [29]. As well known, the on-shell counterterm  $\delta e^2/e^2$  contains large logarithms of light-fermion masses, which are responsible for the running of  $\alpha$  from the scale zero to the characteristic scale of the process. However, owing to the Ward identity, for the case of on-shell photon production these logarithms are cancelled by corresponding terms present in  $\delta Z_{AA}$ . This justifies our choice of  $\alpha$  at the scale zero as input parameter. Owing to the relation (3.41) the Abelian counterterm (3.38) simplifies to

$$\delta C_{q\lambda,\gamma}^A = \delta Z_{q\lambda}^{\text{weak}}. \quad (3.42)$$

The non-Abelian counterterm reads

$$\delta C_{q\lambda,\gamma}^N = -\frac{1}{2s_w c_w} \delta Z_{ZA}, \quad (3.43)$$

where

$$\delta Z_{ZA} = 2 \frac{\Sigma_T^{\text{AZ}}(0)}{M_Z^2} = \frac{\alpha}{4\pi} \frac{4c_w}{s_w} \left[ \bar{\Delta}_{\text{UV}} - \log \left( \frac{M_W^2}{M_Z^2} \right) \right]. \quad (3.44)$$

Thus, we find the ultraviolet divergent contributions of the counterterms to be

$$\delta C_{q\lambda,\gamma}^A \Big|_{\text{UV}} = \delta Z_{q\lambda}^{\text{weak}} \Big|_{\text{UV}} = -\frac{\alpha}{4\pi} \bar{\Delta}_{\text{UV}} \sum_{V=Z,W^\pm} (I^V I^{\bar{V}})_{q\lambda}, \quad (3.45)$$

$$\delta C_{q\lambda,\gamma}^N \Big|_{\text{UV}} = -\frac{\alpha}{2\pi s_w^2} \bar{\Delta}_{\text{UV}}. \quad (3.46)$$

Writing the corresponding amplitude from (3.5) in the form

$$\delta \mathcal{M}_{1,\text{CT}}^{\lambda,\mu\nu} = \left[ I_{q\lambda}^\gamma \delta C_{q\lambda,\gamma}^A - T_{q\lambda}^3 \delta C_{q\lambda,\gamma}^N \right] \mathcal{S}_0^{\mu\nu} \quad (3.47)$$

the cancellation of the ultraviolet singularities from the loop diagrams in (3.33) and the counterterms is manifest.



### 3.3.2 Renormalization of the $Z$ vertex

The Abelian and non-Abelian counterterms corresponding to the  $Z$ -boson vertex in (3.36) are given by

$$\begin{aligned}\delta C_{q\lambda,Z}^A &= \delta Z_{q\lambda}^{\text{weak}} + \frac{1}{2} \left( \delta Z_{ZZ} + \frac{c_W}{s_W} \delta Z_{AZ} + \frac{\delta e^2}{e^2} - \frac{1}{s_W^2} \frac{\delta c_W^2}{c_W^2} \right), \\ \delta C_{q\lambda,Z}^N &= -\frac{1}{2s_W c_W} \delta Z_{AZ} + \frac{1}{s_W^2} \frac{\delta c_W^2}{c_W^2}.\end{aligned}\quad (3.48)$$

The expression for the weak contribution of the quark wave-function renormalization constant  $\delta Z_{q\lambda}^{\text{weak}}$  is the same as in (3.39). The renormalization constants associated with the  $Z$ -boson wave-function read

$$\delta Z_{ZZ} = -\text{Re} \left. \frac{\partial \Sigma_T^{ZZ}(p^2)}{\partial p^2} \right|_{p^2=M_Z^2}, \quad \delta Z_{AZ} = -2\text{Re} \left[ \frac{\Sigma_T^{AZ}(M_Z^2)}{M_Z^2} \right] \quad (3.49)$$

and have been evaluated using the self-energies  $\Sigma_T^{ZZ}$  and  $\Sigma_T^{AZ}$  of Ref. [29].

For the coupling renormalization of  $e$  and  $c_W$  we have considered two different schemes, the  $\overline{\text{MS}}$  and the on-shell scheme. The first one shall be presented here, while the latter is described in Appendix C including a detailed discussion of the differences between the two schemes. The numerical results for  $Z$ +jet production presented in Ch. 8 have been evaluated within the  $\overline{\text{MS}}$  scheme. In this scheme, the counterterms for  $e$  and  $c_W$  read

$$\begin{aligned}\frac{\delta c_W^2}{c_W^2} \Big|_{\overline{\text{MS}}} &\equiv -\frac{\alpha}{4\pi} \bar{\Delta}_{\text{UV}} \left[ \frac{19 + 22s_W^2}{6c_W^2} + 2(\rho - 1) \right], \\ \frac{\delta e^2}{e^2} \Big|_{\overline{\text{MS}}} &\equiv \frac{\alpha}{4\pi} \bar{\Delta}_{\text{UV}} \left[ \frac{11}{3} + \left( \frac{2}{s_W^2} - 4 \right) (\rho - 1) \right]\end{aligned}\quad (3.50)$$

with  $\rho = M_W^2/(c_W^2 M_Z^2)$ . We note that the counterterms (3.50) contain contributions proportional to  $(\rho - 1)$  which depend on the relation between  $M_W$  and  $M_Z$ . In principle, in an  $\mathcal{O}(\alpha)$   $\overline{\text{MS}}$  calculation the value of the  $W$  mass, which appears only in loop diagrams, should be derived from the on-shell  $Z$ -boson mass and the  $\overline{\text{MS}}$  mixing angle using the tree-level relation  $M_W = c_W M_Z$ . In this case the  $(\rho - 1)$  contributions in (3.50) would vanish. However, it seems more natural to use the on-shell value of  $M_W$  as an input parameter in our calculation. This violates the tree-level mass relation and introduces loop corrections that are implicitly contained in the numerical value of  $M_W$ . Their effect on our  $\mathcal{O}(\alpha)$  predictions is formally of  $\mathcal{O}(\alpha^2)$  since  $M_W$  does not contribute at tree level. This procedure is thus consistent at  $\mathcal{O}(\alpha)$ . However, it affects also those  $1/\varepsilon$  poles that appear in  $\delta Z_{AZ}$  since they depend on  $M_W$ . Such singularities give rise to terms proportional to  $(\rho - 1)/\varepsilon$  that are again, formally, of  $\mathcal{O}(\alpha^2)$  and are compensated by the  $(\rho - 1)$  terms that we

have introduced in (3.50). This procedure removes all higher-order effects from the divergent part of the counterterms (3.48), which becomes independent of  $(\rho - 1)$ , and ensures the cancellation of the singularities (3.33) originating from the loop diagrams for arbitrary values of  $\rho$ .

Independently of the renormalization scheme, the above counterterms yield the ultraviolet singularities

$$\delta C_{q_\lambda, Z}^A \Big|_{\text{UV}} = \delta Z_{q_\lambda}^{\text{weak}} \Big|_{\text{UV}} = -\frac{\alpha}{4\pi} \bar{\Delta}_{\text{UV}} \sum_{V=Z, W^\pm} (I^V I^{\bar{V}})_{q_\lambda}, \quad (3.51)$$

$$\delta C_{q_\lambda, Z}^N \Big|_{\text{UV}} = -\frac{\alpha}{2\pi s_W^2} \bar{\Delta}_{\text{UV}}. \quad (3.52)$$

Writing the counterterm amplitude as

$$\delta \mathcal{M}_{1, \text{CT}}^{\lambda, \mu\nu} = \left[ I_{q_\lambda}^Z \delta C_{q_\lambda, Z}^A + \frac{c_W}{s_W} T_{q_\lambda}^3 \delta C_{q_\lambda, Z}^N \right] \mathcal{S}_0^{\mu\nu} \quad (3.53)$$

the cancellation with the  $1/\varepsilon$  poles from loop diagrams in (3.33) is evident.

We note that, similar to the counterterm for the photon coupling, the UV poles associated with the Abelian coupling structure in (3.51) result exclusively from the fermionic wave-function renormalization constant  $\delta Z_{q_\lambda}^{\text{weak}}$ . The poles in  $\delta C_{q_\lambda, Z}^A$  originating from the renormalization of the electroweak coupling constants  $\delta e, \delta c_W$  and the  $Z$ -boson field renormalization constants  $\delta Z_{ZZ}, \delta Z_{AZ}$  cancel. However, in contrast to the photon counterterm, the latter wave-function renormalization constants add finite contributions to  $\delta C_{q_\lambda, Z}^A$ .

### 3.3.3 Renormalization of the $W$ vertex

The coupling of the  $W$  boson to fermions is a purely SU(2) vertex. Hence, the Abelian counterterm is simply given by

$$\delta C_{q_L, W}^A = \frac{1}{2} (\delta Z_{u_L} + \delta Z_{d_L}) \quad (3.54)$$

with the left-handed contribution of the quark wave-function renormalization constant

$$\delta Z_{q_L} = -\text{Re} \left[ \Sigma^{q, L}(0) \right] = \frac{\alpha}{4\pi} \sum_{\Gamma=\gamma, Z, W^\pm} (I^\Gamma I^{\bar{\Gamma}})_{q_L} \left[ \frac{3}{2} - \frac{A_0(M_\Gamma^2)}{M_\Gamma^2} \right]. \quad (3.55)$$

Note, that in contrast to photon and  $Z$  production, also photonic contributions are included. The non-Abelian counterterm reads

$$\delta C_{q_L, W}^N = \frac{1}{2} \left( \delta Z_W + \frac{\delta g_2^2}{g_2^2} \right), \quad (3.56)$$

where

$$\delta Z_W = -\text{Re} \left( \frac{\partial \Sigma_T^W(p^2)}{\partial p^2} \right) \Big|_{p^2=M_W^2} \quad (3.57)$$

is the wave-function renormalization constant of the W boson, that we evaluated using the explicit results for the  $W$  self-energy in Ref. [29]. For the definition and the renormalization of the SU(2) coupling constant,

$$g_2^2 = \frac{4\pi\alpha}{s_W^2}, \quad \frac{\delta g_2^2}{g_2^2} = \frac{\delta\alpha}{\alpha} - \frac{\delta s_W^2}{s_W^2}, \quad (3.58)$$

we adopt the  $G_\mu$ -scheme, where the electromagnetic coupling constant  $\alpha$  is expressed in terms of the Fermi constant  $G_\mu$ , and the weak mixing angle is related to the on-shell masses  $M_Z$ ,  $M_W$  of the gauge bosons,

$$\alpha = \frac{\sqrt{2}G_\mu M_W^2 s_W^2}{\pi}, \quad s_W^2 = 1 - c_W^2 = 1 - M_W^2/M_Z^2. \quad (3.59)$$

The counterterm  $\delta\alpha/\alpha$  in the  $G_\mu$ -scheme can be derived from the on-shell counterterm  $\delta\alpha(0)/\alpha(0)$  for the fine-structure constant in the Thompson limit. Using the one-loop relation  $\alpha = \alpha(0) [1 + \Delta r]$  and requiring  $\alpha + \delta\alpha = \alpha(0) + \delta\alpha(0)$  we have

$$\frac{\delta\alpha}{\alpha} = \frac{\delta\alpha(0)}{\alpha(0)} - \Delta r. \quad (3.60)$$

Combining the relations (3.58)–(3.60) and using the explicit one-loop expression for  $\Delta r$  in [32, 33], we obtain

$$\frac{\delta g_2^2}{g_2^2} = \text{Re} \left[ \frac{\Sigma_T^W(M_W^2) - \Sigma_T^W(0)}{M_W^2} \right] - \frac{\alpha}{\pi s_W^2} \left\{ \bar{\Delta}_{\text{UV}} + \frac{1}{4} \left[ 6 + \frac{7 - 12s_W^2}{2s_W^2} \ln \left( \frac{M_W^2}{M_Z^2} \right) \right] \right\}. \quad (3.61)$$

The above counterterms yield the ultraviolet singularities

$$\begin{aligned} \delta C_{q_L, W}^A \Big|_{\text{UV}} &= -\frac{\alpha}{8\pi} \bar{\Delta}_{\text{UV}} \sum_{q=u,d} \sum_{V=A,Z,W^\pm} (I^V I^{\bar{V}})_{q_L} = -\frac{\alpha}{4\pi} \bar{\Delta}_{\text{UV}} \left( \frac{C_F}{s_W^2} + \frac{Y_{q_L}^2}{4c_W^2} \right), \\ \delta C_{q_L, W}^N \Big|_{\text{UV}} &= -\frac{\alpha}{2\pi s_W^2} \bar{\Delta}_{\text{UV}} \end{aligned} \quad (3.62)$$

and contribute to the counterterm amplitude for  $W$  production with

$$\delta \mathcal{M}_{1, \text{CT}}^{L, \mu\nu} = \left( \delta C_{q_L, W}^A + \delta C_{q_L, W}^N \right) \frac{1}{\sqrt{2}s_W} \mathcal{S}_0^{\mu\nu}, \quad (3.63)$$

in order to cancel the ultraviolet singularities in (3.33).

### 3.4 Soft and collinear singularities for $W$ boson production

In contrast to the weak corrections for photon and  $Z$  boson production, the electroweak loop corrections to  $W$  boson production involve further singularities associated with photonic corrections. More precisely, the loop diagrams and wave-function renormalization constants involve singularities originating from soft and collinear virtual photons (for brevity denoted in the following as IR singularities). According to the KLN-theorem [34], these singularities cancel with the corresponding ones originating from real photon bremsstrahlung. To isolate the IR singularities from the virtual corrections to  $W$  production, we split the corresponding wave-function renormalization constants and the photonic loop contributions to (3.23) in IR-singular (IR) and IR-finite (fin) parts:

$$\begin{aligned}\delta Z_{q_L} &= \delta Z_{q_L}^{\text{IR}} + \delta Z_{q_L}^{\text{fin}}, \\ \delta Z_W &= \delta Z_W^{\text{IR}} + \delta Z_W^{\text{fin}}, \\ \delta \mathcal{A}_{1,I}^{\mu\nu}(M_\gamma^2) &= \delta \mathcal{A}_{1,I}^{\text{IR},\mu\nu} + \delta \mathcal{A}_{1,I}^{\text{fin},\mu\nu}.\end{aligned}\tag{3.64}$$

The singular parts depend on the scheme adopted to regularize IR singularities. The remaining parts are scheme-independent and free from IR singularities, but can contain ultraviolet poles. For the regularization of IR singularities we use, alternatively, two different schemes:

- In the first scheme, which we denote as mass-regularization scheme (MR), we use infinitesimal quark masses  $m$  and a photon-mass regulator,  $M_\gamma = \lambda$  with  $0 < \lambda \ll m$ . Since the quark-mass dependence disappears in the final result, we perform the computation using the same mass  $m$  for all quarks.
- In the second scheme we perform the calculation using massless fermions and photons,  $M_\gamma = m = 0$ , and evaluate IR singularities in dimensional regularization. To denote quantities evaluated in this scheme we use the label DR.

The singular parts of the wave-function renormalization constants (3.55) and (3.57) read

$$\begin{aligned}\delta Z_{q_L}^{\text{IR}} &= \frac{\alpha}{4\pi} \left( \frac{4\pi\mu^2}{M_W^2} \right)^\varepsilon \Gamma(1 + \varepsilon) Q_q^2 h_q^{\text{IR}}, \\ \delta Z_W^{\text{IR}} &= \frac{\alpha}{4\pi} \left( \frac{4\pi\mu^2}{M_W^2} \right)^\varepsilon \Gamma(1 + \varepsilon) h_W^{\text{IR}},\end{aligned}\tag{3.65}$$

with

$$h_{q,\text{MR}}^{\text{IR}} = -\ln\left(\frac{M_W^2}{m^2}\right) - 2\ln\left(\frac{\lambda^2}{m^2}\right) - 4, \quad h_{W,\text{MR}}^{\text{IR}} = -2\ln\left(\frac{\lambda^2}{M_W^2}\right),\tag{3.66}$$

in the MR scheme and

$$h_{q,\text{DR}}^{\text{IR}} = \frac{1}{\varepsilon}, \quad h_{W,\text{DR}}^{\text{IR}} = -\frac{2}{\varepsilon}, \quad (3.67)$$

in the DR scheme. The splitting of the photonic loop contributions  $\delta\mathcal{A}_{1,I}^{\mu\nu}(M_\gamma^2)$  into IR-singular and IR-finite parts is performed at the level of the scalar loop integrals  $J_i(M_\gamma^2)$  with the splitting

$$J_i(M_\gamma^2) = J_i^{\text{IR}} + J_i^{\text{fin}} \quad (3.68)$$

for IR singular integrals. These IR-singular parts depend on the scheme adopted to regularize soft and collinear singularities while the IR-finite parts of these integrals are scheme independent and free from soft-collinear singularities, but can contain ultraviolet poles.

Let us start with the two-point functions (3.27). Here only  $J_{1a}(M_\gamma^2)$  gives rise to IR singularities. This integral is split into

$$\begin{aligned} J_{1a,\text{MR}}^{\text{IR}} &= -\ln\left(\frac{m^2}{M_W^2}\right) + 1, \\ J_{1a,\text{DR}}^{\text{IR}} &= -\left(\frac{4\pi\mu^2}{M_W^2}\right)^\varepsilon \frac{\Gamma(1+\varepsilon)}{\varepsilon} - 1, \\ J_{1a}^{\text{fin}} &= \left(\frac{4\pi\mu^2}{M_W^2}\right)^\varepsilon \frac{\Gamma(1+\varepsilon)}{\varepsilon} + 1. \end{aligned} \quad (3.69)$$

We note that within dimensional regularization the UV and IR singularities cancel each other and the massless two-point function vanishes,  $J_{1a,\text{DR}}^{\text{IR}} + J_{1a}^{\text{fin}} = 0$ . The three-point functions  $J_{9b}(M_\gamma^2)$  and  $J_{11b}(M_\gamma^2)$  in (3.28) are free from IR singularities and the singularities originating from  $J_8(M_\gamma^2)$  and  $J_{10}(M_\gamma^2)$  do not need to be considered since the coefficients associated with these scalar integrals are of order  $M_\gamma^2$  (see Appendix D.1). The remaining three-point functions in (3.28) contain soft and collinear singularities. Using the results of [31] we find

$$\begin{aligned} J_{7,\text{MR}}^{\text{IR}} &= \frac{1}{\hat{s}} \left[ -\frac{1}{2} \ln^2\left(\frac{M_W^2}{m^2}\right) + \ln\left(\frac{M_W^2}{\lambda^2}\right) \ln\left(\frac{-\hat{s}}{m^2}\right) \right], \\ J_{7,\text{DR}}^{\text{IR}} &= \left(\frac{4\pi\mu^2}{M_W^2}\right)^\varepsilon \frac{\Gamma(1+\varepsilon)}{\hat{s}} \left[ \frac{1}{\varepsilon^2} - \frac{1}{\varepsilon} \ln\left(\frac{-\hat{s}}{M_W^2}\right) \right], \\ J_7^{\text{fin}} &= \frac{1}{\hat{s}} \left[ \frac{1}{2} \ln^2\left(\frac{-\hat{s}}{M_W^2}\right) - \frac{\pi^2}{6} \right], \end{aligned} \quad (3.70)$$

and

$$\begin{aligned} J_{9a,\text{MR}}^{\text{IR}} &= \frac{1}{\hat{u} - M_W^2} \left\{ \frac{1}{2} \left[ \ln\left(\frac{M_W^2}{\lambda^2}\right) - \frac{1}{2} \ln\left(\frac{M_W^2}{m^2}\right) \right] \ln\left(\frac{M_W^2}{m^2}\right) \right. \\ &\quad \left. + \ln\left(\frac{M_W^2}{\lambda^2}\right) \ln\left(1 - \frac{\hat{u}}{M_W^2}\right) \right\}, \end{aligned}$$

$$\begin{aligned}
J_{9a,\text{DR}}^{\text{IR}} &= \left( \frac{4\pi\mu^2}{M_W^2} \right)^\varepsilon \frac{\Gamma(1+\varepsilon)}{\hat{u} - M_W^2} \left[ \frac{1}{2\varepsilon^2} - \frac{1}{\varepsilon} \ln \left( 1 - \frac{\hat{u}}{M_W^2} \right) \right], \\
J_{9a}^{\text{fin}} &= \frac{1}{\hat{u} - M_W^2} \left[ \ln^2 \left( 1 - \frac{\hat{u}}{M_W^2} \right) + \text{Li}_2 \left( \frac{\hat{u}}{M_W^2} \right) \right],
\end{aligned} \tag{3.71}$$

where  $\text{Li}_2(x) = -\int_0^x dt \ln(1-t)/t$ . The finite and singular parts for  $J_{11a}(M_\gamma^2) = J_{9a}(M_\gamma^2)|_{\hat{u} \rightarrow \hat{t}}$  are constructed in the same way.

Using the results of [31], the singular parts of the subtracted four-point functions (3.29) can be related to the ones of the three-point functions (as discussed for the example in (3.32)) and read

$$\begin{aligned}
J_{12}^{\text{IR}} &= J_{13}^{\text{IR}}|_{\hat{t} \leftrightarrow \hat{u}} = \frac{1}{\hat{u}} J_7^{\text{IR}}, \\
J_{14a}^{\text{IR}} &= J_{14b}^{\text{IR}}|_{\hat{t} \leftrightarrow \hat{u}} = \frac{1}{\hat{t}} J_{9a}^{\text{IR}},
\end{aligned} \tag{3.72}$$

in both regularization schemes. This implicitly defines the IR finite remainders as

$$\begin{aligned}
J_{12}^{\text{fin}} &= J_{13}^{\text{fin}}|_{\hat{t} \leftrightarrow \hat{u}} = J_{12}(M_A^2) - \frac{1}{\hat{u}} J_7^{\text{IR}}, \\
J_{14a}^{\text{fin}} &= J_{14b}^{\text{fin}}|_{\hat{t} \leftrightarrow \hat{u}} = J_{14a}(M_A^2) - \frac{1}{\hat{t}} J_{9a}^{\text{IR}}.
\end{aligned} \tag{3.73}$$

Using the explicit analytic expressions for the infrared singular four-point and three-point functions from [35, 31] we obtain<sup>4</sup>

$$\begin{aligned}
J_{12}^{\text{fin}} &= \frac{1}{\hat{s}\hat{u}} \left[ \frac{1}{2} \ln^2 \left( \frac{-\hat{s}}{M_W^2} \right) - \ln^2 \left( \frac{\hat{s}}{\hat{u}} \right) - 2\text{Li}_2 \left( 1 - \frac{M_W^2}{\hat{s}} \right) - 2\text{Li}_2 \left( 1 - \frac{M_W^2}{\hat{u}} \right) - \frac{\pi^2}{2} \right], \\
J_{14a}^{\text{fin}} &= \frac{1}{\hat{t}(\hat{u} - M_W^2)} \left[ 2 \ln \left( 1 - \frac{\hat{u}}{M_W^2} \right) \ln \left( \frac{-\hat{t}}{M_W^2} \right) - \frac{1}{2} \ln^2 \left( \frac{-\hat{t}}{M_W^2} \right) \right. \\
&\quad \left. + \text{Li}_2 \left( \frac{\hat{u}}{M_W^2} \right) - \frac{\pi^2}{2} \right].
\end{aligned} \tag{3.74}$$

Combining all singular contributions from the loop integrals  $J_i^{\text{IR}}$  we obtain for the tensors in (3.64)

$$\delta \mathcal{A}_{1,I}^{\text{IR},\mu\nu} = \left( \frac{4\pi\mu^2}{M_W^2} \right)^\varepsilon \Gamma(1+\varepsilon) f_I^{\text{IR}} \mathcal{S}_0^{\mu\nu} \quad \text{with } I = \text{A, N, X, Y}, \tag{3.75}$$

---

<sup>4</sup>Furthermore, the four- and three-point integrals contributing to  $J_{12}(M_F^2)$  have been calculated by hand in both regularization schemes. Agreement was found with the literature.

i.e. the IR singularities, contained in the functions  $f_I^{\text{IR}}$ , factorize<sup>5</sup> with respect to the Born amplitude (3.6). The IR singular part of the renormalized amplitude can be expressed in terms of the electromagnetic charges of the external particles as

$$\delta\mathcal{M}_{1,\text{IR}}^{L,\mu\nu} = \frac{\alpha}{4\pi} \left( \frac{4\pi\mu^2}{M_W^2} \right)^\varepsilon \Gamma(1+\varepsilon) \left[ -Q_q Q_{q'} f_1^{\text{IR}} + \sigma Q_q f_2^{\text{IR}} - \sigma Q_{q'} f_3^{\text{IR}} \right] \mathcal{M}_0^{L,\mu\nu}, \quad (3.76)$$

where  $\sigma = \pm 1$  is the charge of the  $W$  boson and

$$\begin{aligned} f_1^{\text{IR}} &= -f_A^{\text{IR}} - h_q^{\text{IR}}, \\ f_2^{\text{IR}} &= -f_A^{\text{IR}} - f_N^{\text{IR}} + \frac{1}{2} (f_X^{\text{IR}} - f_Y^{\text{IR}} - h_q^{\text{IR}} - h_W^{\text{IR}}), \\ f_3^{\text{IR}} &= -f_A^{\text{IR}} - f_N^{\text{IR}} + \frac{1}{2} (f_X^{\text{IR}} + f_Y^{\text{IR}} - h_q^{\text{IR}} - h_W^{\text{IR}}). \end{aligned} \quad (3.77)$$

In the MR scheme we obtain

$$\begin{aligned} f_{1,\text{MR}}^{\text{IR}} &= -2 \ln \left( \frac{\lambda^2}{M_W^2} \right) \ln \left( \frac{-\hat{s}}{m^2} \right) - \ln^2 \left( \frac{m^2}{M_W^2} \right) + 3 \ln \left( \frac{m^2}{M_W^2} \right) + 2 \ln \left( \frac{\lambda^2}{m^2} \right), \\ f_{2,\text{MR}}^{\text{IR}} &= \ln \left( \frac{\lambda^2}{M_W^2} \right) \left[ \ln \left( \frac{m^2}{M_W^2} \right) - 2 \ln \left( 1 - \frac{\hat{t}}{M_W^2} \right) \right] - \frac{1}{2} \ln^2 \left( \frac{m^2}{M_W^2} \right) \\ &\quad + \frac{1}{2} \ln \left( \frac{m^2}{M_W^2} \right) + 2 \ln \left( \frac{\lambda^2}{M_W^2} \right), \\ f_{3,\text{MR}}^{\text{IR}} &= f_{2,\text{MR}}^{\text{IR}} \Big|_{\hat{t} \rightarrow \hat{u}}, \end{aligned} \quad (3.78)$$

and in the DR scheme

$$\begin{aligned} f_{1,\text{DR}}^{\text{IR}} &= \frac{2}{\varepsilon^2} - \frac{1}{\varepsilon} \left[ 2 \ln \left( \frac{-\hat{s}}{M_W^2} \right) - 3 \right] + 4, \\ f_{2,\text{DR}}^{\text{IR}} &= \frac{1}{\varepsilon^2} - \frac{1}{\varepsilon} \left[ 2 \ln \left( 1 - \frac{\hat{t}}{M_W^2} \right) - \frac{5}{2} \right] + 2, \\ f_{3,\text{DR}}^{\text{IR}} &= f_{2,\text{DR}}^{\text{IR}} \Big|_{\hat{t} \rightarrow \hat{u}}. \end{aligned} \quad (3.79)$$

We note, that the splitting (3.64) has been performed in such a way that in the high-energy limit ( $|\hat{s}|, |\hat{t}|, |\hat{u}| \gg M_W^2$ ) the IR-finite part of the amplitude has the same logarithmic behavior as the virtual corrections regularized by a photon mass  $M_\gamma = M_W$ . Indeed the IR-singular parts  $f_i^{\text{IR}}$  correspond to the contribution

---

<sup>5</sup>To be precise, the tensors  $\delta\mathcal{A}_{1,\text{X}}^{\mu\nu}(M_\gamma^2)$  and  $\delta\mathcal{A}_{1,\text{N}}^{\mu\nu}(M_\gamma^2)$  contain also non-factorizable IR divergences. However these non-factorizable singularities are related by

$$\delta\mathcal{A}_{1,\text{X}}^{\text{non-fact},\mu\nu}(M_\gamma^2) = 2\delta\mathcal{A}_{1,\text{N}}^{\text{non-fact},\mu\nu}(M_\gamma^2),$$

and due to the identity  $C_F - (T_{\text{gl}}^3)^2 = C_A/4$ , which relates the coupling structures associated with the X- and N-terms in (3.23), they cancel.

called purely electromagnetic in Ref. [36]. This implies that, up to terms that are not logarithmically enhanced at high energies, the IR-finite part of the corrections corresponds to the symmetric electroweak contribution of Ref. [36], which is constructed by setting the photon mass equal to  $M_W$ . This property is evident in the asymptotic high-energy expressions presented in (4.9) for the IR-finite part of the diagrams involving virtual photons.

### 3.5 Results

Let us summarize the one-loop results for the processes  $\bar{q}q' \rightarrow Vg$  with  $V = \gamma, Z, W^\pm$ . To  $\mathcal{O}(\alpha^2\alpha_S)$ , the unpolarized squared matrix element is given by

$$\overline{\sum} |\mathcal{M}_1^{\bar{q}q' \rightarrow Vg}|^2 = \overline{\sum} |\mathcal{M}_0^{\bar{q}q' \rightarrow Vg}|^2 + 2\text{Re} \left[ \overline{\sum} \left( \mathcal{M}_0^{\bar{q}q' \rightarrow Vg} \right)^* \delta \mathcal{M}_1^{\bar{q}q' \rightarrow Vg} \right]. \quad (3.80)$$

Using (3.4) and summing over the polarizations we can express the interference term as

$$2\text{Re} \left[ \overline{\sum} \left( \mathcal{M}_0^{\bar{q}q' \rightarrow Vg} \right)^* \delta \mathcal{M}_1^{\bar{q}q' \rightarrow Vg} \right] = 2\pi^2 \alpha \alpha_S (N_c^2 - 1) \\ \times \text{Re} \left[ \sum_{\lambda=R,L} \text{Tr} \left( \not{p}_{q'} \overline{\mathcal{M}}_{0,V}^{\lambda,\mu\nu} \not{p}_{\bar{q}} \delta \mathcal{M}_{1,V}^{\lambda,\mu'\nu'} \right) \right] \mathcal{P}_{\mu\mu'}^V \mathcal{P}_{\nu\nu'}^g, \quad (3.81)$$

with  $\overline{\mathcal{M}} = \gamma^0 \mathcal{M}^\dagger \gamma^0$ . The polarization sums are given by

$$\mathcal{P}_{\nu\nu'}^g = -g_{\nu\nu'}, \\ \mathcal{P}_{\mu\mu'}^V = \begin{cases} -g_{\mu\mu'} & \text{for } V = \gamma, \\ -g_{\mu\mu'} + \frac{p_V^\mu p_{V\mu'}}{p_V^2} & \text{for } V = Z, W^\pm \end{cases} \quad (3.82)$$

for the gluon and the electroweak gauge bosons, respectively. Combining the contributions of the bare one-loop diagrams (3.13) and the counterterms (3.47) and (3.53) for photon and  $Z$  boson production, respectively, we obtain for  $V = \gamma, Z$

$$\overline{\sum} |\mathcal{M}_1^{\bar{q}q' \rightarrow Vg}|^2 = 8\pi^2 \alpha \alpha_S (N_c^2 - 1) \sum_{\lambda=R,L} \left\{ \left( I_{q_\lambda}^V \right)^2 \left[ H_0 \left( 1 + 2 \text{Re} \delta C_{q_\lambda, V}^A \right) \right. \right. \\ \left. \left. + \frac{\alpha}{2\pi} \sum_{\Gamma=Z, W^\pm} \left( I^\Gamma I^{\bar{\Gamma}} \right)_{q_\lambda} H_1^A(M_\Gamma^2) \right] \right. \\ \left. + \frac{U_{VW^3}}{s_W} T_{q_\lambda}^3 I_{q_\lambda}^V \left[ 2H_0 \text{Re} \delta C_{q_\lambda, V}^N + \frac{\alpha}{2\pi} \frac{1}{s_W^2} H_1^N(M_W^2) \right] \right\}. \quad (3.83)$$

The coupling factors are specified in (2.31), (2.32) and (3.10). Similarly, combining the one-loop diagrams (3.23) for  $W$  production and the corresponding counterterms



(3.63) we find

$$\begin{aligned}
\overline{\sum} |\mathcal{M}_1^{\bar{q}q' \rightarrow W^\sigma g}|^2 = & 8\pi^2 \alpha \alpha_S (N_c^2 - 1) \left( I_{q_L}^{W^{-\sigma}} \right)^2 \left\{ H_0 \left[ 1 + 2\text{Re}(\delta C_{q_L, W}^A + \delta C_{q_L, W}^N) \right] \right. \\
& + \frac{\alpha}{2\pi} \sum_{\Gamma=A, Z} \left[ \left( \delta_{\Gamma\Gamma}^{\text{SU}(2)} \frac{C_F}{s_W^2} + \delta_{\Gamma\Gamma}^{\text{U}(1)} \frac{Y_{q_L}^2}{4c_W^2} \right) H_1^A(M_\Gamma^2) \right. \\
& + \delta_{\Gamma\Gamma}^{\text{SU}(2)} \frac{C_A}{2s_W^2} H_1^N(M_\Gamma^2) - \delta_{\Gamma\Gamma}^{\text{SU}(2)} \frac{C_F - (T_{q_L}^3)^2}{s_W^2} H_1^X(M_\Gamma^2) \\
& \left. \left. - X_\Gamma T_{q_L}^3 Y_{q_L} H_1^Y(M_\Gamma^2) \right] + \frac{\alpha}{2\pi} \frac{C_F - (T_{q_L}^3)^2}{s_W^2} H_1^X(M_W^2) \right\}, \quad (3.84)
\end{aligned}$$

with the couplings defined in (2.32), (2.33) and (3.18). The lowest-order contribution in (3.83) and (3.84) is represented through

$$H_0 = \frac{1}{8} \text{Tr} \left[ \not{p}_q \overline{\mathcal{S}}_0^{\mu\nu} \not{p}_{\bar{q}} \mathcal{S}_0^{\mu'\nu'} \right] \mathcal{P}_{\nu\nu'}^g \mathcal{P}_{\mu\mu'}^V = \frac{\hat{t}^2 + \hat{u}^2 + 2\hat{s} p_V^2}{\hat{t}\hat{u}}, \quad (3.85)$$

and the functions  $H_1^I(M_\Gamma^2)$  contain the kinematic information for the unpolarized squared loop amplitudes. They consist of linear combinations of the scalar integrals  $J_i(M_\Gamma^2)$  defined in (3.27)-(3.29) multiplying coefficient functions  $K_i^I(M_\Gamma^2)$  according to

$$H_1^I(M_\Gamma^2) = \sum_j K_j^I(M_\Gamma^2) \text{Re} \left[ J_j(M_\Gamma^2) \right] \quad \text{for } I = A, N, X, Y. \quad (3.86)$$

Explicit expressions for the functions  $K_j^I(M_\Gamma^2)$  are presented in Appendix D.1. In particular,  $H_1^A(M_\Gamma^2)$  and  $H_1^N(M_\Gamma^2)$  are the same functions for photon,  $Z$  and  $W$  production. This is due to our choice of the specific coupling structure for  $W$ -boson production<sup>6</sup>. The functions  $H_1^I(M_\Gamma^2)$  are related to the tensors  $\delta\mathcal{A}_{1,I}^{\mu\nu}(M_\Gamma^2)$  in (3.22) by

$$H_1^I(M_\Gamma^2) = \frac{1}{8} \text{Tr} \left[ \not{p}_{q'} \overline{\mathcal{S}}_0^{\mu\nu} \not{p}_{\bar{q}} \delta\mathcal{A}_{1,I}^{\mu'\nu'}(M_\Gamma^2) \right] \mathcal{P}_{\mu\mu'}^V \mathcal{P}_{\nu\nu'}^g. \quad (3.87)$$

We note that, the crossing and CP symmetry relations (2.24)–(2.25) imply that the functions  $H_1^A$  and  $H_1^N$  are symmetric with respect to the transformation  $\hat{t} \leftrightarrow \hat{u}$ . For neutral gauge boson production this can be trivially seen as the quarks in the initial state are of equal flavor and thus the couplings are the same. For charged gauge boson production it becomes apparent from the observation that the couplings associated with  $H_1^A$  and  $H_1^N$  are the same for  $q = u$  and  $q = d$ . The same argument holds for the function  $H_1^X$ , while  $H_1^Y$  is antisymmetric with respect to  $\hat{t} \leftrightarrow \hat{u}$  exchange since the corresponding coupling is proportional to  $T_{q_L}^3$  and has

---

<sup>6</sup>Furthermore, this structure would simply allow to obtain the photonic one-loop corrections for photon and  $Z$  production in association with a jet, which have not been considered in this work.

thus opposite signs for  $q = u$  and  $q = d$ .

The IR-singular part of the renormalized one-loop correction (3.84) for  $W^\sigma$  production are given by

$$\begin{aligned} \overline{\sum} |\mathcal{M}_{1,\text{IR}}^{\bar{q}q' \rightarrow W^\sigma g}|^2 &= \frac{\alpha}{2\pi} \text{Re} \left[ -Q_q Q_{q'} f_1^{\text{IR}} + \sigma Q_q f_2^{\text{IR}} - \sigma Q_{q'} f_3^{\text{IR}} \right] \\ &\times \left( \frac{4\pi\mu^2}{M_W^2} \right)^\varepsilon \Gamma(1 + \varepsilon) \overline{\sum} |\mathcal{M}_0^{\bar{q}q' \rightarrow W^\sigma g}|^2 \end{aligned} \quad (3.88)$$

with the functions  $f_i^{\text{IR}}$  defined in (3.78) and (3.79).

# Chapter 4

## High energy limit

In this chapter we present compact analytic results for the virtual corrections in the high energy limit, where the electroweak corrections are strongly enhanced by large logarithms. To this end, we derive results in the form of an asymptotic expansion in the limit where all kinematical invariants are much larger than the electroweak gauge boson scale, i.e. we require  $\hat{s}, |\hat{t}|, |\hat{u}| \gg M_W^2$ . In that case, the electroweak  $L$ -loop corrections are dominated by leading logarithmic (LL) contributions of the type  $\alpha^L \log^{2L}(\hat{s}/M_W^2)$  and further by next-to-leading logarithms (NLL) of the form  $\alpha^L \log^{2L-1}(\hat{s}/M_W^2)$ , and so on. At one-loop, the leading double logarithms originate from loop diagrams where virtual gauge bosons are exchanged between pairs of external legs. In particular, they arise from the integration region where the gauge boson momenta are (quasi-) soft and collinear to one of the external legs (cf. Fig. 4a). Single logarithmic contributions of one-loop diagrams result from (quasi-) collinear splittings from external legs where one of the internal lines is a virtual gauge boson (cf. Fig. 4b). Furthermore, the soft and collinear configurations contained in the wave renormalization constants yield single logarithms (cf. Fig. 4c). Logarithms from the coupling renormalization constants are of UV origin. They are controlled by the renormalization group.

In Sect. 4.1 we present the NNLL asymptotic expansion of the one-loop corrections, including leading and next-to-leading logarithms, as well as terms that are not logarithmically enhanced at high energies. Furthermore, in Sect. 4.2 we re-derive results to NLL accuracy using the process independent prescription of [36]. This derivation serves as a check of the NNLL result and introduces the specific notation which we will use to derive the two-loop terms up to NLL accuracy in Sect. 4.3. The leading logarithms at two-loop have been obtained by using the methods of Ref. [37] and include all angular dependent contributions. Furthermore, we use the fixed-order expansion of the process independent resummed expressions proposed in Ref. [38] to derive the NLLs at two-loop.

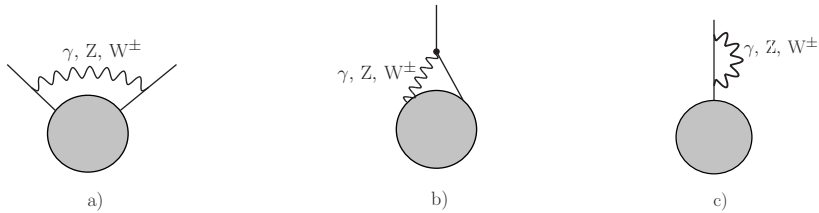


Figure 4.1: Origin of logarithmic contributions: a) Virtual gauge bosons exchange between pairs of external legs; b) Gauge boson splittings from external legs; c) Contributions from wave function renormalization constants.

## 4.1 NNLL approximation at one-loop

In this section we discuss the next-to-next-leading logarithmic (NNLL) approximation to the process  $\bar{q}q' \rightarrow Vg$  with  $V = \gamma, Z, W^\pm$ . This approximation accounts for all contributions that are not suppressed by powers of  $M_W^2/\hat{s}$ . In particular, it includes double and single logarithms as well as terms that are not logarithmically enhanced in the high-energy limit (e.g. logarithms of  $\hat{t}/\hat{s}$  or  $\pi^2$ -terms). In other words, the NNLL approximation provides results with a precision of the order  $(M_W^2/\hat{s}) \ln^2(\hat{s}/M_W^2)$  wrt. the full one-loop calculation. In the following, we sketch the derivation of the NNLL approximation, which has been obtained from the full one-loop calculation.

For charged gauge boson production we derive the high energy approximation for the IR-finite part of the electroweak corrections, obtained by subtracting the IR divergent piece from the renormalized one-loop result (3.84), which cancels with the real corrections. Thus, we derive the high energy approximation for the quantity

$$\overline{\sum} |\mathcal{M}_{1,\text{fin}}^{\bar{q}q' \rightarrow Vg}|^2 = \overline{\sum} |\mathcal{M}_1^{\bar{q}q' \rightarrow Vg}|^2 - \overline{\sum} |\mathcal{M}_{1,\text{IR}}^{\bar{q}q' \rightarrow Vg}|^2, \quad (4.1)$$

where for neutral gauge boson production  $V = \gamma, Z$  the subtracted IR-singular term in (4.1) is absent. We consider the functions  $H_1^{I,\text{fin}}$ , corresponding to the IR-finite part of the functions  $H_1^I$  in (3.86), and perform the following three steps:

- First, we derive analytic expressions in the high energy limit for the IR-finite loop integrals using the general prescription of Ref. [39]. The IR-singular integrals, expressed as  $J_i(M_\gamma^2) = J_i^{\text{IR}} + J_i^{\text{fin}}$  in (3.68), are expanded only for the finite parts while the singular contributions are kept unchanged.
- In a second step, we expand the functions  $H_1^{I,\text{fin}}$  for  $M_W^2/\hat{s} \rightarrow 0$ .
- Finally, we simplify non-logarithmic expressions depending on the ratio  $M_Z/M_W$  by expanding in  $s_w^2 = 1 - M_W^2/M_Z^2$ , keeping only terms up to the first order<sup>1</sup> in  $s_w^2$ .

<sup>1</sup>In practice we find that all terms of  $\mathcal{O}(s_w^2)$  cancel in the result.

In the first step, we reduce the IR-finite four-point functions in (3.29) in terms of four three-point functions according to the general result from Ref. [39]

$$\begin{aligned}
D_0(s_1, s_2, s_3, s_4, s_5, s_6; m_0^2, m_1^2, m_2^2, m_3^2) &\stackrel{\text{NNLL}}{=} -\frac{1}{s_5 s_6} \left[ \ln^2 \left( \frac{-s_5 - i\epsilon}{-s_6 - i\epsilon} \right) + \pi^2 \right] \\
&+ \frac{1}{s_5} \left[ C_0(s_2, s_6, s_3; m_2^2, m_1^2, m_3^2) + C_0(s_4, s_6, s_1; m_0^2, m_3^2, m_1^2) \right] \\
&+ \frac{1}{s_6} \left[ C_0(s_1, s_5, s_2; m_1^2, m_0^2, m_2^2) + C_0(s_3, s_5, s_4; m_3^2, m_2^2, m_0^2) \right]. \quad (4.2)
\end{aligned}$$

Furthermore, all remaining IR-finite three-point functions can be expressed through the relation [39]

$$\begin{aligned}
C_0(s_1, s_{12}, s_2; m_0^2, m_1^2, m_2^2) &\stackrel{\text{NNLL}}{=} \frac{1}{s_{12}} \left[ \frac{1}{2} \ln^2 \left( \frac{-s_{12} - i\epsilon}{m_0^2 - i\epsilon} \right) \right. \\
&- \int_0^1 dx \frac{1}{x} \ln \left( 1 + \frac{m_1^2 - m_0^2 - s_1}{m_0^2 - i\epsilon} x + \frac{s_1^2}{m_0^2 - i\epsilon} x^2 \right) \\
&\left. - \int_0^1 dx \frac{1}{x} \ln \left( 1 + \frac{m_2^2 - m_0^2 - s_2}{m_0^2 - i\epsilon} x + \frac{s_2^2}{m_0^2 - i\epsilon} x^2 \right) \right] \quad (4.3)
\end{aligned}$$

for  $m_0^2 \neq 0$  and

$$\begin{aligned}
C_0(s_1, s_{12}, s_2; m_0^2, m_1^2, m_2^2) &\stackrel{\text{NNLL}}{=} \frac{1}{s_{12}} \left[ \ln \left( \frac{-s_{12} - i\epsilon}{m_1^2 - s_1 - i\epsilon} \right) \ln \left( \frac{-s_{12} - i\epsilon}{m_2^2 - s_2 - i\epsilon} \right) \right. \\
&\left. + \text{Li}_2 \left( -\frac{s_1}{m_1^2 - s_1 - i\epsilon} \right) + \text{Li}_2 \left( -\frac{s_2}{m_2^2 - s_2 - i\epsilon} \right) \right] \quad (4.4)
\end{aligned}$$

for  $m_0^2 = 0$ ,  $s_1 \neq m_1^2$ ,  $s_2 \neq m_2^2$ . Dilogarithms appearing in (4.3) and (4.4) can be further expanded in the limit  $M_W^2/\hat{s} \rightarrow 0$  and yield logarithms.

Finally, the NNLL expansion of the functions  $H_1^{I,\text{fin}}(M_\Gamma^2)$  can be written in the general form

$$H_1^{I,\text{fin}}(M_\Gamma^2) \stackrel{\text{NNLL}}{=} \text{Re} \left[ g_0^I(M_\Gamma^2) \frac{\hat{t}^2 + \hat{u}^2}{\hat{t}\hat{u}} + g_1^I(M_\Gamma^2) \frac{\hat{t}^2 - \hat{u}^2}{\hat{t}\hat{u}} + g_2^I(M_\Gamma^2) \right]. \quad (4.5)$$

This expression involves the rational function  $(\hat{t}^2 + \hat{u}^2)/\hat{t}\hat{u}$ , which has the same angular behavior as the squared Born amplitude (2.38) in the high-energy limit, and two other rational functions, which describe different angular dependencies. The functions  $g_i^I$  consist of logarithms of the kinematical invariants, masses and constants. The loop diagrams involving  $Z$  and  $W$  bosons, with mass  $M_\Gamma = M_Z, M_W$ , yield for the non-Abelian contribution  $H_1^{\text{N,fin}}(M_\Gamma^2)$

$$g_0^{\text{N}}(M_\Gamma^2) = 2 \left[ \bar{\Delta}_{\text{UV}} + (1 - \delta_{VZ}) \ln \left( \frac{M_Z^2}{M_W^2} \right) + \ln \left( \frac{M_\Gamma^2}{M_W^2} \right) \right] + \ln^2 \left( \frac{-\hat{s}}{M_\Gamma^2} \right) - \frac{1}{2} \left[ \ln^2 \left( \frac{-\hat{t}}{M_\Gamma^2} \right) \right]$$

$$\begin{aligned}
& + \ln^2 \left( \frac{-\hat{t}}{M_W^2} \right) + \ln^2 \left( \frac{-\hat{u}}{M_\Gamma^2} \right) + \ln^2 \left( \frac{-\hat{u}}{M_W^2} \right) \Big] + \ln^2 \left( \frac{\hat{t}}{\hat{u}} \right) - \frac{3}{2} \left[ \ln^2 \left( \frac{\hat{t}}{\hat{s}} \right) \right. \\
& \left. + \ln^2 \left( \frac{\hat{u}}{\hat{s}} \right) \right] - 2\pi^2 + 2(1 - \delta_{V\gamma}) \left( -\frac{\pi^2}{9} - \frac{\pi}{\sqrt{3}} + 2 \right), \\
g_1^N(M_\Gamma^2) &= \frac{1}{2} \left[ \ln^2 \left( \frac{\hat{u}}{\hat{s}} \right) - \ln^2 \left( \frac{\hat{t}}{\hat{s}} \right) \right], \\
g_2^N(M_\Gamma^2) &= -2 \left[ \ln^2 \left( \frac{\hat{t}}{\hat{s}} \right) + \ln^2 \left( \frac{\hat{u}}{\hat{s}} \right) + \ln \left( \frac{\hat{t}}{\hat{s}} \right) + \ln \left( \frac{\hat{u}}{\hat{s}} \right) \right] + 2 \ln \left( \frac{M_\Gamma^2}{M_W^2} \right) - 4\pi^2, \quad (4.6)
\end{aligned}$$

where  $\bar{\Delta}_{UV}$  is defined in (3.34) and the symbols  $\delta_{VZ}$  and  $\delta_{V\gamma}$  denote the usual Kronecker-Delta depending on the external gauge boson  $V$ . For the Abelian contributions  $H_1^{A,\text{fin}}(M_\Gamma^2)$  with  $\Gamma = Z, W$  we find

$$\begin{aligned}
g_0^A(M_\Gamma^2) &= \bar{\Delta}_{UV} + \ln \left( \frac{M_Z^2}{M_\Gamma^2} \right) - \ln^2 \left( \frac{-\hat{s}}{M_\Gamma^2} \right) + 3 \ln \left( \frac{-\hat{s}}{M_\Gamma^2} \right) + \frac{3}{2} \left[ \ln^2 \left( \frac{\hat{t}}{\hat{s}} \right) + \ln^2 \left( \frac{\hat{u}}{\hat{s}} \right) \right. \\
& \left. + \ln \left( \frac{\hat{t}}{\hat{s}} \right) + \ln \left( \frac{\hat{u}}{\hat{s}} \right) \right] + \frac{7\pi^2}{3} - 3, \\
g_1^A(M_\Gamma^2) &= -g_1^N(M_W^2) + \frac{3}{2} \left[ \ln \left( \frac{\hat{u}}{\hat{s}} \right) - \ln \left( \frac{\hat{t}}{\hat{s}} \right) \right], \\
g_2^A(M_\Gamma^2) &= -g_2^N(M_W^2). \quad (4.7)
\end{aligned}$$

The functions  $H_1^{X,\text{fin}}(M_\Gamma^2)$  and  $H_1^{Y,\text{fin}}(M_\Gamma^2)$ , which are absent for photon and  $Z$  production, yield for  $W$  production in the high energy limit

$$\begin{aligned}
g_0^X(M_\Gamma^2) &= 0, \\
g_1^X(M_\Gamma^2) &= 0, \\
g_2^X(M_\Gamma^2) &= -2 \left[ 2 \ln \left( \frac{-\hat{s}}{M_\Gamma^2} \right) + \ln \left( \frac{\hat{t}}{\hat{s}} \right) + \ln \left( \frac{\hat{u}}{\hat{s}} \right) - 3 \right], \\
g_0^Y(M_\Gamma^2) &= \ln^2 \left( \frac{-\hat{t}}{M_W^2} \right) - \ln^2 \left( \frac{-\hat{t}}{M_\Gamma^2} \right) - \ln^2 \left( \frac{-\hat{u}}{M_W^2} \right) + \ln^2 \left( \frac{-\hat{u}}{M_\Gamma^2} \right), \\
g_1^Y(M_\Gamma^2) &= 0, \\
g_2^Y(M_\Gamma^2) &= 2 \ln \left( \frac{\hat{t}}{\hat{u}} \right) \quad (4.8)
\end{aligned}$$

for the cases with massive bosons in loops ( $\Gamma = Z, W^\pm$ ). In addition, for the loop diagrams involving photons ( $\Gamma = \gamma$ ), after subtraction of the IR-singular parts, we obtain

$$\begin{aligned}
g_0^N(M_\gamma^2) &= g_0^N(M_W^2) - \frac{7\pi^2}{9} + \frac{2\pi}{\sqrt{3}}, \\
g_0^A(M_\gamma^2) &= g_0^A(M_W^2) + \pi^2,
\end{aligned}$$

$$\begin{aligned}
g_0^I(M_\gamma^2) &= g_0^I(M_W^2) & \text{for } I = X, Y, \\
g_1^I(M_\gamma^2) &= g_1^I(M_W^2) & \text{for } I = A, N, X, Y, \\
g_2^I(M_\gamma^2) &= g_2^I(M_W^2) & \text{for } I = A, N, X, Y.
\end{aligned} \tag{4.9}$$

The results (4.6)–(4.9), for the processes  $\bar{q}q' \rightarrow Vg$ , are defined for arbitrary values of the Mandelstam invariants and can easily be translated to the other partonic processes in (2.3) by means of the crossing relations (2.24) and (2.25). Logarithms with negative arguments in (4.6)–(4.9) are defined through the usual  $i\epsilon$  prescription,  $\hat{r} \rightarrow \hat{r} + i\epsilon$  for  $\hat{r} = \hat{s}, \hat{t}, \hat{u}$ .

Let us now consider the contributions of the counterterms  $\delta C_{q\lambda, V}^A$  and  $\delta C_{q\lambda, V}^N$ . These contributions, consisting of on-shell self-energies and their derivatives, do not depend on the scattering energy and are free from large logarithms. In the case of  $Z$  boson production we present compact approximate expressions for the counterterms (3.48) (in the  $\overline{\text{MS}}$ -scheme). In order to simplify the relatively complicated expressions for the gauge boson self-energies we apply

- a heavy-top expansion including terms of order  $\log(m_t)$  and  $(1/m_t)^0$  and setting  $m_b = 0$ ,
- a first-order expansion in the  $Z$ - $W$  mass difference, using  $1 - M_W^2/M_Z^2 = s_w^2$  as expansion parameter,
- the light-Higgs approximation  $M_H = M_Z$ .

The resulting expressions for the renormalization constants associated with the  $Z$ -boson wave function read

$$\begin{aligned}
\delta \tilde{Z}_{AZ} &= \frac{\alpha}{4\pi} \frac{1}{s_w c_w} \left[ - \left( \frac{7 + 34s_w^2}{3} + 4c_w^2(\rho - 1) \right) \bar{\Delta}_{UV} - \frac{4}{9}(3 - 8s_w^2) \log \left( \frac{m_t^2}{M_Z^2} \right) \right. \\
&\quad \left. + (17 - 36s_w^2) \frac{\pi}{\sqrt{3}} - \frac{8}{27}(78 - 89s_w^2) \right], \\
\delta \tilde{Z}_{ZZ} &= \frac{\alpha}{4\pi} \frac{1}{s_w^2} \left[ - \frac{5 - 10s_w^2 + 46s_w^4}{6c_w^2} \bar{\Delta}_{UV} + \frac{3 - 5s_w^2}{6} \log \left( \frac{m_t^2}{M_Z^2} \right) \right. \\
&\quad \left. + \frac{11 - 37s_w^2}{6} \frac{\pi}{\sqrt{3}} - \frac{113 - 573s_w^2}{36} \right].
\end{aligned} \tag{4.10}$$

For the counterterms in (3.48) we obtain the compact expressions

$$\begin{aligned}
\delta \tilde{C}_{q\lambda, Z}^A &= \frac{\alpha}{4\pi} \left\{ - \sum_{V=Z, W^\pm} (I^V I^{\bar{V}})_{q\lambda} \left( \bar{\Delta}_{UV} - \frac{1}{2} \right) \right. \\
&\quad \left. - \frac{15 - 49s_w^2}{36s_w^2} \log \left( \frac{m_t^2}{M_Z^2} \right) + \frac{113 - 253s_w^2}{12s_w^2} \frac{\pi}{\sqrt{3}} - \frac{105}{8s_w^2} + \frac{4783}{216} \right\},
\end{aligned}$$

$$\delta\tilde{C}_{q\lambda,Z}^N = -\frac{\alpha}{4\pi} \left\{ \frac{2}{s_w^2} \bar{\Delta}_{UV} + \frac{1}{2s_w^2 c_w^2} \left[ -\frac{4}{9} (3 - 8s_w^2) \log\left(\frac{m_t^2}{M_Z^2}\right) + (17 - 36s_w^2) \frac{\pi}{\sqrt{3}} - \frac{8}{27} (78 - 89s_w^2) \right] \right\}. \quad (4.11)$$

The contribution of the counterterms for  $W$  production to the IR-finite part of the one-loop result is obtained by subtracting the IR-divergent part of the wavefunction renormalization constants (3.65). We evaluate these IR-finite parts of the counterterms in numerical form without applying any approximation. Using the input parameters specified in Appendix A we obtain

$$\begin{aligned} \delta C_{qL,W}^{A,\text{fin}} &= \frac{1}{2} (\delta Z_{uL}^{\text{fin}} + \delta Z_{dL}^{\text{fin}}) = \delta C_{qL,W}^A|_{UV} + 5.57 \times 10^{-4}, \\ \delta C_{qL,W}^{N,\text{fin}} &= \frac{1}{2} \left( \delta Z_W^{\text{fin}} + \frac{\delta g_2^2}{g_2^2} \right) = \delta C_{qL,W}^N|_{UV} - 1.49 \times 10^{-3}. \end{aligned} \quad (4.12)$$

For photon production, the corresponding counterterms are quite compact and we do not apply any approximation.

## 4.2 NLL approximation at one-loop

In this section we present the next-to-leading logarithmic (NLL) approximation of the electroweak one-loop corrections to the process  $\bar{q}q' \rightarrow Vg$ . This approximation accounts for contributions from double and single logarithms that grow with energy. We derive these NLL terms using the general prescription of [36], i.e. independently from the complete one-loop calculation. This serves as a cross-check of the large logarithmic contributions that have been derived with the NNLL approximation in the previous section. Furthermore, with the discussion of this method we can introduce the specific notation which will be used to derive the NLLs at the two-loop level.

The method presented in [36] provides a prescription to derive the complete next-to-leading logarithmic corrections at one-loop for exclusive processes with arbitrary external particles. Within this method, the systematic treatment of the electroweak corrections at high energies is performed in a symmetric way for photon,  $Z$  and  $W$  boson loops, rather than to split into electromagnetic and weak parts. To this end, logarithms originating from photon and  $Z$  boson loops are split into two parts: i.) the contributions of a fictitious heavy photon and a  $Z$  boson with mass  $M_W$ , which are added to the  $W$  boson loops resulting in a “symmetric-electroweak” (sew) part and ii.) the remaining contributions originating from the gap of the photon- and  $Z$ -boson mass wrt. the mass of the  $W$  boson. The latter contributions are denoted by the “subtracted electromagnetic” (sem) part and are IR-divergent, regulated with an infinitesimal photon mass  $\lambda$ .

Generally, at  $L$ -loop level the NLL approximation accounts for logarithms of the form  $\ln^{2L}(\hat{s}/M_W^2)$  and  $\ln^{2L-1}(\hat{s}/M_W^2)$ . Using the shorthand  $L_{\hat{r}}^k = \ln^k(|\hat{r}|/M_W^2)$ ,



the angular dependent logarithms with  $\hat{r} = \hat{t}, \hat{u}$  can be systematically expanded according to

$$L_{\hat{r}}^{2L} = L_{\hat{s}}^{2L} + 2L \log \left( \frac{|\hat{r}|}{\hat{s}} \right) L_{\hat{s}}^{2L-1} + \mathcal{O}(L_{\hat{s}}^{2L-2}), \quad L_{\hat{r}}^{2L-1} = L_{\hat{s}}^{2L-1} + \mathcal{O}(L_{\hat{s}}^{2L-2}). \quad (4.13)$$

Denoting the lowest-order matrix element for the process  $\phi_{i_1}(p_1) \dots \phi_{i_n}(p_n) \rightarrow 0$  by

$$\mathcal{M}_0^{i_1 \dots i_n}(p_1, \dots, p_n) \quad (4.14)$$

the NLL corrections at one-loop level assume the form

$$\delta \mathcal{M}_1^{i_1 \dots i_n}(p_1, \dots, p_n) \stackrel{\text{NLL}}{=} \mathcal{M}_0^{i'_1 \dots i'_n}(p_1, \dots, p_n) (\delta_1)_{i'_1 i_1 \dots i'_n i_n}. \quad (4.15)$$

These corrections factorize into the lowest-order matrix element  $\mathcal{M}_0^{i'_1 \dots i'_n}(p_1 \dots p_n)$  for the process  $\phi_{i'_1}(p_1) \dots \phi_{i'_n}(p_n) \rightarrow 0$  and the correction matrix  $\delta_1$  with the external fields as indices. This correction matrix can be split into various contributions according to their origin

$$\delta_1 = \frac{\alpha}{4\pi} \left( \delta^{\text{LSC}} + \delta^{\text{SSC}} + \delta^{\text{C}} + \delta^{\text{PR}} \right). \quad (4.16)$$

In the following we present the general expressions for these contributions and subsequently apply them to the process  $\bar{q}q' \rightarrow Vg$  with  $V = \gamma, Z, W^\pm$ . The leading soft-collinear (LSC) corrections in (4.16) arise from angular-independent contributions of diagrams where virtual gauge bosons are exchanged between pairs of external legs. The explicit form of the LSC correction reads

$$\delta^{\text{LSC}} \mathcal{M}_1^{i_1 \dots i_n} = \sum_{k=1}^n \delta_{i'_k i_k}^{\text{LSC}}(k) \mathcal{M}_0^{i_1 \dots i'_k \dots i_n} \quad (4.17)$$

with

$$\delta_{i'_k i_k}^{\text{LSC}}(k) = -\frac{1}{2} \left[ C_{i'_k i_k}^{\text{ew}}(k) L_{\hat{s}}^2 - 2(I^Z(k))_{i'_k i_k}^2 \ln \left( \frac{M_Z^2}{M_W^2} \right) L_{\hat{s}} + \delta_{i'_k i_k} (I^\gamma)^2_{i_k} L^{\text{sem}}(M_k^2) \right]. \quad (4.18)$$

$C_{i'_k i_k}^{\text{ew}}$  is the electroweak Casimir operator, which is defined together with the couplings  $I^V$  in (2.31)–(2.34).  $\delta_{i'_k i_k}$  is the usual Kronecker symbol. The function  $L^{\text{sem}}$  contains all logarithms of the subtracted electromagnetic part and is given by

$$L^{\text{sem}}(M_k^2) = 2L_{\hat{s}} \ln \left( \frac{M_W^2}{\lambda^2} \right) + \ln^2 \left( \frac{M_W^2}{\lambda^2} \right) - \ln^2 \left( \frac{M_k^2}{\lambda^2} \right), \quad (4.19)$$

where  $M_k$  is the mass of particle  $\phi_k$ . The subleading soft-collinear (SSC) contribution in (4.16) accounts for the angular-dependent parts of virtual gauge bosons exchange

between pairs of external legs. The corresponding correction matrix  $\delta^{\text{SSC}}$  acts on the lowest-order matrix element according to

$$\delta^{\text{SSC}} \mathcal{M}_1^{i_1 \dots i_n} = \sum_{k=1}^n \sum_{l < k} \sum_{V=A,Z,W^\pm} \delta_{i'_k i_k i'_l i_l}^{V,\text{SSC}}(k,l) \mathcal{M}_0^{i_1 \dots i'_k \dots i'_l \dots i_n} \quad (4.20)$$

with

$$\begin{aligned} \delta_{i'_k i_k i'_l i_l}^{V,\text{SSC}} &= 2L_{\hat{s}} \ln \left( \frac{|(p_k + p_l)^2|}{\hat{s}} \right) I_{i'_k i_k}^V(k) I_{i'_l i_l}^{\bar{V}}(l) \\ &+ \delta_{V\gamma} \ln \left( \frac{M_W^2}{\lambda^2} \right) \ln \left( \frac{|(p_k + p_l)^2|}{\hat{s}} \right) I_{i'_k i_k}^\gamma(k) I_{i'_l i_l}^\gamma(l). \end{aligned} \quad (4.21)$$

The remaining contributions from  $\delta^{\text{C}}$  and  $\delta^{\text{PR}}$  in (4.16) correspond to quasi-collinear (C) gauge boson splittings and parameter renormalization (PR), respectively. They contain only single logarithms. The matrix  $\delta^{\text{C}}(k)$  acts in analogy to (4.17) on the lowest-order matrix element and reads for the massless fermionic contributions with isospin index  $\sigma$

$$\delta_{f\sigma f\sigma'}^{\text{C}}(f) = \delta_{\sigma\sigma'} \left\{ \frac{3}{2} C_f^{\text{ew}} L_{\hat{s}} + (I_{f\sigma}^\gamma)^2 \left[ \frac{1}{2} \ln \left( \frac{M_W^2}{m^2} \right) + \ln \left( \frac{M_W^2}{\lambda^2} \right) \right] \right\}. \quad (4.22)$$

The above logarithms depending on the infinitesimal regulators  $m$  and  $\lambda$  correspond to the subtracted electromagnetic part. Logarithms of the form  $L_{\hat{s}}$  resulting from gauge boson matrix elements of  $\delta^{\text{C}}$  have counterparts in the symmetric electroweak part of  $\delta^{\text{PR}}$  and cancel. This is a general feature of gauge boson production in fermion-antifermion annihilation at high energies, which has been proven in [36]. The remaining contributions of this cancellation can be logarithms of electromagnetic origin. These terms will be presented later for the case of gauge boson production in association with a jet.

In the following we present results for the NLL approximation of the electroweak corrections for the processes  $\bar{q}q' \rightarrow Vg$ . In addition, we neglect logarithms of  $M_Z/M_W$  and omit the electromagnetic contributions for the case of neutral gauge boson production. Evaluating the LSC contribution (4.17)–(4.18) for  $V = \gamma, Z$  we find

$$\begin{aligned} \delta^{\text{LSC}} \mathcal{M}_1^{\bar{q}q' \rightarrow Vg} &= -\frac{\alpha}{4\pi} L_{\hat{s}}^2 \left( C_{q\lambda}^{\text{w}} I_{q\lambda}^V + \frac{1}{2} I_{q\lambda}^\gamma C_{\gamma V}^{\text{w}} + \frac{1}{2} I_{q\lambda}^Z C_{ZV}^{\text{w}} \right) \mathcal{H}_0 \\ &= -\frac{\alpha}{4\pi} L_{\hat{s}}^2 \left( C_{q\lambda}^{\text{w}} I_{q\lambda}^V + \frac{U_{VW^3}}{s_w^3} T_{q\lambda}^3 \right) \mathcal{H}_0, \end{aligned} \quad (4.23)$$

where  $U_{VW^3}$  are the elements of the Weinberg mixing matrix defined in (3.10) and the weak Casimir operator for quarks is given by

$$C_{q\lambda}^{\text{w}} = C_{q\lambda}^{\text{w}} = \sum_{\Gamma=Z,W^\pm} \left( I^\Gamma I^{\bar{\Gamma}} \right)_{q'q\lambda} = C_{q\lambda}^{\text{ew}} - Q_q^2. \quad (4.24)$$

The symbol  $\mathcal{H}_0$  is related to the lowest order matrix element by

$$\mathcal{M}_0^{\bar{q}q' \rightarrow Vg} = I_{q'_\lambda q_\lambda}^V \mathcal{H}_0, \quad (4.25)$$

i.e. the gauge boson coupling to quarks is factored out. The SSC contributions for  $V = \gamma, Z$  is given by

$$\begin{aligned} \delta^{\text{SSC}} \mathcal{M}_1^{\bar{q}q' \rightarrow Vg} &= -\frac{\alpha}{4\pi} \frac{U_{VW^3}}{s_w^3} T_{q_\lambda}^3 2L_{\hat{s}} \left[ \ln \left( \frac{|\hat{t}|}{\hat{s}} \right) + \ln \left( \frac{|\hat{u}|}{\hat{s}} \right) \right] \mathcal{H}_0 \\ &= -\frac{\alpha}{4\pi} \frac{U_{VW^3}}{s_w^3} T_{q_\lambda}^3 \left[ L_{\hat{t}}^2 + L_{\hat{u}}^2 - 2L_{\hat{s}}^2 \right] \mathcal{H}_0, \end{aligned} \quad (4.26)$$

where, in the last step, we used the expansion (4.13). Furthermore, the fermionic contribution (4.22) to  $\delta^{\text{C}}$  reads

$$\delta^{\text{C}} \mathcal{M}_1^{\bar{q}q' \rightarrow Vg} = \frac{\alpha}{4\pi} 3L_{\hat{s}}^2 I_{q_\lambda}^V C_{q_\lambda}^{\text{w}} \mathcal{H}_0. \quad (4.27)$$

Indeed, we found a cancellation between  $\delta^{\text{PR}}$  and the corrections matrix elements  $\delta_{\gamma V}^{\text{C}}$  and  $\delta_{Z V}^{\text{C}}$  (defined in [36]). Finally, we present the complete result for the weak NLL approximation for neutral gauge boson production. Writing the unpolarized squared matrix element in the high energy approximation at one-loop as

$$\overline{\sum} |\mathcal{M}_{1,\text{fin}}^{\bar{q}q' \rightarrow Vg}|^2 \stackrel{\text{NLL}}{=} 8\pi\alpha\alpha_s (N_c^2 - 1) \frac{\hat{t}^2 + \hat{u}^2}{\hat{t}\hat{u}} \left[ A_V^{(0)} + \left( \frac{\alpha}{2\pi} \right) A_V^{(1)} \right] \quad (4.28)$$

the contribution of the lowest order for  $V = \gamma, Z$  reads

$$A_V^{(0)} = \sum_{\lambda=\text{R,L}} \left( I_{q_\lambda}^V \right)^2 \quad (4.29)$$

and the corresponding NLL part assumes the compact form

$$A_V^{(1)} = - \sum_{\lambda=\text{L,R}} I_{q_\lambda}^V \left[ I_{q_\lambda}^V C_{q_\lambda}^{\text{ew}} \left( L_{\hat{s}}^2 - 3L_{\hat{s}} \right) + \frac{U_{VW^3}}{s_w^3} T_{q_\lambda}^3 \left( L_{\hat{t}}^2 + L_{\hat{u}}^2 - L_{\hat{s}}^2 \right) \right]. \quad (4.30)$$

This result agrees with the NNLL approximation for photon and  $Z$  production when we neglect all constant terms in (4.6)–(4.9) and set  $M_Z = M_W$ . Furthermore, we find that for  $V = \gamma, Z$  the counterterms do not contribute to the NLL approximation

$$\delta C_{q_\lambda, V}^{\text{A}} \stackrel{\text{NLL}}{=} \delta C_V^{\text{N}} \stackrel{\text{NLL}}{=} 0. \quad (4.31)$$

Let us now turn to the electroweak NLL approximation for charged gauge boson production. For the process  $\bar{q}q' \rightarrow W^\sigma g$  we obtain the LSC contribution

$$\delta^{\text{LSC}} \mathcal{M}_1^{\bar{q}q' \rightarrow W^\sigma g} = -\frac{\alpha}{4\pi} \left\{ L_{\hat{s}}^2 \left( I_{q_L q'_L}^{W^{-\sigma}} C_{q_\lambda}^{\text{ew}} + \frac{1}{2} I_{q_L q'_L}^{W^{-\sigma}} C_{W^\sigma}^{\text{ew}} \right) \right.$$

$$\begin{aligned}
& -\frac{1}{2} \left( Q_W^2 L^{\text{sem}}(M_W^2) + (Q_{q'}^2 + Q_q^2) L^{\text{sem}}(m^2) \right) I_{q_L q'_L}^{W^{-\sigma}} \Big\} \mathcal{H}_0 \\
& = -\frac{\alpha}{4\pi} \left\{ L_{\hat{s}}^2 \left( C_{q_L}^{\text{ew}} + \frac{C_A}{2s_w^2} \right) + Q_q Q_{q'} L^{\text{sem}}(m^2) \right. \\
& \quad \left. - \frac{1}{2} (\sigma Q_q - \sigma Q_{q'}) \left( L^{\text{sem}}(M_W^2) + L^{\text{sem}}(m^2) \right) \right\} I_{q_L q'_L}^{W^{-\sigma}} \mathcal{H}_0 \quad (4.32)
\end{aligned}$$

where  $C_A$  and the electroweak Casimir operators  $C_{q_\lambda}^{\text{ew}}$  are defined in (2.34). As we consider the full electroweak corrections, logarithms of the infinitesimal regulators  $m^2$  and  $\lambda^2$  are present. They are contained in the functions  $L^{\text{sem}}$  given in (4.19). The SSC correction reads

$$\begin{aligned}
\delta^{\text{SSC}} \mathcal{M}_1^{\bar{q}q' \rightarrow W^\sigma g} & = -\frac{\alpha}{4\pi} \left\{ \frac{C_A}{2s_w^2} \left( L_t^2 + L_u^2 - 2L_s^2 \right) + 2 \ln \left( \frac{\lambda^2}{M_W^2} \right) \right. \\
& \quad \left. \times \left[ \sigma Q_q \ln \left( \frac{|\hat{t}|}{\hat{s}} \right) - \sigma Q_{q'} \ln \left( \frac{|\hat{u}|}{\hat{s}} \right) \right] \right\} I_{q_L q'_L}^{W^{-\sigma}} \mathcal{H}_0. \quad (4.33)
\end{aligned}$$

The remaining corrections come from  $\delta^{\text{C}}$  and  $\delta^{\text{PR}}$ . Again, we find the cancellation between the symmetric-electroweak parts of  $\delta^{\text{PR}}$  with the matrix elements of  $\delta^{\text{C}}$  corresponding to the gauge bosons. The resulting expression for the sum of both contributions is

$$\begin{aligned}
(\delta^{\text{C}} + \delta^{\text{PR}}) \mathcal{M}_1^{\bar{q}q' \rightarrow W^\sigma g} & = \frac{\alpha}{4\pi} \left\{ 3L_{\hat{s}} C_{q_L}^{\text{ew}} + 2Q_q Q_{q'} l^{\text{sem}}(m^2) \right. \\
& \quad \left. - (\sigma Q_q - \sigma Q_{q'}) \left( l^{\text{sem}}(M_W^2) + l^{\text{sem}}(m^2) \right) \right\} I_{q_L q'_L}^{W^{-\sigma}} \mathcal{H}_0, \quad (4.34)
\end{aligned}$$

where the term proportional to  $L_{\hat{s}}$  corresponds to the fermionic contributions of  $\delta^{\text{C}}$ . The functions  $l^{\text{sem}}$  in (4.34) contain logarithms originating from the subtracted electromagnetic part

$$l^{\text{sem}}(m) = \frac{1}{2} \ln \left( \frac{M_W^2}{m^2} \right) + \ln \left( \frac{M_W^2}{\lambda^2} \right), \quad (4.35)$$

that originate from photonic loops as a result of the gap between the electromagnetic and weak scales in  $\delta^{\text{C}}$  and  $\delta^{\text{PR}}$ . Finally, combining the contributions from (4.32)–(4.35) we can present the NLL approximation for the process  $\bar{q}q' \rightarrow W^\sigma g$  in the form of (4.28). The lowest-order contribution reads

$$A_W^{(0)} = \left( I_{q_L}^{W^\sigma} \right)^2 = \frac{1}{2s_w^2} \quad (4.36)$$

and the IR-finite part of the NLL approximation can be written in the form

$$A_W^{(1)} = -\frac{1}{2s_w^2} \left[ C_{q_L}^{\text{ew}} \left( L_{\hat{s}}^2 - 3L_{\hat{s}} \right) + \frac{C_A}{2s_w^2} \left( L_t^2 + L_u^2 - L_s^2 \right) \right]. \quad (4.37)$$

The IR-singular terms involving logarithms of the infinitesimal quark and photon masses  $m$  and  $\lambda$ , respectively, originate from the subtracted electromagnetic parts in (4.32), (4.33) and (4.34). Their contributions can be summarized as follows

$$\overline{\sum} |\mathcal{M}_{1,\text{IR}}^{\bar{q}q' \rightarrow W^\sigma g}|^2 \stackrel{\text{NLL}}{=} \frac{\alpha}{2\pi} \left\{ -Q_q Q_{q'} f_{1,\text{NLL}}^{\text{IR}} + \sigma Q_q f_{2,\text{NLL}}^{\text{IR}} - \sigma Q_{q'} f_{2,\text{NLL}}^{\text{IR}} \right\} \overline{\sum} |\mathcal{M}_0^{\bar{q}q' \rightarrow W^\sigma g}|^2 \quad (4.38)$$

with the functions

$$\begin{aligned} f_{1,\text{NLL}}^{\text{IR}} &= L^{\text{sem}}(m^2) - 2l^{\text{sem}}(m^2), \\ f_{2,\text{NLL}}^{\text{IR}} &= \frac{1}{2} \left( L^{\text{sem}}(M_W^2) + L^{\text{sem}}(m^2) \right) - l^{\text{sem}}(M_W^2) - l^{\text{sem}}(m^2) - 2 \ln \left( \frac{\lambda^2}{M_W^2} \right) \ln \left( \frac{|\hat{t}|}{\hat{s}} \right), \\ f_{3,\text{NLL}}^{\text{IR}} &= f_{2,\text{NLL}}^{\text{IR}} \Big|_{\hat{t} \leftrightarrow \hat{u}}. \end{aligned} \quad (4.39)$$

Inserting the definitions of the functions  $L^{\text{sem}}$  and  $l^{\text{sem}}$  (see (4.19), (4.35)) we find the relations

$$\begin{aligned} f_{1,\text{NLL}}^{\text{IR}} &\stackrel{\text{NLL}}{=} f_1^{\text{IR}}, \\ f_{2,\text{NLL}}^{\text{IR}} &\stackrel{\text{NLL}}{=} f_2^{\text{IR}}, \\ f_{3,\text{NLL}}^{\text{IR}} &\stackrel{\text{NLL}}{=} f_3^{\text{IR}}, \end{aligned} \quad (4.40)$$

where the functions  $f_i^{\text{IR}}$ , defined in (3.78), have been extracted from the full one-loop calculation. Thus, we can reproduce to NLL accuracy the IR-singular contributions of the full one-loop correction for  $W$  production by means of the subtracted electromagnetic parts derived within the framework of the NLL approximation [36].

### 4.3 NLL approximation at two-loop

Let us now present our results for the next-to-leading logarithmic approximation of the electroweak corrections up to two loops. As before, we consider corrections to the process  $\bar{q}q' \rightarrow Vg$  and derive all other contributions by CP and crossing symmetry. Using the prescription of Ref. [37], we derive an approximation which accounts for leading logarithms as well as for the angular-dependent subset of the next-to-leading logarithms (NLL<sub>a</sub>), i.e. all contributions of the form  $L_{\hat{r}}^4$  with  $\hat{r} = \hat{s}, \hat{t}, \hat{u}$ . Furthermore, we include the logarithms  $L_{\hat{s}}^3$ , which can be obtained by a fixed-order expansion of process-independent resummed expressions proposed in Ref. [38].

We begin with the discussion of the contribution of the  $L_{\hat{r}}^4$  terms. Similar to the derivation of the NLL corrections at one-loop, the methods of Ref. [37] treats the leading electroweak corrections at two-loop level in such a way that the IR-finite part corresponds to the symmetric electroweak part (sew) in which the electroweak corrections are regularized by a fictitious photon mass  $M_\gamma = M_W$  and furthermore  $M_Z = M_W$ . The remaining subtracted electromagnetic (sem) part corresponds to

the gap between the (vanishing) photon mass and the weak boson mass scale. The latter IR singular contribution is not considered in the present work for the process  $\bar{q}q' \rightarrow Vg$ . It would cancel with the corresponding real corrections of  $\mathcal{O}(\alpha^3)$ . Thus, we present the symmetric part of the electroweak corrections at two-loop level. In analogy to (3.1) the matrix element including two-loop effects can be written as

$$\mathcal{M}_2 = \mathcal{M}_0 + \delta\mathcal{M}_1 + \delta\mathcal{M}_2. \quad (4.41)$$

In Ref. [37] it was shown by an explicit two-loop calculation that the  $\text{NLL}_a$  terms result from the exponentiation of the corresponding one-loop corrections. Thus, up to  $\text{NLL}_a$  accuracy at two-loop we can cast (4.41) into the form

$$\mathcal{M}_2 \stackrel{\text{NLL}_a}{=} \mathcal{M}_0 \exp(\delta^{1,\text{sew}}) \exp(\delta^{1,\text{sem}}), \quad (4.42)$$

where  $\delta^{1,\text{sew}}$  and  $\delta^{1,\text{sem}}$  correspond to the symmetric electroweak and subtracted electromagnetic parts at one-loop, respectively. This splitting in the form of (4.42) is gauge invariant. As stated above, we consider the two-loop contribution from the symmetric electroweak part, and thus the contribution from  $\exp(\delta^{1,\text{sew}})$  only. The expression for  $\delta^{1,\text{sew}}$  is given by the corrections matrices that have been introduced in the previous section for the NLL approximation at one-loop. More precisely, for the considered  $\text{NLL}_a$  approximation at two-loop level we define  $\delta^{1,\text{sew}} = \delta^{\text{LSC}} + \delta^{\text{SSC}}$ , where logarithms involving the photon mass  $\lambda$  are omitted. The contributions of  $\delta^{\text{C}}$  and  $\delta^{\text{PR}}$  to  $\delta^{1,\text{sew}}$  are subleading and do not contribute in this approximation. Combining the relevant expressions of (4.18) and (4.21), we find

$$\delta^{1,\text{sew}} \stackrel{\text{NLL}_a}{=} \frac{\alpha}{4\pi} \left\{ -\frac{1}{2} \sum_{j=1}^n C^{\text{ew}}(j) L_s^2 + \sum_{\substack{j,k=1 \\ k \neq j}}^n \sum_{V=\gamma,Z,W^\pm} I^V(j) I^{\bar{V}}(k) L_s \ln \left( \frac{|2p_j \cdot p_k|}{\hat{s}} \right) \right\}, \quad (4.43)$$

which acts as a matrix with indices corresponding to  $n$  external legs. Using Eq. (4.42) and (4.43) the two-loop contribution to the symmetric electroweak part for the process  $\phi_{i_1}(p_1) \dots \phi_{i_n}(p_n) \rightarrow 0$  can generally be written as

$$\begin{aligned} \delta\mathcal{M}_{2,\text{sew}}^{i_1 \dots i_n} &\stackrel{\text{NLL}_a}{=} \frac{1}{2} \mathcal{M}_0 (\delta^{1,\text{sew}})^2 \\ &= \frac{1}{2} \left( \frac{\alpha}{4\pi} \right)^2 \left\{ \frac{1}{4} L_s^4 \left( \sum_{\substack{j,k=1 \\ k \neq j}}^n \mathcal{M}_0^{i_1 \dots i'_j \dots i'_k \dots i_n} C_{i'_j i_j}^{\text{ew}} C_{i'_k i_k}^{\text{ew}} + \sum_{j=1}^n \mathcal{M}_0^{i_1 \dots i'_j \dots i_n} C_{i'_j i_k}^{\text{ew}} C_{i_k i_j}^{\text{ew}} \right) \right. \\ &\quad - L_s^3 \sum_{\substack{j,k,l=1 \\ k \neq j, l \neq j, k}}^n \sum_{V=\gamma,Z,W^\pm} \mathcal{M}_0^{i_1 \dots i'_j \dots i'_k \dots i'_l \dots i_n} C_{i'_l i_l}^{\text{ew}} I_{i'_j i_j}^V I_{i'_k i_k}^{\bar{V}} \ln \left( \frac{|2p_j \cdot p_k|}{\hat{s}} \right) \\ &\quad \left. - 2L_s^3 \sum_{\substack{j,k=1 \\ k \neq j}}^n \sum_{V=\gamma,Z,W^\pm} \mathcal{M}_0^{i_1 \dots i'_j \dots i'_k \dots i_n} I_{i'_j i_l}^V C_{i'_l i_j}^{\text{ew}} I_{i'_k i_k}^{\bar{V}} \ln \left( \frac{|2p_j \cdot p_k|}{\hat{s}} \right) \right\}. \quad (4.44) \end{aligned}$$

Evaluating (4.44) explicitly for the processes  $\bar{q}q' \rightarrow Vg$  with  $V = \gamma, Z, W^\pm$  we find the two-loop corrections involving the leading logarithms  $L_s^4$  and the subset of angular-dependent next-to-leading logarithms  $L_s^3 \ln(\hat{r}/\hat{s})$  with  $\hat{r} = \hat{t}, \hat{u}$ .

Before presenting the explicit results, let us consider further contributions of the form  $L_s^3$ . These additional NLLs can be obtained using the methods proposed in Ref. [38]. More precisely, these corrections result from resummed double logarithmic contributions that are folded with logarithms from the electroweak renormalization group<sup>2</sup> (RG). To this end, the solutions of the infrared evolution equation (IREE) [14], which yield the leading logarithms to all orders, have been extended in [38] to include also effects from the running couplings. The desired subleading logarithms from the symmetric part of the electroweak two-loop corrections to the process  $\phi_{i_1}(p_1)\dots\phi_{i_n}(p_n) \rightarrow 0$  can be obtained from the expression

$$\delta\mathcal{M}_{2,\text{RG}}^{i_1\dots i_n}(\alpha_w, \alpha_Y) \stackrel{\text{NLL}}{=} \mathcal{M}_0^{i_1\dots i_n}(\alpha_w(\hat{s}), \alpha_Y(\hat{s})) \exp\left(-\sum_{k=1}^n W_{\phi_{i_k}}^{\text{RG}}(\hat{s}, M_W^2)\right), \quad (4.45)$$

by expanding up to two-loop order. We note that in Eq. (4.45) electroweak gauge bosons have to be implemented in the symmetric basis of the electroweak theory and mixing effects for photon and  $Z$  boson production have to be considered. The functions  $W_{\phi_{i_k}}^{\text{RG}}$  depend on the external particle  $\phi_{i_k}$  and read for massless quarks

$$\begin{aligned} W_q^{\text{RG}}(\hat{s}, M_W^2) &= \frac{\alpha_w(M_W^2)}{2\pi} C_F \left\{ \frac{1}{c} L_s \left[ \ln\left(\frac{\alpha_w(M_W^2)}{\alpha_w(\hat{s})}\right) - 1 \right] + \frac{1}{c^2} \frac{\alpha_w(M_W^2)}{\alpha_w(\hat{s})} \right\} \\ &+ \frac{\alpha_Y(M_W^2)}{2\pi} \left(\frac{Y_q}{2}\right)^2 \left\{ \frac{1}{c'} L_s \left[ \ln\left(\frac{\alpha_Y(M_W^2)}{\alpha_Y(\hat{s})}\right) - 1 \right] + \frac{1}{c'^2} \frac{\alpha_Y(M_W^2)}{\alpha_Y(\hat{s})} \right\} \\ &- \left[ \frac{\alpha_w(M_W^2)}{2\pi} C_F + \frac{\alpha_Y(M_W^2)}{2\pi} \left(\frac{Y_q}{2}\right)^2 \right] \frac{3}{2} L_s, \end{aligned} \quad (4.46)$$

and for gauge bosons  $\tilde{V} = W_i, B$  ( $i = 1, 2, 3$ ) in the symmetric basis of the electroweak theory

$$\begin{aligned} W_{\tilde{V}}^{\text{RG}}(\hat{s}, M_W^2) &= \frac{\alpha_w(M_W^2)}{2\pi} \delta_{\tilde{V},W} C_A \left\{ \frac{1}{c} L_s \left[ \ln\left(\frac{\alpha_w(M_W^2)}{\alpha_w(\hat{s})}\right) - 1 \right] + \frac{1}{c^2} \frac{\alpha_w(M_W^2)}{\alpha_w(\hat{s})} \right. \\ &\left. - \frac{1}{2} s_w^2 b_2 L_s \right\} - \delta_{\tilde{V},B} \frac{\alpha_Y(M_W^2)}{4\pi} c_w^2 b_1 L_s, \end{aligned} \quad (4.47)$$

where  $c = \alpha_w(M_W^2) b_2 s_w^2 / (4\pi)$  and  $c' = \alpha_Y(M_W^2) b_1 c_w^2 / (4\pi)$ . The running couplings in (4.45)–(4.47) have to be evaluated with

$$\alpha_Y(\hat{s}) = \frac{\alpha}{c_w^2} \frac{1}{1 + \frac{\alpha}{4\pi} b_1 L_s}, \quad \alpha_w(\hat{s}) = \frac{\alpha}{s_w^2} \frac{1}{1 + \frac{\alpha}{4\pi} b_2 L_s}, \quad (4.48)$$

---

<sup>2</sup>The resummation proposed in Ref. [38] relies on the assumption that effects from spontaneous breaking of the  $SU(2) \times U(1)$  symmetry can be neglected in the high-energy limit.

and correspond to the U(1) and SU(2) gauge symmetries, respectively. The one-loop  $\beta$ -function coefficients associated with these couplings are given by  $b_1 = -41/(6c_w^2)$  and  $b_2 = 19/(6s_w^2)$ .

Extending Eq. (4.28) for two-loop corrections, we can write the unpolarized squared matrix element in the high energy limit for the processes  $\bar{q}q' \rightarrow Vg$  as

$$\overline{\sum} |\mathcal{M}_{2,\text{fin}}^{\bar{q}q' \rightarrow Vg}|^2 \stackrel{\text{NLL}}{=} 8\pi\alpha\alpha_s(N_c^2 - 1) \frac{\hat{t}^2 + \hat{u}^2}{\hat{t}\hat{u}} \left[ A_V^{(0)} + \left(\frac{\alpha}{2\pi}\right) A_V^{(1)} + \left(\frac{\alpha}{2\pi}\right)^2 A_V^{(2)} \right]. \quad (4.49)$$

The functions  $A_V^{(0)}$  and  $A_V^{(1)}$  correspond to the contributions of the lowest-order and the NLL approximation of the one-loop corrections, respectively. They have been defined in (4.29),(4.30),(4.36) and (4.37). The two-loop correction factors  $A_V^{(2)}$  include the squared one-loop contributions and the interference of  $\delta\mathcal{M}_{2,\text{sew}}^{\bar{q}q' \rightarrow Vg}$  (4.44) plus the two-loop terms of  $\delta\mathcal{M}_{2,\text{RG}}^{\bar{q}q' \rightarrow Vg}$  (4.45) with the lowest-order contribution. For neutral gauge boson production ( $V = \gamma, Z$ ) this factor reads

$$\begin{aligned} A_V^{(2)} = & \sum_{\lambda=L,R} \left\{ \frac{1}{2} \left( I_{q_\lambda}^V C_{q_\lambda}^{\text{ew}} + \frac{U_{VW^3}}{s_w^3} T_{q_\lambda}^3 \right) \left[ I_{q_\lambda}^V C_{q_\lambda}^{\text{ew}} (L_s^4 - 6L_s^3) \right. \right. \\ & + \left. \frac{U_{VW^3}}{s_w^3} T_{q_\lambda}^3 (L_t^4 + L_u^4 - L_s^4) \right] - (\delta_{VZ} - \delta_{V\gamma}) \frac{T_{q_\lambda}^3 Y_{q_\lambda}}{8s_w^4} (L_t^4 + L_u^4 - L_s^4) \\ & \left. + \frac{1}{6} I_{q_\lambda}^V \left[ I_{q_\lambda}^V \left( \frac{b_1}{c_w^2} \left( \frac{Y_{q_\lambda}}{2} \right)^2 + \frac{b_2}{s_w^2} C_{F,q_\lambda} \right) + \frac{U_{VW^3}}{s_w^3} T_{q_\lambda}^3 b_2 \right] L_s^3 \right\}, \quad (4.50) \end{aligned}$$

where  $b_1$  and  $b_2$  are the one-loop  $\beta$ -function coefficients defined above, and the electroweak mixing matrix elements  $U_{VW^3}$  are given in (3.10). We stress that although the above results for photon and  $Z$  boson production can be put in the same form, their derivation requires separate calculation for each of the processes.

Finally, for the production of  $W$  bosons we find the two-loop correction factors

$$\begin{aligned} A_W^{(2)} = & \frac{1}{2s_w^2} \left\{ \frac{1}{2} \left( C_{q_L}^{\text{ew}} + \frac{C_A}{2s_w^2} \right) \left[ C_{q_L}^{\text{ew}} (L_s^4 - 6L_s^3) + \frac{C_A}{2s_w^2} (L_t^4 + L_u^4 - L_s^4) \right] \right. \\ & \left. + \frac{1}{6} \left[ \frac{b_1}{c_w^2} \left( \frac{Y_{q_L}}{2} \right)^2 + \frac{b_2}{s_w^2} \left( C_{F,q_L} + \frac{C_A}{2} \right) \right] L_s^3 \right\}, \quad (4.51) \end{aligned}$$

where  $b_1$  and  $b_2$  are the one-loop  $\beta$ -function coefficients defined above.



# Chapter 5

## Real photonic corrections for $W$ +jet production

As we have seen in Ch. 3, the virtual electroweak corrections to  $W$  boson production involve soft and collinear singularities associated with photonic loops. To cancel those IR singularities, real photon emission needs to be calculated. In this chapter, we consider the tree-level process  $\bar{q}q' \rightarrow W^\sigma g \gamma$ , which allows to cancel the corresponding singularities from the virtual corrections to the process  $\bar{q}q' \rightarrow W^\sigma g$  in a well-defined observable. The Feynman diagrams for this process are shown in Fig. 5.1. As discussed in (2.27), all other partonic reactions for  $W$  production are related by crossing and CP symmetry. Thus, the explicit calculation of the squared matrix elements needs to be done only once.

Similar to (3.4), we write the real emission matrix element for the process  $\bar{q}q' \rightarrow W^\sigma g \gamma$  as

$$\mathcal{M}_0^{\bar{q}q' \rightarrow W^\sigma g \gamma} = i e^2 g_S t^a \bar{v}(p_{\bar{q}}) \mathcal{M}_0^{L, \mu\nu\rho} \omega_L u(p_{q'}) \varepsilon_\mu^*(p_W) \varepsilon_\nu^*(p_g) \varepsilon_\rho^*(p_\gamma), \quad (5.1)$$

where the charge of the  $W$  boson is denoted by  $\sigma$ . The contribution from the Feynman diagrams in Fig. 5.1 can then be written in terms of three coupling structures

$$\mathcal{M}_0^{L, \mu\nu\rho} = \left( I^\gamma I^{W^{-\sigma}} \right)_{q_L q'_L} D_5^{\mu\nu\rho} + \left( I^{W^{-\sigma}} I^\gamma \right)_{q_L q'_L} D_6^{\mu\nu\rho} + \frac{i}{s_W} \varepsilon^{W^{-\sigma} W^\sigma \gamma} I_{q_L q'_L}^{W^{-\sigma}} D_7^{\mu\nu\rho}, \quad (5.2)$$

where the tensors  $D_5^{\mu\nu\rho}$  and  $D_6^{\mu\nu\rho}$  describe the contributions of the diagrams r1, r5, r6 and r2, r3, r7, respectively.  $D_7^{\mu\nu\rho}$  corresponds to the diagrams r4, r8 involving the Yang-Mills coupling. The gauge boson coupling matrices  $I^\gamma$  and  $I^W$  are defined in Sect. 2.4. The squared matrix element, summed over polarization and color as well as averaged over initial-state polarization, is obtained by

$$\overline{|\mathcal{M}_0^{\bar{q}q' \rightarrow W^\sigma g \gamma}|^2} = 32\pi^3 \alpha^2 \alpha_S (N_c^2 - 1) \text{Tr} \left[ \not{p}_{q'} \overline{\mathcal{M}}_0^{L, \mu\nu\rho} \not{p}_{\bar{q}} \mathcal{M}_0^{L, \mu'\nu'\rho'} \right] \mathcal{P}_{\mu\mu'}^V \mathcal{P}_{\nu\nu'}^g \mathcal{P}_{\rho\rho'}^\gamma \quad (5.3)$$

with  $\overline{\mathcal{M}} = \gamma^0 \mathcal{M}^\dagger \gamma^0$ . The tensors  $\mathcal{P}_{\mu\mu'}^V$ , corresponding to the vector boson polarization sums, are defined in (3.82). Evaluating the trace and the polarization sums

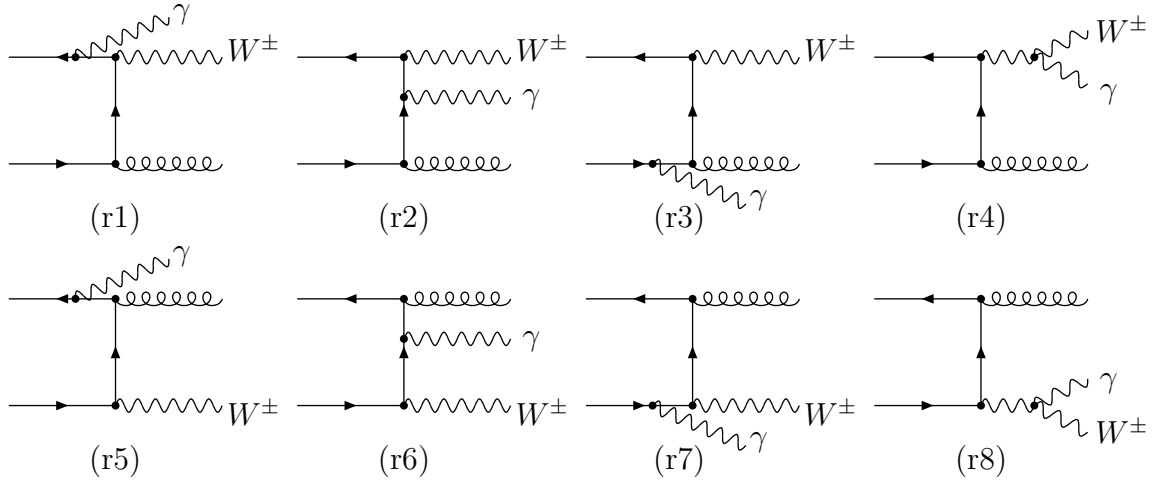


Figure 5.1: Tree-level diagrams for the process  $\bar{q}q' \rightarrow W^\pm g\gamma$ .

explicitely we obtain the squared matrix element (5.3) in terms of three kinematical functions and coupling factors

$$\begin{aligned} \overline{\sum} |\mathcal{M}_0^{\bar{q}q' \rightarrow W^\sigma g\gamma}|^2 &= 32\pi^3 \alpha^2 \alpha_s (N_c^2 - 1) (I_{q_L}^{W^{-\sigma}})^2 \\ &\times \left[ -Q_q Q_{q'} H_r^1 + \sigma Q_q H_r^2 - \sigma Q_{q'} H_r^3 \right]. \end{aligned} \quad (5.4)$$

The functions  $H_r^i$  depend on the kinematic invariants defined in (2.15) and are explicitely given in Appendix D.2.

In the limit of soft and/or collinear photon emission, the squared matrix element (5.4) exhibits IR singularities. To combine these singularities with those originating from the virtual corrections we extract them in analytic form. This is done with the help of the dipole subtraction formalism [40, 41, 42]. Within this framework the partonic differential cross section for the generic process  $ab \rightarrow W^\sigma k\gamma$  can be schematically written as

$$\frac{d\hat{\sigma}^{ab \rightarrow W^\sigma k\gamma}}{dp_T} = \mathcal{N}_{ab} \int d\Phi_3 \left[ M^{ab}(\Phi_3) - M_{\text{sub}}^{ab}(\Phi_3) \right] + \frac{d\hat{\sigma}_A^{ab}}{dp_T}, \quad (5.5)$$

with  $\mathcal{N}_{ab}$  given in (2.10). The quantity  $M^{ab}$  reads

$$M^{ab}(\Phi_3) = \overline{\sum} |\mathcal{M}_0^{ab \rightarrow W^\sigma k\gamma}|^2 F_{O,3}(\Phi_3). \quad (5.6)$$

The auxiliary function  $M_{\text{sub}}^{ab}$  is chosen such that it has the same singular behavior as  $M^{ab}$  in the soft and collinear limits. This ensures that the difference  $M^{ab} - M_{\text{sub}}^{ab}$  can be integrated numerically. To compensate for the subtraction, the integral of the auxiliary function  $M_{\text{sub}}^{ab}$ , denoted here  $d\hat{\sigma}_A^{ab}/dp_T$ , is then added back. The analytical form of  $d\hat{\sigma}_A^{ab}/dp_T$  is obtained after performing integration over the subspace

of the radiated photon. The result of this one-particle subspace integration contains singular contributions which must be combined with those from the virtual corrections. The algorithms for constructing the auxiliary subtraction function and its integrated counterpart have been developed both for the case of photon radiation off massless or massive fermions [40] and QCD radiation off massless [41] or massive partons [42]. In Sects. 5.1 and 5.2 we discuss the application of both formalisms to calculate the  $\mathcal{O}(\alpha)$  real corrections to the  $W$ +jet production process. Utilizing both formalism serves as a check of our calculation. To describe the photon emission off a  $W$  boson we use expressions for the emission off a massive fermion, since only soft singularities are present in this case and they depend only on the charge of the external particle and not on its spin.

After adding the real and virtual corrections, collinear singularities remain. Final-state singularities are avoided by recombining collinear photon-quark configurations as discussed in Sect. 2.2. Initial-state singularities are absorbed in the definition of renormalized PDFs using the  $\overline{\text{MS}}$  scheme. Finally, this yields a finite and well-defined cross section.

## 5.1 Mass regularization

The formalism of Ref. [40] employs small photon and fermion masses to regularize soft and collinear singularities. The subtraction term for the squared matrix element is constructed from the appropriate dipole factors. Keeping the original notation of Ref. [40] we can write for the process  $ab \rightarrow W^\sigma k \gamma$  (where  $a, b$  can be  $\bar{q}, q', g$ )

$$\begin{aligned}
M_{\text{sub}}^{ab}(\Phi_3) = & -4\pi\alpha \sum_{\tau=\pm} \left\{ \left( Q_a Q_b g_{ab,\tau}^{\text{sub}}(p_a, p_b, p_\gamma) M_0^{a'b'}(\tilde{\Phi}_{2,ab}) \right. \right. \\
& - Q_a \sigma g_{aW,\tau}^{\text{sub}}(p_a, p_W, p_\gamma) M_0^{a'b'}(\tilde{\Phi}_{2,aW}) \\
& - \sigma Q_a g_{Wa,\tau}^{\text{sub}}(p_W, p_a, p_\gamma) M_0^{a'b'}(\tilde{\Phi}_{2,Wa}) \\
& - Q_a Q_k g_{ak,\tau}^{\text{sub}}(p_a, p_k, p_\gamma) M_0^{a'b'}(\tilde{\Phi}_{2,ak}) \\
& \left. \left. - Q_k Q_a g_{ka,\tau}^{\text{sub}}(p_k, p_a, p_\gamma) M_0^{a'b'}(\tilde{\Phi}_{2,ka}) + (a \leftrightarrow b) \right) \Big|_{\{a'=a, b'=b\}} \right. \\
& + Q_k \sigma g_{kW,\tau}^{\text{sub}}(p_k, p_W, p_\gamma) M_0^{ab}(\tilde{\Phi}_{2,kW}) \\
& \left. + \sigma Q_k g_{Wk,\tau}^{\text{sub}}(p_W, p_k, p_\gamma) M_0^{ab}(\tilde{\Phi}_{2,Wk}) \right\}, \tag{5.7}
\end{aligned}$$

with

$$M_0^{ab}(\tilde{\Phi}_{2,nm}) = \overline{\sum} |\mathcal{M}_0^{ab \rightarrow W^\sigma k}(\tilde{\Phi}_{2,nm})|^2 F_{O,2}(\tilde{\Phi}_{2,nm}). \tag{5.8}$$

Due to  $Q_g = 0$  the dipole terms with gluon indices do not contribute to (5.7) and for each subprocess the subtraction term  $M_{\text{sub}}^{ab}$  is constructed from six dipole terms, characterized by the  $g^{\text{sub}}$  functions. Expressions for these functions are taken directly

Dipole	Type (emitter, spectator)	Eq. no.	$\tilde{\Phi}_{2,nm}$
$g_{ab,\tau}^{\text{sub}}$	massless IS, massless IS	(3.22)	(3.25)–(3.27)
$g_{aW,\tau}^{\text{sub}}$	massless IS, massive FS	(A.1)	(3.12)
$g_{Wa,\tau}^{\text{sub}}$	massive FS, massless IS	(A.1)	(3.12)
$g_{ak,\tau}^{\text{sub}}$	massless IS, massless FS	(3.9)	(3.12)
$g_{ka,\tau}^{\text{sub}}$	massless FS, massless IS	(3.9)	(3.12)
$g_{kW,\tau}^{\text{sub}}$	massless FS, massive FS	(4.4)	(4.5)
$g_{Wk,\tau}^{\text{sub}}$	massive FS, massless FS	(4.4)	(4.5)

Table 5.1: Dipole subtraction terms from Ref. [40] used to calculate  $M_{\text{sub}}^{ab}$  in (5.7) for the massive regularization (IS = initial-state, FS = final-state).

from Ref. [40]. In Table 5.1 we list all the functions which are used to calculate (5.7), together with the corresponding equation numbers in Ref. [40].

For each subprocess the six dipole terms fall into three groups, each containing two dipole terms and coming with a specific charge combination, either  $-Q_q Q_{q'}$  or  $\sigma Q_q$ , or  $-\sigma Q_{q'}$ . In the soft and collinear limits, the subtraction term  $M_{\text{sub}}^{ab}$  has then the same structure as  $M^{ab}$  in (5.4) and the IR-singular part of the virtual corrections (3.88). Thus the cancellation of singularities can be analyzed for each charge combination separately.

The construction of the reduced phase space  $\tilde{\Phi}_{2,nm}$  follows the prescriptions of Ref. [40]. Generally  $\tilde{\Phi}_{2,nm}$  is a mapping from the three-particle phase space into a two-particle phase space. The mapping respects all mass shell conditions. For different types of dipoles, different mappings are necessary. In Table 5.1 we list numbers of equations in Ref. [40] which we used to perform mapping for the dipole terms appearing in our calculations. In particular, the observable-defining function  $F_{O,2}(\tilde{\Phi}_{2,nm})$  in (5.8) is then

$$F_{O,2}(\tilde{\Phi}_{2,nm}) = \delta(p_{\text{T}} - \tilde{p}_{\text{T},W}) \theta(\tilde{p}_{\text{T},j} - p_{\text{T},j}^{\text{min}}), \quad (5.9)$$

with  $\tilde{p}_{\text{T},W}$  and  $\tilde{p}_{\text{T},j}$  belonging to  $\tilde{\Phi}_{2,nm}$ .

The expression for the subtraction term integrated over the phase space of the photon reads

$$\begin{aligned} \frac{d\hat{\sigma}_{\text{A}}^{ab}}{dp_{\text{T}}} = & -\frac{\alpha}{2\pi} \left\{ 2Q_a Q_b \left[ G_{\text{I,I}}^{\text{sub}}(\hat{r}_{ab}) \frac{d\hat{\sigma}_{\text{fwd}}^{ab \rightarrow W^{\sigma k}}}{dp_{\text{T}}}(\hat{s}, p_{\text{T}}) \right. \right. \\ & \left. \left. + \int_0^1 dx \left[ \mathcal{G}_{\text{I,I}}^{\text{sub}}(\hat{r}_{ab}, x) \right]_+ \frac{d\hat{\sigma}_{\text{fwd}}^{ab \rightarrow W^{\sigma k}}}{dp_{\text{T}}}(x\hat{s}, p_{\text{T}}) + (a \leftrightarrow b) \right] \right. \\ & \left. - Q_a \sigma \left[ G_{\text{I,FM}}^{\text{sub}}(\hat{r}_{aW}) \frac{d\hat{\sigma}_{\text{fwd}}^{ab \rightarrow W^{\sigma k}}}{dp_{\text{T}}}(\hat{s}, p_{\text{T}}) \right] \right\} \end{aligned}$$

$$\begin{aligned}
& + \int_0^1 dx \left[ \mathcal{G}_{\text{I,FM}}^{\text{sub}}(\hat{r}_{aW}(x), x) \right]_+ \frac{d\hat{\sigma}_{\text{fwd}}^{ab \rightarrow W^{\sigma k}}}{dp_{\text{T}}}(x\hat{s}, p_{\text{T}}) + (a \leftrightarrow b) \Big] \\
& - Q_b \sigma \left[ G_{\text{I,FM}}^{\text{sub}}(\hat{r}_{bW}) \frac{d\hat{\sigma}_{\text{fwd}}^{ab \rightarrow W^{\sigma k}}}{dp_{\text{T}}}(\hat{s}, p_{\text{T}}) \right. \\
& \quad \left. + \int_0^1 dx \left[ \mathcal{G}_{\text{I,FM}}^{\text{sub}}(\hat{r}_{bW}(x), x) \right]_+ \frac{d\hat{\sigma}_{\text{fwd}}^{ab \rightarrow W^{\sigma k}}}{dp_{\text{T}}}(x\hat{s}, p_{\text{T}}) + (a \leftrightarrow b) \right] \\
& - Q_a Q_k \left[ G_{\text{I,F}}^{\text{sub}}(\hat{r}_{ak}) \frac{d\hat{\sigma}_{\text{fwd}}^{ab \rightarrow W^{\sigma k}}}{dp_{\text{T}}}(\hat{s}, p_{\text{T}}) \right. \\
& \quad \left. + \int_0^1 dx \left[ \mathcal{G}_{\text{I,F}}^{\text{sub}}(\hat{r}_{ak}(x), x) \right]_+ \frac{d\hat{\sigma}_{\text{fwd}}^{ab \rightarrow W^{\sigma k}}}{dp_{\text{T}}}(x\hat{s}, p_{\text{T}}) + (a \leftrightarrow b) \right] \\
& - Q_b Q_k \left[ G_{\text{I,F}}^{\text{sub}}(\hat{r}_{bk}) \frac{d\hat{\sigma}_{\text{fwd}}^{ab \rightarrow W^{\sigma k}}}{dp_{\text{T}}}(\hat{s}, p_{\text{T}}) \right. \\
& \quad \left. + \int_0^1 dx \left[ \mathcal{G}_{\text{I,F}}^{\text{sub}}(\hat{r}_{bk}(x), x) \right]_+ \frac{d\hat{\sigma}_{\text{fwd}}^{ab \rightarrow W^{\sigma k}}}{dp_{\text{T}}}(x\hat{s}, p_{\text{T}}) + (a \leftrightarrow b) \right] \\
& \left. + Q_k \sigma \left[ G_{\text{F,FM}}^{\text{sub}}(\hat{r}_{kW}) \frac{d\hat{\sigma}_{\text{fwd}}^{ab \rightarrow W^{\sigma k}}}{dp_{\text{T}}}(\hat{s}, p_{\text{T}}) + (a \leftrightarrow b) \right] \right\}. \tag{5.10}
\end{aligned}$$

The relevant invariants in (5.10) are defined as  $\hat{r}_{ab} = (p_a + p_b)^2 = \hat{s}$ ,  $\hat{r}_{kW} = (p_k + p_W)^2 = \hat{s}$ , and

$$\begin{aligned}
\hat{r}_{aW}(x) &= (xp_a - p_W)^2, \\
\hat{r}_{ak}(x) &= (xp_a - p_k)^2, \\
\hat{r}_{nl} &= \hat{r}_{nl}(1).
\end{aligned} \tag{5.11}$$

The terms proportional to  $d\hat{\sigma}_{\text{fwd}}^{ab \rightarrow W^{\sigma k}}/dp_{\text{T}}$  in (5.10) represent the contributions originating from the forward hemisphere in the two-particle phase space [see (2.13)-(2.14)]. The  $(a \leftrightarrow b)$  terms are the contributions from the backward hemisphere, and

$$\left. \frac{d\hat{\sigma}_{\text{fwd}}^{ab \rightarrow W^{\sigma k}}}{dp_{\text{T}}} \right|_{a \leftrightarrow b} = \frac{d\hat{\sigma}_{\text{bkwd}}^{ab \rightarrow W^{\sigma k}}}{dp_{\text{T}}}. \tag{5.12}$$

Note that the first argument of  $d\hat{\sigma}_{\text{fwd}}^{ab \rightarrow W^{\sigma k}}/dp_{\text{T}}$  in (5.10) directly indicates the  $x$ -dependence of the actual values of the  $\hat{t}$ ,  $\hat{u}$  invariants defined in (2.8). The plus-distributions appearing in Eq. (5.10) are evaluated according to the prescription

$$\begin{aligned}
& \int_0^1 dx \left[ \mathcal{G}^{\text{sub}}(\hat{r}(x), x) \right]_+ \frac{d\hat{\sigma}}{dp_{\text{T}}}(x\hat{s}, p_{\text{T}}) = \\
& = \int_0^1 dx \left[ \mathcal{G}^{\text{sub}}(\hat{r}(x), x) \frac{d\hat{\sigma}}{dp_{\text{T}}}(x\hat{s}, p_{\text{T}}) \theta(x - \hat{\tau}) - \mathcal{G}^{\text{sub}}(\hat{r}(1), x) \frac{d\hat{\sigma}}{dp_{\text{T}}}(\hat{s}, p_{\text{T}}) \right],
\end{aligned} \tag{5.13}$$

where  $\hat{r} = \left(p_T + \sqrt{p_T^2 + M_W^2}\right)^2 / \hat{s}$  guarantees the minimal center-of-mass energy to produce the final state. The expressions for the integrated dipole functions  $G^{\text{sub}}$  and  $\mathcal{G}^{\text{sub}}$  in (5.10) follow directly<sup>1</sup> from the results in Ref. [40]. For the functions  $G^{\text{sub}}$  they read

$$G_{\text{I,I}}^{\text{sub}}(\hat{r}) = \frac{1}{2} \left[ \text{Re} \left( f_{1,\text{MR}}^{\text{IR}} \right) + \ln^2 \left( \frac{\hat{r}}{M_W^2} \right) - 3 \ln \left( \frac{\hat{r}}{M_W^2} \right) - \frac{2}{3} \pi^2 + 4 \right], \quad (5.14)$$

$$\begin{aligned} G_{\text{I,FM}}^{\text{sub}}(\hat{r}) &= \text{Re} \left( f_{2,\text{MR}}^{\text{IR}} \right) \Big|_{\hat{t} \leftrightarrow \hat{r}} + 2 \ln^2 \left( 1 - \frac{\hat{r}}{M_W^2} \right) - \ln^2 \left( 2 - \frac{\hat{r}}{M_W^2} \right) \\ &+ \ln \left( 1 - \frac{\hat{r}}{M_W^2} \right) \left( \frac{M_W^4}{\hat{r}^2} - \frac{3M_W^2}{\hat{r}} - 3 \right) - 2 \text{Li}_2 \left( \frac{M_W^2}{2M_W^2 - \hat{r}} \right) \\ &+ 2 \text{Li}_2 \left( \frac{\hat{r}}{2M_W^2 - \hat{r}} \right) - 2 \text{Li}_2 \left( \frac{-\hat{r}}{2M_W^2 - \hat{r}} \right) + \frac{M_W^2}{\hat{r}} + \frac{\pi^2}{6} + \frac{1}{2}, \end{aligned} \quad (5.15)$$

$$G_{\text{I,F}}^{\text{sub}}(\hat{r}) = \text{Re} \left( f_{1,\text{MR}}^{\text{IR}} \right) \Big|_{\hat{s} \leftrightarrow \hat{r}} + \ln^2 \left( \frac{-\hat{r}}{M_W^2} \right) - 3 \ln \left( \frac{-\hat{r}}{M_W^2} \right) - \frac{\pi^2}{3} + \frac{1}{2}, \quad (5.16)$$

$$\begin{aligned} G_{\text{F,FM}}^{\text{sub}}(\hat{r}) &= \text{Re} \left( f_{2,\text{MR}}^{\text{IR}} \right) \Big|_{\hat{t} \leftrightarrow \hat{r}} + \ln^2 \left( \frac{\hat{r}}{M_W^2} - 1 \right) + \ln^2 \left( 1 - \frac{M_W^2}{\hat{r}} \right) \\ &+ \frac{1}{2} \ln \left( \frac{\hat{r}}{M_W^2} \right) - \frac{7}{2} \ln \left( \frac{\hat{r}}{M_W^2} - 1 \right) - \frac{3}{2} \ln \left( \frac{\sqrt{\hat{r}} - M_W}{\sqrt{\hat{r}} + M_W} \right) \\ &+ 4 \text{Li}_2 \left( \frac{M_W^2}{\hat{r}} \right) - 4 \text{Li}_2 \left( \sqrt{\frac{M_W^2}{\hat{r}}} \right) + \frac{M_W^2}{2\hat{r}} - \frac{2\pi^2}{3} + 3. \end{aligned} \quad (5.17)$$

The IR-singular contributions in (5.14)-(5.17) are contained in the functions  $f_{i,\text{MR}}^{\text{IR}}$ , which are defined in (3.78). This reveals the explicit cancellation with the IR-singularities of the virtual corrections in (3.88).

The functions  $\mathcal{G}^{\text{sub}}$  are given by

$$\begin{aligned} \mathcal{G}_{\text{I,I}}^{\text{sub}}(\hat{r}, x) &= \chi(x) + \frac{1+x^2}{1-x} \left\{ \ln \left( \frac{\hat{r}}{\mu_{\text{QED}}^2} \right) + 2 \ln(1-x) \right\} + 1-x, \quad (5.18) \\ \mathcal{G}_{\text{I,FM}}^{\text{sub}}(\hat{r}, x) &= \chi(x) + \frac{1+x^2}{1-x} \left\{ \ln \left( \frac{M_W^2 - \hat{r}}{x \mu_{\text{QED}}^2} \right) + \ln \left( (1-x)(1-z_1(\hat{r}, x)) \right) \right\} \\ &+ \frac{z_1(\hat{r}, x) - 1}{2(1-x)} \left( 3 + z_1(\hat{r}, x) - \frac{4M_W^2 x}{(\hat{r} - M_W^2)(1-x)} \right) + 1-x, \end{aligned} \quad (5.19)$$

---

<sup>1</sup>The function  $G_{\text{F,FM}}^{\text{sub}}(\hat{r})$  in (5.17) corresponds to the end-point contribution of an integrated dipole with the combination of a massless and massive emitter and spectator pair in the final state. This function is not available in the literature. We derived the corresponding expression (5.17) from Eq. (4.10) in Ref. [40], which gives the result for the case where both the emitter and spectator are massive, by taking the limit of an infinitesimal quark mass for either the emitter or spectator mass. This limit has been checked numerically and furthermore, in a subsequent massless limit for the remaining mass the complete massless result in Ref. [40] could be reproduced.

$$\mathcal{G}_{1,F}^{\text{sub}}(\hat{r}, x) = \chi(x) + \frac{1+x^2}{1-x} \left\{ \ln \left( \frac{-\hat{r}}{x\mu_{\text{QED}}^2} \right) + \ln(1-x) \right\} - \frac{3}{2(1-x)} + 1 - x, \quad (5.20)$$

with

$$z_1(\hat{r}, x) = \frac{M_W^2 x}{M_W^2 - (1-x)\hat{r}} \quad (5.21)$$

and

$$\chi(x) = \frac{1+x^2}{1-x} \left\{ \ln \left( \frac{\mu_{\text{QED}}^2}{m^2} \right) - 2 \ln(1-x) - 1 \right\}, \quad (5.22)$$

where  $\mu_{\text{QED}}$  is the factorization scale and  $m$  stands for the quark-mass regulator. The functions  $\chi(x)$  are singular. These singularities are related to the collinear photon radiation off an initial-state quark and are absorbed in the definition of renormalized PDFs, yielding the hadronic cross section finite. The procedure bears complete analogy to absorbing collinear QCD singularities into the definition of the PDFs. In the  $\overline{\text{MS}}$  factorization scheme, the renormalized PDFs to  $\mathcal{O}(\alpha)$  are given by [15]

$$f_{h,q}(x, \mu_{\text{QCD}}^2) = f_{h,q}^{\overline{\text{MS}}}(x, \mu_{\text{QCD}}^2, \mu_{\text{QED}}^2) - \frac{\alpha}{2\pi} Q_q^2 \int_x^1 \frac{dz}{z} f_{h,q}^{\overline{\text{MS}}}\left(\frac{x}{z}, \mu_{\text{QCD}}^2, \mu_{\text{QED}}^2\right) [\chi(z)]_+. \quad (5.23)$$

In order to make the cancellation of the singular functions  $\chi(z)$  more explicit, let us write the hadronic cross section of  $\mathcal{O}(\alpha^2)$  in the simplified form

$$d\sigma^{h_1 h_2} = \int_0^1 dx_1 dx_2 f_{h_1,q}(x_1) f_{h_2,q'}(x_2) d\hat{\sigma}^{qq'}(\hat{s}) \Big|_{\mathcal{O}(\alpha^2)}, \quad (5.24)$$

where we assume  $\hat{s} = x_1 x_2 s$  and suppress the dependence on  $\mu_{\text{QCD}}$  in the PDFs. Considering the  $x_1$  dependent parton distribution function, the insertion of (5.23) into Eq.(5.24) yields to  $\mathcal{O}(\alpha^2)$

$$\begin{aligned} d\sigma^{h_1 h_2} &= \int_0^1 dx_1 dx_2 f_{h_1,q}^{\overline{\text{MS}}}(x_1, \mu_{\text{QED}}^2) f_{h_2,q'}^{\overline{\text{MS}}}(x_2, \mu_{\text{QED}}^2) d\hat{\sigma}^{qq'}(\hat{s}) \Big|_{\mathcal{O}(\alpha^2)} \\ &\quad - \frac{\alpha}{2\pi} Q_q^2 \int_0^1 dx_1 dx_2 f_{h_2,q'}^{\overline{\text{MS}}}(x_2, \mu_{\text{QED}}^2) \int_{x_1}^1 \frac{dz}{z} f_{h_1,q}^{\overline{\text{MS}}}\left(\frac{x_1}{z}, \mu_{\text{QED}}^2\right) [\chi(z)]_+ d\hat{\sigma}^{qq'}(\hat{s}) \Big|_{\mathcal{O}(\alpha)} \\ &= \int_0^1 dx_1 dx_2 f_{h_1,q}^{\overline{\text{MS}}}(x_1, \mu_{\text{QED}}^2) f_{h_2,q'}^{\overline{\text{MS}}}(x_2, \mu_{\text{QED}}^2) \left\{ d\hat{\sigma}^{qq'}(\hat{s}) \Big|_{\mathcal{O}(\alpha^2)} \right. \\ &\quad \left. - \frac{\alpha}{2\pi} Q_q^2 \int_0^1 dz [\chi(z)]_+ d\hat{\sigma}^{qq'}(z\hat{s}) \Big|_{\mathcal{O}(\alpha)} \right\} \end{aligned} \quad (5.25)$$

and similar for the PDF depending on  $x_2$ . In this form, the singular function  $\chi(z)$  is isolated in a convolution over  $z$  multiplying the lowest-order cross section, which is evaluated with a reduced center-of-mass energy corresponding to  $z\hat{s}$ . The integrated dipole contributions (5.18)-(5.20) in (5.10) carry exactly the same structure and thus cancel with the above singularities contained in the function  $\chi(z)$  resulting from renormalized PDFs.

## 5.2 Dimensional regularization

In an independent calculation we used the results of Refs. [41, 42] to evaluate the dipole subtraction terms and their integrated counterparts. The formalism of [41, 42] is concerned with QCD radiation and expressions for dipoles are given as matrices in color and helicity space. Since we consider photon emission off a fermion line, the color and helicity structure disappears and the dipole matrices reduce to simple expressions. More precisely, to adapt the formalism Refs. [41, 42] for the calculation of QED corrections, we make use of expressions describing gluon radiation off a fermion line in Refs. [41, 42] and replace

$$\alpha_S \rightarrow \alpha, \quad \mathbf{T}_i \rightarrow \sigma_i Q_i, \quad C_F \rightarrow Q_i^2, \quad T_R \rightarrow 1, \quad C_A \rightarrow 0, \quad (5.26)$$

where  $\mathbf{T}_i$  indicates the color of the emitting parton,  $Q_i$  is the electric charge in units of the positron charge for this parton, and  $\sigma_i = +1$  ( $-1$ ) for incoming (outgoing) partons. Adopting notation analogous to Refs. [41, 42], the subtraction term for the process  $ab \rightarrow W^\sigma k \gamma$  can be then written

$$\begin{aligned} \mathbf{M}_{\text{sub}}^{ab}(\Phi_3) = & \left[ \mathcal{D}_{\text{QED}}^{a\gamma,b} + \mathcal{D}_{W,\text{QED}}^{a\gamma} + \mathcal{D}_{\gamma W,\text{QED}}^a + \mathcal{D}_{k,\text{QED}}^{a\gamma} + \mathcal{D}_{\gamma k,\text{QED}}^a + (a \leftrightarrow b) \right] \\ & + \mathcal{D}_{\gamma k,W,\text{QED}} + \mathcal{D}_{\gamma W,k,\text{QED}}, \end{aligned} \quad (5.27)$$

where

$$\mathcal{D}_{F,\text{QED}}^I = F_{O,2}(\tilde{\Phi}_{2,nm}) \mathcal{D}_F^I(p_W, p_k, p_\gamma; p_a, p_b) \Big|_{\text{replacements of eq. (5.26)}}. \quad (5.28)$$

It is understood in Eq. (5.27) that dipole subtraction terms with a gluon index do not contribute to  $\mathbf{M}_{\text{sub}}^{ab}$ . In a complete analogy to Eq. (5.7), for any initial state  $ab$  the expression for  $\mathbf{M}_{\text{sub}}^{ab}$  is constructed from six dipole subtraction terms  $\mathcal{D}_{F,\text{QED}}^I$ , each associated with one of the three possible charge combinations  $-Q_q Q_{q'}$ ,  $\sigma Q_q$  or  $-\sigma Q_{q'}$ . The dipole subtraction functions  $\mathcal{D}_F^I$  are taken directly from Refs. [41, 42]. A list of the functions  $\mathcal{D}_F^I$  used to calculate the subtraction term  $\mathbf{M}_{\text{sub}}^{ab}$  in (5.27), together with the corresponding equation numbers in Refs. [41, 42], is presented in Table 5.2. Additionally, for each dipole subtraction term appearing in (5.27) we include a description of its type. The mappings from  $\Phi_3$  to  $\tilde{\Phi}_{2,nm}$  agree between the formalism of Refs. [41, 42] and [40]. However, for the sake of completeness, Table 5.2 contains numbers of equations which provide mapping formulae in Refs. [41, 42]. The function  $F_{O,2}$  in (5.28) is given by expression (5.9).

Moreover, apart from the final-state emitter, final-state spectator case, i.e. the dipoles  $\mathcal{D}_{\gamma k,W,\text{QED}}$  and  $\mathcal{D}_{\gamma W,k,\text{QED}}$ , there is a direct correspondence between the dipole subtraction terms in the two formalisms of the form

$$\begin{aligned} \mathcal{D}_{\text{QED}}^{a\gamma,b} & \xrightarrow{\varepsilon \rightarrow 0} -Q_a Q_b 4\pi\alpha \sum_{\tau=\pm} g_{ab,\tau}^{\text{sub}}(p_a, p_b, p_\gamma) \mathbf{M}_0^{ab}(\tilde{\Phi}_{2,ab}), \\ \mathcal{D}_{W,\text{QED}}^{a\gamma} & \xrightarrow{\varepsilon \rightarrow 0} Q_a \sigma 4\pi\alpha \sum_{\tau=\pm} g_{aW,\tau}^{\text{sub}}(p_a, p_W, p_\gamma) \mathbf{M}_0^{ab}(\tilde{\Phi}_{2,aW}), \end{aligned}$$



Dipole	Type (emitter, spectator)	Eq. nos.	$\tilde{\Phi}_{2, nm}$
$\mathcal{D}_{\text{QED}}^{a\gamma, b}$	massless IS, massless IS	(5.136), (5.145) in Ref. [41]	(5.137), (5.139), (5.140) in Ref. [41]
$\mathcal{D}_{W, \text{QED}}^{a\gamma}$	massless IS, massive FS	(5.71), (5.81) in Ref. [42]	(5.73), (5.74) in Ref. [42]
$\mathcal{D}_{\gamma W, \text{QED}}^a$	massive FS, massless IS	(5.40), (5.50) in Ref. [42]	(5.42), (5.43) in Ref. [42]
$\mathcal{D}_{k, \text{QED}}^{a\gamma}$	massless IS, massless FS	(5.61), (5.65) in Ref. [41]	(5.62)-(5.64) in Ref. [41]
$\mathcal{D}_{\gamma k, \text{QED}}^a$	massless FS, massless IS	(5.36), (5.39) in Ref. [41]	(5.37), (5.38) in Ref. [41]
$\mathcal{D}_{\gamma k, W, \text{QED}}$	massless FS, massive FS	(5.2), (5.16) in Ref. [42]	(5.3), (5.7), (5.9) in Ref. [42]
$\mathcal{D}_{\gamma W, k, \text{QED}}$	massive FS, massless FS	(5.2), (5.16) in Ref. [42]	(5.3), (5.7), (5.9) in Ref. [42]

Table 5.2: Dipole expressions from Refs. [41, 42] used to calculate  $\mathbf{M}_{\text{sub}}^{ab}$  in (5.27) for the dimensional regularization.

$$\begin{aligned}
\mathcal{D}_{\gamma W, \text{QED}}^a &\xrightarrow{\varepsilon \rightarrow 0} Q_a \sigma \, 4\pi\alpha \sum_{\tau=\pm} g_{W a, \tau}^{\text{sub}}(p_W, p_a, p_\gamma) \mathbf{M}_0^{ab}(\tilde{\Phi}_{2, Wa}), \\
\mathcal{D}_{k, \text{QED}}^{a\gamma} &\xrightarrow{\varepsilon \rightarrow 0} Q_a Q_k \, 4\pi\alpha \sum_{\tau=\pm} g_{ak, \tau}^{\text{sub}}(p_a, p_k, p_\gamma) \mathbf{M}_0^{ab}(\tilde{\Phi}_{2, ak}), \\
\mathcal{D}_{\gamma k, \text{QED}}^a &\xrightarrow{\varepsilon \rightarrow 0} Q_a Q_k \, 4\pi\alpha \sum_{\tau=\pm} g_{ka, \tau}^{\text{sub}}(p_k, p_a, p_\gamma) \mathbf{M}_0^{ab}(\tilde{\Phi}_{2, ka}). \tag{5.29}
\end{aligned}$$

The subtraction term integrated over the photon phase space is constructed according to

$$\frac{d\hat{\sigma}_{\text{A}}^{ab}}{dp_{\text{T}}} = \frac{\alpha}{2\pi} \left[ \mathcal{I}^{ab}(\hat{s}, p_{\text{T}}) + \int_0^1 dx \left( \mathcal{K}^{ab}(x, \hat{s}, p_{\text{T}}) + \mathcal{P}^{ab}(x, \hat{s}, p_{\text{T}}) \right) \right], \tag{5.30}$$

where the expressions for  $\mathcal{I}, \mathcal{K}$  and  $\mathcal{P}$  functions follow from the  $\mathbf{I}, \mathbf{P}(x)$  and  $\mathbf{K}(x)$  operators in Refs. [41, 42] after evaluating the replacements of Eq. (5.26). For the photonic corrections to any of the subprocesses  $ab \rightarrow W^\sigma k$  we can write

$$\mathcal{I}^{ab}(\hat{s}, p_{\text{T}}) = Q_a Q_b \left[ \tilde{\mathcal{I}}(\hat{s}_{ab}) \frac{d\hat{\sigma}_{\text{fwd}}^{ab \rightarrow W^\sigma k}}{dp_{\text{T}}}(\hat{s}, p_{\text{T}}) + (a \leftrightarrow b) \right]$$

$$\begin{aligned}
& - Q_a \sigma \left[ \mathcal{I}'(\hat{s}_{aW}) \frac{d\hat{\sigma}_{\text{fwd}}^{ab \rightarrow W^{\sigma k}}}{dp_{\text{T}}}(\hat{s}, p_{\text{T}}) + (a \leftrightarrow b) \right] \\
& - Q_b \sigma \left[ \mathcal{I}'(\hat{s}_{bW}) \frac{d\hat{\sigma}_{\text{fwd}}^{ab \rightarrow W^{\sigma k}}}{dp_{\text{T}}}(\hat{s}, p_{\text{T}}) + (a \leftrightarrow b) \right] \\
& - Q_a Q_k \left[ \tilde{\mathcal{I}}(\hat{s}_{ak}) \frac{d\hat{\sigma}_{\text{fwd}}^{ab \rightarrow W^{\sigma k}}}{dp_{\text{T}}}(\hat{s}, p_{\text{T}}) + (a \leftrightarrow b) \right] \\
& - Q_b Q_k \left[ \tilde{\mathcal{I}}(\hat{s}_{bk}) \frac{d\hat{\sigma}_{\text{fwd}}^{ab \rightarrow W^{\sigma k}}}{dp_{\text{T}}}(\hat{s}, p_{\text{T}}) + (a \leftrightarrow b) \right] \\
& + Q_k \sigma \left[ \mathcal{I}'(\hat{s}_{kW}) \frac{d\hat{\sigma}_{\text{fwd}}^{ab \rightarrow W^{\sigma k}}}{dp_{\text{T}}}(\hat{s}, p_{\text{T}}) + (a \leftrightarrow b) \right], \tag{5.31}
\end{aligned}$$

where  $\hat{s}_{nm} = 2p_n \cdot p_m$ , and we make use of  $Q_g = 0$ . As in (5.10), the terms proportional to  $d\hat{\sigma}_{\text{fwd}}^{ab \rightarrow W^{\sigma k}}/dp_{\text{T}}$  originate from the forward hemisphere and the  $(a \leftrightarrow b)$  terms from the backward hemisphere. The integrated dipole functions in (5.31) read

$$\begin{aligned}
\tilde{\mathcal{I}}(\hat{s}_{nm}) &= - \left( \frac{4\pi\mu^2}{M_W^2} \right)^\varepsilon \Gamma(1 + \varepsilon) \text{Re} \left( f_{1,\text{DR}}^{\text{IR}} \right) \Big|_{\hat{s}=\hat{s}_{nm}} - \ln^2 \left( \frac{\hat{s}_{nm}}{M_W^2} \right) + 3 \ln \left( \frac{\hat{s}_{nm}}{M_W^2} \right) \\
&\quad + \frac{4\pi^2}{3} - 6, \\
\mathcal{I}'(\hat{s}_{nm}) &= - \left( \frac{4\pi\mu^2}{M_W^2} \right)^\varepsilon \Gamma(1 + \varepsilon) \text{Re} \left( f_{2,\text{DR}}^{\text{IR}} \right) \Big|_{\hat{t}=M_W^2+(\delta_{nk}-\delta_{na})\hat{s}_{nm}} - \ln^2 \left( \frac{\hat{s}_{nm}}{M_W^2} \right) \\
&\quad + 3 \ln \left( \frac{\hat{s}_{nm}}{M_W^2} \right) - \ln \left( \frac{\hat{s}_{nm}}{M_W^2 + \hat{s}_{nm}} \right) \left[ \ln \left( \frac{\hat{s}_{nm}}{M_W^2} \right) - \ln \left( \frac{M_W^2}{M_W^2 + \hat{s}_{nm}} \right) + 1 \right] \\
&\quad + 3 \ln \left( 1 - \sqrt{\frac{M_W^2}{M_W^2 + \hat{s}_{nm}}} \right) + \frac{M_W^2}{\hat{s}_{nm}} \ln \left( \frac{M_W^2}{M_W^2 + \hat{s}_{nm}} \right) + 2\text{Li}_2 \left( \frac{\hat{s}_{nm}}{M_W^2 + \hat{s}_{nm}} \right) \\
&\quad + \frac{3M_W}{\sqrt{\hat{s}_{nm} + M_W^2} + M_W} + \pi^2 - 6. \tag{5.32}
\end{aligned}$$

The structure of the singular terms  $f_{i,\text{DR}}^{\text{IR}}$  in (5.32) is kept the same as in (3.88) to manifestly show cancellation of singularities between virtual and real corrections. For the  $x$ -dependent functions we have

$$\begin{aligned}
\mathcal{K}^{ab}(x, \hat{s}, p_{\text{T}}) &= (Q_a^2 + Q_b^2) \left[ \bar{\mathcal{K}}(x) \frac{d\hat{\sigma}_{\text{fwd}}^{ab \rightarrow W^{\sigma k}}}{dp_{\text{T}}}(x\hat{s}, p_{\text{T}}) + (a \leftrightarrow b) \right] \\
&\quad + 2 Q_a Q_b \left[ \tilde{\mathcal{K}}(x) \frac{d\hat{\sigma}_{\text{fwd}}^{ab \rightarrow W^{\sigma k}}}{dp_{\text{T}}}(x\hat{s}, p_{\text{T}}) + (a \leftrightarrow b) \right] \\
&\quad - Q_a \sigma \left[ \mathcal{K}'(x, \hat{s}_{aW}) \frac{d\hat{\sigma}_{\text{fwd}}^{ab \rightarrow W^{\sigma k}}}{dp_{\text{T}}}(x\hat{s}, p_{\text{T}}) + (a \leftrightarrow b) \right] \\
&\quad - Q_b \sigma \left[ \mathcal{K}'(x, \hat{s}_{bW}) \frac{d\hat{\sigma}_{\text{fwd}}^{ab \rightarrow W^{\sigma k}}}{dp_{\text{T}}}(x\hat{s}, p_{\text{T}}) + (a \leftrightarrow b) \right]
\end{aligned}$$

$$\begin{aligned}
& - (Q_a Q_k + Q_b Q_k) \left[ \mathcal{K}''(x) \frac{d\hat{\sigma}_{\text{fwd}}^{ab \rightarrow W^\sigma k}}{dp_\Gamma}(x\hat{s}, p_\Gamma) + (a \leftrightarrow b) \right], \\
\mathcal{P}^{ab}(x, \hat{s}, p_\Gamma) = & 2Q_a Q_b \left[ \mathcal{P}(x, \hat{s}_{ab}) \frac{d\hat{\sigma}_{\text{fwd}}^{ab \rightarrow W^\sigma k}}{dp_\Gamma}(x\hat{s}, p_\Gamma) + (a \leftrightarrow b) \right] \\
& - Q_a \sigma \left[ \mathcal{P}(x, \hat{s}_{aW}) \frac{d\hat{\sigma}_{\text{fwd}}^{ab \rightarrow W^\sigma k}}{dp_\Gamma}(x\hat{s}, p_\Gamma) + (a \leftrightarrow b) \right] \\
& - Q_b \sigma \left[ \mathcal{P}(x, \hat{s}_{bW}) \frac{d\hat{\sigma}_{\text{fwd}}^{ab \rightarrow W^\sigma k}}{dp_\Gamma}(x\hat{s}, p_\Gamma) + (a \leftrightarrow b) \right] \\
& - Q_a Q_k \left[ \mathcal{P}(x, \hat{s}_{ak}) \frac{d\hat{\sigma}_{\text{fwd}}^{ab \rightarrow W^\sigma k}}{dp_\Gamma}(x\hat{s}, p_\Gamma) + (a \leftrightarrow b) \right] \\
& - Q_b Q_k \left[ \mathcal{P}(x, \hat{s}_{bk}) \frac{d\hat{\sigma}_{\text{fwd}}^{ab \rightarrow W^\sigma k}}{dp_\Gamma}(x\hat{s}, p_\Gamma) + (a \leftrightarrow b) \right], \tag{5.33}
\end{aligned}$$

with

$$\begin{aligned}
\bar{\mathcal{K}}(x) &= P_{\text{reg}}(x) \ln\left(\frac{1-x}{x}\right) + (1-x) + \left[\frac{2}{1-x} \ln\left(\frac{1-x}{x}\right)\right]_+ \\
&\quad - \delta(1-x)(5 - \pi^2), \\
\tilde{\mathcal{K}}(x) &= -P_{\text{reg}}(x) \ln(1-x) - \left(2 \left[\frac{\ln(1-x)}{1-x}\right]_+ - \frac{\pi^2}{3} \delta(1-x)\right), \\
\mathcal{K}'(x, \hat{s}_{nm}) &= -2 \left[\frac{\ln(1-x)}{1-x}\right]_+ + \frac{2 \ln(2-x)}{1-x} \\
&\quad - \left[\frac{1-x}{2(1-x + M_W^2/\hat{s}_{nm})^2} - \frac{2}{1-x} \left\{1 + \ln\left(1-x + \frac{M_W^2}{\hat{s}_{nm}}\right)\right\}\right]_+ \\
&\quad - \left[\frac{2}{1-x}\right]_+ \left\{\ln\left(2-x + \frac{M_W^2}{\hat{s}_{nm}}\right) + \ln\left(\frac{(2-x)\hat{s}_{nm}}{(2-x)\hat{s}_{nm} + M_W^2}\right)\right\} \\
&\quad - P_{\text{reg}}(x) \ln\left(\frac{(1-x)\hat{s}_{nm}}{(1-x)\hat{s}_{nm} + M_W^2}\right) \\
&\quad - \delta(1-x) \left\{-\frac{3}{2} + \frac{M_W^2}{\hat{s}_{nm}} \ln\left(\frac{M_W^2}{\hat{s}_{nm} + M_W^2}\right) + \frac{3M_W}{\sqrt{\hat{s}_{nm} + M_W^2} + M_W}\right. \\
&\quad \left. + \frac{3}{2} \ln\left(\frac{\hat{s}_{nm} - 2M_W \sqrt{\hat{s}_{nm} + M_W^2} + 2M_W^2}{\hat{s}_{nm}}\right) + \frac{1}{2} \frac{M_W^2}{\hat{s}_{nm} + M_W^2}\right\}, \\
\mathcal{K}''(x) &= \frac{3}{2} \left(\left[\frac{1}{1-x}\right]_+ + \delta(1-x)\right), \\
\mathcal{P}(x, \hat{s}_{nm}) &= \left[\frac{1+x^2}{1-x}\right]_+ \ln\left(\frac{\mu_{\text{QED}}^2}{x\hat{s}_{nm}}\right), \tag{5.34}
\end{aligned}$$

and

$$P_{\text{reg}}(x) = \left[ \frac{1+x^2}{1-x} \right]_+ - \left[ \frac{2}{1-x} \right]_+ - \frac{3}{2} \delta(1-x). \quad (5.35)$$

Note that in contrast to Eq. (5.31), the quantity  $\hat{s}_{nm}$  in (5.33) can be implicitly dependent on the fraction  $x$ . More precisely, it is the case if  $\hat{s}_{nm}$  involves the momentum of a final-state particle. The final-state momentum belongs then to the phase space for which the squared center-of-mass energy is  $x\hat{s} = 2xp_a \cdot p_b$  [42].

The evaluation of the terms involving the plus-distribution is carried out as indicated in Ref. [42], i.e. according to

$$\begin{aligned} & \int_0^1 dx [\mathcal{R}(x, \hat{s}_{nm}(x))]_+ \frac{d\hat{\sigma}}{dp_{\text{T}}}(x\hat{s}, p_{\text{T}}) = \\ & = \int_0^1 dx \left[ \mathcal{R}(x, \hat{s}_{nm}(x)) \frac{d\hat{\sigma}}{dp_{\text{T}}}(x\hat{s}, p_{\text{T}}) \theta(x - \hat{\tau}) - \mathcal{R}(x, \hat{s}_{nm}(1)) \frac{d\hat{\sigma}}{dp_{\text{T}}}(\hat{s}, p_{\text{T}}) \right], \end{aligned} \quad (5.36)$$

with  $\hat{\tau} = \left( p_{\text{T}} + \sqrt{p_{\text{T}}^2 + M_W^2} \right)^2 / \hat{s}$ .

In the formalism of Refs. [41, 42] the collinear counterterms associated with PDF renormalization are included in the expressions for integrated dipole functions, i.e. the final results which we use are free from collinear singularities. The expressions presented here are calculated using the  $\overline{\text{MS}}$  factorization scheme.

As can be seen from the presented formulae, the explicit expressions for the integrated dipole functions in the two formalisms are different. In particular, the expressions for the end-point contributions have different forms due to specific conventions wrt. calculating the plus-distribution terms in the two formalisms. However we have checked that, after subtraction of the IR singularities, for each charge combination apart from  $\sigma Q_k$  the integrated dipole contributions to  $d\sigma_{\text{A}}^{ab}/dp_{\text{T}}$  in the two formalisms are equivalent.

# Chapter 6

## Phase space integrations

In this chapter we present two different approaches to parameterize the phase space integration for final state particles. In Sect. 6.1 we discuss an explicit parameterization via angle and energies for three particles in the final state. This version has been used for the numerical results presented in Ch. 8. A more general method is described in Sect. 6.2, which allows to perform a phase space integration with arbitrary many particles in the final state. The method is extended to generate soft and collinear limits for massless external momenta. This option allows to systematically check the numerical cancellations associated with the dipole subtraction method. It has been used to ensure the correctness of the dipole terms for the real corrections to  $W$ +jet production.

### 6.1 Three-particle phase space generation

We start with the discussion of the phase space generation for three particles in the final state. The corresponding Lorentz-invariant phase-space element is given by

$$d\Phi_3 = \frac{d^3p_1}{(2\pi)^3 2p_1^0} \frac{d^3p_2}{(2\pi)^3 2p_2^0} \frac{d^3p_3}{(2\pi)^3 2p_3^0} (2\pi)^4 \delta^4(p_a + p_b - p_1 - p_2 - p_3). \quad (6.1)$$

$p_a$  and  $p_b$  denote the momentum vectors of the incoming particles whereas  $p_1$ ,  $p_2$  and  $p_3$  correspond to the final state particles. The incoming particles are assumed to be massless, while  $m_1$ ,  $m_2$  and  $m_3$  are the masses of  $p_1$ ,  $p_2$  and  $p_3$ , respectively. The delta function guarantees energy-momentum conservation.

The integration over the three-particle phase space involves five free parameters, which we choose to be three angle and two energies. In the partonic center-of-mass frame with  $p_a + p_b = (\sqrt{\hat{s}}, 0, 0, 0)$  we use the azimuth and polar angle  $\varphi_3$  and  $\theta_3$  of momentum  $p_3$  wrt. the beam axis. The third angle is the azimuth  $\eta$  of  $p_1$  wrt. momentum  $p_3$ , as shown in Fig. 6.1. Furthermore, we choose the energies  $p_1^0$  and  $p_3^0$  as remaining integration variables. All other parameters are fixed by kinematic constraints.

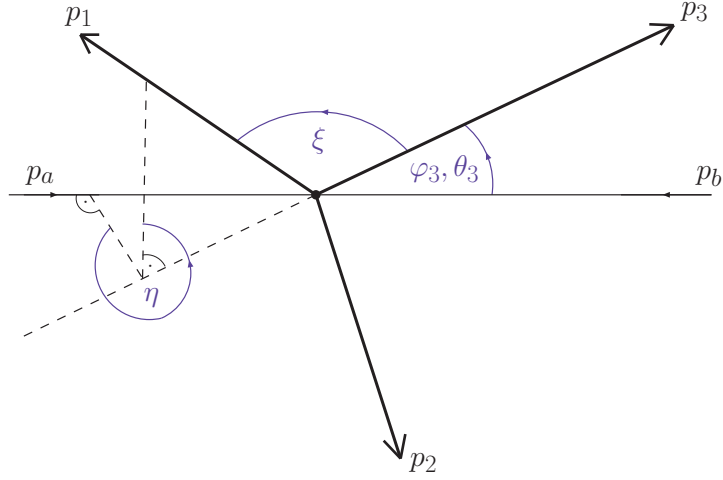


Figure 6.1: Parameterization of the three-particle phase space in terms of the three angle  $\varphi_3, \theta_3, \eta$  and the particle energies  $p_1^0$  and  $p_3^0$ .

Reparameterizing the one-particle phase space elements in (6.1) as

$$\frac{d^3 p_i}{2p_i^0} = \frac{|\vec{p}_i|^2 d|\vec{p}_i|}{2p_i^0} d\varphi_i d\cos\theta_i = \frac{|\vec{p}_i|}{2} dp_i^0 d\varphi_i d\cos\theta_i \quad (6.2)$$

and exploiting energy-momentum conservation to eliminate the integration over  $p_2$ , we can write the three-particle phase space element as

$$d\Phi_3 = \frac{1}{4(2\pi)^5} dp_1^0 d\xi d\eta dp_3^0 d\varphi_3 d\theta_3 |\vec{p}_1||\vec{p}_3| \delta(p_2^2 - m_2^2). \quad (6.3)$$

The polar angle  $\xi$  of  $p_1$  wrt. the momentum  $p_3$  can be fixed by evaluation of the delta function in (6.3), which yields

$$\cos\xi = \frac{|\vec{p}_2|^2 - |\vec{p}_1|^2 - |\vec{p}_3|^2}{2|\vec{p}_1||\vec{p}_3|}. \quad (6.4)$$

We note that this step introduces the factor  $1/(2|\vec{p}_1||\vec{p}_3|)$  to (6.3) resulting from the substitution of the delta function's argument.

Now, we can explicitly parameterize the final state momenta. Using the relation  $|\vec{p}_k| = \sqrt{(p_k^0)^2 - m_k^2}$  we simply have

$$\vec{p}_3 = |\vec{p}_3| \begin{pmatrix} \cos\varphi_3 \sin\theta_3 \\ \sin\varphi_3 \sin\theta_3 \\ \cos\theta_3 \end{pmatrix}. \quad (6.5)$$

The momentum vector  $p_1$  is parameterized in polar coordinates  $\eta$  and  $\xi$  wrt. to  $p_3$ . Thus, in the partonic center-of-mass frame the spacial components of  $p_1$  are given by

$$\vec{p}_1 = |\vec{p}_1| \begin{pmatrix} \cos \varphi_3 & -\sin \varphi_3 & 0 \\ \sin \varphi_3 & \cos \varphi_3 & 0 \\ 0 & 0 & 1 \end{pmatrix} \begin{pmatrix} \cos \theta_3 & 0 & \sin \theta_3 \\ 0 & 1 & 0 \\ -\sin \theta_3 & 0 & \cos \theta_3 \end{pmatrix} \begin{pmatrix} \cos \eta \sin \xi \\ \sin \eta \sin \xi \\ \cos \xi \end{pmatrix}. \quad (6.6)$$

The remaining momentum vector  $p_2$  is fixed by the relation for energy-momentum conservation, i.e.  $p_2 = p_a + p_b - p_1 - p_3$ . Finally, we have to specify the integration limits for the integration over the phase space measure (6.3). For the angle we simply have

$$\varphi_3 \in [0, 2\pi], \quad \cos \theta_3 \in [-1, 1], \quad \eta \in [0, 2\pi]. \quad (6.7)$$

The energies  $p_1^0$  and  $p_3^0$  are fixed by the condition  $|\cos \xi| \leq 1$  which yields the final form

$$\int d\Phi_3 = \frac{1}{8(2\pi)^5} \int_{m_3}^{(p_3^0)^{\max}} dp_3^0 \int_{(p_1^0)^{\min}}^{(p_1^0)^{\max}} dp_1^0 \int_0^{2\pi} d\varphi_3 \int_{-1}^1 d\cos \theta_3 \int_0^{2\pi} d\eta \quad (6.8)$$

with

$$(p_3^0)^{\max} = \frac{\sqrt{\hat{s}}}{2} - \frac{(m_1 + m_2)^2 - m_3^2}{2\sqrt{\hat{s}}}, \quad (6.9)$$

$$(p_1^0)^{\max, \min} = \frac{\sqrt{\hat{s}} - p_3^0}{2\tau} (\tau + m_1^2 - m_2^2) \pm \frac{|\vec{p}_3|}{2\tau} \sqrt{(\tau - (m_1 + m_2)^2)(\tau - (m_1 - m_2)^2)}$$

and  $\tau = \hat{s} - 2\sqrt{\hat{s}}p_3^0 + m_3^2$ . The three-particle phase space integration in the form of Eq. (6.8) allows for a straightforward implementation of the three-particle phase space integration in a Monte Carlo program.

## 6.2 Multi-particle phase space generation

In addition to the previously discussed parameterization of the three-particle phase space, we describe a method for arbitrary many particles in the final state. Unlike the explicit parameterization via angle and energies, the considered approach is based on sequential splitting of 2-particle subspaces [43]. In order to generate the momentum vectors for  $N$  particles,  $N - 1$  splittings are necessary (cf. Fig. 6.2).

Analogous to (6.1), we write the Lorentz-invariant phase-space for  $N$  external final state particles as

$$\int d\Phi_N = \int \left( \prod_{k=1}^N \frac{d^3 p_k}{(2\pi)^3 2p_k^0} \right) (2\pi)^4 \delta^4 \left( p_a + p_b - \sum_{k=1}^N p_k \right). \quad (6.10)$$

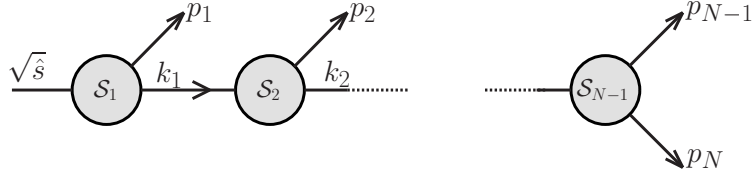


Figure 6.2:  $N$ -particle phase space generation via sequential splitting of 2-particle subspaces.

The number of independent parameters is  $3N - 4$ . It has been shown [43] that the  $N$ -particle phase-space (6.10) can be expressed as a product of a  $1 \rightarrow 2$ -decay process with  $p \rightarrow p_1 + k_1$  and a  $N - 1$ -particle phase-space describing the decays  $k_1 \rightarrow p_2 + \dots + p_N$ , integrated over all possible values for the invariant mass. These results can be translated into the following iterative form of integrations

$$\begin{aligned}
\int d\Phi_N &= \frac{1}{2M_0} \int_{m_2+\dots+m_N}^{M_0-m_1} dM_1 \mathcal{S}_1(M_0; M_1, m_1) \\
&\quad \times \int_{m_3+\dots+m_N}^{M_1-m_2} dM_2 \mathcal{S}_2(M_1; M_2, m_2) \\
&\quad \times \dots \\
&\quad \times \int_{m_{N-1}+m_N}^{M_{N-3}-m_{N-2}} dM_{N-2} \mathcal{S}_{N-2}(M_{N-3}; M_{N-2}, m_{N-2}) \\
&\quad \times \mathcal{S}_{N-1}(M_{N-2}; M_{N-1}, m_{N-1})
\end{aligned} \tag{6.11}$$

where  $m_i$  is the mass of the  $i$ th external particle with momentum vector  $p_i$ . Furthermore,  $M_0 = \sqrt{\hat{s}}$  and  $M_{N-1} = m_N$ . As illustrated in Fig. 6.2, the function  $\mathcal{S}_l(M_{l-1}; M_l, m_l)$  corresponds to the  $l$ th iteration of an  $1 \rightarrow 2$  decay process. Thus, we can write

$$\mathcal{S}_l(M_{l-1}; M_l, m_l) = \frac{1}{4M_{l-1}} \lambda^{1/2}(M_{l-1}^2, M_l^2, m_l^2) \int_0^{2\pi} d\varphi_l \int_{-1}^1 d\cos\theta_l, \tag{6.12}$$

where  $\varphi_l$  and  $\theta_l$  are the azimuth and polar angle given in the rest frame of the decaying particle with momentum  $k_{l-1}$  and mass  $M_{l-1}$ .  $\lambda(x, y, z) = x^2 + y^2 + z^2 - 2xy - 2xz - 2yz$  is the Källén-function. The momenta  $p'_l$  and  $k_l$  corresponding to the decay products in the rest frame of  $k_{l-1}$  are given by

$$\begin{aligned}
\vec{k}_l &= -\vec{p}'_l = |\vec{k}_l| \begin{pmatrix} \cos\varphi_l \sin\theta_l \\ \sin\varphi_l \sin\theta_l \\ \cos\theta_l \end{pmatrix}, \\
p_l^0 &= \sqrt{|\vec{k}_l|^2 + m_l^2}, \\
k_l^0 &= \sqrt{|\vec{k}_l|^2 + M_l^2},
\end{aligned} \tag{6.13}$$



where  $|\vec{k}_l| = 1/(2M_{l-1}) \lambda^{1/2}(M_{l-1}^2, M_l^2, m_l^2)$ . While  $k_l$  corresponds to the momentum vector for the decay of the next iteration,  $p'_l$  results in the external momentum  $p_l$  after a Lorentz-boost into the partonic center-of-mass frame. Thus, for each momentum vector  $p'_l$  we need  $l - 1$  iterative boosts wrt. the frames of  $k_{l-1}, k_{l-2}, \dots, k_1$ , in order to arrive in the partonic center-of-mass frame. Such a single boost for the momentum  $p'$ , which is defined in the rest frame of  $k$ , into the frame of  $k$  is given by

$$\begin{aligned}\vec{p} &= \vec{p}' + \vec{k} \left( \frac{\vec{k} \cdot \vec{p}'}{M^2(\gamma + 1)} + \frac{p'^0}{M} \right), \\ p^0 &= \frac{1}{M} (k^0 p'^0 + \vec{k} \cdot \vec{p}')\end{aligned}\tag{6.14}$$

with  $k^2 = M^2$  and  $\gamma = k^0/M$ .

### 6.2.1 Generation of soft and collinear limits

Let us now consider the method discussed above for the special case of soft and collinear configurations. Generating those exceptional phase space points is extremely helpful in order to perform checks of the dipole subtraction method. Through having systematic control over the strength of a soft or collinear singularity, one can check the cancellations between dipoles and squared matrix elements. Furthermore, the numerical stability of squared matrix elements can be tested. We present a simple modification of the sequential splitting method, which offers the possibility to successively generate the limit for one soft momentum vector or two collinear ones. We note that when generating those singular events special care has to be taken in order to keep all momenta on-shell and fulfill the energy-momentum relation with high precision.

For the generation of collinear momentum vectors we restrict the method to generate only one pair of collinear momentum vectors, while the remaining configurations are assumed to be non-exceptional. This still allows to check all possible dipole types. Furthermore, without loss of generality we choose the first two momenta  $p_1$  and  $p_2$  from (6.11) to be the collinear pair. Starting with the first splitting, we obtain the momentum vector  $p_1^\mu = (p_1^0, \vec{p}_1)^\mu$  with

$$\vec{p}_1 = p_1^0 \begin{pmatrix} \cos \varphi_1 \sin \theta_1 \\ \sin \varphi_1 \sin \theta_1 \\ \cos \theta_1 \end{pmatrix}.\tag{6.15}$$

$p_1$  is given in the partonic center-of-mass frame and needs not to be boosted. The second splitting yields  $p_2^\mu = (p_2^0, \vec{p}_2)^\mu$  with

$$\vec{p}_2 = p_2^0 \begin{pmatrix} \cos \varphi_2 \sin \theta_2 \\ \sin \varphi_2 \sin \theta_2 \\ \cos \theta_2 \end{pmatrix}\tag{6.16}$$

in the rest frame of  $-\vec{p}_1$ . Thus, the vector  $p'_2$  is related to  $p_2$  by a boost in the direction of  $+\vec{p}_1$ . Assuming that this boost does not strongly alter the angle  $\varphi_2$  and  $\theta_2$  in the situation where  $p_1$  and  $p_2$  are collinear, we can simply write

$$\begin{aligned} p_1 \cdot p_2 &\stackrel{\text{coll.}}{=} p_1^0 p_2^0 - \vec{p}_1 \cdot \vec{p}'_2 \\ &= p_1^0 p_2^0 (1 - \sin \theta_1 \sin \theta_2 \cos(\varphi_1 - \varphi_2) - \cos \theta_1 \cos \theta_2). \end{aligned} \quad (6.17)$$

In order to parameterize the collinear limit we introduce the abbreviations  $\cos \theta_k =: 2X_k - 1$  and  $\varphi_k =: 2\pi Y_k$  with  $X_k, Y_k \in [0, 1]$  and write

$$\begin{aligned} X_2 &= (1 - \eta)X_1, \\ Y_2 &= (1 - \eta)Y_1. \end{aligned} \quad (6.18)$$

Hence, we can generate a collinear configuration through  $\eta \rightarrow 0$ , which corresponds to a rotation of  $p_2$  towards the fixed direction of  $p_1$ . Inserting (6.18) into Eq. (6.17) and expanding up to  $\mathcal{O}(\eta^2)$ , we can solve for  $\eta^2$  and obtain

$$\eta^2 = \Delta_{12} \frac{2(1 - X_1)}{X_1(1 + 16\pi^2 Y_1^2(1 - X_1)^2)} \quad (6.19)$$

with  $\Delta_{ij} = p_i \cdot p_j / (p_i^0 p_j^0)$ . Now, for a fixed configuration<sup>1</sup> of  $p_1$  we can specify the desired strength of the collinear singularity  $\Delta_{12}$  and rotate  $p_2$  accordingly. All remaining momenta  $p_3, \dots, p_N$  can be obtained from further splittings as described in Sect. 6.2 without modifications. Thus, we can generate a  $N$ -particle phase space with any collinear singularity between two final-state momenta, while total energy-momentum conservation and all on-shell relations are guaranteed.

It is also necessary to consider the case of a final-state momentum vector that is collinear with the beam axis. We choose  $p_1$  from the first splitting to be collinear with one of the momentum vectors from the initial-state particles in the partonic center-of-mass frame. Their momentum vectors are given by  $p_{a/b} = \sqrt{\hat{s}}(1, 0, 0, \pm 1)$  and yield

$$p_{a/b} \cdot p_1 = p_1^0 p_{a/b}^0 (1 \mp \cos \theta_1). \quad (6.20)$$

Using the abbreviation  $\cos \theta_1 = 2X_1 - 1$  we find the conditions

$$X_1 = 1 - \frac{1}{2}\Delta_{a1}, \quad X_1 = \frac{1}{2}\Delta_{b1} \quad (6.21)$$

for  $p_1$  being collinear to  $p_a$  or  $p_b$ , respectively, given the desired strength of the collinear singularity  $\Delta_{ij}$ .

---

<sup>1</sup>The cases  $X_1 = 0, 1$  have to be excluded. They correspond to events along the beam axis and will be considered separately.

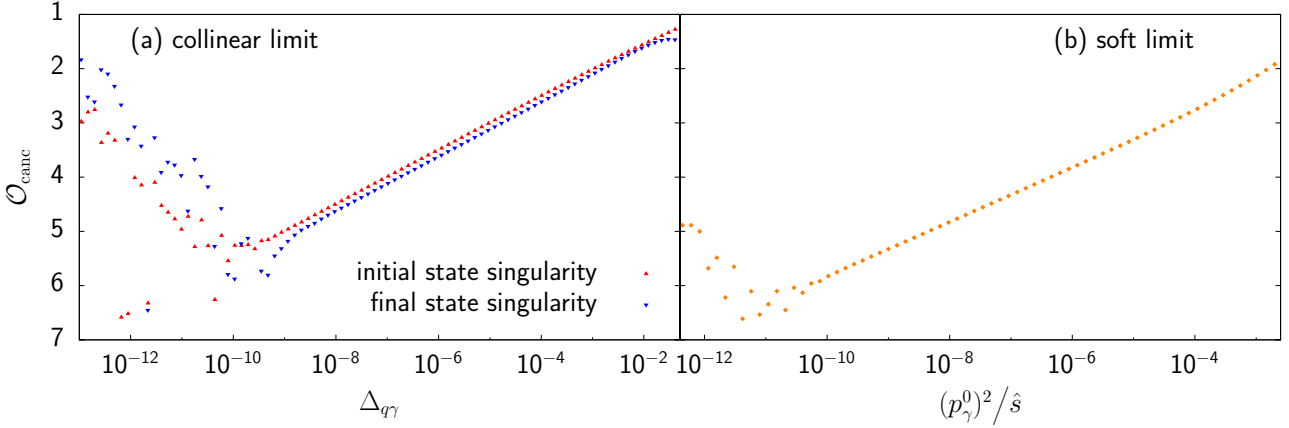


Figure 6.3: Magnitude of cancellations between the squared matrix element and the dipole subtraction terms for collinear quark-photon configurations (a) and a soft photon configuration (b) in the process  $q'g \rightarrow W^+q\gamma$  at  $\sqrt{\hat{s}} = 500$  GeV.

The generation of a soft configuration is simple if we choose again the momentum vector  $p_1$  from the first splitting in (6.11). As no Lorentz-boost is involved in the first splitting, the energy component of this vector is given by

$$p_1^0 = \frac{\sqrt{\hat{s}}}{2} \left( 1 - \frac{M_1^2}{\hat{s}} \right), \quad (6.22)$$

where  $M_1$  is the first integration variable from the phase space integration (6.11). By choosing  $M_1$  accordingly it is possible to generate a soft singularity for any desired strength  $p_1^0/\sqrt{\hat{s}}$ . The remaining momentum vectors  $p_2, \dots, p_N$  can be obtained from further splittings as described in Sect. 6.2 without modifications.

To demonstrate the methods discussed above we give two examples for the three-particle phase space of the real photonic corrections for  $W$ +jet production. In particular, we consider the contribution of the partonic process  $q'g \rightarrow W^+q\gamma$  and generate the limit for collinear quark-photon configurations as well as the soft photon limit. The unpolarized squared matrix element  $M^{q'g}$  in (5.6) exhibits collinear singularities for the cases  $p_{q'} \cdot p_\gamma \rightarrow 0$  and  $p_q \cdot p_\gamma \rightarrow 0$ , i.e. where the photon becomes collinear to the initial or final state quark, respectively. Furthermore, the soft photon limit is represented through  $p_\gamma^0 \rightarrow 0$ . In order to check the proper cancellation of these singularities with the corresponding dipole subtraction term  $M_{\text{sub}}^{q'g}$  (5.6) we define

$$\mathcal{O}_{\text{canc}} = -\log_{10} \left| \frac{M^{q'g} - M_{\text{sub}}^{q'g}}{M_{\text{sub}}^{q'g}} \right| \quad (6.23)$$

and generate the limits

$$\Delta_{q\gamma} = 10^{-2} \dots 10^{-13}, \quad (6.24)$$

$$\frac{(p_\gamma^0)^2}{\hat{s}} = 10^{-2} \dots 10^{-12}. \quad (6.25)$$

The numerical result for the collinear limit (6.24) is shown in Fig. 6.3a. For the initial- as well as for the final-state singularity the order of the cancellation  $\mathcal{O}_{\text{canc}}$  constantly increases with the strength of the singularity in the range  $10^{-9} \leq \Delta_{q\gamma} \leq 10^{-2}$ . Furthermore, in this range we observe a slope of  $\mathcal{O}_{\text{canc}}$  as a function of  $\Delta_{q\gamma}$  of about 0.5. This is the expected behavior resulting from the dipole method: The leading singularities of the form  $(p_q \cdot p_\gamma)^{-1}$  cancel between the squared matrix element and the dipoles, while an (integrable) square root singularity  $1/\sqrt{p_q \cdot p_\gamma}$  remains. This requires  $\mathcal{O}_{\text{canc}}$  in (6.23) to behave like  $1/2 \log_{10}(\Delta_{q\gamma})$  for collinear or soft configurations, which corresponds exactly to the observed slope of 0.5 in Fig. 6.3a. This behavior demonstrates the correctness of the implementation of the dipole subtraction terms. However, for  $\Delta_{q\gamma} > 10^{-9}$  the cancellations fail and fluctuate. The reasons are numerical instabilities in the expressions of the squared matrix element for these very collinear configurations. This is due to the limited numerical precision in a computer implementation.

We find a similar picture for the soft photon limit in Fig. 6.3b. The dipole subtraction method works well for photon energies down to  $10^{-5} \times \sqrt{\hat{s}}$ . Again, we find the expected behavior of  $\mathcal{O}_{\text{canc}}$  vs.  $(p_\gamma^0)^2/\hat{s}$  with a slope of 0.5 in the range  $10^{-10} \leq (p_\gamma^0)^2/\hat{s} \leq 10^{-2}$ . For even softer photons the numerical expressions become unstable by the same reasons as above.

Thus, in order to obtain a numerically stable implementation of the dipole subtraction method, one has to cut out these highly singular regions, where the accurate evaluation of the squared matrix element fails. If chosen small enough, this cut does not affect the value of the cross section because the difference of the squared matrix element and the dipoles is free from singularities and the removed phase space volume is proportional to the value of the cut. The numerical results presented in Ch. 8 have been obtained with a cut at  $10^{-8}$  for  $\Delta_{q\gamma}$  and  $(p_\gamma^0)^2/\hat{s}$ . We checked that the variation of this cut by a factor 10 does not affect the results for the cross section.

# Chapter 7

## Checks and implementations

Every part of the presented calculation was performed in at least two completely independent ways. On the one hand, the results were derived by S. Pozzorini and A. Kulesza, on the other hand by M. S.

The tensor integrals had been reduced analytically using two different MATHEMATICA [44] codes and were checked against results in FEYNCALC [30]. The algebraic reduction to standard matrix elements as well as their interference had been implemented in FORM [45] and MATHEMATICA, independently. We verified the cancellation of ultraviolet divergencies analytically and numerically. Similar, for the IR singularities of  $W$  production we checked analytically the cancellation between virtual and real corrections for both, the massive and dimensional regularization scheme. Furthermore, we verified that the one-loop corrections (3.24) satisfy the Ward identity

$$\varepsilon_\mu^*(p_V) p_{g\nu} \bar{v}(p_{\bar{q}}) \left[ \delta \mathcal{A}_{1,I}^{\mu\nu}(M_\Gamma^2) \omega_\lambda \right] u(p_q) = 0 \quad \text{for } I=A,N,X,Y, \quad (7.1)$$

i.e. the polarization vector of the gluon  $\varepsilon_\nu^*(p_g)$  has been replaced by its momentum vector  $p_{g\nu}$ . A similar Ward identity holds for the lowest-order amplitude. We note that the Abelian one-loop contribution and the non-Abelian contribution in the case of neutral gauge boson production satisfy two additional Ward identities<sup>1</sup>

$$\begin{aligned} p_{V\mu} \varepsilon_\nu^*(p_g) \bar{v}(p_{\bar{q}}) \left[ \delta \mathcal{A}_{1,I}^{\mu\nu}(M_\Gamma^2) \omega_\lambda \right] u(p_q) &= 0, \\ p_{V\mu} p_{g\nu} \bar{v}(p_{\bar{q}}) \left[ \delta \mathcal{A}_{1,I}^{\mu\nu}(M_\Gamma^2) \omega_\lambda \right] u(p_q) &= 0 \quad \text{for } I=A,(N). \end{aligned}$$

The NLL approximation at one-loop that had been derived from the general prescription of [36] was checked against the NLL terms of the full one-loop calculation.

---

<sup>1</sup>Similar identities for the N-, X- and Y- form factors for  $W$  boson production exist but are less trivial due to the non-vanishing contributions from would-be Goldstone bosons on the right-hand side. This means that the calculation of the unpolarized cross section requires the use of the exact expression for the  $W$ -boson polarization sum. Instead, owing to (7.1), the gluon polarization sum can be implemented as  $-g_{\nu\nu'}$ .

Also the IR-singular contributions for  $W$  production in the high-energy limit were reproduced within this framework, as shown in (4.40).

For the numerical evaluation we implemented the results in two independent FORTRAN programs. For the evaluation of the IR-finite loop integrals we used a set of routines by A. Denner and, alternatively, the FF library [46]. The squared matrix element for the real corrections of  $W$  production was checked numerically against MADGRAPH [47]. In order to perform the 3-particle phase-space integration we implemented the parameterization described in Sect. 6.1 and used the adaptive Monte-Carlo routine VEGAS [48]. Furthermore, the phase space generator RAMBO [49] had been used for testing. The dipole subtraction terms were derived and implemented in two different ways, using the mass regularization of IR singularities and the dimensional regularization. Detailed comparisons at analytical and numerical level were performed, and the agreement between the predictions generated within two different regularization schemes provides a strong check on the calculation of the real corrections. As the dipole method relies on the subtraction of large numbers in the integrand, we also checked the numerical stability of the squared real emission matrix element for soft and collinear configurations. The numerical cancellations for these configurations was tested with the method described in Sect. 6.2.1 and is implemented in the C programming language.

Finally, we can state that we found complete agreement for the final results at analytical level and fully consistent results within the statistical errors for the numerical comparison.

As far as comparisons were possible we also checked with results in the literature. The revised results of Ref. [17] for photon and  $Z$  production at large transverse momenta agree with our result. In Ref. [23] a slightly different observable for  $W$  production at large  $p_T$  has been studied. Nevertheless, we find qualitatively similar results.

# Chapter 8

## Numerical results

In this chapter we present numerical results for the previously discussed electroweak corrections to gauge boson production at large transverse momenta. We consider hadronic initial states for the LHC and the Tevatron. In Sect. 8.1 the discussion begins with a first look on numerical results at parton level for  $Z$  production. Results for the hadronic production of a photon, a  $Z$  or a  $W$  boson in association with a jet are presented in Sect. 8.2 for the LHC and in Sect. 8.3 for the Tevatron. In these sections, we study the transverse momentum ( $p_T$ ) distributions as well as  $p_T$ -integrated cross sections. Furthermore, we present various ratios of  $p_T$ -distributions for different gauge bosons. Technical plots are also given, concerning the quality of the high-energy approximations and the relative size of virtual and real corrections for  $W$ +jet production. The various input parameters are specified in Appendix A.

### 8.1 Results for $Z$ production at partonic level

We begin by investigating the weak one-loop results for  $Z$  production at partonic level and consider the unpolarized differential cross section

$$\frac{d\hat{\sigma}^{ab \rightarrow Zk}}{d\cos\theta} = \frac{\hat{s} - M_Z^2}{32\pi N_{ab}\hat{s}^2} \overline{\sum} |\mathcal{M}^{ab \rightarrow Zk}|^2, \quad (8.1)$$

where  $\cos\theta$  corresponds to the cosine of the scattering angle in the partonic center-of-mass frame. The correction of the weak next-to-leading order (NLO) calculation wrt. the lowest order (LO) is expressed through

$$\hat{\mathcal{R}}_{\text{NLO/LO}}^{ab} = \frac{d\hat{\sigma}_{\text{NLO}}^{ab}/d\cos\theta}{d\hat{\sigma}_{\text{LO}}^{ab}/d\cos\theta} - 1. \quad (8.2)$$

Similarly the quality of the next-to-leading-logarithmic (NLL) and the next-to-next-leading-logarithmic (NNLL) approximations wrt. to the exact NLO calculation are denoted by  $\hat{\mathcal{R}}_{\text{NLL/NLO}}^{ab}$  and  $\hat{\mathcal{R}}_{\text{NNLL/NLO}}^{ab}$ , respectively. These ratios, calculated at

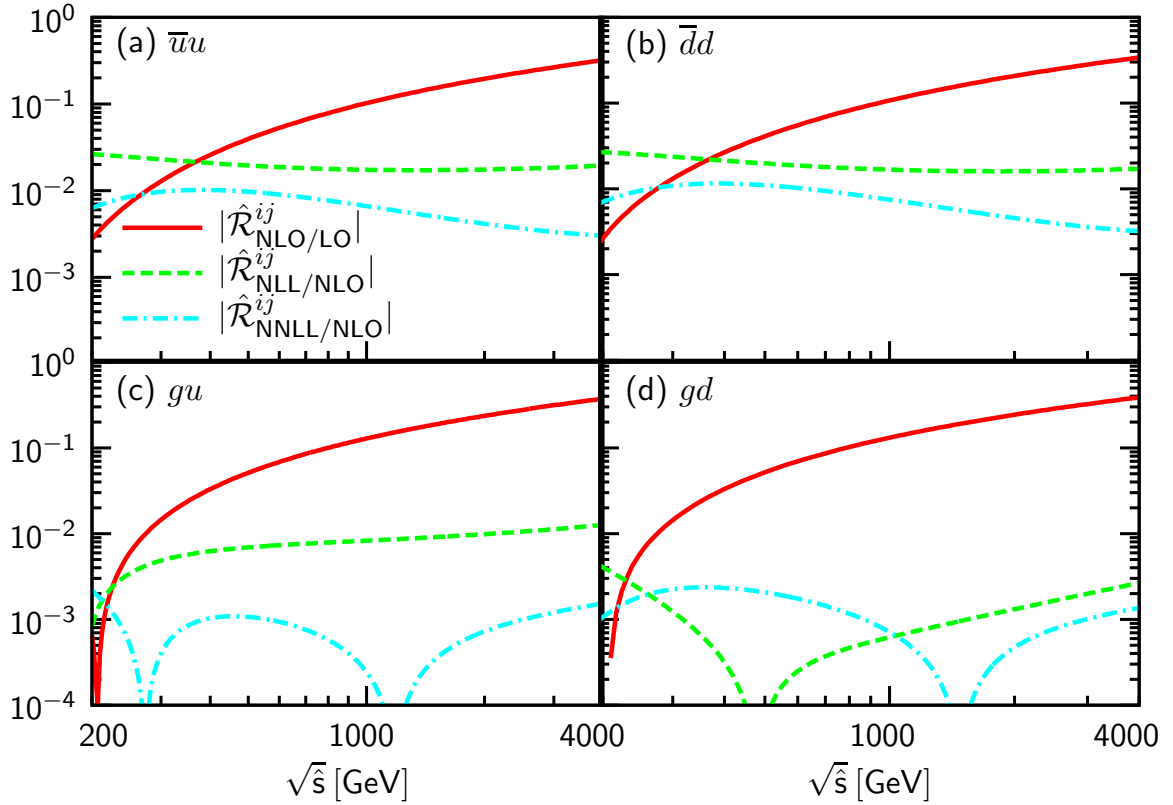


Figure 8.1: Relative one-loop corrections for  $Z$  boson production to the partonic differential cross sections  $d\hat{\sigma}^{ab}/d\cos\theta$  at  $\cos\theta = 0$  for (a)  $\bar{u}u$  channel, (b)  $\bar{d}d$  channel, (c)  $gu$  channel, (d)  $gd$  channel. The solid, dashed and dot-dashed lines denote the modulus of the  $\hat{\mathcal{R}}$  ratios, as defined in (8.2), for the full NLO cross section, the NLL approximation and the NNLL approximation of the one-loop cross section, respectively.

$\cos\theta=0$ , are displayed as a function of  $\sqrt{\hat{s}}$  in Fig. 8.1. We present results for the four partonic processes:  $\bar{u}u \rightarrow Zg$  (Fig. 8.1a),  $\bar{d}d \rightarrow Zg$  (Fig. 8.1b),  $gu \rightarrow Zu$  (Fig. 8.1c),  $gd \rightarrow Zd$  (Fig. 8.1d).

The size of the weak NLO correction grows with the energy and reaches 30% for all channels at  $\sqrt{\hat{s}} \approx 4$  TeV. The sign of this correction is negative. From Fig. 8.1 we conclude that the NLL terms provide a fairly good approximation to the full NLO result for  $\sqrt{\hat{s}} \geq 200$  GeV, with the remaining terms responsible for less than 3% of the cross section in the  $u\bar{u}$  and  $d\bar{d}$  channels, and less than 1% in the  $gu$  and  $gd$  channels. The quality of the NNLL approximation is very good in all channels, better or comparable to 1% in the full region under consideration.



## 8.2 Results for the LHC

Let us now turn to the numerical results for the LHC, i.e. proton-proton collisions at  $\sqrt{s} = 14$  TeV, producing an electroweak gauge boson in association with a jet. We choose the cut on the transverse momentum of the jet to be  $p_{T,j}^{\min} = 100$  GeV and present results for  $p_T$  of the gauge boson in the range 100 GeV–2 TeV. In the case of  $W$ +jet production, we treat the emission of an additional photon fully inclusive unless otherwise stated and choose the value of the separation parameter below which quark-photon recombination is applied to be  $R_{\text{sep}} = 0.4$ . The dependence of our predictions on  $R_{\text{sep}}$  is negligible. We have verified that the shift of the transverse-momentum distribution induced by variations of this parameter in the range  $0.1 \leq R_{\text{sep}} \leq 1.0$  does not exceed a few permille.

The transverse-momentum distributions for the reactions  $pp \rightarrow \gamma j$  and  $pp \rightarrow Z j$  are shown in Fig. 8.2 and for  $pp \rightarrow W^\pm j$  in Fig. 8.3. The LO results are depicted in Fig. 8.2a and Fig. 8.3a for neutral and charged gauge boson production, respectively. In the considered range of  $p_T$  the cross sections fall off by about seven orders of magnitude but still, the 1–2 TeV region will be accessible by LHC and provide sizable event rates (cf. (2.39)). The different size of the LO cross sections for photon and  $Z$  boson production in Fig. 8.2a is mainly due to the different numerical values for the vector boson couplings to quarks. In contrast, the cross sections for  $W^+$  and  $W^-$  production in Fig. 8.3a differ as a reason of the quark content in the proton initial state at the LHC. In (b) and (c) of Fig. 8.2 and Fig. 8.3 the relative size of the NLO, one-loop NLL, one-loop NNLL and NNLO corrections wrt. the LO predictions is shown for each gauge boson separately<sup>1</sup>. Equally for all gauge boson processes, the one-loop contributions are negative and increase with  $p_T$ , while the leading two-loop contributions are of positive size increasing with  $p_T$ . We also observe that the one-loop NLL and NNLL approximations for all gauge boson processes are in good agreement (at the 1–2% level) with the full NLO result for  $p_T \geq 100$  GeV. The NLO correction for photon production in Fig. 8.2b ranges from  $-6\%$  at  $p_T = 500$  GeV up to  $-17\%$  at  $p_T = 2$  TeV. The corresponding NNLO contribution amounts to  $+3\%$  at  $p_T = 2$  TeV, yielding a total (i.e. together with the NLO) correction of  $-14\%$  wrt. the LO. For the production of the massive gauge bosons  $Z$  and  $W^\pm$  we find even larger corrections. The NLO corrections for  $Z$  production in Fig. 8.2c amounts to  $-13\%$  at  $p_T = 500$  GeV and increases up to  $-37\%$  at  $p_T = 2$  TeV of the LO cross section. The two-loop contributions have an effect of  $+8\%$  at  $p_T = 2$  TeV. The size of the corrections to photon and  $Z$  production differs by roughly a factor of two. This is mainly due to the different numerical values of the coupling factors, which multiply

---

<sup>1</sup>We note that for the case of photon and  $Z$  boson production the symbols NLO, NLL and NNLL correspond to the weak one-loop correction and its approximations. For  $W$  boson production NLO denotes the full  $\mathcal{O}(\alpha)$  correction including virtual and real corrections, whereas NLL and NNLL refer to the approximations of the IR-finite one-loop terms as defined in (4.1). The symbol NNLO denotes the sum of NLO and dominant two-loop contributions in the high-energy limit, cf. Eq. (4.50), (4.51).

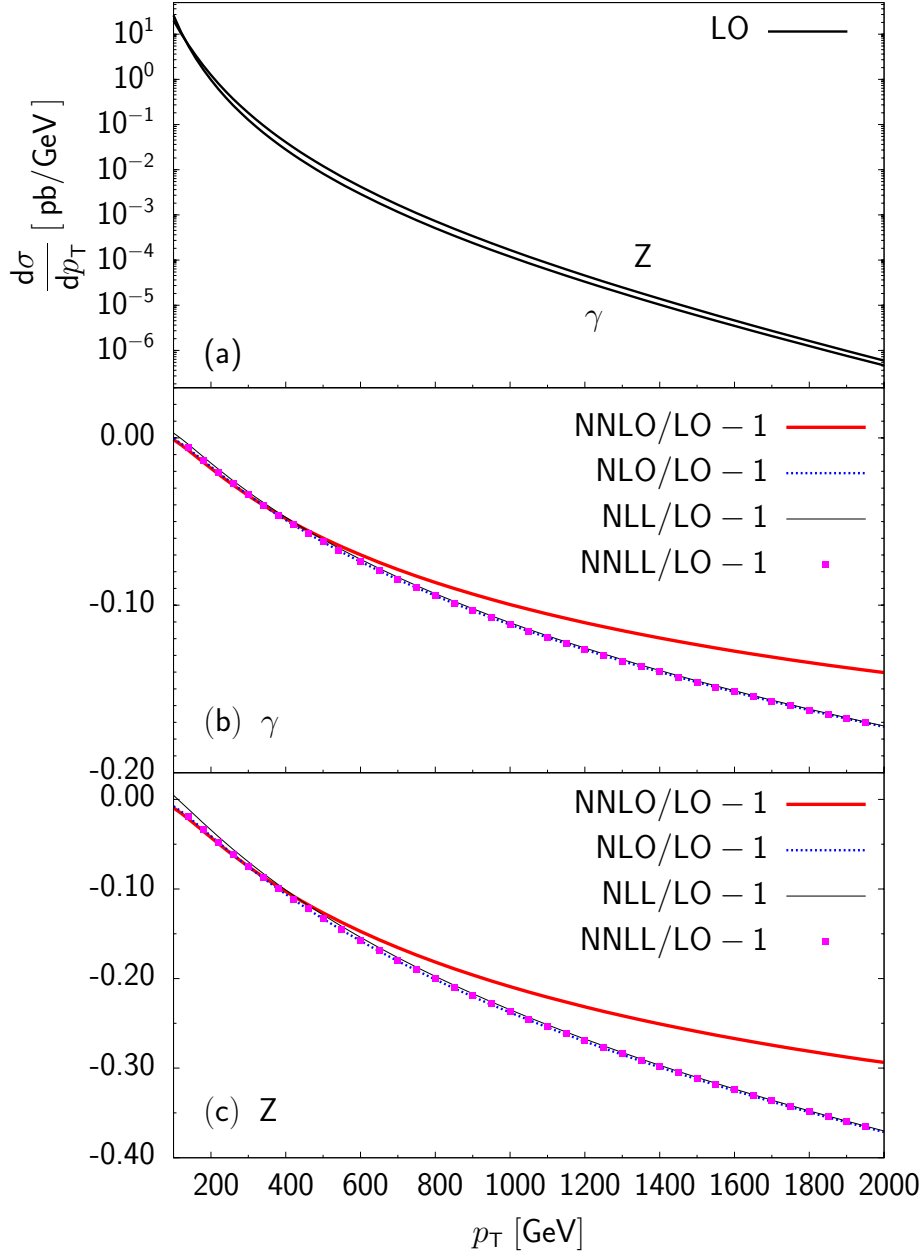


Figure 8.2: Transverse-momentum distribution for neutral gauge boson production at the LHC. (a) LO distribution for  $pp \rightarrow \gamma j$  and  $pp \rightarrow Z j$ . Relative NLO (dotted), NLL (thin solid), NNLL (squares) and NNLO (two-loop approximation, thick solid) electroweak correction wrt. the LO distribution for  $pp \rightarrow \gamma j$  in (b) and similar for  $pp \rightarrow Z j$  in (c).

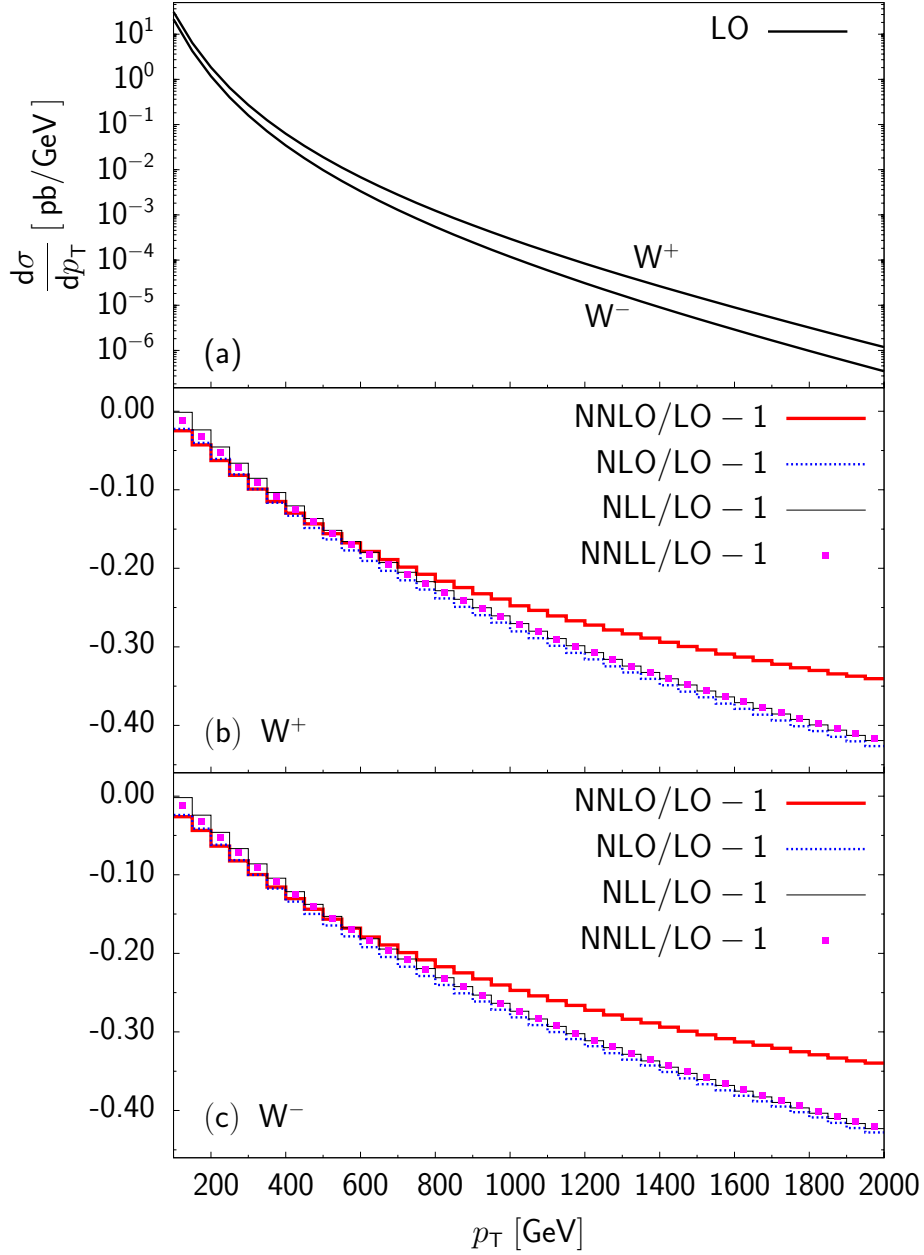


Figure 8.3: Transverse-momentum distribution for  $W$ -boson production at the LHC. (a) LO distribution for  $pp \rightarrow W^+ j$  and  $pp \rightarrow W^- j$ . Relative NLO (dotted), NLL (thin solid), NNLL (squares) and NNLO (two-loop approximation, thick solid) electroweak correction wrt. the LO distribution for  $pp \rightarrow W^+ j$  in (b) and similar for  $pp \rightarrow W^- j$  in (c).

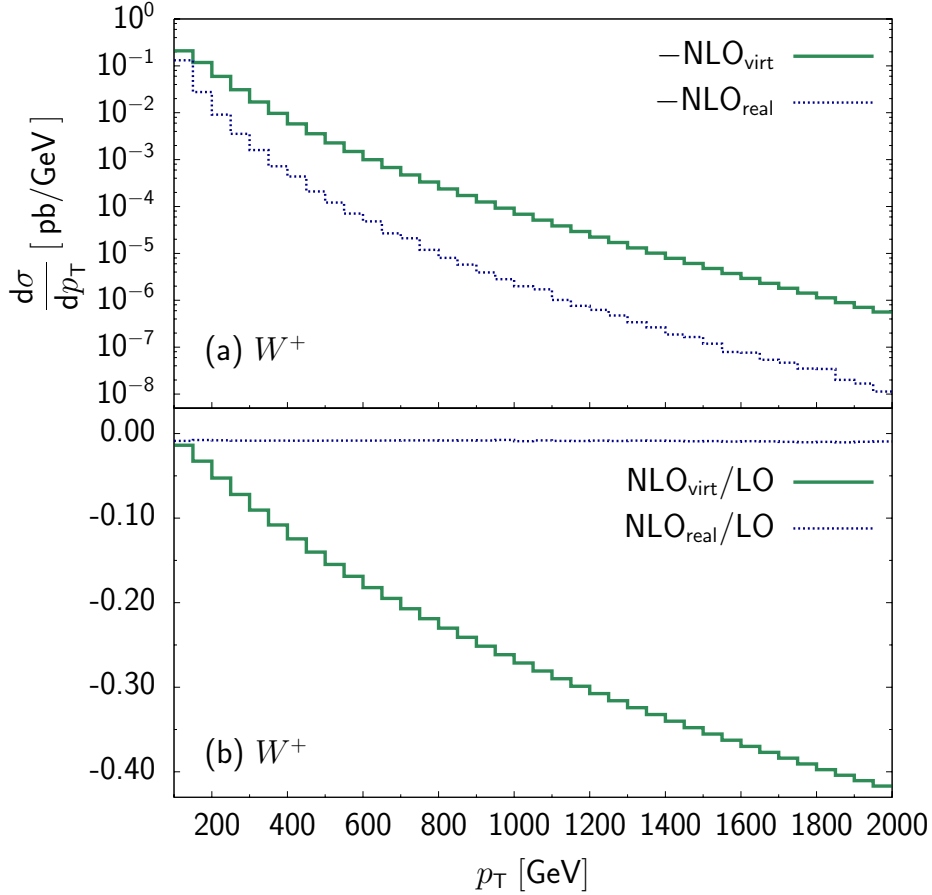


Figure 8.4: IR-finite parts of the virtual ( $\text{NLO}_{\text{virt}}$ ) and real ( $\text{NLO}_{\text{real}}$ ) contributions to the  $p_T$ -distribution of  $W$  bosons in the process  $pp \rightarrow W^+ j$  at  $\sqrt{s} = 14$  TeV.

the corresponding leading logarithms. The behavior of the relative corrections to  $W^+$  and  $W^-$  production in Fig. 8.3b and Fig. 8.3c, respectively, is very similar. The importance of the NLO contribution increases significantly with  $p_T$  and leads to a negative correction ranging from  $-15\%$  at  $p_T = 500$  GeV to  $-43\%$  at  $p_T = 2$  TeV. The two-loop terms are positive and amount to  $+3\%$  at  $p_T = 1$  TeV and  $+9\%$  at  $p_T = 2$  TeV. This shifts the relative corrections for  $W^+$  and  $W^-$  production up to  $-25\%$  at  $p_T = 1$  TeV and  $-34\%$  at  $p_T = 2$  TeV.

The IR-finite parts of the virtual ( $\text{NLO}_{\text{virt}}$ ) and real ( $\text{NLO}_{\text{real}}$ ) corrections to  $W^+$ +jet production at the LHC are shown separately in Fig. 8.4a. These IR-finite parts are constructed by subtracting the IR divergencies (3.88) from the virtual corrections and adding it to the real ones. Fig. 8.4b shows the relative size of the  $\text{NLO}_{\text{virt}}$  and  $\text{NLO}_{\text{real}}$  corrections wrt. the LO predictions. The  $\text{NLO}_{\text{virt}}$  contribution dominates the full NLO correction and amounts up to  $-42\%$  at  $p_T = 2$  TeV. The  $\text{NLO}_{\text{real}}$  part contributes with a smaller and nearly constant correction of about  $-1\%$  in the entire  $p_T$ -range. This means that, for the case of fully inclusive photon radiation, the  $\text{NLO}_{\text{virt}}$  part represents a good approximation of the full NLO

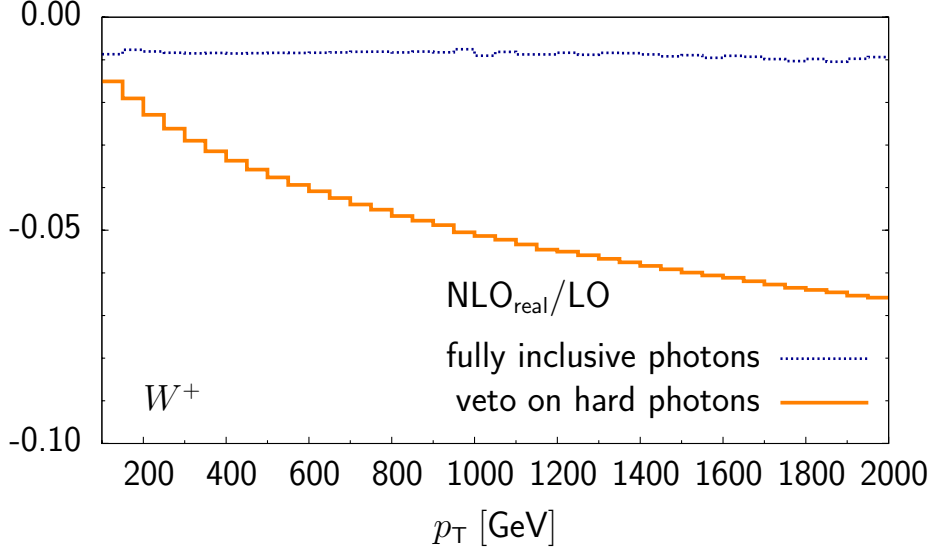


Figure 8.5: Relative size of the real correction ( $\text{NLO}_{\text{real}}$ ) wrt. the LO for fully inclusive photon radiation and the case where visible photons are rejected, plotted as a function of  $p_T$  for the process  $pp \rightarrow W^+ j$  at  $\sqrt{s} = 14$  TeV.

correction. For less inclusive observables where a veto on hard photons is imposed, the  $\text{NLO}_{\text{real}}$  contribution can become important. This is shown in Fig. 8.5 for  $W^+$  production. We compare the relative contribution of  $\text{NLO}_{\text{real}}$  for the case of fully inclusive photon radiation (as already shown in Fig. 8.4) with the case where visible photons with  $p_{T,\gamma} > 10$  GeV and  $R(\gamma, j) > 0.4$  are rejected. This veto leads to a significant enhancement of the (absolute size of the)  $\text{NLO}_{\text{real}}$  part, which can exceed  $-5\%$  for  $p_T \geq 1$  TeV.

The high-energy behavior of the virtual one-loop corrections is described by the compact NLL and NNLL approximations presented in Sect. 4. The quality of these approximations is shown in Fig. 8.6a–c for neutral and charged gauge boson production. From Fig. 8.6a we conclude that the NLL approximation for photon production works very well, differing from the full NLO prediction by about 3 permille at low  $p_T$  and by less than 1 permille at  $p_T \approx 2$  TeV. The quality of the NNLL approximation is extremely good, with an accuracy of  $10^{-3}$  or better in the entire  $p_T$ -range. Also for  $Z$  boson production, in Fig. 8.6b, we find that the NLL approximation works well. It differs from the full NLO prediction by about 1% at low  $p_T$  and by 0.2% at  $p_T = 2$  TeV. The quality of the NNLL approximation is at the permille level (or better) in the entire  $p_T$ -range. For the case of the electroweak corrections to  $W$  production the high energy approximations are derived for the IR-finite part  $\text{NLO}_{\text{virt}}$ . Thus, in Fig. 8.6 we compare the corresponding NLL and NNLL approximations with  $\text{NLO}_{\text{virt}}$  for  $W^+$  production. The NLL approximation works well differing from the exact  $\text{NLO}_{\text{virt}}$  result by less than 1% for  $p_T \geq 200$  GeV. The quality of the NNLL approximation is about 2 permille at low  $p_T$  and better than 0.3 permille for

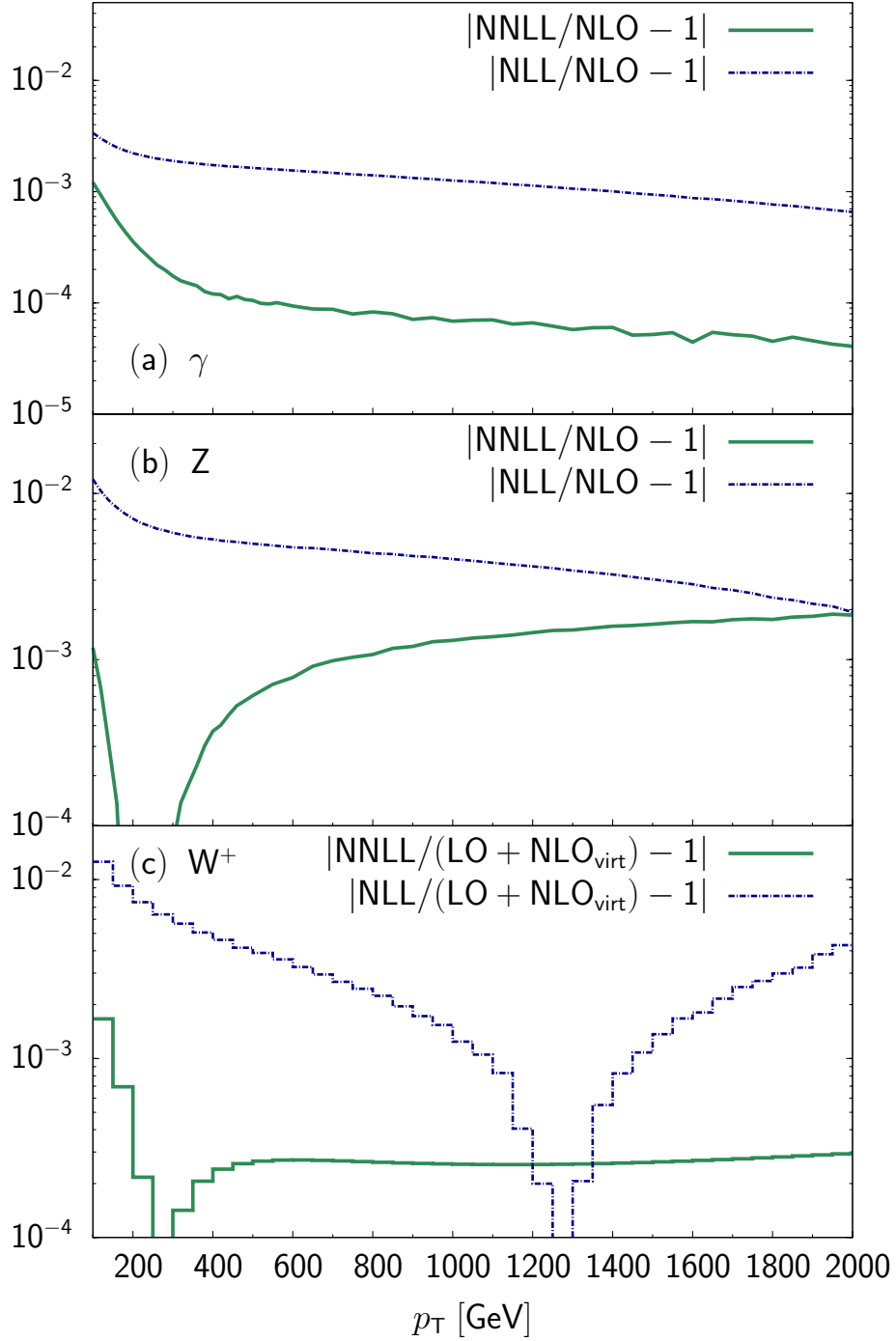


Figure 8.6: Relative precision of the high-energy approximations at one-loop in the processes  $pp \rightarrow \gamma j$  (a),  $pp \rightarrow Z j$  (b) and  $pp \rightarrow W^+ j$  (c) at  $\sqrt{s} = 14$  TeV as a function of  $p_T$ : NNLL (solid) and NLL (dash-dotted) wrt. the exact one-loop result.

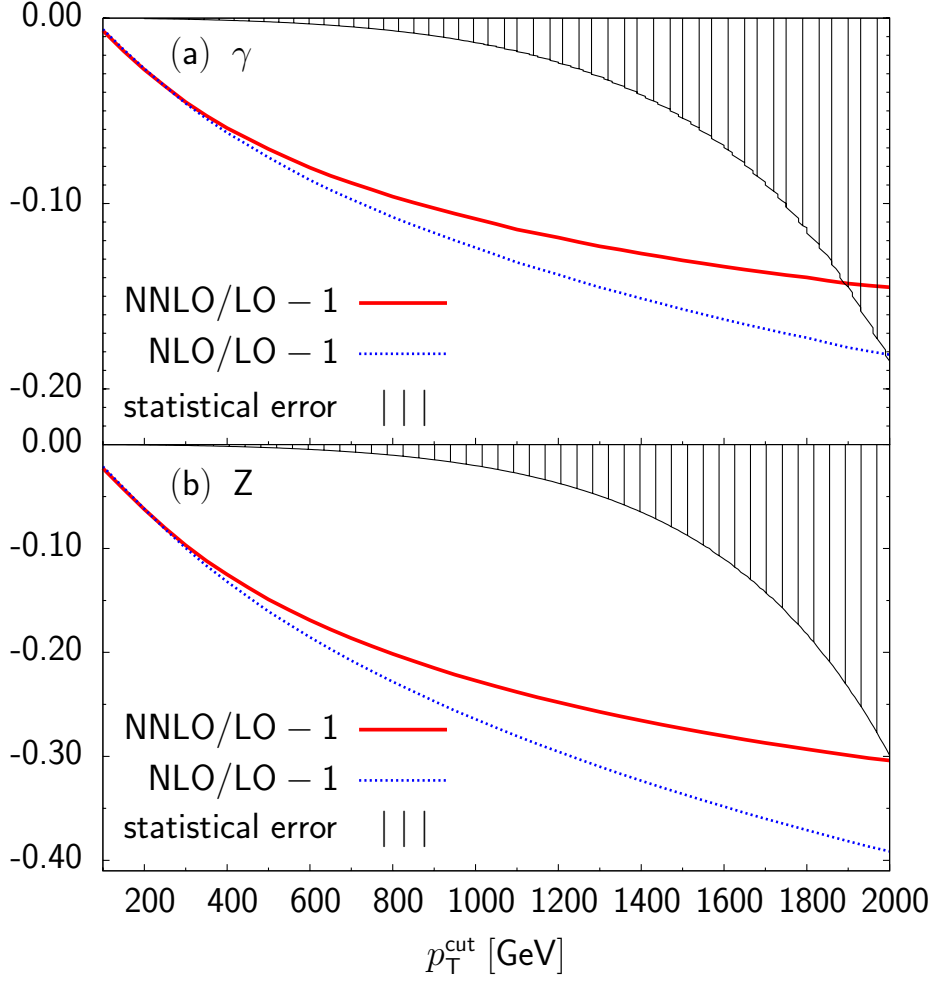


Figure 8.7: Relative NLO (dotted) and NNLO (two-loop approximation, solid) electroweak corrections wrt. the LO and statistical error (shaded area) for the integrated cross section of the reactions (a)  $pp \rightarrow \gamma j$  and (b)  $pp \rightarrow Z j$  at  $\sqrt{s} = 14$  TeV as a function of  $p_T^{\text{cut}}$ .

higher values of  $p_T$ . We find very similar results for the relative accuracy of the high energy approximations for  $W^-$  production.

To underline the relevance of the large electroweak corrections at the LHC, we present the relative NLO and NNLO corrections to the cross sections integrated over  $p_T$  starting from  $p_T = p_T^{\text{cut}}$ , as a function of  $p_T^{\text{cut}}$ . Cf. Fig. 8.7 and Fig. 8.8 for neutral and charge gauge boson production, respectively. The results are compared with the statistical error, estimated as  $\Delta\sigma_{\text{stat}}/\sigma = 1/\sqrt{N}$  with  $N = \mathcal{L} \times \text{BR} \times \sigma_{\text{LO}}$ . We assume a total integrated luminosity  $\mathcal{L} = 300\text{fb}^{-1}$  for the LHC [27] and use the LO cross section  $\sigma_{\text{LO}}$  for the corresponding gauge boson. Furthermore, we choose the branching ratios  $\text{BR}(\gamma) = 1$ ,  $\text{BR}(Z \rightarrow l^+l^-, \bar{\nu}_l\nu_l) = 0.306$  and  $\text{BR}(W \rightarrow e\nu_e, \mu\nu_\mu) = 2/9$ . We note that decays into neutrinos correspond to missing energy events in the de-

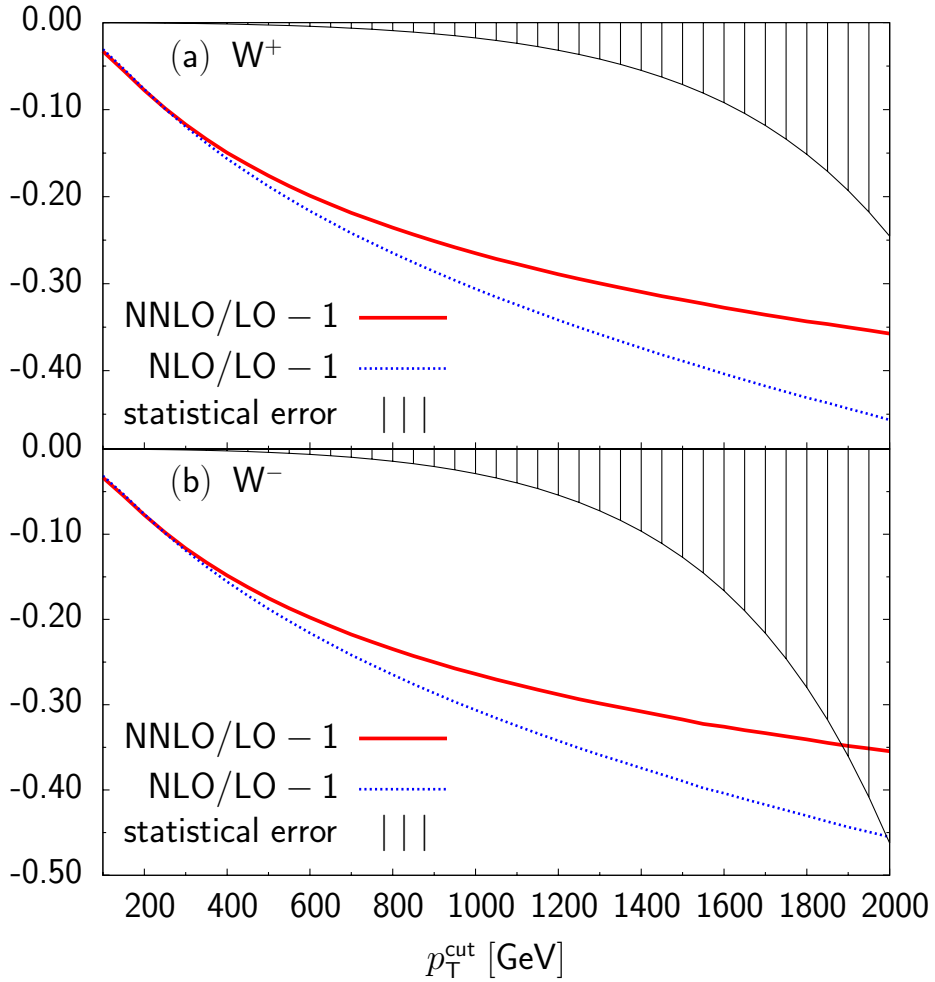


Figure 8.8: Relative NLO (dotted) and NNLO (two-loop approximation, solid) electroweak corrections wrt. the LO and statistical error (shaded area) for the integrated cross section of the reactions (a)  $pp \rightarrow W^+ j$  and (b)  $pp \rightarrow W^- j$  at  $\sqrt{s} = 14$  TeV as a function of  $p_T^{\text{cut}}$ .



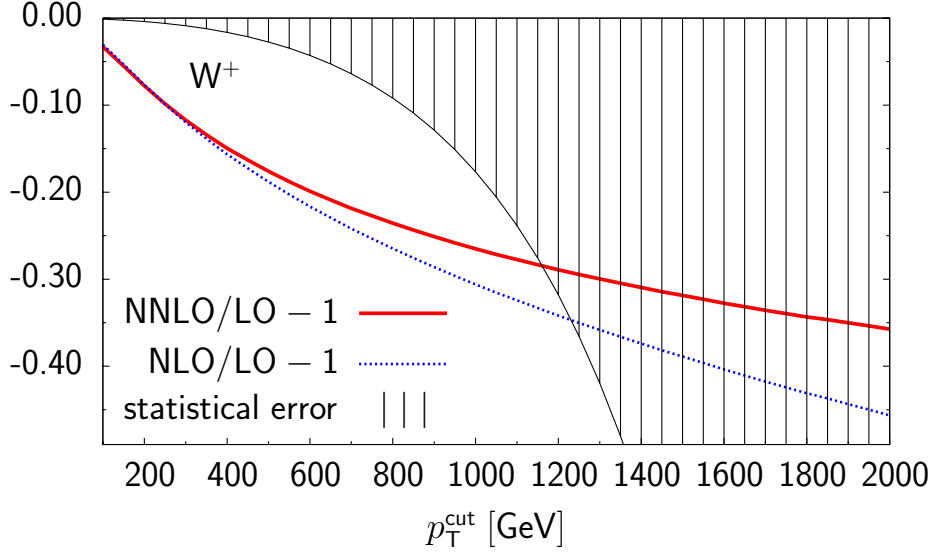


Figure 8.9: Modification of Fig. 8.8a with a statistical error corresponding to a hundredth ( $3 \text{ fb}^{-1}$ ) of the previously assumed luminosity.

tector. Thus, the  $p_T$ -measurement relies on measuring the jet recoil, which carries systematic errors of a few percent [8] and can translate to larger uncertainties on the cross section for steeply falling distributions.

It is clear from Fig. 8.7 and Fig. 8.8 that the size of the NLO corrections are bigger than the statistical error in a wide range of  $p_T$ . Also the differences between the NNLO and NLO corrections, due to two-loop logarithmic effects, is significant. In terms of the estimated statistical error, these two-loop contributions amount to 1–3 standard deviations for  $p_T \approx 1 \text{ TeV}$  for all gauge bosons production processes. As shown in Fig. 8.9 for  $W^+$  production, even with a very low luminosity of  $3 \text{ fb}^{-1}$ , which corresponds to the early phase of data-taking at the LHC, and  $p_T \lesssim 800 \text{ GeV}$  the electroweak corrections are of significant size and correspond to a two standard deviation effect.

Ratios of  $p_T$ -distributions for  $W^+$ ,  $W^-$ ,  $Z$  bosons and photons are expected to be less sensitive to theoretical errors than the distributions themselves, since uncertainties such as the scale at which  $\alpha_s$  is calculated or the choice of PDFs cancel to a large extent in these ratios. Moreover, due to a similar cancellation mechanism, the ratio should remain stable against QCD corrections and lead to important experimental tests of  $W$  and  $Z$  couplings in the high-energy region. In Fig. 8.10–Fig. 8.12 we present several ratios and study the impact of the electroweak corrections to these quantities.

From Fig. 8.10 we observe that the weak corrections modify the ratio of photon and  $Z$  production considerably. The effect is the strongest at high  $p_T$ . In this region, the LO photon cross section is smaller than the cross section for  $Z$  boson production by

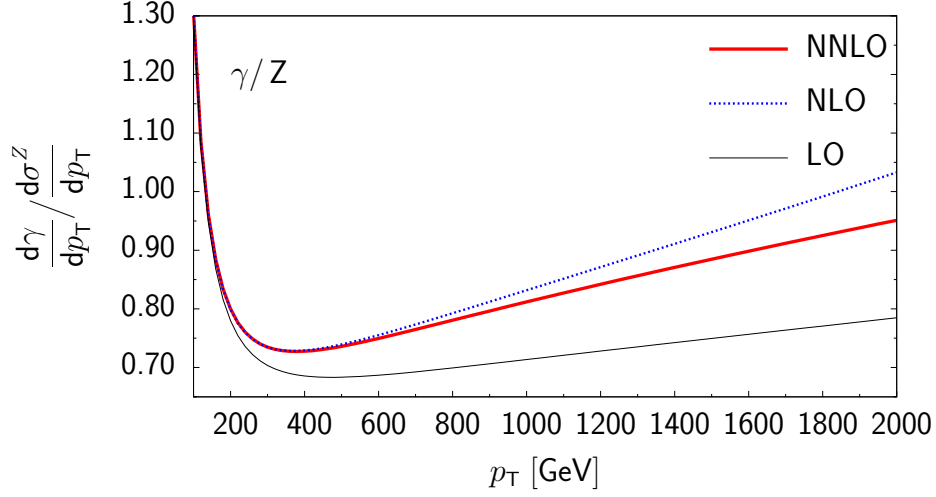


Figure 8.10: Ratio of the  $p_T$ -distributions for the processes  $pp \rightarrow \gamma j$  and  $pp \rightarrow Z j$  at  $\sqrt{s} = 14$  TeV: LO (thin solid), NLO(dotted) and NNLO (two-loop approximation, thick solid) predictions.

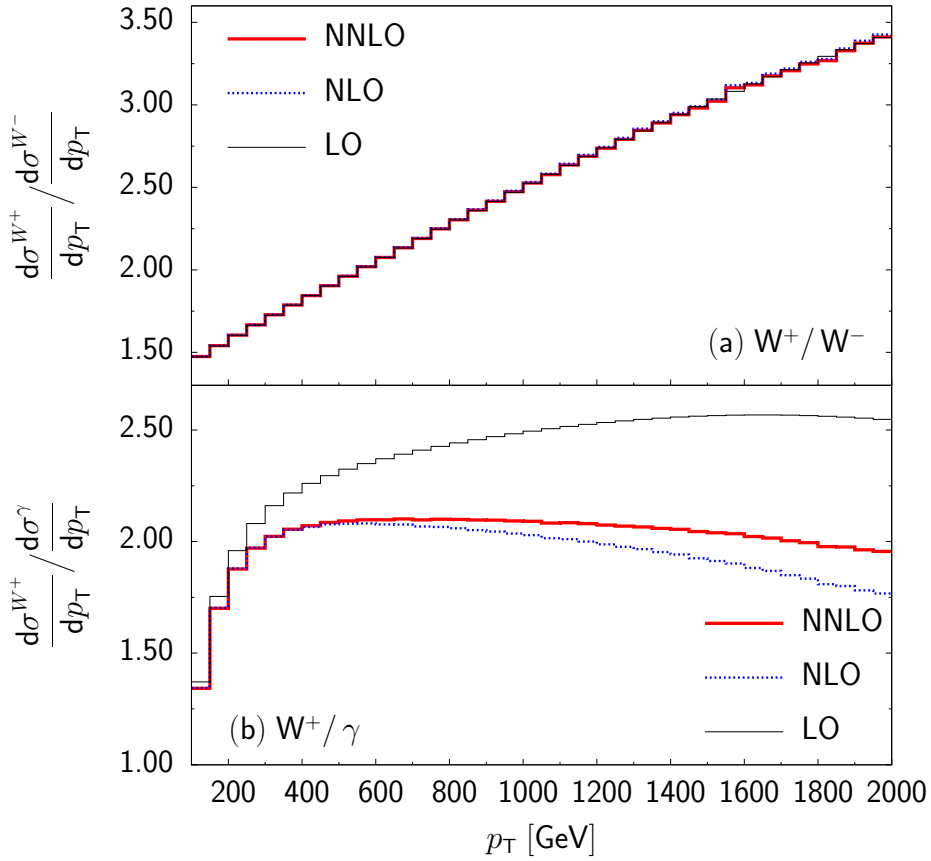


Figure 8.11: Ratio of the  $p_T$ -distributions for the processes (a)  $pp \rightarrow W^+ j$  and  $pp \rightarrow W^- j$  and (b)  $pp \rightarrow W^+ j$  and  $pp \rightarrow \gamma j$  at  $\sqrt{s} = 14$  TeV: LO (thin solid), NLO(dotted) and NNLO (two-loop approximation, thick solid) predictions.

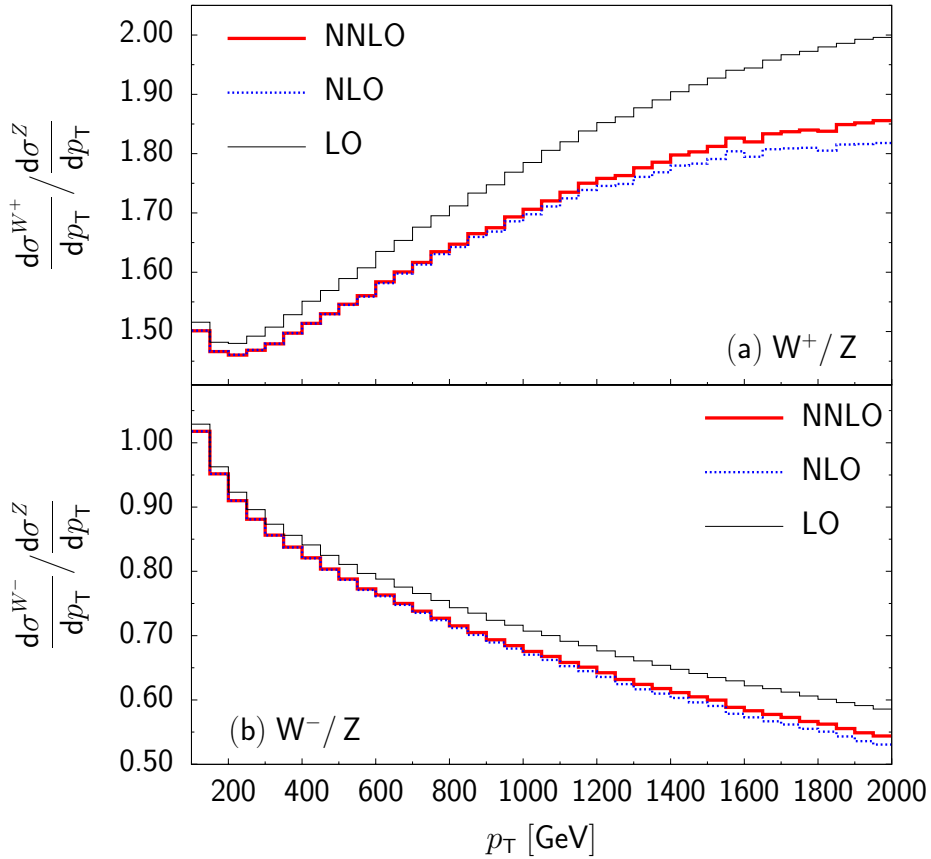


Figure 8.12: Ratio of the  $p_T$ -distributions for the processes (a)  $pp \rightarrow W^+ j$  and  $pp \rightarrow Z j$  and (b)  $pp \rightarrow W^- j$  and  $pp \rightarrow Z j$  at  $\sqrt{s} = 14$  TeV: LO (thin solid), NLO (dotted) and NNLO (two-loop approximation, thick solid) predictions.

about 25%. The relatively large NLO corrections for  $Z$  production, as compared to  $\gamma$  production, cause the full NLO production rates to become equal at the highest  $p_T$  considered here, i.e.  $p_T \approx 2$  TeV. The two-loop corrections modify the ratio and lead to a few percent decrease at high  $p_T$ .

The ratio for the  $W^+$  and  $W^-$   $p_T$ -distributions is presented in Fig. 8.11a. The LO value increases from 1.5 at  $p_T = 100$  GeV to 3.4 at  $p_T = 2$  TeV. As already observed, the relative electroweak corrections to the  $W^+$ - and  $W^-$ -boson  $p_T$ -distributions are almost identical. In consequence, the LO, NLO and NNLO curves in Fig. 8.11a overlap. In contrast, the impact of the electroweak corrections on the  $W^+/\gamma$  ratio (cf. Fig. 8.11b) at the LHC is clearly visible. The LO prediction, ranging from 1.4 to 2.5, receives a negative NLO correction that grows with  $p_T$  and amounts to  $-0.5$  for  $p_T = 1$  TeV. At  $p_T = 2$  TeV the difference between the NNLO and NLO curves is about 0.2.

The ratios of  $p_T$ -distributions for  $W^+/Z$  and  $W^-/Z$  are shown in Fig. 8.12a and Fig. 8.12b, respectively. For the  $W^+/Z$  ratio the LO prediction ranges from 1.5 to

2. For  $p_T \geq 1$  TeV it is reduced by 4–9% by the NLO corrections. The logarithmic two-loop corrections to these ratios are small. We find a qualitatively similar behavior for the corrections to the  $W^-/Z$  ratio. In the considered range of  $p_T$  the ratio varies between 1.0 and 0.5. The NLO corrections reduce the LO prediction by 5–7% for  $1 \text{ TeV} \leq p_T \leq 2 \text{ TeV}$ .

### 8.3 Results for the Tevatron

We also perform a similar analysis for electroweak gauge boson production in association with a jet at the Tevatron. We consider the reactions  $p\bar{p} \rightarrow Vj$  with a hadronic center-of-mass energy of 2 TeV and present results for transverse momenta in the range  $50 \text{ GeV} \leq p_T \leq 400 \text{ GeV}$ . The cut on the transverse momentum of the jet is  $p_{T,j}^{\text{min}} = 50 \text{ GeV}$  and, as for the LHC, the separation parameter for  $Wj\gamma$  final states is taken to be  $R_{\text{sep}} = 0.4$ .

In Fig. 8.13a the LO  $p_T$ -distributions for photon and  $Z$  boson production are shown. The corresponding relative corrections for the NLO, NLL, NNLL and NNLO calculations are presented in Fig. 8.13b and Fig. 8.13c. The effects of electroweak corrections are generally much smaller at the Tevatron than at the LHC. We find that the NLO corrections for photon production increase with  $p_T$  but do not exceed  $-4\%$  wrt. the LO at the highest  $p_T$  considered, i.e. at  $p_T = 400 \text{ GeV}$ . For the case of  $Z$  boson production the relative NLO corrections range almost linearly between 0% and  $-8.5\%$  for  $50 \text{ GeV} \leq p_T \leq 400 \text{ GeV}$ . Furthermore, we observe for photon as well as for  $Z$  boson production that the NNLL approximation is significantly better than the NLL approximation. Two-loop contributions have little impact on the size of the corrections. The LO  $p_T$ -distribution for  $W$  boson production at the Tevatron is shown in Fig. 8.14a. In contrast to LHC, the production rates for positively and negatively charged  $W$  bosons are equal. For the electroweak corrections, which are presented in Fig. 8.14b, we find a similar picture as for  $Z$  boson production. The NLO corrections grow with  $p_T$  and reach  $-11\%$  at  $p_T = 400 \text{ GeV}$ . The one-loop NLL and NNLL approximations describe the exact NLO results with about 3% and 1% precision, respectively. The size of the two-loop contributions is very small.

A more precise study concerning the quality of the high-energy approximations is shown in Fig. 8.15a–c for photon,  $Z$  and  $W$  boson production. As for the LHC, we compare the NLL and NNLL approximations with the corresponding exact one-loop calculations. The latter are the weak corrections (denoted as NLO) for neutral gauge boson production, and the IR-finite part of the electroweak corrections (denoted as  $\text{NLO}_{\text{virt}}$ ) for the case of charged gauge boson production. In the  $p_T$ -range under consideration both, the NLL and the NNLL approximation are less precise than at the LHC. Nevertheless, the precision of the NNLL approximation is always better than 6 permille for all gauge bosons, and thus sufficient for all practical purposes.

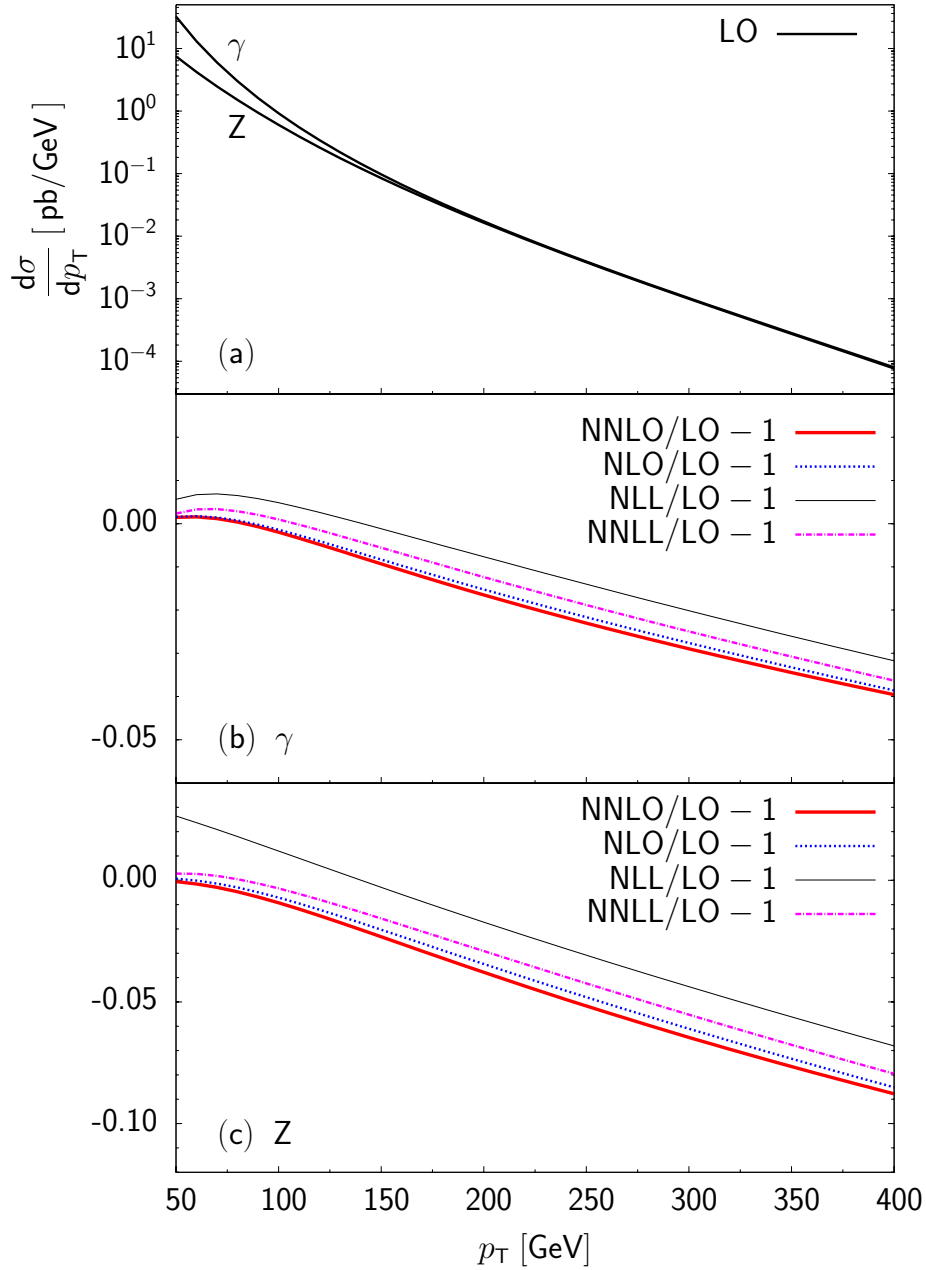


Figure 8.13: Transverse-momentum distribution for neutral gauge boson production at the Tevatron. (a) LO distribution for  $p\bar{p} \rightarrow \gamma j$  and  $p\bar{p} \rightarrow Zj$ . Relative NLO (dotted), NLL (thin solid), NNLL (squares) and NNLO (two-loop approximation, thick solid) electroweak correction wrt. the LO distribution for  $p\bar{p} \rightarrow \gamma j$  in (b) and similar for  $p\bar{p} \rightarrow Zj$  in (c).

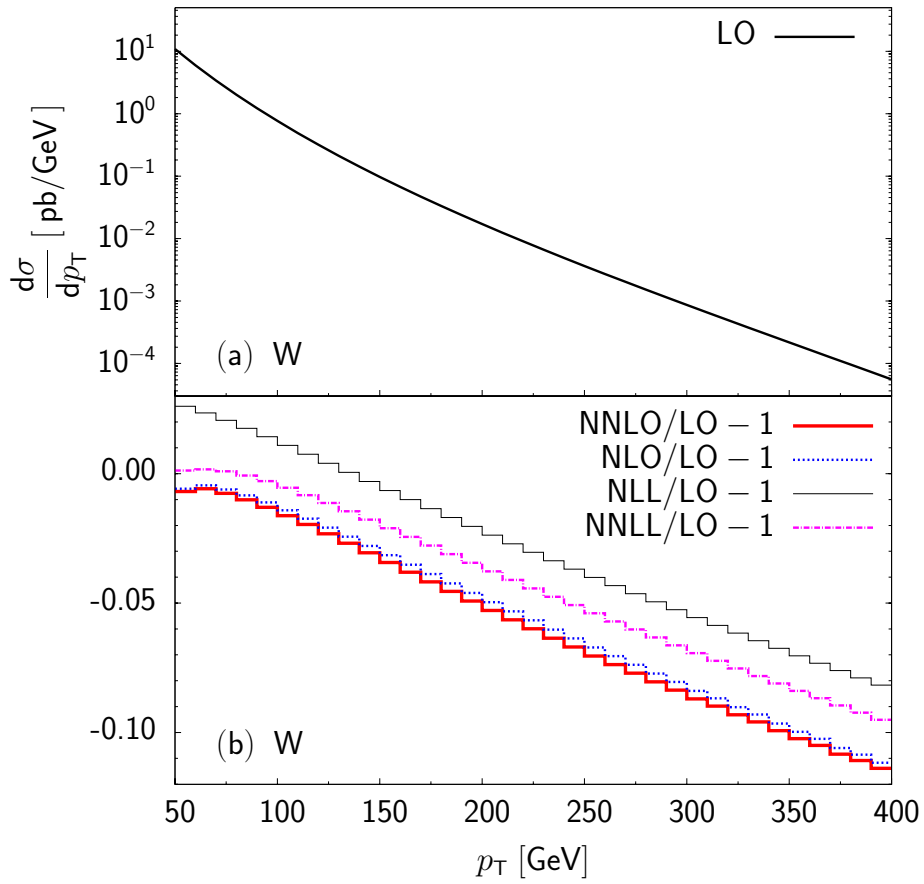


Figure 8.14: Transverse-momentum distribution for  $W$ -boson production at the Tevatron. (a) LO distribution for  $p\bar{p}\rightarrow W^{+(-)} j$  (solid). (b) Relative NLO (dotted), NLL (thin solid), NNLL (squares) and NNLO (two-loop approximation, thick solid) electroweak correction wrt. the LO distribution for  $pp\rightarrow W^{+(-)} j$ .

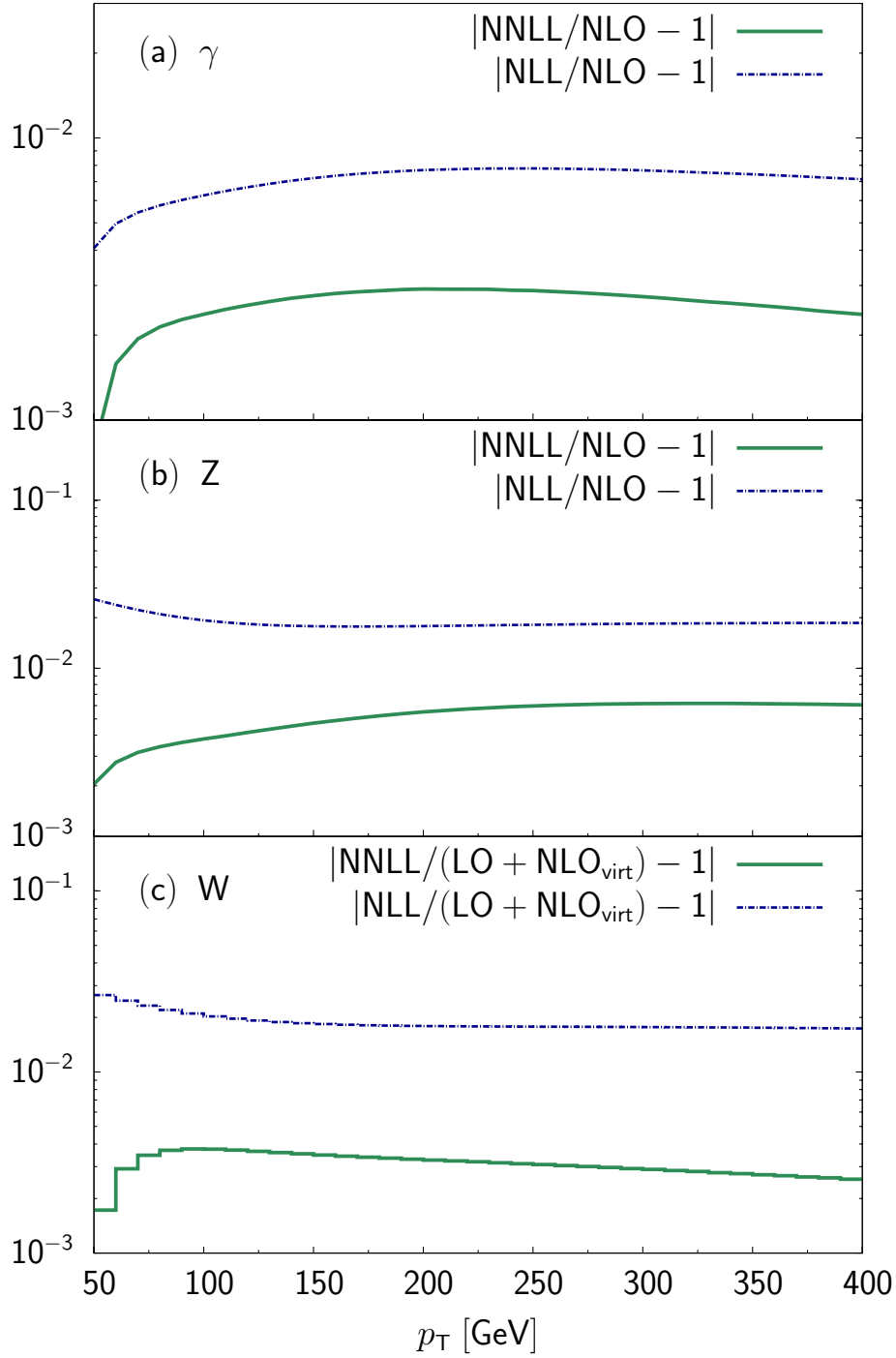


Figure 8.15: Relative precision of the high-energy approximations at one-loop in the process (a)  $p\bar{p} \rightarrow \gamma j$ , (b)  $p\bar{p} \rightarrow Z j$  and  $p\bar{p} \rightarrow W^{+(-)} j$  (c) at  $\sqrt{s} = 2$  TeV as a function of  $p_T$ : NNLL (solid) and NLL (dashed) wrt. the exact one-loop result.

In Fig. 8.16a–c the relative NLO and NNLO corrections to the  $p_T$ -integrated cross section with  $p_T \geq p_T^{\text{cut}}$  are compared with the estimated statistical error for an integrated luminosity  $\mathcal{L} = 7\text{fb}^{-1}$  [50]. The NLO weak correction for photon production in Fig. 8.16a is of the order of the statistical error and we conclude it should be taken into account when considering precision measurements. The two-loop terms do not bear much significance for a precise measurement. The size of the NLO electroweak corrections for  $Z$  and  $W$  boson production is larger and well above the statistical error for a significant range of  $p_T$ -values. Therefore they should be included in the analysis when considering precision measurements. In contrast, the impact of the dominant two-loop corrections is negligible.

The effect of the electroweak corrections on the ratios of  $p_T$ -distributions for  $\gamma/Z$  and  $W/Z$ ,  $W/\gamma$  is shown in Fig. 8.17 and Fig. 8.18a–b, respectively. Since the electroweak corrections to the photon,  $Z$  and  $W$  boson production at the Tevatron are moderate, their effect on the ratio is fairly small and stays within a few percent range for all values of  $p_T$  considered here.



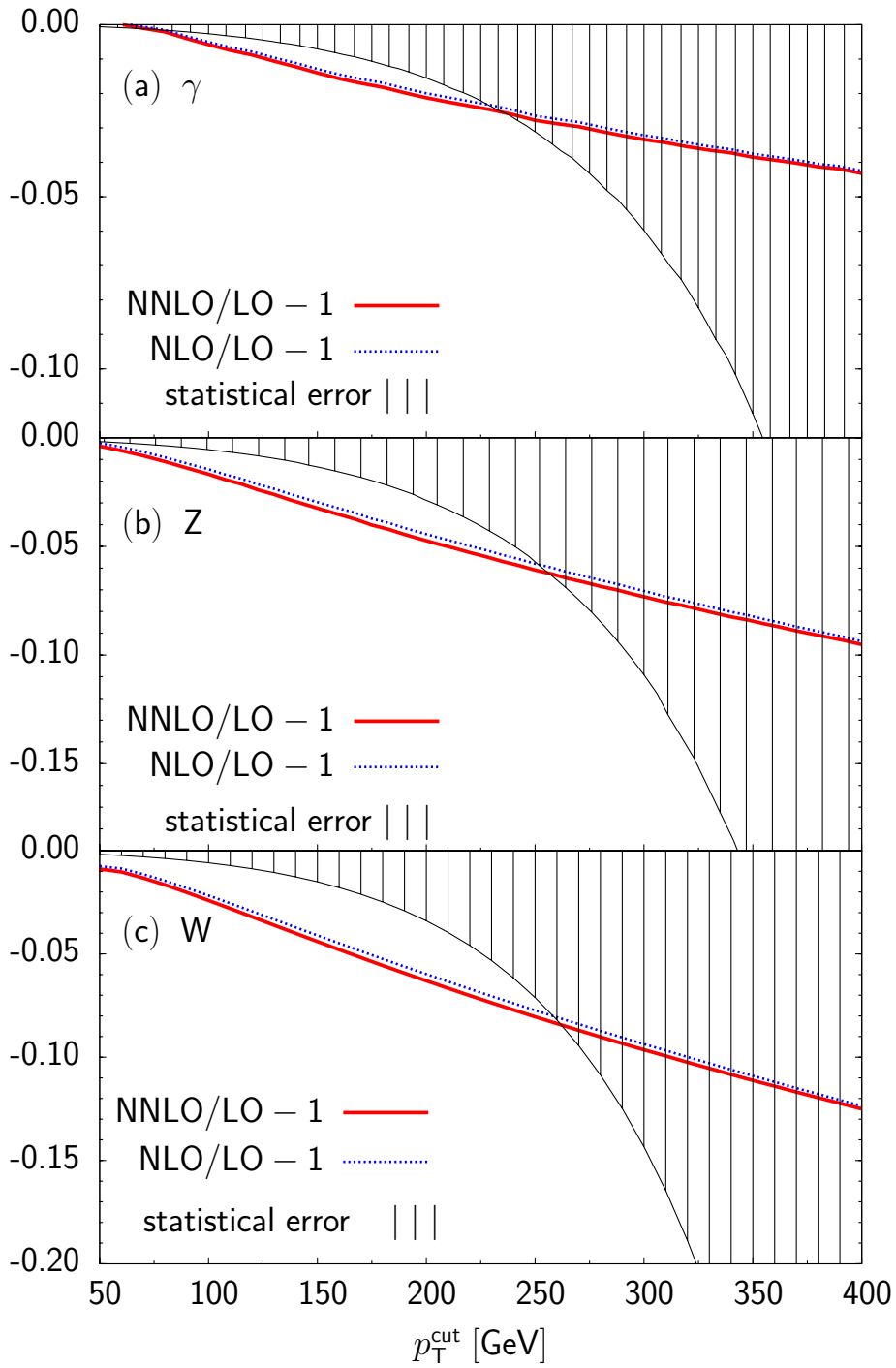


Figure 8.16: Relative NLO (dotted) and NNLO (two-loop approximation, solid) electroweak corrections wrt. the LO and statistical error (shaded area) for the integrated cross section of the processes (a)  $p\bar{p} \rightarrow \gamma j$ , (b)  $p\bar{p} \rightarrow Z j$  and (c)  $p\bar{p} \rightarrow W^{+(-)} j$  at  $\sqrt{s} = 2 \text{ TeV}$  as a function of  $p_T^{\text{cut}}$ .

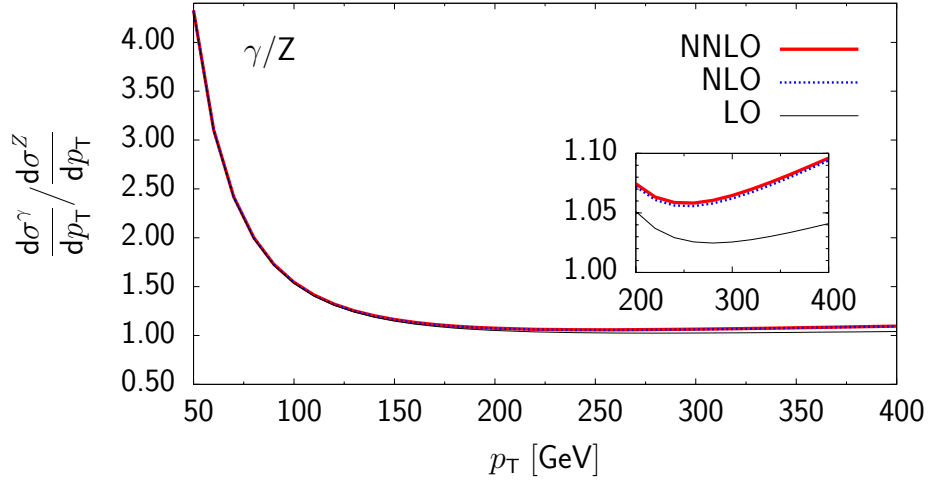


Figure 8.17: Ratio of the  $p_T$ -distributions for the processes  $p\bar{p} \rightarrow \gamma j$  and  $p\bar{p} \rightarrow Z j$  at  $\sqrt{s} = 2$  TeV: LO (thin solid), NLO(dotted) and NNLO (two-loop approximation, thick solid) predictions.

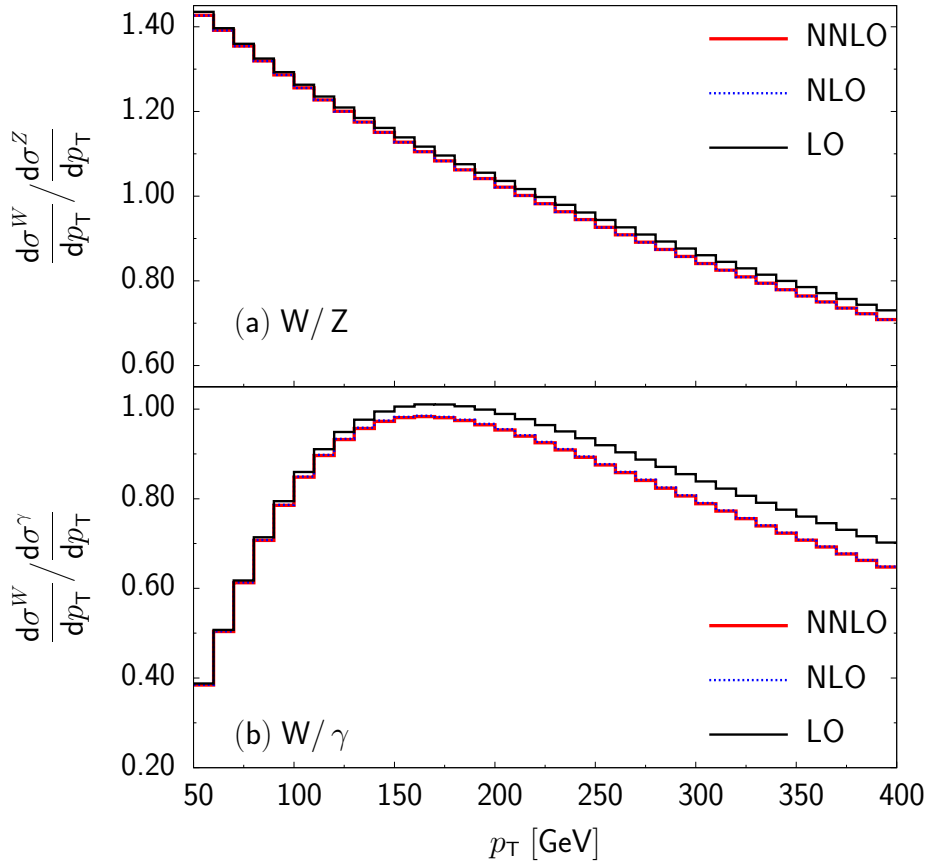


Figure 8.18: Ratio of the  $p_T$ -distributions (a) for the processes  $p\bar{p} \rightarrow W^{+(-)} j$  and  $p\bar{p} \rightarrow Z j$  and (b) for the processes  $p\bar{p} \rightarrow W^{+(-)} j$  and  $p\bar{p} \rightarrow \gamma j$  at  $\sqrt{s} = 2$  TeV: LO (thin solid), NLO(dotted) and NNLO (two-loop approximation, thick solid) predictions.

# Chapter 9

## Conclusions

In this work the electroweak corrections to large transverse momentum production of gauge bosons at the hadron colliders Tevatron and LHC were calculated. For photon and  $Z$  boson production we have considered the pure weak corrections at one-loop level. These contributions can be separated from the purely photonic corrections in a gauge-invariant manner. For the corrections to charged gauge boson production this is not possible. Thus, we have calculated the full electroweak one-loop corrections for  $W$  production and included real photon emission.

Special attention has been devoted to the high-energy region, where the weak corrections are enhanced by logarithms of  $\hat{s}/M_W^2$ . We have derived compact approximate expressions, which describe the complete asymptotic high-energy behavior at one-loop. Furthermore, we have derived dominant contributions at two-loop level. These two-loop terms include the leading and next-to-leading logarithms.

At the Tevatron,  $p_T$ -values up to around 300 GeV can be reached with reasonable event rates. In this region the  $\mathcal{O}(\alpha)$  electroweak corrections to the  $p_T$ -distribution reach up to  $-9\%$  for  $Z$  and  $W$  boson production and are thus of relevance for precision measurements. The corresponding corrections for photon production at large  $p_T$  are of minor importance and reach up to  $-4\%$ . Two-loop electroweak corrections are negligible at the Tevatron. With  $p_T$  below 400 GeV the relative rates for  $W$ ,  $Z$  and  $\gamma$  production are hardly affected by electroweak corrections.

In contrast, for transverse momenta in the TeV region accessible at the LHC, electroweak corrections play an important role. The  $\mathcal{O}(\alpha)$  corrections for  $Z$  and  $W$  boson production lead to a reduction of the  $p_T$ -distribution by about  $-15\%$  at transverse momenta of 500 GeV and reach more than  $-35\%$  at 2 TeV. For photon production we find  $\mathcal{O}(\alpha)$  corrections of  $-17\%$  at  $p_T = 2$  TeV. The dominant two-loop corrections at the LHC are positive and will be relevant for precision studies. Their size amounts to 5–10% for  $Z$  and  $W$  bosons, while for photon production they contribute with up to 3% corrections at high  $p_T$ . The study of relative rates for  $W^+$ ,  $W^-$ ,  $Z$  and  $\gamma$  production constitutes an interesting subject at the LHC. These rates are expected to be stable with respect to QCD effects and uncertainties in the PDFs. We find that the electroweak corrections cancel almost completely in the  $W^+/W^-$  ratio. In contrast, their impact on the  $\gamma/Z$ ,  $W^+/Z$  and the  $W^+/\gamma$  ratios is significant and leads to a shift of  $\mathcal{O}(10\%)$  for  $p_T \geq 1$  TeV.

# Appendix A

## Input parameters for the numerical results

In this appendix we specify the input parameters that have been used for the numerical results presented in this work. Common to all  $V$ +jet processes are the masses of the gauge bosons [51]

$$\begin{aligned}M_W &= 80.39 \text{ GeV}, \\M_Z &= 91.19 \text{ GeV}.\end{aligned}\tag{A.1}$$

Furthermore, all hadronic cross sections are obtained by using the parton distributions functions (PDFs) LO MRST2001 [52]. We choose  $\mu_{\text{QCD}}^2 = p_{\text{T}}^2$  as the factorization scale and adopt, in agreement with the value used in the PDF analysis,

$$\alpha_s(M_Z^2) = 0.13\tag{A.2}$$

for the strong coupling constant. We use the resummed one-loop running expression

$$\alpha_s(p_{\text{T}}^2) = \frac{\alpha_s(M_Z^2)}{1 + \frac{\alpha_s(M_Z^2)}{4\pi} \left(11 - \frac{2}{3}n_f\right) \ln\left(\frac{p_{\text{T}}^2}{M_Z^2}\right)}\tag{A.3}$$

with  $n_f = 5$  active quark flavors<sup>1</sup>.

The results for photon production in association with a jet are obtained with the on-shell definitions for the coupling parameters

$$\begin{aligned}\alpha &= 1/137, \\s_{\text{w}}^2 &= 1 - c_{\text{w}}^2 = 1 - \frac{M_W^2}{M_Z^2} = 0.2228.\end{aligned}\tag{A.4}$$

---

<sup>1</sup>Note that when calculating the contribution to the hadronic cross section coming from the dipole subtraction terms for the real corrections to  $W$ +jet production, we take the transverse momentum of the  $W$  boson in the reduced phase space,  $\tilde{p}_{\text{T},W}$ , as the factorization scale and the argument of  $\alpha_s$ .

For  $Z$ -boson production we have adopted the  $\overline{\text{MS}}$ -values

$$\begin{aligned}\alpha &= 1/128.1, \\ s_w^2 &= 1 - c_w^2 = 0.2314.\end{aligned}\tag{A.5}$$

Furthermore, the gauge boson field renormalization constants introduce the dependence on the masses

$$\begin{aligned}m_t &= 176.9 \text{ GeV}, \\ m_b &= 4.3 \text{ GeV}, \\ M_H &= 120 \text{ GeV}\end{aligned}\tag{A.6}$$

of the top and bottom quarks as well as the Higgs boson, respectively. We note, that the dependence of our results on these masses is very small.

In the case of  $W$ +jet production we have evaluated the coupling parameters in the  $G_\mu$ -scheme. Thus, the electromagnetic coupling constant is expressed in terms of the Fermi constant  $G_\mu$  and the weak mixing angle is related to the on-shell masses of the gauge bosons

$$\begin{aligned}G_\mu &= 1.16637 \times 10^{-5} \text{ GeV}^{-2}, \\ s_w^2 &= 1 - c_w^2 = 1 - \frac{M_W^2}{M_Z^2} = 0.2228, \\ \alpha &= \frac{\sqrt{2}G_\mu M_W^2 s_w^2}{\pi} = 1/132.3.\end{aligned}\tag{A.7}$$

In this case, the masses in the counterterms have been evaluated with

$$\begin{aligned}m_t &= 171.4 \text{ GeV}, \\ m_b &= 0 \text{ GeV}, \\ M_H &= 120 \text{ GeV}.\end{aligned}\tag{A.8}$$

The relevant values for effects of quark mixing via the CKM matrix are given by

$$\begin{aligned}|V_{ub}| &= 0.004, & |V_{us}| &= 0.224, & |V_{ud}| &= \sqrt{1 - |V_{ub}|^2 - |V_{us}|^2}, \\ |V_{cb}| &= 0.041, & |V_{cd}| &= 0.224, & |V_{cs}| &= \sqrt{1 - |V_{cb}|^2 - |V_{cd}|^2}.\end{aligned}\tag{A.9}$$

In our calculation of the real corrections for  $W$  boson production we choose the  $\overline{\text{MS}}$  factorization scheme in order to absorb collinear singularities from initial state radiation into the PDFs. The corresponding scale is set to  $\mu_{\text{QED}}^2 = M_W^2$ . We note that in order to consistently include  $\mathcal{O}(\alpha)$  corrections in a calculation of a hadronic cross section, PDFs that are used in the calculation need to take into account QED effects. Such PDF analysis has been performed in [53] and the  $\mathcal{O}(\alpha)$  effects are

known to be small for  $\mu_{\text{QED}} \lesssim 100 \text{ GeV}$ , both concerning the change in the quark distribution functions (below  $\mathcal{O}(1\%)$  [54]) and the size of the photon distribution function. Moreover, the currently available PDFs incorporating  $\mathcal{O}(\alpha)$  corrections, MRST2004QED [53], include QCD effects at the NLO in  $\alpha_S$ . Since our calculations are of the lowest order in QCD, and QED effects on PDFs are estimated to be small for  $\mu_{\text{QED}} \lesssim 100 \text{ GeV}$ , we prefer to use a LO QCD PDF set without QED corrections incorporated, rather than MRST2004QED, and we set  $\mu_{\text{QED}} = M_W$ .

We note that, the use of different factorization scales,  $\mu_{\text{QCD}} = p_T$  and  $\mu_{\text{QED}} = M_W$ , is due to the fact that  $\mu_{\text{QCD}}$  and  $\mu_{\text{QED}}$  play a different role in our calculation. The dependence on  $\mu_{\text{QCD}}$  is due to the LO evolution of the PDFs and represents an effect of  $\mathcal{O}(\alpha_S \ln(\mu_{\text{QCD}}/\mu_0))$ , where  $\mu_0$  is the scale at which the PDF evolution starts. This dependence would be compensated by NLO QCD contributions of  $\mathcal{O}(\alpha_S \ln(p_T/\mu_{\text{QCD}}))$  and, although QCD corrections are not included in our calculation, choosing  $\mu_{\text{QCD}} = p_T$  we can absorb large NLO QCD logarithms of the scale  $p_T$  in the LO PDF evolution. In contrast, the  $\mu_{\text{QED}}$  dependence of our predictions is due to  $\mathcal{O}(\alpha \ln(p_T/\mu_{\text{QED}}))$  terms in the photon bremsstrahlung corrections. This dependence is not compensated by the PDF evolution since we use a PDF set that does not include QED effects, assuming that these effects are negligible. This approach makes sense only if the scale  $\mu_{\text{QED}}$  is chosen in such a way that the (potential) impact of QED effects on the PDFs is very small. In Ref. [54] it was shown that the QED corrections to the PDFs grow with  $\mu_{\text{QED}}$  but do not exceed one percent for  $\mu_{\text{QED}} \lesssim 100 \text{ GeV}$ . This motivates our choice  $\mu_{\text{QED}} = M_W$  for the QED factorization scale.

Moreover we do not include photon-induced contributions, which are parametrically suppressed by a factor  $\alpha/\alpha_S$ . However, in Ref. [23] it has been reported that photon-induced contributions are of numerical significance for large  $p_T$   $W$ -boson production at the LHC. Estimates of the exact size of these effects are obscured by large theoretical uncertainty on the photon's PDF, as demonstrated in Ref. [23].

# Appendix B

## Recombination and exclusive $W$ +jet cross section

As discussed in Sect. 2.2, the recombination prescription that we use to regularize photon-quark final-state collinear singularities implies a different treatment of final-state quarks and gluons. While for final-state gluons we apply a cut on  $p_{T,g}$  within the entire phase space, for final-state quarks the recombination effectively removes the cut on  $p_{T,q}$  inside the collinear cone  $R(q, \gamma) < R_{\text{sep}}$ . As a consequence the recombined  $gq' \rightarrow W^\sigma q\gamma$  cross section (2.21) has a logarithmic dependence on the cut-off parameter  $R_{\text{sep}}$ . In order to quantify this  $R_{\text{sep}}$ -dependence, let us consider the contribution of real photon radiation inside the recombination cone. To this end, assuming that the cone is sufficiently small ( $R_{\text{sep}} \ll 1$ ), we adopt a collinear approximation

$$\int_{R(q,\gamma) < R_{\text{sep}}} d\hat{\sigma}^{gq' \rightarrow W^\sigma q\gamma} = \hat{\sigma}^{gq' \rightarrow W^\sigma q} \int_0^1 dz F_{q\gamma}(z), \quad (\text{B.1})$$

where<sup>1</sup>  $z = p_{T,\gamma}/(p_{T,q} + p_{T,\gamma}) = 1 - p_{T,q}/p_{T,W}$  is the photon momentum fraction and [41]

$$\begin{aligned} F_{q\gamma}(z) &= \frac{\alpha Q_q^2}{2\pi} P_{q\gamma}(z, \varepsilon) \frac{(4\pi\mu^2)^\varepsilon}{\Gamma(1-\varepsilon)} \int_0^{k_{\perp,\text{max}}^2} \frac{dk_{\perp}^2}{(k_{\perp}^2)^{1+\varepsilon}} \\ &= -\frac{\alpha Q_q^2}{2\pi} P_{q\gamma}(z) \frac{(4\pi)^\varepsilon}{\varepsilon\Gamma(1-\varepsilon)} + \bar{F}_{q\gamma}(z, \mu^2) \end{aligned} \quad (\text{B.2})$$

with

$$\bar{F}_{q\gamma}(z, \mu^2) = -\frac{\alpha Q_q^2}{2\pi} \left[ P_{q\gamma}(z) \ln \left( \frac{\mu^2}{k_{\perp,\text{max}}^2} \right) - z \right]. \quad (\text{B.3})$$

Here  $P_{q\gamma}(z, \varepsilon) = P_{q\gamma}(z) - \varepsilon z$  with  $P_{q\gamma}(z) = [1 + (1-z)^2]/z$  is the  $q \rightarrow \gamma$  splitting function in  $4-2\varepsilon$  dimensions,  $k_{\perp}$  is the photon transverse momentum wrt. the photon-quark system, and  $k_{\perp,\text{max}} = z(1-z)R_{\text{sep}} p_{T,W}$ . The  $1/\varepsilon$  collinear singularity resulting

---

<sup>1</sup>Here we assume lowest-order kinematics, i.e.  $p_{T,q} + p_{T,\gamma} = p_{T,W}$  in the collinear region.

from inclusive photon radiation, i.e. integrating over the complete energy spectrum  $0 \leq z \leq 1$ , cancels against the virtual corrections.

The  $R_{\text{sep}}$ -dependence of the recombined cross section (2.21) is due to the fact that, inside the recombination cone quarks with  $p_{T,q} < p_{T,j}^{\text{min}}$  (or equivalently photons with  $z > 1 - p_{T,j}^{\text{min}}/p_{T,W}$ ) are not rejected. Thus the variation of  $\hat{\sigma}_{\text{rec.}}$  induced by a rescaling  $R_{\text{sep}} \rightarrow \xi_{\text{sep}} R_{\text{sep}}$  amounts to

$$\frac{\Delta \hat{\sigma}_{\text{rec.}}^{gq' \rightarrow W^\sigma q \gamma}}{\hat{\sigma}_{gq' \rightarrow W^\sigma q}} = \frac{\alpha Q_q^2}{2\pi} \ln \xi_{\text{sep}}^2 \int_{z_{\text{min}}}^1 dz P_{q\gamma}(z) \quad \text{with} \quad z_{\text{min}} = 1 - p_{T,j}^{\text{min}}/p_{T,W}. \quad (\text{B.4})$$

For relatively small transverse momenta ( $p_{T,W} \simeq 2p_{T,j}^{\text{min}}$ ) a rescaling of  $R_{\text{sep}}$  by a factor  $\xi_{\text{sep}} = 10$  shifts the  $gq' \rightarrow W^\sigma q(\gamma)$  cross section by less than 2 (0.5) permille for up- (down-) type quarks. Moreover it is obvious that at high  $p_{T,W}$ , where  $z_{\text{min}} \rightarrow 1$ , this effect tends to disappear.

Let us now compare the recombination procedure with a realistic definition of exclusive  $pp \rightarrow Wj$  production, where final-state quarks ( $a = q$ ) and gluons ( $a = g$ ) are subject to the same cut  $p_{T,a} > p_{T,j}^{\text{min}}$  within the entire phase space (including collinear quark-photon configurations). Since the recombination procedure does not affect final-state gluons, only channels involving final-state quarks need to be considered. The difference between the recombined  $gq' \rightarrow W^\sigma q \gamma$  cross section (2.21) and the exclusive cross section (2.22) corresponds to the contribution of hard collinear photons with  $R(q, \gamma) < R_{\text{sep}}$  and  $z_{\text{min}} \leq z \leq 1$ . This collinear hard-photon radiation can be described by means of quark fragmentation functions [55, 56, 57, 58, 59, 60] as

$$\Delta \hat{\sigma}_{\text{excl.}} = \hat{\sigma}_{\text{rec.}}^{gq' \rightarrow W^\sigma q \gamma} - \hat{\sigma}_{\text{excl.}}^{gq' \rightarrow W^\sigma q \gamma} = \hat{\sigma}_{gq' \rightarrow W^\sigma q} \int_{z_{\text{min}}}^1 dz \mathcal{D}_{q\gamma}(z). \quad (\text{B.5})$$

Here the effective quark fragmentation function  $\mathcal{D}_{q\gamma}(z) = F_{q\gamma}(z) + D_{q\gamma}(z)$  consists of the perturbative contribution  $F_{q\gamma}$  and the bare fragmentation function  $D_{q\gamma}$ . The collinear singularity resulting from the perturbative contribution is factorized into the bare fragmentation function at the scale  $\mu$ , such that in the  $\overline{\text{MS}}$  scheme [55]

$$\mathcal{D}_{q\gamma}(z) = \bar{F}_{q\gamma}(z, \mu^2) + \bar{D}_{q\gamma}(z, \mu^2), \quad (\text{B.6})$$

and the renormalized fragmentation function  $\bar{D}_{q\gamma}$  can be extracted from experimental measurements. Using the parameterization [56, 60]

$$\bar{D}_{q\gamma}(z, \mu_0^2) = \frac{\alpha Q_q^2}{2\pi} \left[ -P_{q\gamma}(z) \ln(1-z)^2 - 13.26 \right], \quad (\text{B.7})$$

obtained by the ALEPH collaboration at  $\mu_0 = 0.14 \text{ GeV}$ , we arrive at

$$\mathcal{D}_{q\gamma}(z) = \frac{\alpha Q_q^2}{2\pi} \left[ P_{q\gamma}(z) \ln \left( \frac{z R_{\text{sep}} p_{T,W}}{\mu_0} \right)^2 + z - 13.26 \right]. \quad (\text{B.8})$$



With this expression we derive a conservative upper bound for  $\Delta\hat{\sigma}_{\text{excl.}}$ . To this end we consider  $Q_q = 2/3$ ,  $R_{\text{sep}} \simeq 1$ , and a wide range of transverse momenta,  $2p_{T,j}^{\text{min}} \leq p_{T,W} \leq 2 \text{ TeV}$ . With these parameters we obtain

$$\frac{\Delta\hat{\sigma}_{\text{excl.}}}{\hat{\sigma}} \lesssim 2 \times 10^{-3}. \quad (\text{B.9})$$

We conclude that, for  $R_{\text{sep}} \lesssim \mathcal{O}(1)$ , the recombined cross section has a negligible dependence on the recombination parameter  $R_{\text{sep}}$  and provides a fairly precise description of exclusive  $pp \rightarrow Wj$  production at high transverse momentum.

# Appendix C

## On-shell coupling renormalization for $Z$ +jet production

In this appendix we discuss effects from the on-shell renormalization of the weak mixing angle and the electromagnetic coupling constant in the process for  $Z$  boson production. We compare this approach to the result found in Sect. 3.3.2, where the  $\overline{\text{MS}}$ -scheme was adopted to define the coupling constants.

In the on-shell (OS) scheme, the weak mixing angle is defined as  $c_w^2 = M_W^2/M_Z^2$  and the corresponding counterterms reads

$$\frac{\delta c_w^2}{c_w^2} \stackrel{\text{OS}}{=} \text{Re} \left[ \frac{\Sigma_{\text{T}}^{WW}(M_W^2)}{M_W^2} - \frac{\Sigma_{\text{T}}^{ZZ}(M_Z^2)}{M_Z^2} \right]. \quad (\text{C.1})$$

As on-shell input parameter for the electromagnetic coupling constant we used  $\alpha = \alpha(M_Z^2)$ , defined as

$$\alpha(M_Z^2) = \frac{\alpha(0)}{1 - \Delta\alpha(M_Z^2)}, \quad \Delta\alpha(M_Z^2) = \text{Re} \left[ \Pi_{\text{ferm}}^{AA}(0) - \Pi_{\text{ferm}}^{AA}(M_Z^2) \right], \quad (\text{C.2})$$

where  $\alpha(0) = e(0)^2/(4\pi)$  is the fine-structure constant in the Thompson limit and  $\Pi_{\text{ferm}}^{AA}$  represents the fermionic contribution to the photonic vacuum polarization. The counterterm associated with  $e^2 = 4\pi\alpha(M_Z^2)$  is given by

$$\frac{\delta e^2}{e^2} \stackrel{\text{OS}}{=} \frac{\delta e(0)^2}{e(0)^2} - \Delta\alpha(M_Z^2) = \text{Re} \left[ \Pi_{\text{fer}}^{AA}(M_Z^2) \right] + \Pi_{\text{bos}}^{AA}(0) - \frac{2s_w}{c_w} \frac{\Sigma_{\text{T}}^{AZ}(0)}{M_Z^2}, \quad (\text{C.3})$$

where  $\delta e(0)$  is the counterterm in the Thompson limit, and  $\Pi_{\text{bos}}^{AA}(0)$  represents the bosonic contribution to the photon propagator.

In order to see the numerical effects between the OS- and  $\overline{\text{MS}}$ -scheme we consider the ratio of the NLO transverse momentum distributions for  $pp \rightarrow Zj$  at the LHC. The input values are specified in Appendix A. In Fig. C.1 we illustrate the

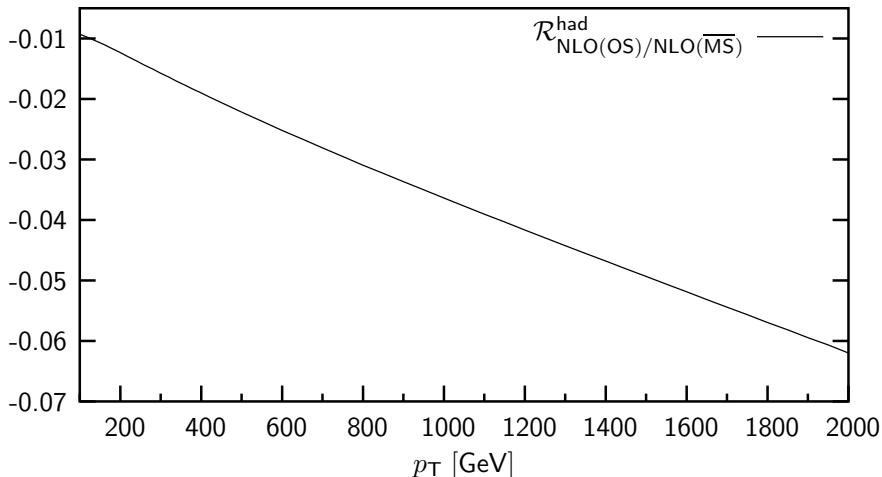


Figure C.1: Relative difference of the NLO transverse momentum distribution for  $pp \rightarrow Zj$  calculated in the  $\overline{\text{MS}}$  and on-shell (OS) schemes at  $\sqrt{s} = 14$  TeV.

dependence of the NLO  $p_T$ -distribution on the choice of the renormalization scheme with

$$\mathcal{R}_{\text{NLO(OS)/NLO}(\overline{\text{MS}})}^{\text{had}} = \frac{d\sigma_{\text{NLO}}^{\text{OS}}/dp_T}{d\sigma_{\text{NLO}}^{\overline{\text{MS}}}/dp_T} - 1. \quad (\text{C.4})$$

At low  $p_T$  the results in the OS and  $\overline{\text{MS}}$  schemes differ by around 1% and the difference grows with  $p_T$  reaching 6% at  $p_T = 2$  TeV. This effect is mainly due to the different treatment of the weak mixing angle in the two renormalization schemes. As well known, the relation between the  $\overline{\text{MS}}$  and on-shell definitions of the weak mixing angle is provided by the  $\rho$  parameter [61] as

$$\frac{c_w^2}{\hat{c}_w^2} = \frac{M_W^2}{M_Z^2 \hat{c}_w^2} = \rho, \quad \frac{\hat{s}_w^2}{s_w^2} - 1 = \Delta s_w^2 = \frac{c_w^2}{s_w^2} \Delta\rho, \quad (\text{C.5})$$

where  $\rho = (1 - \Delta\rho)^{-1}$  and the symbols with and without hat denote  $\overline{\text{MS}}$  and on-shell quantities, respectively. The input parameters used in our calculation,  $\hat{s}_w^2 = 0.2314$  and  $s_w^2 = 1 - M_W^2/M_Z^2 \simeq 0.2228$ , correspond to  $\Delta s_w^2 \simeq 3.8\%$  and are extracted from precision electroweak measurements taking all available loop corrections into account. Instead, loop corrections beyond  $\mathcal{O}(\alpha)$  are not included in our calculation and, in particular, the deviation observed in Fig. C.1 is due to missing two-loop (and higher-order) corrections related to the  $\rho$  parameter. The scheme dependence resulting from  $\alpha/s_w^2$  terms amounts to

$$\frac{\alpha}{s_w^2} (1 - \Delta^{(1)} s_w^2) - \frac{\alpha}{\hat{s}_w^2} \simeq \frac{\alpha}{\hat{s}_w^2} (\Delta s_w^2 - \Delta^{(1)} s_w^2), \quad (\text{C.6})$$

where  $\Delta^{(1)} s_w^2 = (c_w^2/s_w^2) \Delta\rho^{(1)} \simeq 4.5\%$  corresponds to the one-loop corrections to the  $\rho$  parameter, which are included in our on-shell predictions through the counterterm

(C.1). This scheme dependence (C.6) is thus due to the higher-order contributions  $\Delta s_w^2 - \Delta^{(1)} s_w^2 \simeq -0.7\%$ . Their relatively large size results from the combined effect of  $\mathcal{O}(\alpha\alpha_S m_t^2)$  [62],  $\mathcal{O}(\alpha\alpha_S^2 m_t^2)$  [63],  $\mathcal{O}(\alpha^2 m_t^4)$  [64] and  $\mathcal{O}(\alpha^2 m_t^2)$  [65] corrections to the  $\rho$  parameter and is consistent with the effect observed in Fig. C.1 at small  $p_T$ . In addition, the scheme-dependence resulting from the one-loop logarithmic terms is of order

$$-\left(\frac{\alpha^2}{s_w^4} - \frac{\alpha^2}{\hat{s}_w^4}\right) \log^2(\hat{s}/M_W^2) \simeq -2\Delta s_w^2 \frac{\alpha^2}{s_w^4} \log^2(\hat{s}/M_W^2). \quad (\text{C.7})$$

This effect is due to missing two-loop corrections of order  $\Delta\rho \alpha \log^2(\hat{s}/M_W^2)$ . Its size is proportional to  $\Delta s_w^2 \simeq 3.8\%$  and grows with energy. This explains the high- $p_T$  behavior in Fig. C.1.

We stress that the effects (C.6)–(C.7) are entirely due to missing higher-order terms related to  $\Delta\rho$  and that such missing terms concern only the calculation in the on-shell scheme. Indeed,  $\Delta\rho$  enters our predictions only through the relation between the weak mixing angle and the weak-boson masses in the on-shell scheme whereas the  $\overline{\text{MS}}$  calculation does not receive any contribution from  $\Delta\rho$ . The large scheme-dependence in Fig. C.1 has thus to be interpreted as large uncertainty of the one-loop prediction in the on-shell scheme whereas such uncertainties are absent in the  $\overline{\text{MS}}$  scheme. This motivates the choice of the  $\overline{\text{MS}}$  scheme adopted in this work.

# Appendix D

## Explicit results

In this appendix we present explicit analytic expressions of our calculation. The result for the full one-loop calculations to the processes  $\bar{q}q' \rightarrow Vg$  with  $V = \gamma, Z, W^\pm$  are given in D.1. In D.2 we present explicit results for the real photon emission process  $\bar{q}q' \rightarrow W^\sigma g\gamma$ .

### D.1 Virtual corrections

We present explicit analytic expression for the functions  $H_{1,V}^I(M_\Gamma^2)$  defined in (3.87). These functions describe the contribution of the unrenormalized one-loop Feynman diagrams of Fig. 3.1 to the unpolarized cross section. They consist of linear combinations of the scalar integrals defined in (3.27)–(3.29)

$$H_{1,V}^I(M_\Gamma^2) = \sum_j K_j^I(M_\Gamma^2) \operatorname{Re} [J_j(M_\Gamma^2)] \quad \text{for } I = \text{A, N, X, Y.} \quad (\text{D.1})$$

The coefficients of the function  $H_{1,V}^{\text{A}}(M_\Gamma^2)$  read

$$\begin{aligned} K_0^{\text{A}}(M_\Gamma^2) &= -\frac{4\hat{s}^2 + 3(\hat{t}^2 + \hat{u}^2)}{\hat{t}\hat{u}} + \hat{s} \left( \frac{1}{\hat{s} + \hat{t}} + \frac{1}{\hat{s} + \hat{u}} - \frac{5}{\hat{u}} - \frac{5}{\hat{t}} + \frac{4}{\hat{t} + \hat{u}} \right), \\ K_{1a}^{\text{A}}(M_\Gamma^2) &= M_\Gamma^2 \left\{ - \left[ \frac{3\hat{s}}{(\hat{s} + \hat{t})^2} + \frac{3\hat{s}}{(\hat{s} + \hat{u})^2} \right] + \left( \frac{1}{\hat{s} + \hat{t}} + \frac{1}{\hat{s} + \hat{u}} \right) \right. \\ &\quad \left. - 2 \left( \frac{\hat{s} + \hat{u}}{\hat{t}^2} + \frac{\hat{s} + \hat{t}}{\hat{u}^2} \right) + \frac{2\hat{s}^2(2\hat{s} + \hat{t} + \hat{u})}{\hat{t}\hat{u}(\hat{s} + \hat{t})(\hat{s} + \hat{u})} \right\} + 4 \frac{(\hat{s} + \hat{t})^2 + (\hat{s} + \hat{u})^2}{\hat{t}\hat{u}}, \\ K_{1b}^{\text{A}}(M_\Gamma^2) &= 0, \\ K_2^{\text{A}}(M_\Gamma^2) &= p_V^2 \left[ \frac{6\hat{s}M_\Gamma^2}{(\hat{s} + \hat{t})^3} + \frac{6\hat{s}M_\Gamma^2}{(\hat{s} + \hat{u})^3} + \frac{2\hat{s}M_\Gamma^2}{(\hat{s} + \hat{t})^2\hat{u}} + \frac{2\hat{s}M_\Gamma^2}{(\hat{s} + \hat{u})^2\hat{t}} + \frac{4(\hat{s} + \hat{t} + \hat{u})}{(\hat{t} + \hat{u})^2} - \frac{3}{\hat{t}} \right. \\ &\quad \left. - \frac{3}{\hat{u}} + \frac{2\hat{s} + \hat{t} - 2M_\Gamma^2}{(\hat{s} + \hat{t})^2} + \frac{2\hat{s} + \hat{u} - 2M_\Gamma^2}{(\hat{s} + \hat{u})^2} - \frac{\hat{s}(2\hat{s} + \hat{t} + \hat{u})(2M_\Gamma^2 + 3\hat{s})}{\hat{t}\hat{u}(\hat{s} + \hat{t})(\hat{s} + \hat{u})} \right], \end{aligned}$$

$$\begin{aligned}
K_3^A(M_\Gamma^2) &= 0, \\
K_4^A(M_\Gamma^2) &= -\frac{4\hat{s}(\hat{s} + 2\hat{t} + 2\hat{u})}{(\hat{t} + \hat{u})^2}, \\
K_{5a}^A(M_\Gamma^2) &= -\frac{6M_\Gamma^2\hat{s}\hat{u}}{(\hat{s} + \hat{t})^3} + \frac{M_\Gamma^2(2\hat{u} - 5\hat{s}) - \hat{s}\hat{u}}{(\hat{s} + \hat{t})^2} + \frac{2M_\Gamma^2(\hat{s} + \hat{t} + \hat{u})}{\hat{u}^2} - \frac{M_\Gamma^2 + 4\hat{s} + \hat{u}}{\hat{s} + \hat{t}}, \\
K_{5b}^A(M_\Gamma^2) &= 0, \\
K_{6a}^A(M_\Gamma^2) &= K_{5a}^A(M_\Gamma^2)\Big|_{\hat{t} \leftrightarrow \hat{u}}, \\
K_{6b}^A(M_\Gamma^2) &= 0, \\
K_7^A(M_\Gamma^2) &= -\frac{\hat{s}}{\hat{t}\hat{u}} \left[ 2(\hat{s} + M_\Gamma^2)(\hat{t} + \hat{u}) + \hat{t}^2 + \hat{u}^2 \right], \\
K_8^A(M_\Gamma^2) &= \frac{p_V^2 M_\Gamma^2}{\hat{u}(\hat{u} - p_V^2)^3} \left[ 2\hat{t}M_\Gamma^2(\hat{u} - \hat{s} - \hat{t}) - 4p_V^2\hat{s}(\hat{s} + \hat{t} + M_\Gamma^2) \right], \\
K_{9a}^A(M_\Gamma^2) &= K_{9b}^A(M_\Gamma^2) = 0, \\
K_{10}^A(M_\Gamma^2) &= K_8^A(M_\Gamma^2)\Big|_{\hat{t} \leftrightarrow \hat{u}}, \\
K_{11a}^A(M_\Gamma^2) &= K_{11b}^A(M_\Gamma^2) = 0, \\
K_{12}^A(M_\Gamma^2) &= -\frac{M_\Gamma^2(\hat{t} + \hat{u}) + \hat{s}\hat{u}}{\hat{t}\hat{u}} \left[ 2(\hat{s} + M_\Gamma^2)(\hat{s} + M_\Gamma^2 + \hat{t}) + \hat{t}^2 \right], \\
K_{13}^A(M_\Gamma^2) &= K_{12}^A(M_\Gamma^2)\Big|_{\hat{t} \leftrightarrow \hat{u}}, \\
K_{14a}^A(M_\Gamma^2) &= K_{14b}^A(M_\Gamma^2) = 0.
\end{aligned} \tag{D.2}$$

For the coefficients of the function  $H_{1,V}^N(M_\Gamma^2)$  we obtain

$$\begin{aligned}
K_0^N(M_\Gamma^2) &= \frac{4\hat{s}}{\hat{t}\hat{u}}(\hat{s} + \hat{t} + \hat{u}) - 2\hat{s} \left( \frac{1}{\hat{s} + \hat{u}} + \frac{1}{\hat{s} + \hat{t}} + \frac{2}{\hat{t} + \hat{u}} \right) + 2 \left( \frac{\hat{t}}{\hat{u}} + \frac{\hat{u}}{\hat{t}} \right), \\
K_{1a}^N(M_\Gamma^2) &= -\frac{M_\Gamma^2}{2} \left\{ \frac{4\hat{s}}{\hat{t}\hat{u}} + (\hat{t}\hat{u} - 2\hat{s}(\hat{s} + \hat{t} + \hat{u})) \left[ \frac{1}{\hat{t}(\hat{s} + \hat{u})^2} + \frac{1}{\hat{u}(\hat{s} + \hat{t})^2} \right] \right\} \\
&\quad - \frac{\hat{s}(4\hat{s} + 3\hat{t} + 3\hat{u}) + \hat{t}^2 + \hat{u}^2}{\hat{t}\hat{u}}, \\
K_{1b}^N(M_\Gamma^2) &= -K_{1a}^N(M_\Gamma^2)\Big|_{M_\Gamma^2 \leftrightarrow M_W^2}, \\
K_2^N(M_\Gamma^2) &= -K_2^A(M_\Gamma^2), \\
K_3^N(M_\Gamma^2) &= (M_W^2 + M_\Gamma^2) \left[ \frac{3\hat{s}\hat{t}}{(\hat{s} + \hat{u})^3} + \frac{3\hat{s}\hat{u}}{(\hat{s} + \hat{t})^3} \right] - \frac{1}{\hat{t}\hat{u}} \left[ \frac{1}{(\hat{s} + \hat{t})^2} + \frac{1}{(\hat{s} + \hat{u})^2} \right] \\
&\quad \times \left\{ \hat{s}^4 - 2\hat{t}^2\hat{u}^2 + \hat{s}^2(\hat{t} + \hat{u})(2\hat{s} + \hat{t} + \hat{u}) + (M_W^2 + M_\Gamma^2) \right. \\
&\quad \left. \times \left[ \hat{s}^2(\hat{s} + \hat{t} + \hat{u}) - \hat{t}\hat{u}(2\hat{s} - \hat{t} - \hat{u}) \right] \right\},
\end{aligned}$$

$$\begin{aligned}
K_4^{\text{N}}(M_\Gamma^2) &= -K_4^{\text{A}}(M_\Gamma^2), \\
K_{5a}^{\text{N}}(M_\Gamma^2) &= \frac{2\hat{s}(\hat{s} + \hat{t}) - 2\hat{t}\hat{u}}{2(\hat{s} + \hat{t})^2} - \left[ \frac{\hat{s} + \hat{t}}{\hat{u}} - \frac{2\hat{s}}{\hat{s} + \hat{t}} - \frac{\hat{u}(2\hat{s} + \hat{t})}{2(\hat{s} + \hat{t})^2} \right] - M_\Gamma^2 \left[ \frac{1}{\hat{u}} - \frac{2\hat{s} + \hat{t}}{2(\hat{s} + \hat{t})^2} \right] \\
&\quad + (2M_\Gamma^2 - M_W^2) \left[ \frac{2\hat{s}}{(\hat{s} + \hat{t})^2} + \frac{\hat{u}(2\hat{s} - \hat{t})}{(\hat{s} + \hat{t})^3} \right], \\
K_{5b}^{\text{N}}(M_\Gamma^2) &= \frac{2\hat{s}(\hat{s} + \hat{t}) - 2\hat{t}\hat{u}}{2(\hat{s} + \hat{t})^2} + \left[ \frac{\hat{s} + \hat{t}}{\hat{u}} - \frac{2\hat{s}}{\hat{s} + \hat{t}} - \frac{\hat{u}(2\hat{s} + \hat{t})}{2(\hat{s} + \hat{t})^2} \right] + M_W^2 \left[ \frac{1}{\hat{u}} - \frac{2\hat{s} + \hat{t}}{2(\hat{s} + \hat{t})^2} \right] \\
&\quad - M_\Gamma^2 \left[ \frac{2\hat{s}}{(\hat{s} + \hat{t})^2} + \frac{\hat{u}(2\hat{s} - \hat{t})}{(\hat{s} + \hat{t})^3} \right], \\
K_{6a}^{\text{N}}(M_\Gamma^2) &= K_{5a}^{\text{N}}(M_\Gamma^2) \Big|_{\hat{t} \leftrightarrow \hat{u}}, \\
K_{6b}^{\text{N}}(M_\Gamma^2) &= K_{5b}^{\text{N}}(M_\Gamma^2) \Big|_{\hat{t} \leftrightarrow \hat{u}}, \\
K_7^{\text{N}}(M_\Gamma^2) &= -K_7^{\text{A}}(M_\Gamma^2), \\
K_8^{\text{N}}(M_\Gamma^2) &= -K_8^{\text{A}}(M_\Gamma^2), \\
K_{9a}^{\text{N}}(M_\Gamma^2) &= \hat{u} - \frac{\hat{s}^2 - \hat{s}\hat{t}}{2\hat{t}} + \frac{\hat{s}^2 + \hat{s}\hat{t}}{2\hat{u}} + (M_W^2 + M_\Gamma^2) \left[ \frac{2\hat{s}^2 + \hat{t}\hat{s} + \hat{t}^2}{2\hat{t}\hat{u}} - \frac{\hat{t} - \hat{s}}{2\hat{t}} \right] \\
&\quad - \frac{2M_\Gamma^2\hat{t}\hat{u}}{(\hat{s} + \hat{t})^2} + \frac{M_\Gamma^2}{\hat{s} + \hat{t}} \left[ \frac{M_W^2\hat{s}^2}{\hat{t}\hat{u}} - \frac{M_\Gamma^2\hat{u}(2\hat{s} - \hat{t})}{(\hat{s} + \hat{t})^2} - \frac{2(M_W^2 + M_\Gamma^2)\hat{s}}{\hat{s} + \hat{t}} \right], \\
K_{9b}^{\text{N}}(M_\Gamma^2) &= K_{9a}^{\text{N}}(M_\Gamma^2) \Big|_{M_\Gamma^2 \leftrightarrow M_W^2}, \\
K_{10}^{\text{N}}(M_\Gamma^2) &= K_8^{\text{N}}(M_\Gamma^2) \Big|_{\hat{t} \leftrightarrow \hat{u}} = -K_{10}^{\text{A}}(M_\Gamma^2), \\
K_{11a}^{\text{N}}(M_\Gamma^2) &= K_{9a}^{\text{N}}(M_\Gamma^2) \Big|_{\hat{t} \leftrightarrow \hat{u}}, \\
K_{11b}^{\text{N}}(M_\Gamma^2) &= K_{9b}^{\text{N}}(M_\Gamma^2) \Big|_{\hat{t} \leftrightarrow \hat{u}}, \\
K_{12}^{\text{N}}(M_\Gamma^2) &= -K_{12}^{\text{A}}(M_\Gamma^2), \\
K_{13}^{\text{N}}(M_\Gamma^2) &= K_{12}^{\text{N}}(M_\Gamma^2) \Big|_{\hat{t} \leftrightarrow \hat{u}} = -K_{13}^{\text{A}}(M_\Gamma^2), \\
K_{14a}^{\text{N}}(M_\Gamma^2) &= \frac{M_W^2\hat{t} + M_\Gamma^2\hat{u} - \hat{t}\hat{u}}{2\hat{t}\hat{u}} \left[ 2M_W^2M_\Gamma^2 + (2\hat{s} + \hat{t} + \hat{u})(M_W^2 + M_\Gamma^2) - 2\hat{t}\hat{u} \right. \\
&\quad \left. - \hat{s}(\hat{t} + \hat{u}) \right], \\
K_{14b}^{\text{N}}(M_\Gamma^2) &= K_{14a}^{\text{N}}(M_\Gamma^2) \Big|_{M_\Gamma^2 \leftrightarrow M_W^2}. \tag{D.3}
\end{aligned}$$

The only non-vanishing coefficients of the function  $H_{1,V}^{\text{X}}(M_\Gamma^2)$  read

$$\begin{aligned}
K_0^{\text{X}}(M_\Gamma^2) &= -\frac{\hat{t}^2 + \hat{u}^2 + \hat{s}(\hat{t} + \hat{u})}{\hat{t}\hat{u}}, \\
K_{1a}^{\text{X}}(M_\Gamma^2) &= -\left[ K_{5a}^{\text{X}}(M_\Gamma^2) + K_{6a}^{\text{X}}(M_\Gamma^2) \right],
\end{aligned}$$

$$\begin{aligned}
K_{5a}^X(M_\Gamma^2) &= \frac{2(M_\Gamma^2 - \hat{u})(\hat{s} + \hat{t})}{\hat{u}^2}, \\
K_{6a}^X(M_\Gamma^2) &= K_{5a}^X(M_\Gamma^2)|_{\hat{t} \leftrightarrow \hat{u}}.
\end{aligned} \tag{D.4}$$

Finally, for  $H_{1,V}^Y(M_\Gamma^2)$  we obtain

$$\begin{aligned}
K_0^Y(M_\Gamma^2) &= \frac{(\hat{u} - \hat{t})(\hat{s} + \hat{t} + \hat{u})}{\hat{t}\hat{u}}, \\
K_{1a}^Y(M_\Gamma^2) &= M_\Gamma^2 \left[ \frac{2}{\hat{t}} + \frac{3\hat{s}}{(\hat{s} + \hat{t})^2} - \frac{1}{\hat{s} + \hat{t}} - \frac{2}{\hat{u}} - \frac{3\hat{s}}{(\hat{s} + \hat{u})^2} + \frac{1}{\hat{s} + \hat{u}} \right] \\
&\quad + M_\Gamma^2 \left[ \frac{2(\hat{s} + \hat{u})}{\hat{t}^2} - \frac{2(\hat{s} + \hat{t})}{\hat{u}^2} \right], \\
K_{1b}^Y(M_\Gamma^2) &= -M_W^2 \left[ \frac{2}{\hat{t}} + \frac{3\hat{s}}{(\hat{s} + \hat{t})^2} - \frac{1}{\hat{s} + \hat{t}} - \frac{2}{\hat{u}} - \frac{3\hat{s}}{(\hat{s} + \hat{u})^2} + \frac{1}{\hat{s} + \hat{u}} \right] \\
&\quad - \left[ \frac{2(\hat{s} + \hat{u})}{\hat{t}} - \frac{2(\hat{s} + \hat{t})}{\hat{u}} \right], \\
K_2^Y(M_\Gamma^2) &= 0, \\
K_3^Y(M_\Gamma^2) &= \frac{2(M_W^2 - M_\Gamma^2)(\hat{t} - \hat{u})(\hat{s} + \hat{t} + \hat{u})}{(\hat{s} + \hat{t})^3(\hat{s} + \hat{u})^3} \left[ -7\hat{s}^3 + (\hat{t}\hat{u} - 6\hat{s}^2)(\hat{t} + \hat{u}) \right. \\
&\quad \left. - \hat{s}(2\hat{t}^2 - \hat{t}\hat{u} + 2\hat{u}^2) \right], \\
K_4^Y(M_\Gamma^2) &= 0, \\
K_{5a}^Y(M_\Gamma^2) &= -\frac{2\hat{s}^2 + 3\hat{t}\hat{u} + 2\hat{s}(\hat{t} + \hat{u})}{(\hat{s} + \hat{t})^2} - M_W^2 \left[ \frac{4\hat{s}}{(\hat{s} + \hat{t})^2} + \frac{2\hat{u}(2\hat{s} - \hat{t})}{(\hat{s} + \hat{t})^3} \right] \\
&\quad - M_\Gamma^2 \left[ \frac{2\hat{s} + \hat{t}}{(\hat{s} + \hat{t})^2} - \frac{2}{\hat{u}} - \frac{2(\hat{s} + \hat{t})}{\hat{u}^2} \right], \\
K_{5b}^Y(M_\Gamma^2) &= \frac{2\hat{s}^2 + 3\hat{t}\hat{u} + 2\hat{s}(\hat{t} + \hat{u})}{(\hat{s} + \hat{t})^2} + M_\Gamma^2 \left[ \frac{4\hat{s}}{(\hat{s} + \hat{t})^2} + \frac{2\hat{u}(2\hat{s} - \hat{t})}{(\hat{s} + \hat{t})^3} \right] \\
&\quad + M_W^2 \left[ \frac{2\hat{s} + \hat{t}}{(\hat{s} + \hat{t})^2} - \frac{2}{\hat{u}} \right] - \frac{2(\hat{s} + \hat{t})}{\hat{u}}, \\
K_{6a}^Y(M_\Gamma^2) &= -K_{5a}^Y(M_\Gamma^2)|_{\hat{t} \leftrightarrow \hat{u}}, \\
K_{6b}^Y(M_\Gamma^2) &= -K_{5b}^Y(M_\Gamma^2)|_{\hat{t} \leftrightarrow \hat{u}}, \\
K_7^Y(M_\Gamma^2) &= 0, \\
K_8^Y(M_\Gamma^2) &= 0, \\
K_{9a}^Y(M_\Gamma^2) &= \frac{1}{(\hat{s} + \hat{t})^3 \hat{t}\hat{u}} \left\{ 2M_\Gamma^4 \hat{t}\hat{u} \left[ 2\hat{s}^2 - \hat{t}\hat{u} + 2\hat{s}(\hat{t} + \hat{u}) \right] \right. \\
&\quad \left. - M_\Gamma^2(\hat{s} + \hat{t}) \left[ (\hat{s} + \hat{t})^2(2\hat{s}^2 + \hat{s}\hat{t} + \hat{t}^2) + (\hat{s} - \hat{t})(\hat{s} + \hat{t})^2 \hat{u} - 4\hat{t}^2 \hat{u}^2 \right] \right\}
\end{aligned}$$



$$\begin{aligned}
& + 2M_W^2 \hat{s} \left( \hat{s}(\hat{s} + \hat{t}) - 2\hat{t}\hat{u} \right) \Big] - (\hat{s} + \hat{t})^3 \left[ \hat{s}^2(\hat{t} - \hat{u}) + 2\hat{t}\hat{u}^2 \right. \\
& \left. + \hat{s}\hat{t}(\hat{t} + \hat{u}) + M_W^2 \left( 2\hat{s}^2 + \hat{t}(\hat{t} - \hat{u}) + \hat{s}(\hat{t} + \hat{u}) \right) \right] \Big\}, \\
K_{9b}^Y(M_\Gamma^2) &= -K_{9a}^Y(M_\Gamma^2) \Big|_{M_\Gamma^2 \leftrightarrow M_W^2}, \\
K_{10}^Y(M_\Gamma^2) &= 0, \\
K_{11a}^Y(M_\Gamma^2) &= -K_{9a}^Y(M_\Gamma^2) \Big|_{\hat{t} \leftrightarrow \hat{u}}, \\
K_{11b}^Y(M_\Gamma^2) &= -K_{9b}^Y(M_\Gamma^2) \Big|_{\hat{t} \leftrightarrow \hat{u}}, \\
K_{12}^Y(M_\Gamma^2) &= 0, \\
K_{13}^Y(M_\Gamma^2) &= 0, \\
K_{14a}^Y(M_\Gamma^2) &= -2K_{14a}^N(M_\Gamma^2), \\
K_{14b}^Y(M_\Gamma^2) &= 2K_{14b}^N(M_\Gamma^2) = -K_{14a}^Y(M_\Gamma^2) \Big|_{M_\Gamma^2 \leftrightarrow M_W^2}. \tag{D.5}
\end{aligned}$$

## D.2 Real corrections for $W + \text{jet}$

We present explicit analytic expression for the functions  $H_r^i$  of Eq.(5.4) for the real photon emission process  $\bar{q}q' \rightarrow W^\sigma g\gamma$ . These functions describe the contribution of the real photon emission Feynman diagrams of Fig. 5.1 to the unpolarized squared amplitude and depend on the kinematical invariants  $\hat{s}, \hat{t}, \hat{u}, \hat{t}'$  and  $\hat{u}'$ . To simplify the expressions we introduce a further decomposition into the functions  $H_{55}, H_{56a}, H_{67}$  and  $H_{77a}$  according to

$$\begin{aligned}
H_r^1 &= [H_{55} + H_{56a}] + (T \leftrightarrow U), \\
H_r^2 &= [H_{77a} - H_{55}] \Big|_{T \leftrightarrow U} + H_{67}, \\
H_r^3 &= H_r^2 \Big|_{T \leftrightarrow U}. \tag{D.6}
\end{aligned}$$

The operation  $(T \leftrightarrow U)$  means the combined permutation of  $(\hat{t} \leftrightarrow \hat{u})$  and  $(\hat{t}' \leftrightarrow \hat{u}')$ . The kinematic invariants are defined in (2.15) and the above functions are given by

$$\begin{aligned}
H_{55} &= \frac{2}{(-p_W^2 + \hat{s} + \hat{t} + \hat{t}')(-p_W^2 + \hat{s} + \hat{u} + \hat{u}')} \left\{ \hat{u} \left( \frac{\hat{s}}{\hat{t}'} - \frac{\hat{u}'}{p_W^2} + 2 \right) \right. \\
& + \frac{p_W^2(p_W^2 - \hat{s} - \hat{u}')}{\hat{t}'\hat{u}^2} \left( p_W^4 - 2p_W^2(\hat{s} + \hat{t} + \hat{t}') + (\hat{s} + \hat{t})^2 + 2\hat{t}'^2 + 2\hat{t}'(\hat{s} + \hat{t}) \right) \\
& - \frac{(p_W^2 - \hat{s} - \hat{t})}{\hat{t}'\hat{u}} \left( p_W^4 - p_W^2(3\hat{s} + 2\hat{t}) + (\hat{s} + \hat{u}')(2\hat{s} + \hat{t} + \hat{u}') \right) \\
& \left. + \frac{1}{\hat{u}} \left( 4p_W^4 - p_W^2(7\hat{s} + 4\hat{t} + 2\hat{u}') + 3\hat{s}^2 + \hat{u}'(\hat{t} + 2\hat{u}') + \hat{s}(\hat{t} + 4\hat{u}') \right) \right\}
\end{aligned}$$

$$\begin{aligned}
& + \frac{1}{\hat{t}'} \left( 3\hat{s}^2 + 4\hat{s}(\hat{t} + \hat{t}') + \hat{s}\hat{u}' + 2(\hat{t} + \hat{t}')^2 + \hat{u}'(\hat{t} + 4\hat{t}') \right) \\
& - \left. \frac{2p_W^2(3\hat{s} + 2\hat{t} + 4\hat{t}' + \hat{u}')}{2\hat{t}'} - \frac{(\hat{t} + \hat{t}')^2 + \hat{u}^2 + \hat{u}'^2}{2p_W^2} + \frac{\hat{t}'(\hat{s} - 3p_W^2)}{\hat{u}} \right\},
\end{aligned}$$

$$\begin{aligned}
H_{56a} = & \frac{1}{(-p_W^2 + \hat{s} + \hat{t} + \hat{t}')(-p_W^2 + \hat{s} + \hat{u} + \hat{u}')} \left\{ -\frac{\hat{s}^3(2p_W^2 - 2\hat{s})^2}{2\hat{t}'\hat{u}\hat{u}'} + \frac{2\hat{s}(7p_W^2 - 9\hat{s})}{\hat{u}'} \right. \\
& + \frac{2\hat{u}'^2}{p_W^2} + 4(p_W^2 - 2\hat{s}) + \hat{u}^2 \left( \frac{2}{p_W^2} - \frac{4}{\hat{u}'} \right) + \hat{u}' \left( \frac{6p_W^2 - 8\hat{s}}{\hat{t}'} - 12 \right) + \frac{8\hat{u}'(p_W^2 - \hat{s})}{\hat{t}} \\
& + \hat{u} \left( \frac{6p_W^2 - 8\hat{s}}{\hat{t}} + \frac{4\hat{u}'}{p_W^2} + \frac{4(p_W^2 - 2\hat{s}) - 2\hat{t}'}{\hat{u}'} - 12 \right) + \frac{1}{\hat{u}} \left( -4\hat{u}'^2 - 4\hat{u}'(p_W^2 + 2\hat{s}) \right. \\
& \left. - 2\hat{t}\hat{u}' + 2\hat{s}(5p_W^2 - 9\hat{s}) \right) + \frac{1}{\hat{t}\hat{u}} \left( 4\hat{u}'^2(p_W^2 - \hat{s}) + 2\hat{u}'(p_W^2 - \hat{s})(p_W^2 + 3\hat{s}) - 4p_W^2\hat{t}'\hat{u}' \right. \\
& \left. + 2\hat{s}(p_W^2 - \hat{s})(p_W^2 + 3\hat{s}) \right) + \frac{1}{\hat{t}'\hat{u}} \left( 4\hat{u}'^2(p_W^2 - \hat{s}) - 2\hat{t}\hat{u}'^2 + 12\hat{s}\hat{u}'(p_W^2 - \hat{s}) \right) \\
& + \frac{2(p_W^2 - 4\hat{s})\hat{t}}{\hat{u}'} + \frac{1}{\hat{t}'\hat{u}'} \left( -4\hat{s}\hat{u}^2 + 6\hat{s}\hat{u}(p_W^2 - \hat{s}) - 2\hat{s}(p_W^4 - 2\hat{s}p_W^2 + 3\hat{s}^2) \right) \\
& + \frac{1}{\hat{t}\hat{u}'} \left( 2\hat{u}^2(p_W^2 - 2\hat{s}) - 2\hat{t}'\hat{u}^2 + 2\hat{t}'\hat{u}(p_W^2 - 4\hat{s}) - 2\hat{u}(p_W^2 - 3\hat{s})(p_W^2 - 2\hat{s}) \right. \\
& \left. - 4\hat{s}(p_W^2 - 4\hat{s})(p_W^2 - \hat{s}) \right) + \frac{1}{\hat{u}\hat{u}'} \left( -4\hat{s}(2p_W^2 - 3\hat{s})(p_W^2 - \hat{s}) - 2\hat{t}(p_W^2 - 3\hat{s})(p_W^2 - \hat{s}) \right. \\
& \left. - 2\hat{t}'(2p_W^2 - 3\hat{s})(p_W^2 - \hat{s}) \right) + \frac{1}{\hat{t}\hat{u}\hat{u}'} \left( -2\hat{s}^2(2p_W^2 - 2\hat{s})^2 - (6\hat{s}\hat{t}' + 2\hat{t}'^2)(p_W^2 - \hat{s})^2 \right) \\
& \left. + \frac{1}{\hat{t}'\hat{u}\hat{u}'} \left( -4\hat{s}^2(p_W^2 - 2\hat{s})(p_W^2 - \hat{s}) + 2\hat{t}'^2\hat{s}(p_W^2 - \hat{s}) - 2\hat{t}\hat{s}(p_W^2 - 3\hat{s})(p_W^2 - \hat{s}) \right) \right\},
\end{aligned}$$

$$\begin{aligned}
H_{67} = & \frac{2}{(p_W^2 - \hat{s}_5)(-p_W^2 + \hat{s} + \hat{t} + \hat{t}')(-p_W^2 + \hat{s} + \hat{u} + \hat{u}')} \left\{ -p_W^4 - p_W^2(9\hat{s} + \frac{19\hat{t}'}{2} + 5\hat{u}) \right. \\
& + 4\hat{s}^2 + 2\hat{t}'^2 + 2\hat{u}^2 + \frac{15\hat{s}\hat{t}'}{2} + 8\hat{s}\hat{u} + \frac{23\hat{t}'\hat{u}}{2} + \frac{\hat{u}'}{2} \left( -9p_W^2 + 9\hat{s} + 14\hat{t}' + 6\hat{u} + \frac{3\hat{s}_5\hat{u}}{p_W^2} \right) \\
& + \hat{t}'^2 \left( \frac{\hat{s}_5}{p_W^2} + \frac{2(p_W^2 - \hat{u})}{\hat{u}'} \right) + \frac{1}{\hat{t}} \left( p_W^4(\hat{s} - 2\hat{t}' + \hat{u}) - 2p_W^2(\hat{s}^2 + 3\hat{t}'\hat{s} + \hat{t}'^2) + \hat{s}(\hat{s} + 2\hat{t}')^2 \right. \\
& \left. - (\hat{s} + \hat{t}')\hat{u}^2 - 2\hat{t}'\hat{u}'^2 + (\hat{s} + 2\hat{t}')^2\hat{u} + \hat{u}'[3p_W^4 - 4\hat{s}p_W^2 + \hat{s}^2 + 2\hat{t}'^2 + 2\hat{s}\hat{t}' \right. \\
& \left. - \hat{u}(p_W^2 + \hat{s} + 2\hat{t}')] + \frac{(\hat{s} + \hat{t}')}{\hat{u}'} \left[ (p_W^2 - \hat{s} - \hat{u})(p_W^2(2\hat{s} + \hat{t}' + \hat{u}) - 2\hat{t}'\hat{u} - \hat{s}(\hat{t}' + \hat{u})) \right] \right) \\
& \left. + \hat{t} \left( -5p_W^2 + 5\hat{s} + 3\hat{t}' + 8\hat{u} + \frac{11\hat{u}'}{2} + \frac{1}{\hat{u}'} \left[ -(p_W^2 + \hat{s} - \hat{t}')(\hat{s}_5 + \hat{t} + \hat{t}' + \hat{u} + \hat{u}') \right] \right) \right\}
\end{aligned}$$

$$\begin{aligned}
& +2\hat{u}^2 + 2\hat{u}(\hat{s} - \hat{t}') + \frac{3\hat{s}_5\hat{t}'}{2p_W^2} \Big] \Big) + \frac{p_W^2}{\hat{u}'} \left( 2p_W^4 + p_W^2(3\hat{s} + \hat{t}' - 2\hat{u}) - 4\hat{s}^2 - 2\hat{s}(\hat{t}' + 4\hat{u}) \right. \\
& \left. + \hat{t}'(\hat{t}' - 5\hat{u}) \right) + \frac{1}{\hat{u}'} \left( +\hat{s}^3 - \hat{t}'\hat{u}(\hat{t}' - 4\hat{u}) + \hat{s}^2(\hat{t}' + 4\hat{u}) + \hat{s}(-\hat{t}'^2 + 4\hat{u}\hat{t}' + 4\hat{u}^2) \right) \\
& \left. + \frac{\hat{s}_5\hat{u}'^2}{p_W^2} + \frac{\hat{s}_5(\hat{t}'^2 + \hat{u}^2)}{p_W^2} \right\},
\end{aligned}$$

$$\begin{aligned}
H_{77a} = & \frac{1}{(p_W^2 - \hat{s}_5)^2(-p_W^2 + \hat{s} + \hat{t} + \hat{t}')(-p_W^2 + \hat{s} + \hat{u} + \hat{u}')} \left\{ -5p_W^6 + p_W^4(10\hat{t} + 7\hat{t}') \right. \\
& + p_W^2 \left[ \hat{s}^2 + 4\hat{t}'\hat{s} - 3\hat{t}^2 - \hat{t}(7\hat{t}' + 2\hat{u}) + 2\hat{t}'(\hat{u}' - 2\hat{t}') \right] + \hat{s}_5 \left[ -2\hat{t}^2 + (\hat{t}' + 2\hat{u} + 3\hat{u}')\hat{t} \right. \\
& \left. \left. + \hat{s}(2\hat{t} + \hat{t}') + \hat{t}'(\hat{u}' - 2\hat{t}') \right] + \frac{\hat{s}_5^2(\hat{t}^2 + \hat{t}'\hat{t} + \hat{t}'^2)}{p_W^2} \right\}. \tag{D.7}
\end{aligned}$$

# Bibliography

- [1] H. Fritzsch and P. Minkowski, Phys. Lett. B **69** (1977) 316. Also, for a review see: J. F. Owens, Rev. Mod. Phys. **59** (1987) 465.
- [2] P. Aurenche *et al.*, Phys. Lett. B **140** (1984) 87; P. Aurenche *et al.*, Nucl. Phys. B **297** (1988) 661; H. Baer, J. Ohnemus and J. F. Owens, Phys. Lett. B **234** (1990) 127; Phys. Rev. D **42** (1990) 61; E. L. Berger and J. w. Qiu, Phys. Lett. B **248** (1990) 371; Phys. Rev. D **44** (1991) 2002; P. Aurenche *et al.*, Nucl. Phys. B **399** (1993) 34; L. E. Gordon and W. Vogelsang, Phys. Rev. D **48** (1993) 3136; Phys. Rev. D **50** (1994) 1901; S. Catani *et al.*, JHEP **0205** (2002) 028 [hep-ph/0204023].
- [3] F. Abe *et al.* [CDF Collaboration], Phys. Rev. Lett. **73** (1994) 2662 [Erratum-ibid. **74** (1995) 1891]; D. Acosta *et al.* [CDF Collaboration]; Phys. Rev. D **65** (2002) 112003 [hep-ex/0201004]; B. Abbott *et al.* [D0 Collaboration], Phys. Rev. Lett. **84** (2000) 2786 [hep-ex/9912017]; V. M. Abazov *et al.* [D0 Collaboration], Phys. Rev. Lett. **87** (2001) 251805 [hep-ex/0106026]; L. Apanasevich *et al.* [Fermilab E706 Collaboration], Phys. Rev. Lett. **81** (1998) 2642 [hep-ex/9711017]; Phys. Rev. D **70** (2004) 092009 [hep-ex/0407011]; G. Balocchi *et al.* [UA6 Collaboration], Phys. Lett. B **436** (1998) 222. For a review of older data, see: W. Vogelsang and M. R. Whalley, J. Phys. G **23** (1997) A1.
- [4] P. Aurenche, R. Baier and M. Fontannaz, Phys. Rev. D **42** (1990) 1440; W. Vogelsang and A. Vogt, Nucl. Phys. B **453** (1995) 334 [hep-ph/9505404].
- [5] A. Kumar *et al.*, Phys. Rev. D **67** (2003) 014016.
- [6] Yu. L. Dokshitzer, D. I. D'Yakonov, and S. I. Troyan, Phys. Lett. B **79** (1978) 269; G. Parisi and R. Petronzio, Nucl. Phys. B **154** (1979) 427; G. Altarelli, R. K. Ellis, M. Greco and G. Martinelli, Nucl. Phys. B **246** (1984) 12; J. C. Collins and D. E. Soper, Nucl. Phys. B **193** (1981) 381 [Erratum-ibid. B **213** (1983) 545]; Nucl. Phys. B **197** (1982) 446; J. C. Collins, D. E. Soper and G. Sterman, Nucl. Phys. B **250** (1985) 199; C. T. H. Davies and W. J. Stirling, Nucl. Phys. B **244** (1984) 337; C. T. H. Davies, B. R. Webber and W. J. Stirling, Nucl. Phys. B **256** (1985) 413; P. B. Arnold and R. P. Kauffman, Nucl. Phys. B **349** (1991) 381.

- [7] C. Balázs and C. P. Yuan, *Phys. Rev. D* **56** (1997) 5558 [hep-ph/9704258]; R. K. Ellis and S. Veseli, *Nucl. Phys. B* **511** (1998) 649 [hep-ph/9706526]; A. Kulesza and W. J. Stirling, *Nucl. Phys. B* **555** (1999) 279 [hep-ph/9902234]; *Eur. Phys. J. C* **20** (2001) 349 [hep-ph/0103089]; J.-W. Qiu and X.-F. Zhang *Phys. Rev. Lett.* **86** (2001) 2724 [hep-ph/0012058]; *Phys. Rev. D* **63** (2001) 114011 [hep-ph/0012348]; A. Kulesza, G. Sterman and W. Vogelsang, *Phys. Rev. D* **66** (2002) 014011 [hep-ph/0202251].
- [8] CMS Technical Design Reports, “Volume II: Physics Performance”, CERN/LHCC/2006-021, CMS TDR 8.2, 26 June 2006
- [9] S. Catani *et al.*, [hep-ph/0005025].
- [10] J. Huston *et al.*, *Phys. Rev. D* **51** (1995) 6139 [hep-ph/9501230]; P. Aurenche *et al.*, *Eur. Phys. J. C* **9** (1999) 107 [hep-ph/9811382].
- [11] R. K. Ellis, G. Martinelli and R. Petronzio, *Nucl. Phys. B* **211** (1983) 106; P. B. Arnold and M. H. Reno, *Nucl. Phys. B* **319** (1989) 37 [Erratum-ibid. B **330** (1990) 284]; R. J. Gonsalves, J. Pawlowski and C. F. Wai, *Phys. Rev. D* **40** (1989) 2245; W. T. Giele, E. W. N. Glover and D. A. Kosower, *Nucl. Phys. B* **403** (1993) 633 [hep-ph/9302225]; J. Campbell and R. K. Ellis, *Phys. Rev. D* **65** (2002) 113007 [hep-ph/0202176]; J. Campbell, R. K. Ellis and D. L. Rainwater, *Phys. Rev. D* **68** (2003) 094021 [hep-ph/0308195].
- [12] A. Gehrmann-De Ridder, T. Gehrmann and E. W. N. Glover, *Nucl. Phys. Proc. Suppl.* **135** (2004) 97 [hep-ph/0407023]; S. Weinzierl, [hep-ph/0408278].
- [13] J. H. Kühn, A. A. Penin and V. A. Smirnov, *Eur. Phys. J. C* **17** (2000) 97 [hep-ph/9912503]; M. Ciafaloni, P. Ciafaloni and D. Comelli, *Phys. Rev. Lett.* **84** (2000) 4810 [hep-ph/0001142]; A. Denner and S. Pozzorini, *Eur. Phys. J. C* **18** (2001) 461 [hep-ph/0010201]; *Eur. Phys. J. C* **21** (2001) 63 [hep-ph/0104127]; B. Jantzen *et al.*, *Nucl. Phys. B* **731** (2005) 188 [Erratum-ibid. B **752** (2006) 327] [hep-ph/0509157]; J. H. Kühn *et al.*, *Nucl. Phys. B* **616** (2001) 286 [hep-ph/0106298].
- [14] V. S. Fadin *et al.*, *Phys. Rev. D* **61** (2000) 094002 [hep-ph/9910338]; W. Beenakker and A. Werthenbach, *Nucl. Phys. B* **630** (2002) 3 [hep-ph/0112030]; A. Denner, M. Melles and S. Pozzorini, *Nucl. Phys. B* **662** (2003) 299 [hep-ph/0301241]; S. Pozzorini, *Nucl. Phys. B* **692** (2004) 135 [hep-ph/0401087].
- [15] S. Dittmaier and M. Krämer, *Phys. Rev. D* **65** (2002) 073007 [hep-ph/0109062].
- [16] U. Baur, O. Brein, W. Hollik, C. Schappacher and D. Wackerroth, *Phys. Rev. D* **65** (2002) 033007 [hep-ph/0108274]; E. Accomando, A. Denner and S. Pozzorini, *Phys. Rev. D* **65** (2002) 073003 [hep-ph/0110114]; W. Hollik

- and C. Meier, Phys. Lett. B **590** (2004) 69 [hep-ph/0402281]; U. Baur and D. Wackeroth, Phys. Rev. D **70** (2004) 073015 [hep-ph/0405191]; E. Accomando, A. Denner and A. Kaiser, Nucl. Phys. B **706** (2005) 325 [hep-ph/0409247]; E. Accomando, A. Denner and C. Meier, Eur. Phys. J. C **47** (2006) 125 [hep-ph/0509234]; J. H. Kühn, A. Scharf and P. Uwer, Eur. Phys. J. C **45** (2006) 139 [hep-ph/0508092]; [hep-ph/0610335]; S. Moretti, M. R. Nolten and D. A. Ross, Phys. Lett. B **639** (2006) 513 [hep-ph/0603083]; C. M. Carloni Calame, G. Montagna, O. Nicrosini and A. Vicini, JHEP **0612** (2006) 016 [hep-ph/0609170]; W. Bernreuther, M. Fuecker and Z. G. Si, Phys. Rev. D **74** (2006) 113005 [hep-ph/0610334].
- [17] E. Maina, S. Moretti and D. A. Ross, Phys. Lett. B **593** (2004) 143 [Erratum-ibid. B **614** (2005) 216] [hep-ph/0403050].
- [18] J. H. Kühn, A. Kulesza, S. Pozzorini and M. Schulze, Phys. Lett. B **609** (2005) 277 [hep-ph/0408308].
- [19] J. H. Kühn, A. Kulesza, S. Pozzorini and M. Schulze, Nucl. Phys. B **727** (2005) 368 [hep-ph/0507178].
- [20] J. H. Kühn, A. Kulesza, S. Pozzorini and M. Schulze, JHEP **0603** (2006) 059 [hep-ph/0508253].
- [21] U. Baur, Phys. Rev. D **75** (2007) 013005 [hep-ph/0611241].
- [22] J. H. Kühn, A. Kulesza, S. Pozzorini and M. Schulze, Phys. Lett. B **651** (2007) 160 [hep-ph/0703283].
- [23] W. Hollik, T. Kasprzik, B.A. Kniehl, arXiv:0707.2553 [hep-ph].
- [24] J. H. Kühn, A. Kulesza, S. Pozzorini and M. Schulze, Nucl. Phys. B **797** (2008) 22 arXiv:0708.0476 [hep-ph].
- [25] W. Hollik *et al.*, Acta Phys. Polon. B **35** (2004) 2533 [hep-ph/0501246].
- [26] S. Pozzorini, *doctoral thesis, Universität Zürich, 2001*, [hep-ph/0201077].
- [27] V. A. Mitsou, [hep-ph/0004161].
- [28] G. Passarino and M. J. G. Veltman, Nucl. Phys. B **160** (1979) 151.
- [29] A. Denner, Fortsch. Phys. **41** (1993) 307.
- [30] R. Mertig, M. Böhm and A. Denner, Comput. Phys. Commun. **64** (1991) 345; <http://www.feyncalc.org/>.
- [31] S. Dittmaier, Nucl. Phys. B **675** (2003) 447 [hep-ph/0308246].

- [32] A. Sirlin, *Phys. Rev. D* **22** (1980) 971; W. J. Marciano and A. Sirlin, *Phys. Rev. D* **22** (1980) 2695 [Erratum-ibid. *D* **31**, 213 (1985)]; *Nucl. Phys. B* **189** (1981) 442.
- [33] M. Böhm, A. Denner and H. Joos, “Gauge theories of the strong and electroweak interaction”, *Stuttgart, Germany: Teubner (2001) 784 p.*
- [34] T. Kinoshita, *J. Math. Phys.* **3** (1962) 650; T. D. Lee and M. Nauenberg, *Phys. Rev.* **133** (1964) B1549.
- [35] W. Beenakker and A. Denner, *Nucl. Phys. B* **338** (1990) 349.
- [36] A. Denner and S. Pozzorini, *Eur. Phys. J. C* **18** (2001) 461 [hep-ph/0010201]; *Eur. Phys. J. C* **21** (2001) 63 [hep-ph/0104127].
- [37] A. Denner, M. Melles and S. Pozzorini, *Nucl. Phys. B* **662** (2003) 299 [hep-ph/0301241].
- [38] M. Melles, *Phys. Rev. D* **63** (2001) 034003 [hep-ph/0004056]; *Phys. Rev. D* **64** (2001) 014011 [hep-ph/0012157]; *Phys. Rev. D* **64** (2001) 054003 [hep-ph/0102097]; *Phys. Rept.* **375** (2003) 219 [hep-ph/0104232]; *Eur. Phys. J. C* **24** (2002) 193 [hep-ph/0108221].
- [39] M. Roth and A. Denner, *Nucl. Phys. B* **479** (1996) 495 [hep-ph/9605420].
- [40] S. Dittmaier, *Nucl. Phys. B* **565** (2000) 69 [hep-ph/9904440].
- [41] S. Catani and M. H. Seymour, *Nucl. Phys. B* **485** (1997) 291 [Erratum-ibid. *B* **510** (1998) 503] [hep-ph/9605323].
- [42] S. Catani, S. Dittmaier, M. H. Seymour and Z. Trocsanyi, *Nucl. Phys. B* **627** (2002) 189 [hep-ph/0201036].
- [43] E. Byckling, K. Kajantie, “Particle Kinematics”, *John Wiley & Sons Ltd. (1973).*
- [44] Wolfram Research, Inc., *Mathematica*, Version 4.2, Champaign, IL (2002).
- [45] J. A. M. Vermaseren,
- [46] G. J. van Oldenborgh, *Comput. Phys. Commun.* **66** (1991) 1.
- [47] T. Stelzer and W. F. Long, *Comput. Phys. Commun.* **81** (1994) 357.
- [48] G. P. Lepage, Cornell preprint CLNS 80-447.
- [49] R. Kleiss, W. J. Stirling and S. D. Ellis, *Comput. Phys. Commun.* **40** (1986) 359.

- [50] R. Dixon, presentation at the Fermilab Users' Meeting, Batavia, IL, June 2007. [http://www.fnal.gov/orgs/fermilab\\_users\\_org/users\\_mtg/2007/agenda-for-web.htm](http://www.fnal.gov/orgs/fermilab_users_org/users_mtg/2007/agenda-for-web.htm)
- [51] S. Eidelman *et al.* [Particle Data Group], Phys. Lett. B **592** (2004) 1.
- [52] A. D. Martin, R. G. Roberts, W. J. Stirling and R. S. Thorne, Phys. Lett. B **531** (2002) 216 [hep-ph/0201127].
- [53] A. D. Martin, R. G. Roberts, W. J. Stirling and R. S. Thorne, Eur. Phys. J. C **39** (2005) 155 [hep-ph/0411040].
- [54] M. Roth and S. Weinzierl, Phys. Lett. B **590** (2004) 190 [hep-ph/0403200].
- [55] E. W. N. Glover and A. G. Morgan, Z. Phys. C **62** (1994) 311.
- [56] D. Buskulic *et al.* [ALEPH Collaboration], Z. Phys. C **69** (1996) 365.
- [57] L. Bourhis, M. Fontannaz and J. P. Guillet, Eur. Phys. J. C **2** (1998) 529 [hep-ph/9704447].
- [58] M. Fontannaz, J. P. Guillet and G. Heinrich, Eur. Phys. J. C **21** (2001) 303 [hep-ph/0105121].
- [59] M. Klasen, Rev. Mod. Phys. **74** (2002) 1221 [hep-ph/0206169].
- [60] A. Gehrmann-De Ridder, T. Gehrmann and E. Poulsen, Eur. Phys. J. C **47** (2006) 395 [hep-ph/0604030].
- [61] G. Degrassi, S. Fanchiotti and A. Sirlin, Nucl. Phys. B **351** (1991) 49.
- [62] A. Djouadi and C. Verzegnassi, Phys. Lett. B **195** (1987) 265; B. A. Kniehl, Nucl. Phys. B **347** (1990) 86.
- [63] K. G. Chetyrkin, J. H. Kühn and M. Steinhauser, Phys. Lett. B **351** (1995) 331 [hep-ph/9502291].
- [64] R. Barbieri, M. Beccaria, P. Ciafaloni, G. Curci and A. Vicere, Phys. Lett. B **288** (1992) 95 [Erratum-ibid. B **312** (1993) 511] [hep-ph/9205238]; R. Barbieri, M. Beccaria, P. Ciafaloni, G. Curci and A. Vicere, Nucl. Phys. B **409** (1993) 105; J. Fleischer, O. V. Tarasov and F. Jegerlehner, Phys. Lett. B **319** (1993) 249; G. Degrassi, S. Fanchiotti and P. Gambino, Int. J. Mod. Phys. A **10** (1995) 1377 [hep-ph/9403250].
- [65] G. Degrassi, P. Gambino and A. Vicini, Phys. Lett. B **383** (1996) 219 [hep-ph/9603374]; G. Degrassi, P. Gambino and A. Sirlin, Phys. Lett. B **394** (1997) 188 [hep-ph/9611363].







# Acknowledgment

My special thanks go to Prof. Johann H. Kühn for giving me the opportunity to work on this interesting topic. In particular, I am grateful for his advice and numerous discussions through which I have learned a lot about physics. I thank Prof. Dieter Zeppenfeld for agreeing to be the second referee for my dissertation.

Also many thanks go to my collaborators Anna Kulesza and Stefano Pozzorini. I have profited a lot from their experience and support during our work on this project. I would like to thank Peter Uwer for his interesting and helpful suggestions concerning the dipole method and phase space integrations.

Without the financial support from the Graduiertenkolleg “Hochenergiephysik und Teilchenastrophysik” this work would not have been possible. I have profited a lot from the annual workshops in Freudenstadt and the opportunity to join various conferences. In particular, the time at the summer school in Les Houches 2006 and the LoopFest VI conference at Fermilab are unforgettable impressions.

Throughout my time at the Institute for Theoretical Particle Physics in Karlsruhe I have always enjoyed the pleasant and inspiring atmosphere. Special thanks go to Philipp Maierhöfer, Kristof Schulze, Tobias Selz and Peter Uwer for carefully reading parts of the manuscript. I am grateful to Andreas Scharf for countless discussions and his help during the final phase of my thesis.

Last, but certainly not least, möchte ich mich bei allen Freunden und insbesondere bei meiner Familie bedanken, die mir moralischen Rückhalt und finanzielle Unterstützung während meines Studiums bot.



# Curriculum Vitae

## Personal Information:

Name: Markus Christian Schulze  
Date of Birth: 12th October 1978  
Place of Birth: Karlsruhe, Germany  
Nationality: German  
Marital Status: Single

## Education:

1998: General qualification for university entrance  
Carl-Engler-Schule Karlsruhe,  
Technisches Gymnasium

1998-1999: Civil service,  
Institute for Water and River Basin Management,  
University of Karlsruhe

1999-2005: Studies in Physics at the University of Karlsruhe

January 2005: Diploma in Physics,  
Diploma thesis: “Electroweak corrections  
to the hadronic production of  $Z$ +jet final states”

May 2005 - April 2008: Dissertation,  
Fellow of the Graduiertenkolleg “Hochenergiephysik  
und Teilchenastrophysik”

Title: “Electroweak corrections to gauge boson production  
at large transverse momenta”

Date of Exam: 18th April 2008

Referees: Prof. Dr. Johann H. Kühn,  
Prof. Dr. Dieter Zeppenfeld